National Library of Canada
Bibliothèque nationale du Canada

Canadian Theses Service
Service des thèses canadiennes

Ottawa, Canada
K1A 0N4

NOTICE

The quality of this microform is heavily dependent upon the quality of the original thesis submitted for microfilming. Every effort has been made to ensure the highest quality of reproduction possible.

If pages are missing, contact the university which granted the degree.

Some pages may have indistinct print especially if the original pages were typed with a poor typewriter ribbon or if the university sent us an inferior photocopy.

Reproduction in full or in part of this microform is governed by the Canadian Copyright Act, R.S.C. 1970, c. C-30, and subsequent amendments.

AVIS

La qualité de cette microforme dépend grandement de la qualité de la thèse soumise au microfilmage. Nous avons tout fait pour assurer une qualité supérieure de reproduction.

S'il manque des pages, veuillez communiquer avec l'université qui a conféré le grade.

La qualité d'impression de certaines pages peut laisser à désirer, surtout si les pages originales ont été dactylographiées à l'aide d'un ruban usé ou si l'université nous a fait parvenir une photocopie de qualité inférieure.

La reproduction, même partielle, de cette microforme est soumise à la Loi canadienne sur le droit d'auteur, SRC 1970, c. C-30, et ses amendements subséquents.

NL-339 (r. 88/04) c

Canada

UNIVERSITY OF ALBERTA

NATURAL CONVECTION in a CYLINDRICAL POROUS MEDIUM: ONE and TWO FLUID PHASES

by

Douglas A. Lillico

A Thesis

Submitted to the Faculty of Graduate Studies and Research
In Partial Fulfillment of the Requirements for
the Degree of Doctor of Philosophy
In

Mechanical Engineering
Department of Mechanical Engineering

Edmonton, Alberta

Spring 1992

National Library of Canada
Bibliothèque nationale du Canada

Canadian Theses Service
Service des thèses canadiennes

Ottawa, Canada
K1A 0N4

The author has granted an irrevocable non-exclusive licence allowing the National Library of Canada to reproduce, loan, distribute or sell copies of his/her thesis by any means and in any form or format, making this thesis available to interested persons.

L'auteur a accordé une licence irrévocable et non exclusive permettant à la Bibliothèque nationale du Canada de reproduire, prêter, distribuer ou vendre des copies de sa thèse de quelque manière et sous quelque forme que ce soit pour mettre des exemplaires de cette thèse à la disposition des personnes intéressées.

The author retains ownership of the copyright in his/her thesis. Neither the thesis nor substantial extracts from it may be printed or otherwise reproduced without his/her permission.

L'auteur conserve la propriété du droit d'auteur qui protège sa thèse. Ni la thèse ni des extraits substantiels de celle-ci ne doivent être imprimés ou autrement reproduits sans son autorisation.

ISBN 0-315-73220-2

Canada

UNIVERSITY OF ALBERTA

RELEASE FORM

NAME OF AUTHOR: **DOUGLAS A. LILLICO**

TITLE OF THESIS: **NATURAL CONVECTION in a CYLINDRICAL POROUS MEDIUM: ONE and TWO FLUID PHASES**

DEGREE: **DOCTOR OF PHILOSOPHY IN MECHANICAL ENGINEERING**

Permission is hereby granted to the University of Alberta Library to reproduce single copies for private, scholarly or scientific research purposes only.

The author reserves all other publication and other rights in association with the copyright in the thesis, and except as hereinbefore provided neither the thesis nor any substantial portion thereof may be printed or otherwise reproduced in any material form whatever without the author's prior written permission.

5403 92AVE., Edmonton, Alberta

Date: APRIL 16, 1992

UNIVERSITY OF ALBERTA

FACULTY OF GRADUATE STUDIES AND RESEARCH

The undersigned certify that they have read, and recommend to the Faculty of Graduate Studies and Research for acceptance, a thesis entitled **NATURAL CONVECTION in a CYLINDRICAL POROUS MEDIUM: ONE and TWO FLUID PHASES** submitted by Douglas A. Lillico in partial fulfillment of the requirements for the degree of Doctor in Philosophy in Mechanical Engineering.

Dr. J.D. Dale (Supervisor)

Dr. J. Masliyah (Supervisor)

Dr. T.W. Forest

Dr. R.E. Hayes

Dr. K.C. Cheng

Dr. G. Sedgwick

Dr. D. Ruth (External Examiner)

Date: April 14, 1992

ABSTRACT

Due to the reducing supply of oil producible from Alberta's conventional oil reservoirs, attention has been drawn to increasing the production capability of Alberta's immense heavy oil and oil sands reservoirs. Most of these reserves are too deep to be economically strip mined and effective exploitation of these deeper reservoirs requires the improvement of existing thermal in-situ production technology. One area of potential improvement in thermal recovery is improving the heat transfer from the high temperature injected steam to the reservoir. Forced convection and conduction dominate the thermal processes, but thermal natural convection may have considerable effect, particularly in regions of low pressure gradient and favorable temperature gradient.

The purpose of this work is to examine experimentally and theoretically the steady state natural convection of reservoir-like fluids at relatively high pressures (2 MPa) and temperatures (190°C) in a porous medium. This was done for a single fluid (water), for a liquid and a condensible gas (water/steam) and for different mixtures of two immiscible liquids (oil/water, tetrachloroethylene/water). The porous media used were quartz sand packed to permeabilities ranging from 26.5 darcies (26.5×10^{-12} m^2) to 2100 darcies (2100×10^{-12} m^2) and porosities of between 32.4% and 34.0%. The sand packs were contained in a steady state, guarded heat transfer cell that was heated from above for conductivity measurements and from below for convection experiments. The cylindrical sand packs were 0.45 m in diameter and 0.67 m. tall. The heat fluxes were measured using 0.45 m diameter heat flux meters located above and below the sand pack.

The natural convection of a single fluid in a porous medium heated from below has previously been described in the literature. A novel method for handling viscosity variations was developed that greatly increases the applicability of the previous models to real systems. A new set of boundary conditions representing finitely conductive layers above and below the porous medium were formulated in an attempt to more closely match the actual boundary conditions encountered experimentally.

The natural convection of a liquid and a condensible gas was found to develop an overlying liquid zone when the permeability of the porous medium was below an upper limit. New models describing the behaviour of the critical overlying liquid zone were developed. These models explained the apparently contradictory evidence previously reported in the literature.

The onset of natural convection of a mixture of two immiscible liquids was found to be adequately described by a novel model, developed in this work, based predominantly on relative permeability concepts.

ACKNOWLEDGMENTS

I must express my appreciation to my academic supervisors, Dr. J.D. Dale and Dr. J. Masliyah and to my project managers, Dr. T.W. Stone and Dr. G. Sedgwick, for their valuable guidance, encouragement, and thoughtful suggestions throughout the preparation of this thesis.

I feel indebted to the Alberta Research Council and the Alberta Oil Sands Technology and Research Authority for funding this study. I would also like to thank all the staff at the Alberta Research Council who participated in the completion of this thesis.

TABLE OF CONTENTS

ABSTRACT i

ACKNOWLEDGEMENTS iii

1. INTRODUCTION 1
   - 1.1 Heat Transfer in Oil Sands 1
   - 1.2 Thermal Natural Convection in Porous Media 3
   - 1.3 Natural Convection in an Enclosed Porous Medium 4
   - 1.4 Objectives of this Study 4

2. LITERATURE SURVEY 7
   - 2.1 Single Fluid Natural Convection 7
   - 2.2 Single Fluid Natural Convection in a Porous Medium 7
     - 2.2.1 Onset of Convection 8
     - 2.2.2 Heat Transfer Rates 9
     - 2.2.3 Confinement Effects 9
     - 2.2.4 Viscosity Variation Effects 11
     - 2.2.5 Boundary Condition Effects 12
   - 2.3 Steam/Water Natural Convection in a Porous Medium 12
   - 2.4 Two Immiscible Fluids Natural Convection in a Porous Medium 13
   - 2.5 Literature Survey Summary 13
   - 2.6 Studies Performed in this Work 14

3. EXPERIMENTAL APPARATUS 15

4. NATURAL CONVECTION OF A SINGLE FLUID IN POROUS MEDIA 19
   - 4.1 Single Fluid Model 21
     - 4.1.1 Onset of Convection 21
     - 4.1.2 Heat Transfer Rate 29
   - 4.2 Single Fluid Experiments 30

TABLE OF CONTENTS cont.

4.3 Single Fluid: Comparison of Results....33
4.3.1 Onset of Convection....33
4.3.2 Heat Transfer Rate....33

5. NATURAL CONVECTION OF LIQUID/CONDENSIBLE VAPOUR....36
5.1 Steam/Water Models....38
5.2 Steam/Water Experiments....43
5.3 Steam/Water: Comparison of Results....47

6. NATURAL CONVECTION OF TWO IMMISCIBLE LIQUIDS....53
6.1 Two Immiscible Fluids Models....53
6.1.1 Psuedo-Fluid Model....53
6.1.2 Relative Permeability Models....54
6.2 Tetrachloroethylene/Water Experiments....57
6.3 Mentor 29/Water Experiments....59
6.4 Two Immiscible Liquids: Comparison of Results....63
6.4.1 Psuedo-Fluid Model Results....63
6.4.2 Relative Permeability Models Results....68
6.4.2.1 Relative Permeability Sensitivity....73

7. CONCLUSIONS....76

8. REFERENCES....78

APPENDICES:

A. Heat Transfer Cell....83
B. Heat Transfer Cell Calibration....104
C. Single Fluid: Onset of Convection....109
D. Critical Rayleigh Values....135
E. Single Fluid: Onset Models Comparison....170
F. Single Fluid: Heat Transfer Rate....172

TABLE OF CONTENTS cont.

G. Single Fluid: Experimental Analysis.....182
H. Liquid/Condensible Vapour: Steam/Water Interface Stability.....186
I. Liquid/Condensible Vapour: Experimental Analysis.....192
J. Liquid/Condensible Vapour: Two Phase Zone Theoretical Analysis.....194
K. Two Immiscible Liquids: Experimental Analysis.....196
L. Two Immiscible Liquids: Pseudo-Fluid.....199
M. Relative Permeability Experiments.....202
N. Two Immiscible Liquids: Relative Permeability.....203
O. Water/Sand Thermal Conductivity.....206

LIST OF FIGURES

2.1 Isotherms and Streamlines in Natural Convection in a Porous Layer....10
3.1 Heat Transfer Cell Diagram....16
4.1 Convective Mode Planforms in a Cylindrical Porous Medium Heated from Below....20
4.2 Variable Viscosity Predictions....23
4.3 Sand Pack Layout....24
4.4 Convective Isotherms (Elevation), Water in Sand, Run W-S #5....31
4.5 Measured Heat Transfer Rates, Water in Sand, Runs W-S #1-#5....32
4.6 Comparison of Predicted and Measured Critical Rayleigh Values, Water in Sand, Runs W-S #1-#5....34
4.7 Comparison of Predicted and Measured Heat Transfer Rates, Water in Sand, Runs W-S #1-#5....35
5.1 Schematic of the Natural Convection of a Liquid/Vapour in a Porous Medium Heated from Below....37
5.2 Moderate Permeability Isotherm Contours (Elevation), Water/Steam in Sand, Run W/S-S #1....40
5.3 Experimental Results,Water/Steam in Sand, Runs W/S-S #1-#3....45
5.4 High Permeability Isotherms Contour (Elevation), Water/Steam in Sand, Run W/S-S II #4....48
5.5 Overlying Water Zone Nusselt Number Model Predictions....52
6.1 Proposed Relative Permeability Models....56
6.2 Experimental Results, Tetrachloroethylene/Water in Sand, Runs T/W-S #1-#4....58
6.3 Experimental Results, Tetrachloroethylene/Water in High Permeability Sand, Runs T/W-S II #1-#4....60
6.4 Experimental Results, Mentor 29/Water in High Permeability Sand, Runs O/W-S #1-#3, #5-#7....61
6.5 Experimental Results, Mentor 29/Water in High Permeability Sand, Runs O/W-S II #1-#5....62

LIST OF FIGURES cont.

6.6 Comparison of Predicted and Measured Critical Rayleigh Values, Psuedo-Fluid, Tetrachloroethylene/Water in Sand, Runs T/W-S #1-#4.....64

6.7 Comparison of Predicted and Measured Critical Rayleigh Values, Psuedo-Fluid, Tetrachloroethylene/Water in High Permeability Sand, Runs T/W-S II #1-#4.....65

6.8 Comparison of Predicted and Measured Critical Rayleigh Values, Psuedo-Fluid, Mentor 29/Water in High Permeability Sand, Runs O/W-S #1-#3, #5-#7.....66

6.9 Comparison of Predicted and Measured Critical Rayleigh Values, Psuedo-Fluid, Mentor 29/Water in High Permeability Sand, Runs O/W-S II #1-#5.....67

6.10 Comparison of Predicted and Measured Critical Rayleigh Values, Relative Permeability Model 1,Tetrachloroethylene/Water in Sand, Runs T/W-S #1-#4.....69

6.11 Comparison of Predicted and Measured Critical Rayleigh Values, Relative Permeability Model 1, Tetrachloroethylene/Water in High Permeability Sand, Runs T/W-S II #1-#4.....70

6.12 Comparison of Predicted and Measured Critical Rayleigh Values, Relative Permeability Model 1, Mentor 29/Water in High Permeability Sand, Runs O/W-S #1-#3, #5-#7.....71

6.13 Comparison of Predicted and Measured Critical Rayleigh Values, Relative Permeability Model 1, Water/Mentor 29 in High Permeability Sand, Runs O/W-S II #1-#5.....72

6.14 Comparison of Predicted and Measured Critical Rayleigh Values, Relative Permeability Model 1, Mentor 29/Water in High Permeability Sand, Runs O/W-S #1-#3, #5-#7, Water Rel Perm + 10%.....74

6.15 Comparison of Predicted and Measured Critical Rayleigh Values, Relative Permeability Model 1, Mentor 29/Water in High Permeability Sand, Runs O/W-S #1-#3, #5-#7, Water Rel Perm - 10%.....75

LIST OF FIGURES cont.

A.1 Heat Transfer Cell....90
A.2 Lower Heating/Cooling Head section....91
A.3 Upper Heating/Cooling Head and Overburden Assembly Section....92
A.4 Main Heater Plate....93
A.5 Heat Transfer Fluid Circuits....94
A.6 Cooling Plate....95
A.7 Pore Fluid Control System....96
A.8 Primary Thermocouple Locations....97
A.9 Heat Flux Meter....98
A.10 Temperature Probes....99
A.11 Cell Power System....100
A.12 Lower Gasket Assembly....101
A.13 Basic Flow Chart of Data Acquisition and Control Program....102
A.14 Subroutine Flow Chart of Data Acquisition and Control Program....103
C.1 Sand Pack Layout....120
C.2 Convective Motion Planforms....134
D.1-D.17
Predicted Critical Rayleigh Values, Modes 1 - 17....136
G.1 Lower Surface Temperature Profile....185

LIST OF TABLES

5.1 Water/Steam in Sand: Experimental Results....44
5.2 Water/Steam in Sand: Comparison of Models....49
5.3 Water/Steam in Sand: Overlying Water Zone Modes....50
6.1 Psuedo-Fluid Model Predictions....63
6.2 Relative Permeability Model 1 Predictions....68

B.1 Heat Transfer Cell Calibration....108
C.1 Model Eigenvalues....133
D.1-D.17
Predicted Critical Rayleigh Values, Modes 1 - 17....137
G.1 Single Fluid: Experimental Results....184
I.1 Liquid/Condensible Vapour: Experimental Results....193
K.1 Tetrachloroethylene/Water in Sand: Experimental Results....197
K.2 Two Immiscible Liquids: Experimental Results....198
L.1 Tetrachloroethylene/Water in Sand: Pseudo-fluid Rayleigh Values....200
L.2 Two Immiscible Liquids: Pseudo-fluid Rayleigh Values....201
N.1 Tetrachloroethylene/Water in Sand: Tetrachloroethylene Phase
Relative Permeability Rayleigh Values....204
N.2 Two Immiscible Liquids: Relative Permeability Rayleigh Values....205

LIST OF SYMBOLS

a	Dimensionless temporary function in r, λ describing fluid motion
A^*	Horizontal cross-sectional area of sand pack [m^2]
A	Dimensionless sand pack area A^* / L^2
b	Dimensionless temporary function in ϕ, λ describing fluid motion
B	Dimensionless parameter, $[k/\phi_p L^2] \{Pr\}^{-1}$
B_i	Finite dimensionless amplitudes of convective fluid motion
C_p	Heat capacity, in Ra definitions at cold end conditions [J/kg K]
C_i	Temporary constants used in development of equations
$\vec{F}^*$	Body force vector [$kg/m^2 s^2$]
g_a	Acceleration of gravity [m/s^2]
g	Dimensionless height function describing fluid motion
G_i	Dimensionless constants dependent on λ
Gr	Grashof number, the ratio between buoyancy and viscous forces $(g_a \beta L^3 \Delta T) / \nu^2$
h	Dimensionless temporary function in r, λ, ϕ describing fluid motion
h_{lv},h_{fg}	Heat of vapourization [J/kg]
$I_{1,2}$	Integrals used for predicting Nusselt numbers
J_m	Bessel function of first kind, mode m
k	Permeability [m^2]
k_{rf}	Relative permeability of fluid
k_{ro}	Relative permeability of oil phase
k_{rw}	Relative permeability of water phase
k_{rl}	Relative permeability of liquid phase
k_{rv}	Relative permeability of vapour phase
$\hat{k}$	Unit vector in vertical (z) direction
L	Height of porous medium [m]
L_L	Thickness of finitely conductive layer used in second boundary condition set to model heat flux meters [m]
$\hat{n}$	Unit vector normal to surface

LIST OF SYMBOLS cont.

Nu	Nusselt number, ratio of actual heat flux to heat flux if conduction only was occurring
Nu_o	Overall Nusselt number, $q\ L / \lambda_m\ (T_1 - T_0)$
Nu_w	Overlying water zone Nusselt number, $q\ \Delta y_w / \lambda_m\ (T_M - T_0)$
Nu_{sw}	Two phase zone Nusselt number, $q\ \Delta y_{sw} / \lambda_m\ (T_1 - T_M)$
$\dot{m}$	mass flow rate [kg/s]
P^*	Pressure [Pa]
P_0^*	Applied pore pressure [Pa]
P	Dimensionless pressure p. 113
p^*	Perturbed pressure [Pa] p. 111
p	Dimensionless perturbed pressure p. 113
Pr	Prandtl Number, the ratio of the diffusivity of momentum to the diffusivity of heat $C_p\ \mu / \lambda_f$
Q,q	Heat flux [W/m^2]
q_{max}	Dryout heat flux [W/m^2]
Q_b	Heat flux at the onset of boiling [W/m^2]
r^*	Radial direction [m]
r	Dimensionless radial direction, r^* / L
$\hat{r}$	Unit vector in radial (r) direction
R	Outer radius of porous medium [m]
Ra_{sf}	Rayleigh number, single fluid layer
Ra	Rayleigh number, as modified for porous media
Ra_c	Critical Rayleigh number, Ra value at the onset of convection
Ra_b	Rayleigh number at the onset of boiling
Ra_{rf}	Rayleigh number of a fluid in a porous medium containing another immiscible fluid, defined using relative permeability concepts.
R_c	Zebib's[32] critical rayleigh value Ra_c
s	aspect ratio, dimensionless outer radius (R/L)
S	Surface
S_l	Saturation ratio of primary liquid, fraction of pore space occupied by primary liquid
S_o	Saturation of oil phase

LIST OF SYMBOLS cont.

t^*	Time [s]
t	Dimensionless time p. 113
T	Temperature [°C, K]
T_{sat}	Boiling point temperature [°C, K]
ΔT	Temperature difference across a zone [°C, K]
T_z	Average temperature over horizontal cross-section of pack at height z^* in pack [°C, K]
u^*	Local fluid velocity [m/s]
u_b^*	Bulk fluid velocity [m/s]
u	Dimensionless local fluid velocity p. 113
u_b	Dimensionless bulk fluid velocity p. 113
W	Stability number for steam/water interface
W_b	Interface stability number at the onset of boiling
W_{bc}	Critical onset of boiling interface stability number
Δy_w	Thickness of overlying water zone [m]
Δy_{sw}	Thickness of two phase zone [m]
z^*	Vertical direction [m]
z	Dimensionless vertical direction, z^* / L
$z_{m,k}$	Zebib's[23] eigenvalue source function (m,k) = modes

Greek Symbols

α	Dimensionless finite heat flux meter thermal conductivity $(\lambda_L / L_L) / (\lambda_m / L)$
β	Coefficient of volume expansion, in Ra definitions at average conditions [1/K]
γ	Heat capacity ratio of matrix to fluid $(\rho C_p)_m / (\rho_0 C_p)_f$
λ	Eigenvalue
λ_m	Thermal conductivity of saturated porous medium, in Ra definitions at average conditions [W/m K]
λ_L	Thermal conductivity of layer used in second boundary condition set to model heat flux meters [W/m K]

LIST OF SYMBOLS cont.

λ_{sT}	Thermal conductivity of medium saturated with water @ temperature T [W/m K]
λ_s	Thermal conductivity of water saturated porous medium [W/m K]
λ_w	Thermal conductivity of water [W/m K]
λ_{solid}	Thermal conductivity of solid in matrix [W/m K]
μ	Fluid dynamic viscosity, in Ra definitions at cold end conditions [Pa s]
μ_R	Viscosity ratio (μ_0 / μ_1)
ϕ	Angle [Radians]
ϕ_p	Porosity
ρ	Fluid density, in Ra definitions at cold end conditions [kg/m^3]
τ^*	Temperature fluctuation [°C, K]
τ	Dimensionless temperature fluctuation p. 175
θ	Dimensionless perturbed temperature $(((T - T_0) + (T_1 - T_0)(z^* / L))/(T_1 - T_0))$
Θ	Dimensionless temperature p. 175
Θ_z	Dimensionless T_z p. 175
υ	Kinematic viscosity [m^2/s]
ω^*	Bulk fluid velocity in $\hat{k}$ direction [m/s]
ω	Dimensionless bulk fluid velocity in $\hat{k}$ direction $\tilde{u}_b \bullet \hat{k}$
Ω	Correction factor for predicting liquid/vapour Nusselt number

Subscripts and superscripts

$()_0$	Value at cold end conditions
$()_1$	Value at hot end conditions
$()_M$	Value at top of two phase zone (bottom of overlying water zone)
$(\tilde{})$	Vector value
$()^i$	Derivative of variable
$()_m$	Value of porous medium, including fluid and matrix

LIST OF SYMBOLS cont.

$()_f$	Value of fluid
$()_g$	Value of gas
$()_l$	Value of liquid
$()_v$	Value of vapour
$()_{hfm}$	Value of heat flux meter
$()_{bot}$	Value at bottom of sand pack
$()_{top}$	Value at top of sand pack
$()_{sat}$	Value at saturation point (boiling point)
$()_{psuedo}$	Value used in pseudo-fluid model

CHAPTER 1. INTRODUCTION

Due to the reducing supply of oil which can be produced by conventional methods from Alberta light oil reservoirs attention is being attracted to the high viscosity oil contained in the immense 413.6 x 10^9 m^3 Alberta oil sands deposits and heavy oil reservoirs[1] . The oil sands reserves are characteristically composed of water-wet unconsolidated, predominantly quartz, sand with pore spaces filled with water, bitumen, and, sometimes, gas phases[2] . The liquid water phase typically also contains fines (fine sand and clay particles), and dissolved components (salts, gases, oil). The bitumen phase usually includes a wide range of extremely high viscosity hydrocarbons, and some dissolved gases and water. The bitumen phase viscosity is too high for conventional reservoir production techniques to succeed.

The oil sands deposits near the surface may be successfully, and economically, strip mined, as is done near Ft. McMurray. Some 5.8 x 10^9 m^3 of the oil sands and heavy oil reserves are shallow enough, under less than 50 m of overburden[1] , to be potentially strip-mined. The bulk of the recoverable reserves, 57.0 x 10^9 m^3 , must be extracted in-situ.[1] In-situ recovery techniques are predominantly thermal, utilizing the injection of hot fluids to increase oil temperatures and, thus, reduce viscosity. The reduced viscosity, and attendant increased oil mobility, allow the production of the oil. The injected fluids are usually steam or hot water, and may include additives for improved conformance, etc.. One of the critical factors controlling the thermal stimulation of a heavy oil reservoir or oil sands deposit is the rate of heat transfer from the injected fluids to the produced oil.

1.1 Heat Transfer in Oil Sands

Heat transfer through oil sands reservoirs is extremely complicated. All three of the basic modes of heat transfer (conduction, convection, and radiation)[3] may be involved in series and in parallel combinations. Additionally, the effects of multiple phases and components, as are present in oil sands reservoirs, tend to complicate further the already convoluted heat transfer processes.

Radiative heat transfer is the transport of energy in the form of electromagnetic radiation. In porous media radiative heat transfer usually occurs from solid particle to solid particle through the pore space. Oil sands reservoirs have relatively low spatial temperature

gradients and the pore spaces are predominantly filled with opaque liquids. The low temperature gradients result in small temperature differences between adjacent sand grains and reduced radiative heat transfer. The liquid in the pore spaces absorb the radiative energy, halting radiation heat transfer. These two factors combine to make heat transfer by radiation negligible in most situations related to this work.

Conductive heat transfer is the transport of energy from a high temperature region to a lower temperature region by the drift of electrons (solid metals), vibrational impact of molecules (other solids), and kinetic impact of molecules (fluids). In porous media, conductive heat transfer follows an extremely complicated and convoluted path.[4] Conduction can occur through the pore space fluids, through the solid phase alone, and through a series path from solid particle to pore fluid to solid particle. The three paths can combine in parallel and series and the relative significance of each depends greatly on the characteristics of the porous medium. The most significant media characteristics include the thermal properties of the various solid, liquid and gas phases, porosity, fluid saturations, and wettability. The extreme complexity of modelling the conduction heat transfer through the complicated structure of the oil sands material causes thermal conductivity to be best predicted by relationships fitted to experimental data garnered from tests on materials which are as similar as possible to the actual reservoir materials[5] .

Convective heat transfer in porous media is the transport of energy by fluids flowing through a porous medium in which a temperature difference exists. Convective heat transfer can be separated into forced convective heat transfer and natural convective heat transfer.

Forced convective heat transfer in porous media is the transport of thermal energy by fluids flowing through the porous media under the driving force of an imposed pressure gradient. The presence of three different fluid phases (oil, water, gas) greatly increases the complexity of describing this process in oil sands reservoirs. There has been a large amount of laboratory scale production testing, field piloting, and numerical modelling resulting in considerable knowledge of forced convective heat transfer in oil sands.[6]

Natural convective heat transfer in porous media is the transport of thermal energy by fluids moving through the porous media due to the influence of body forces, such as those resulting from concentration gradients or density gradients in a gravitational field.

Natural convection in thermally stimulated oil sands deposits is expected to be buoyancy induced flow due to thermal gradients. Additionally, heat transfer can be particularly large when phase changes combine with natural convection, as large amounts of energy can be transferred in the boiling and condensation zones.

Pilot plant scale and larger projects intending to utilize in-situ production from heavy oil reservoirs and oil sands are preceded by extensive numerical reservoir modelling examining the proposed production scheme. The numerical modellers have a considerable amount of knowledge available to them about all the possible heat transfer paths, except for natural convection. The intent of this work is to enhance the available knowledge on thermal natural convection in reservoir-like materials, in particular the natural convection of steam-water and oil-water systems.

1.2 Thermal Natural Convection in Porous Media

Natural convection of a fluid, not in a porous medium, has been studied for almost two hundred years. Modelling of the thermal natural convection of a single fluid in porous media has been done for less than fifty years and primarily differs from the fluid only case in the treatment of fluid motion.[7] The constraining effect of the porous media simplifies the equations of fluid motion considerably. In most circumstances the equations of motion can be simplified to Darcy's Law, where fluid velocity has a linear dependence on pressure gradient.[8] Single fluid natural convection in a porous medium has been studied for many different spatial arrangements,[7,9] and modelling has been done using more realistic assumptions about the fluid properties.[10]

Natural convection in oil sands reservoirs can involve two or three different fluid phases. Multi-phase natural convection in porous media has not been thoroughly explored. Multi-phase systems are quite different from single fluid systems, as the different phases interfere considerably with each other's behaviour. These effects include condensation of a gas phase into a liquid phase, dissolution of one phase into another, and the reduction of the effective permeability of the porous media. The natural convection of two completely miscible fluids (one phase, two components) in porous media has been examined to a limited extent,[11-13] as has the natural convection of a liquid and a condensible gas (steam/water).[14-20] Natural convection of two immiscible liquids (oil/water) has not been reported for the two immiscible liquids distributed throughout a porous medium,

only for two separate liquid layers not contained in a porous medium.[21]

1.3 Natural Convection in an Enclosed Porous Medium

A typical oil sands reservoir has a thin pay zone, but a relatively large horizontal extent. The resulting large aspect ratio, defined as horizontal extent / vertical extent, would allow the use of the assumption of a layer of infinite horizontal extent in describing the natural convection occurring in the reservoir. Studies of thermal natural convection in a porous layer of infinite horizontal extent heated from below showed convection to occur as a large number of discrete roll cells, the dimensions of which are primarily determined by the layer thickness.[7]

However, in a laboratory scale experiment the effect of horizontal confinement is, of necessity, much greater. Horizontal dimensions of a laboratory sand pack are necessarily limited by spatial requirements, while the necessary sand pack thickness for the convection of viscous liquids to occur remains the same or is increased. The aspect ratio is therefore small, particularly when compared with a typical reservoir. In order to describe the convection mechanisms tested in a laboratory scale experiment, the effects of the small aspect ratio must be considered. Natural convection of a fluid in a confined porous medium will usually occur as a few roll cells[22] or as a single roll cell.[23] Additionally, the confinement effects will increase the critical Rayleigh value,[23] and delay the onset of convection.

1.4 Objectives of this Study

The primary objective of this study was to increase the understanding of the thermal natural convection of fluids in oil sands reservoirs. The particular application of this information would be to aid the numerical reservoir modelling that is essential to predicting the behaviour of in-situ reservoir production schemes.

These objectives were met by developing models to predict the onset of natural convection and to predict some of the heat transfer correlations for experiments using two fluids saturating a sand pack heated from below. Parameters for this study, as noted below, were chosen to provide a closer look at heat transfer under conditions experienced in the in-situ thermal recovery of bitumen or heavy oil. The three fluid phases present in

a steam stimulated oil sands reservoir are oil, water, and steam. Most commonly, there exists a high water saturation zone between the zones of high oil and steam saturation.

To represent the most common situation, fluid combinations representing the oil/water and water/steam contact zones were tested at high pressures and temperatures. The water/steam system was examined by boiling water in a sand pack heated from below. The oil/water system was examined by detecting the onset of convection of a mixture of oil and water in a water wet sand pack heated from below.

Selection of higher permeability sand packs and less viscous oils than typical for oil sands reservoirs allowed natural convection to be studied effectively in a laboratory setting. The study concentrated on the critical parameters determining the onset of convection and on the heat transfer correlations for the water/steam system.

The initial series of experiments was conducted with a single fluid, water, in order to provide baseline performance. Three fluid combinations were studied: water/steam, tetrachloroethylene/water and Mentor 29/water. Tetrachloroethylene and Mentor 29, a light oil, were selected as they are immiscible in water. The sand packs used in the experiments were: 40-70 quartz sand, packed to 32.4% porosity and 26.5 Darcy (26.5×10^{-12} m^2) permeability; 6-9 quartz sand, packed to 34.0% porosity and 2100 Darcy (2100×10^{-12} m^2) permeability; and 6-9 quartz sand packed to 33.4% porosity and 1950 Darcy (1950×10^{-12} m^2) permeability. During the course of the experiments temperatures reached 190°C and pressures reached 2 MPa. To provide calibration and baseline information, five experiments were done with water alone. Eight experiments were done with water/steam, eight with water/tetrachloroethylene, and eleven with water/Mentor 29.

The initial single fluid experimental series was used to provide corroboration for conventional analytical and numerical models of the onset of convection and heat transfer rate. The conventional onset of convection model was altered in this study by changing the relationship used to describe the fluid viscosity dependence on temperature. The alteration was introduced to improve the utility of the conventional model when applied to experimental results. The water/steam system was analytically modelled using interface stability concepts to predict the convective behaviour of and the heat transfer correlations for the system. The experimental results from this study and earlier studies published by others were used to corroborate these models and to provide key parameter values. A novel analytical and numerical model of the onset of convection was

developed. The model was based on relative permeability concepts, and to corroborate it, experiments with two different pairs of immiscible fluids were conducted.

CHAPTER 2. LITERATURE SURVEY

The thermal natural convection of fluids has been studied experimentally, analytically and numerically. These examinations have encompassed a large number of possible spatial arrangements, such as heated from below, from the side, uniformly within (reactions, irradiation, etc.), and by immersed bodies. Additionally, studies have investigated transient and/or steady state heat transfer. The fluids used have ranged from pure water and other liquids, to gases, to miscible and immiscible mixtures, and to discrete layers of immiscible liquids. In most of the investigations, the fluids were not constrained by a porous medium, but a large amount of work has been done to examine thermal natural convection of fluids in a porous medium. The tremendous amount of literature published on the topic of thermal natural convection requires the restriction of the literature survey to the steady state thermal natural convection of fluids in a porous medium heated from below. Some discussion of the fluid only case will be presented as an introductory measure.

2.1 Single Fluid Natural Convection

The steady state thermal natural convection of a single fluid layer heated from below was first examined by Rayleigh.[24] Natural convection in this situation occurs when the temperature gradient is large enough for the buoyancy forces to exceed the viscous shear forces. Rayleigh developed a dimensionless number that represented the balance of forces (Ra_{sf}) and determined the critical value for the point of marginal stability (onset of convection) of an ideal fluid layer of infinite horizontal extent . The Rayleigh number is a dimensionless group that is the product of the Grashof and Prandtl numbers. The Grashof number represents the ratio between buoyancy and viscous forces, and the Prandtl number represents the ratio of the fluid's momentum diffusivity (viscosity) to its thermal diffusivity. Rayleigh's technique was to linearize and simplify the equations of conservation of mass, momentum, and energy, and then solve for the critical Rayleigh value at the point of instability. An ideal fluid was defined as one with constant properties except for the effect of thermally induced density variations on the buoyancy force (Boussinesq approximation).[25]

2.2 Single Fluid Natural Convection in a Porous Medium

Natural convection of a single fluid in porous media differs from the fluid only case in the

treatment of fluid motion. The constraining effect of the porous media simplifies the equations of fluid motion considerably. In most circumstances the equations of motion can be simplified to Darcy's Law, where fluid velocity has a linear dependence on driving force and porous media permeability.[8] Darcy's Law fails when fluid velocities become high enough for inertial effects to be significant. Suitable extensions to Darcy's Law are then implemented to allow an adequate description of the fluid motion within the porous medium.[26,27]

2.2.1 Onset of Convection

A description of the onset of convection in a porous layer of infinite horizontal extent heated from below and saturated with an ideal fluid was first attempted in 1945 by Horton and Rogers.[28] Lapwood, in 1948, also described a similar system,[7] using the technique first developed by Rayleigh[24] for a fluid that is not constrained by a porous medium. Lapwood used Darcy's Law and found a modified dimensionless Rayleigh number that reflected the changes in the equations of motion. He determined the critical value for the onset of convection in a porous layer of infinite horizontal extent, saturated with an ideal fluid, heated from below ($Ra_c = 39.5$). Values of the modified Rayleigh number have little to do with the original Rayleigh number and henceforth the modified Rayleigh number will be referred to as the Rayleigh number. The Rayleigh number is defined as:

$$Ra = [g_a \, k \, \beta \, (T_{bot} - T_{top}) \, L \, \rho^2 \, C_p] / (\mu_{bot} \, \lambda_m) \qquad 2.1$$

Other researchers later attempted improved descriptions and experimental corroboration. It was not until 1966 that Katto and Masuoka[29] found the correct form for the effective thermal diffusivity of the system that allowed experimental corroboration. Katto and Masuoka[29] corroborated their results by an experiment using nitrogen gas as the fluid in a high permeability porous medium. Since gas viscosity has less temperature dependence than liquid viscosity, their predictive model ignored viscosity variations. Additionally, the high permeability porous medium they used enabled the utilization of a cell of high aspect ratio. This high aspect ratio allowed their model to ignore confinement effects. Considerable effort has been expended on describing the combined effects of temperature dependent properties and confinement,[14,23,30-32] with success being primarily dependent on how closely the assumptions matched the experiment.

2.2.2 Heat Transfer Rates

The prediction of heat transfer rate at supercritical Rayleigh numbers (after the onset of convection) has been studied by many researchers.[14,26,27,33-38] An excellent review of natural convection heat transfer in porous media was done by Cheng[39] in 1978. Experiments have shown that when fluid velocity levels are high, models based upon Darcy's law do not accurately predict heat transfer rates and that models utilizing extensions to Darcy's law[26,27] need to be used. A flow model by Bau[14] found the amplitude of fluid motion and hence heat transfer rate by using power integral techniques to extend the linearized equations, used for predicting the onset of convection, that described the form of the fluid motion. This method is applicable for Rayleigh numbers of up to approximately five times the critical Rayleigh value.[37,40]

2.2.3 Confinement Effects

Natural convection in a porous layer of infinite horizontal extent occurs as a large number of discrete roll cells, the dimensions of which are primarily dependent on the layer thickness.[7] However, natural convection of a fluid in a confined porous medium will usually occur as only a few roll cells, and often as a single roll cell which occupies the entire porous medium.[22,23] Additionally, the confinement effects delay the onset of convection, thus increasing the critical Rayleigh value. The isotherms and streamlines that delineate the roll cells found in natural convection are shown as a schematic in Figure 2.1.

Different confinement geometries have been used in studies of confinement effects, with most being either rectangular or cylindrical. Beck, in 1972,[22] examined the natural convection of a fluid in a rectangular box, filled with a porous medium, heated from below. He found the preferred forms of fluid motion to be square roll cells. Holst and Aziz, in 1972,[25] conducted an experimental and numerical study of convection in a rectangular porous medium. Later studies in rectangular boxes tended to concentrate on the transitions through the fluid motion modes at higher Ra values.[41-43]

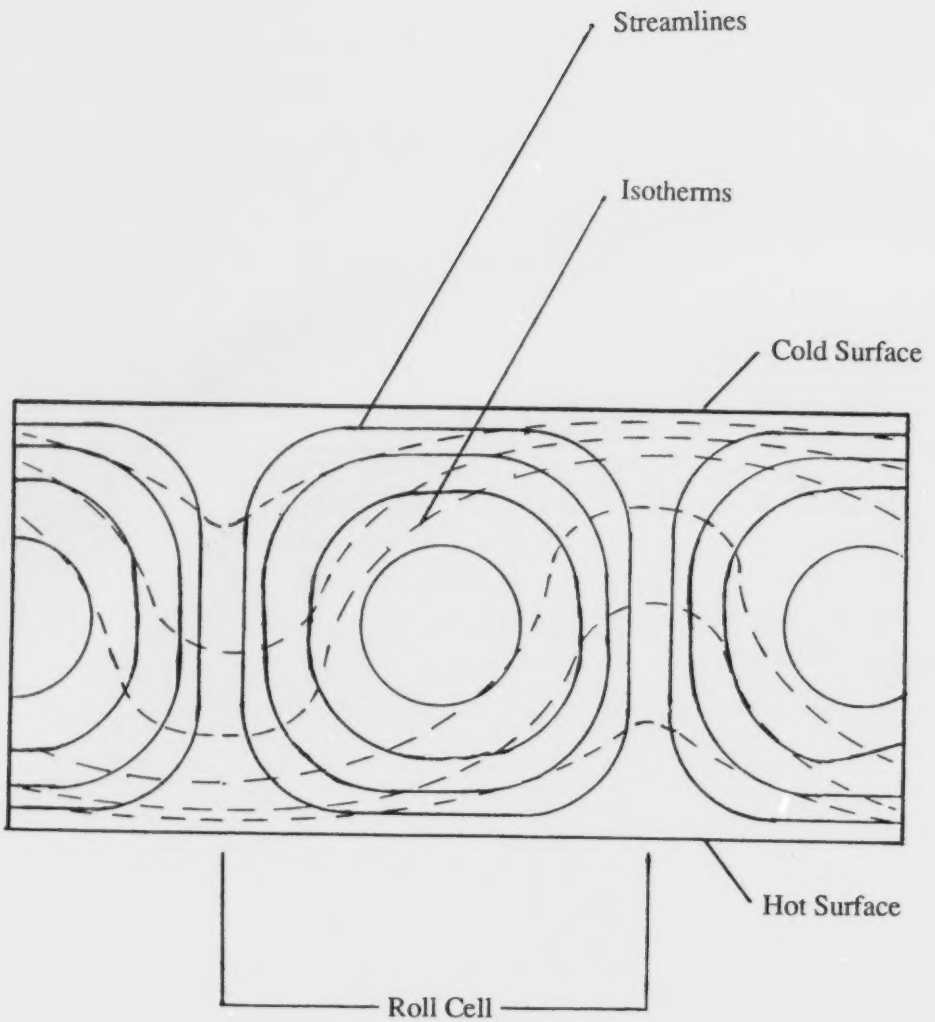

Figure 2.1 Isotherms and Streamlines in Natural Convection in a Porous Layer

Zebib, in 1978,[23] published an excellent theoretical model of natural convection in a cylindrical porous medium heated from below. He found the predominant fluid motion modes to be asymmetric, and the critical Rayleigh value to increase for small aspect ratios. Bories and Deltour, in 1979,[44] examined the case of a cylindrical porous medium confined in an infinite slab. Bau and Torrance, in 1982,[45] published a theoretical and experimental study on the natural convection of water in a cylindrical porous medium heated from below, in which the top surface was isothermal and permeable. The correlation between experiment and model was limited, as viscosity variation effects were not considered.

2.2.4 Viscosity Variation Effects

The effects of the variation of viscosity with temperature on thermal natural convection of a fluid in a porous layer was first theoretically studied by Rogers and Morrison in 1950,[46] using an exponential relationship between viscosity and temperature. The enhanced analysis improved their comparison between experimental results and theory. An empirical viscosity-temperature relationship was used by Kassoy and Zebib in their 1975 theoretical study.[10] They found that the critical Rayleigh value was reduced from 39.5 (constant viscosity) to 8.9 (variable viscosity) for a water saturated layer of infinite horizontal extent with upper and lower boundary temperatures of 25°C and 275°C. Zebib later applied the analysis to a porous medium confined in a rectangular box,[32] and then to a cylindrical porous medium[23] and similar Ra_c reductions were noted. In 1977, Straus and Schubert conducted a theoretical analysis of geothermal convection[47] in which all the fluid properties were allowed to vary and they found a reduction in Ra_c of up to 31 times. Wooding, in 1957,[48] used a numerical model of a specific New Zealand geothermal area that included an empirical dependence of viscosity on temperature. Holst and Aziz, in 1972,[25] conducted a numerical and experimental investigation into convection in a rectangular porous medium that included variable viscosity effects. Sorey, in 1976,[38] numerically studied the onset of convection and the heat transfer rate in a confined box and included tabulated viscosity values. The results of his numerical study clearly illustrated the importance of the viscosity variation effect on the onset of convection.

Gary et al[33] found the effect of viscosity variation on heat transfer rates to be manifested primarily through the critical Rayleigh value and the predicted fluid velocity profiles at onset. In confirmation, an examination of the illustrations published by Sorey[38] show his reported increase in heat transfer with an increase in viscosity variation was due

primarily to a shift in Ra_c to lower values.

2.2.5 Boundary Condition Effects

Several different thermal boundary conditions have been used for the study of a confined porous layer heated from below. Usually, the side walls have been considered adiabatic,[22,23,25,45] so as to avoid any effects of an imposed horizontal temperature gradient. Bories and Deltour,[44] however, considered a cylindrical porous medium contained in an infinite slab of finite conductivity. The common thermal boundary conditions used for the upper and lower surfaces are to assume they are isothermal. However, Ribando and Torrance[31] also examined the case of uniform heat flux through the lower surface of the porous medium. Also, Riahi[49] examined a porous layer of infinite horizontal extent sandwiched between two semi-infinite volumes of finite conductivity. The volumes were assumed to initially be at steady state conditions just prior to the onset of convection. Theoretical analysis shows that non-isothermal boundary conditions reduce the critical Rayleigh value.[31,49]

Several different flow boundary conditions have been used for the study of a confined porous layer heated from below. The side walls have universally been assumed to be impermeable (no flow boundary conditions). The flow boundary conditions for the horizontal surfaces have been assumed to be either impermeable or permeable. The most common boundary condition sets have been either both surfaces assumed impermeable,[10,22,23,25] or the lower surface assumed impermeable and the upper permeable (reduced Ra_c).[14,40,45]

2.3 Steam/Water Natural Convection in a Porous Medium

Liquid which saturates a porous medium heated from below will begin to boil when the temperature of the lower surface exceeds the liquid boiling point. Boiling in moderately permeable porous media creates an almost isothermal two phase (vapour/liquid) zone in which the vapour rises as bubbles from the bottom surface to the top of the two phase zone, where it condenses and flows downwards as a liquid.[18] The overlying liquid zone position is maintained by the condensation of penetrating vapour fingers as they enter the colder liquid zone.[50]

Sondergeld and Turcotte, in 1977,[16] conducted an experimental study of the boiling of water in a rectangular sand pack heated from below. They found a convective overlying water zone. They modelled the two phase zone as one-dimensional, and attempted to explain the overlying water zone convection using a flawed buoyancy argument. They conducted a later visualization study[19] which confirmed the overlying water zone convection, and that it was triggered by the onset of boiling. Bau and Torrance, in 1981,[18] experimentally studied the boiling of water in a cylindrical porous medium. They found no evidence of overlying water zone convection until a later study[17] where convection occurred prior to boiling. They modelled the two phase zone in a similar manner to Sondergeld and Turcotte. Udell, in 1985,[15] published a one dimensional theoretical analysis of the two phase zone that more accurately modelled the fluid behaviour. He extended the simple relative permeability models and saturation relationships previously used. Schubert and Straus, in 1977,[20] published a study of the convection of a steam/water mixture in a geothermal system. They found the steam/water system to convect more readily than the water only system.

2.4 Two Immiscible Fluids Natural Convection in a Porous Medium

Natural convection of two immiscible liquids (oil/water) has been studied only as two separate layers not contained in a porous medium.[21] The natural convection of two immiscible liquids (i.e. oil/water) distributed throughout a porous medium has not been previously reported. The natural convection of three or more fluid phases (oil/water/gas) in porous media has also not been documented.

2.5 Literature Survey Summary

The documentation of the natural convection of a single fluid saturating a confined porous medium heated from below is quite complete. Previous treatments of variable viscosity effects have been laborious in application to analysing experimental results. Published treatments of the natural convection of steam/water systems in moderately permeable porous media heated from below have concentrated primarily on the two phase zone and descriptions of the overlying water zone have not been adequate to predict its behaviour. There has been no published work on the natural convection of a mixture of two immiscible liquids in a porous medium.

2.6 Studies Performed in this Work

This study examined the natural convection of a single fluid, water, in a confined cylindrical porous medium heated from below as an experimental baseline for following experiments. Additionally, a new treatment of the variable viscosity effect allowed the development of a model for the rapid prediction of single fluid natural convection for different fluids and different temperatures.

The natural convection of steam/water systems in a porous medium heated from below was then examined. Relationships, based on interface stability, were used to form models used to predict the heat transfer mode and Nusselt number of the overlying water zone were developed.

Finally, the onset of natural convection of mixtures of two immiscible liquids in a confined porous medium heated from below was experimentally determined. Relative permeability extensions to the single fluid model developed during the single fluid portion of this study were found to adequately describe the behaviour of the system.

CHAPTER 3. EXPERIMENTAL APPARATUS

The experiments were performed in a vertically standing cylindrical heat transfer cell. A cross-section of the shell is shown in Figure 3.1. The sand pack was sandwiched between two calibrated heat flux meters, which were also sandwiched between two, constant temperature, horizontal surfaces. Provisions were made to apply a controlled overburden pressure to the sample, and to control the sample's pore fluid pressure. Most oils convect less easily than water and in order for them to convect the sand pack must be taller or the imposed temperature difference greater than that required for water convection. Hence, the cell was made as tall as possible and the cell was designed to operate at temperatures of up to 190°C. The high temperature required that the cell be built to withstand pore fluid pressures of up to 2 MPa, as the pore fluids were to be maintained as liquids in many experiments. Overburden pressures of 100 to 200 kPa above the pore fluid pressures were applied both to ensure particle to particle contact (critical to consistent thermal conduction behaviour) and to avoid bed fluidization. In the following, a brief description of the cell is given. A complete description of the cell and operating procedures can be found in Appendix A. The process used to calibrate the heat transfer cell is described in Appendix B.

The cell wall has an inner diameter of 0.45 m, and was made of an asbestos-cement water pipe internally clad with 26 gauge 316 stainless steel lined with Dow-Corning 730 fluoro-silicone rubber. The asbestos-cement water pipe was the largest that could be readily obtained with an adequate pressure rating. The optimum height for a given pack diameter occurs when the convection enhancement of greater height and the convection suppression of the resulting smaller aspect ratio are balanced. The optimum height for the convection of water in a 0.45 m diameter sand pack was calculated, using the equations presented later in this work, as 0.67 m, and the sand pack height was fixed at that value.

Both the top and bottom surfaces of the cell wall were seated against gaskets located in upper and lower heating/cooling heads. The upper and lower heating/cooling heads were clamped between flanges by studs. The studs were tightened with a hydraulic stud tensioner.

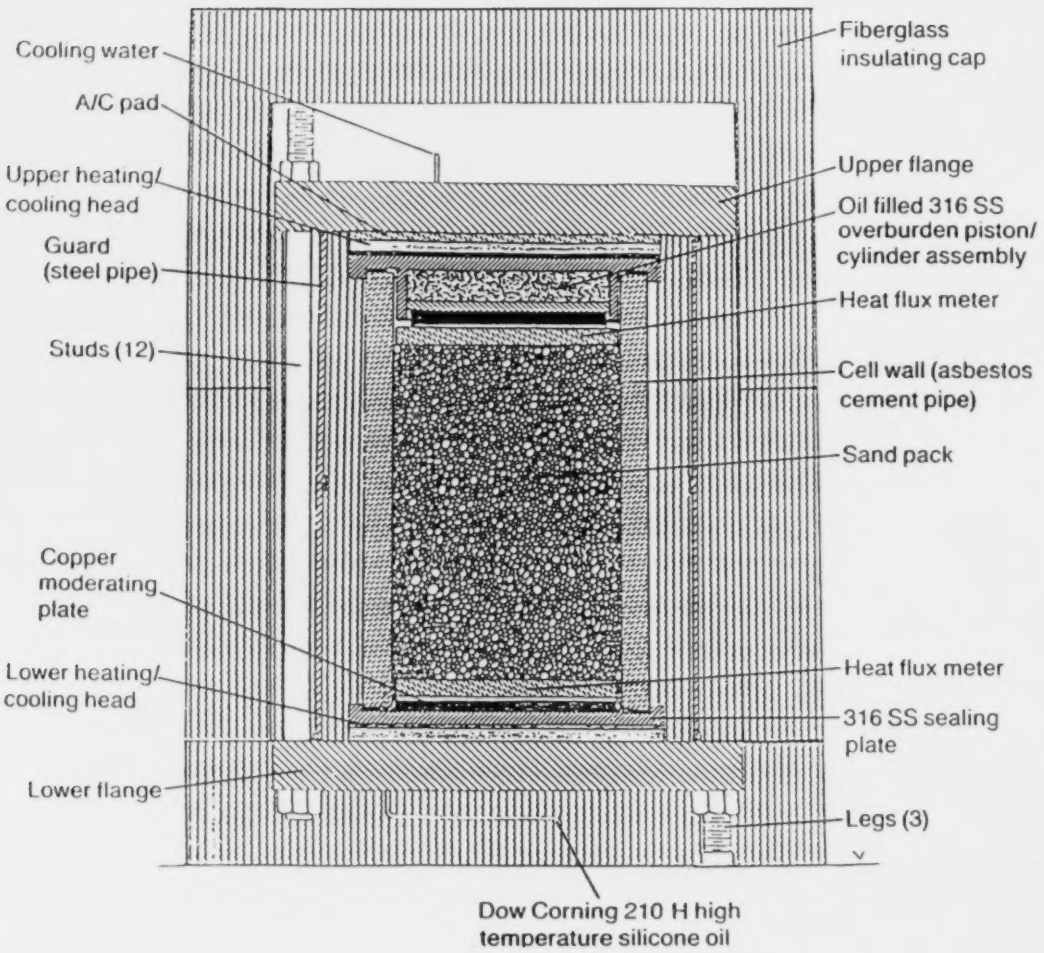

Figure 3.1 Heat Transfer Cell Diagram

The upper heating/cooling head contained a piston assembly that applied overburden pressure. Both the upper and lower heating/cooling heads had their temperatures set and maintained by computer controlled electric heaters. Additional temperature control of the heating/cooling heads was obtained by flowing cooling water through the upper heating/cooling head and hot Dow-Corning 210H silicone oil from a Haake N3-B circulator through the lower heating/cooling head. The upper and lower heating/cooling heads also contained six injection/extraction ports each, through which pore fluids were pumped to saturate the sand pack and to control the pore fluid pressure when the cell was operating.

A heat flux meter separated the bottom of the sand pack from the constant temperature lower heating/cooling head. Another heat flux meter separated the top of the sand pack from the constant temperature upper heating/cooling head. The heat flux meters were discs made of Colorceran, a robust, inorganic mixture of calcium, aluminum, silicate and asbestos fibres. The thermal conductivity of this material was measured by both Tempest Engineering and the Institute for Research in Construction, National Research Council of Canada. The results of the measurements were obtained too late to be used in the calibration of the heat flux meters and are not reported in this work. Sand pack temperatures were monitored by layers of thermocouple probes distributed throughout the pack. There were four layers of probes in the initial experiments and six layers in the later experiments.

The cell wall was surrounded by a 0.09 m thick layer of mineral wool insulation and then a 7.6 mm wall thickness steel pipe that functioned as a containment system and as a thermal guard. The guard pipe had one cooler attached to its upper outer surface and three temperature controlled electric heaters fastened to its outer surface, at the top, the middle, and the bottom. Guard heaters were controlled by stand alone controllers such that there existed no more than a 5°C temperature difference across the insulation between the cell wall and guard. The outer perimeter of the complete cell assembly was enclosed in a three piece fibreglass insulation assembly. The minimum thickness of this assembly was 0.15 m.

The complicated structure of the cell wall was developed to overcome severe leakage problems. Considerable gasket seating surface damage to the ends of the asbestos-cement pipe resulting from the high gasket seating stresses required the use of stainless steel rings as gasket seating surfaces. The stainless steel cladding was welded to the rings to seal them. The cladding buckled against the asbestos-cement pipe under the gasket

seating load and caused small cracks to develop in the many welds in the cladding. The small cracks were sealed by applying the fluoro-silicone rubber lining. This system stopped the leaks through the cell wall, but extensive gasket leaking persisted until a sophisticated multi-piece system was utilized. The sophisticated gasketing system included Flexitallic gaskets, Loctite 515 Gasket Eliminator sealant, Nomex sand control collars and Teflon collapsible O-rings.

Primary control and data acquisition were handled with a Hewlett-Packard 3054A data acquisition and control system. The system was used to record thermocouple temperatures and pressures, and to control the primary heaters in the heating/cooling heads. The system was designed to be operator-independent, as steady state for each data point usually took ten to fourteen days of continuous uninterrupted operation to achieve. The long duration of each experiment made the reliability of the apparatus and control system critical, and did not allow for the use of manual control of the critical operating parameters.

The initial series of experiments showed the rates of heat transfer measured by the upper heat flux meter were inaccurate, due to the effect of the overburden assembly. The overburden assembly conducted heat through its thick cylinder walls of stainless steel and through its cylinder fluid. The parallel heat flow combination disrupted the heat flow path through the upper heat flux meter. The use of the upper heat flux meter was then discontinued and the thermocouple points freed up were utilized by replacing the four layers of probes initially used to measure sand pack temperatures with six layers of probes. An analysis of the experimental errors was done during the development of the heat transfer cell[4] ,and the experimental uncertainty was found to be ± 7.2 % for a conductive state in the 0.67 m tall heat transfer cell.

CHAPTER 4. NATURAL CONVECTION OF A SINGLE FLUID IN POROUS MEDIA

Fluid saturating a porous medium heated from below will be cold and dense at the top and hot and less dense at the bottom. This potentially unstable arrangement is tempered both by the fluid viscosity resisting fluid motion and by thermal diffusivity damping thermal disturbances. Onset of convection will not occur until the destabilizing effect of the temperature gradient overcomes these stabilizing factors. Fluid in a confined porous medium heated from below has a certain mode of movement that is the least stable. The aspect ratio (radius/height) of the heat transfer cell used in these experiments resulted in the least stable mode at the onset of convection incorporating flow up one side of the cell and down the other, as shown as mode 1 in Figure 4.1. As the applied temperature gradient is steepened fluid motion occurs in other modes. For example, the third mode of motion in a cell of the present configuration is flow up the centre and down the sides, as shown as mode three in Figure 4.1. The least stable mode of motion can be predicted by modelling the system, or be determined by analyzing the temperature contours from an experiment.

Onset of convection occurs at a critical value of the Rayleigh number (Ra_c). Heat transfer is by conduction alone when Ra is less than Ra_c and by conduction and convection for values above Ra_c. The Rayleigh number (Ra) is a dimensionless group that is the product of the Grashof and Prandtl numbers. The Grashof number represents the ratio between buoyancy and viscous forces, and the Prandtl number represents the ratio of the fluid's momentum diffusivity (viscosity) to its thermal diffusivity. The Rayleigh number commonly used to describe natural convection of a lone fluid was modified by Lapwood[7] to form the Rayleigh number used in the study of natural convection in porous media. The modifications take account of the differences in both the equations of motion and, hence, inertial forces, and the thermal diffusivity. Unfortunately, the porous media Rayleigh number does not represent the natural convection of a single fluid in a porous medium as well as the lone fluid Rayleigh number represents lone fluid natural convection. Much larger temperature differences are required to initiate the natural convection of viscous liquids in a porous medium heated from below than are required for a fluid not confined in a porous medium. The larger temperature differences result in larger variations in viscosity and correspondingly larger variations in the critical Rayleigh number values.[10]

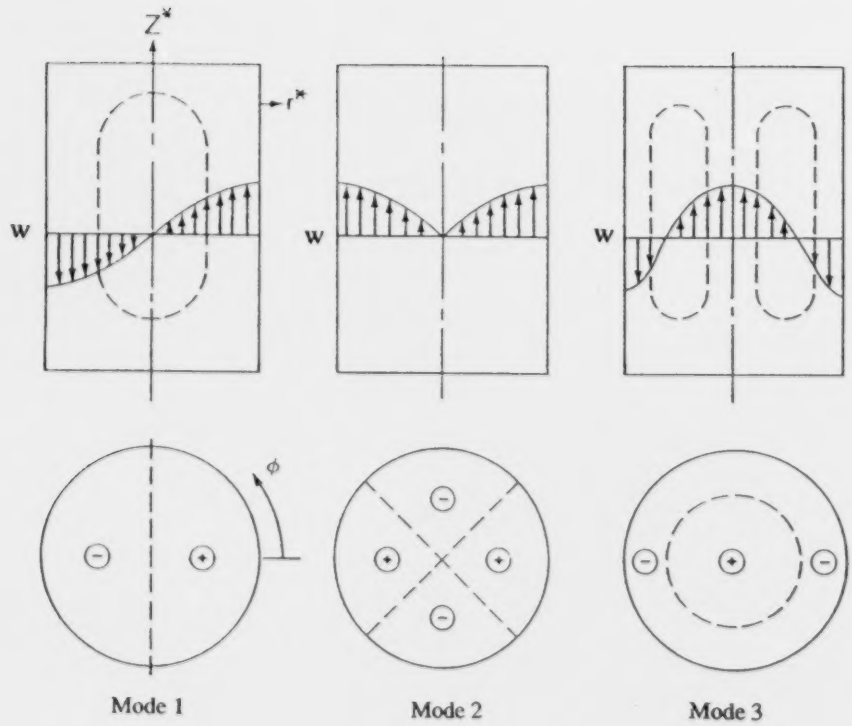

Figure 4.1 Convective Mode Planforms in a Cylindrical Porous Medium Heated from Below

The Nusselt number (Nu) is a dimensionless group representing the ratio of the actual heat transfer rate to the rate if only conduction were occurring. Therefore, for Ra values below Ra_c, Nu equals one, and for Ra values above Ra_c, Nu is greater than one.

4.1 Single Fluid Model

Natural convection of a single fluid in a cylindrical porous medium heated from below can best be modelled in two parts. The first part is the onset of convection, the point at which large scale fluid motion begins. The second part is the rate of heat transfer after the onset of convection, which varies with the mass flow rate of the convective motion.

4.1.1 Onset of Convection

Zebib, in 1978,[23] published a theoretical model of the natural convection of water in a cylindrical porous medium heated from below. His work was used in this study as the basis for the analysis of the onset of convection of a single fluid in a porous medium. Unfortunately, direct use of Zebib's model for analysis of the experiments conducted in this study would be very time consuming. This is because Zebib's treatment of the effects of viscosity variation require the complete numerical solution of his model for every bottom and top temperature combination considered in the iterative procedure used to predict Ra_c for each actual experiment. Additionally, the application of Zebib's method to a fluid other than water would require the insertion of the fluid's viscosity-temperature relationship into the model. Both of these difficulties with the actual application of his work to this study forced the development of a more "user-friendly" model.

Thus, in this study, a model of the natural convection of a single fluid in a porous medium was developed that included a novel viscosity-temperature relationship applicable to all the liquids used. The relationship was an exponential approximation of the viscosity variation, based on the ratio between the fluid viscosity at the top temperature and the fluid viscosity at the bottom temperature. The viscosity variation relationship developed was:

$$\mu = \mu_0 \left(\frac{\mu_0}{\mu_1} \right)^{-\left[\frac{T - T_0}{T_1 - T_0} \right]} \qquad 4.1$$

where:

μ = fluid viscosity at intermediate temperature [Pa s]
μ_0 = fluid viscosity at upper (cold) temperature [Pa s]
μ_1 = fluid viscosity at lower (hot) temperature [Pa s]
T = intermediate temperature [°C, K]
T_0 = upper (cold) temperature [°C, K]
T_1 = lower (hot) temperature [°C, K]

This new viscosity variation relationship allowed the modelling of the onset of natural convection for a given viscosity ratio of any liquid. The relationship developed in this study approximated the actual viscosity much more closely than other possible simplifying assumptions, such as: constant viscosity at the cold temperature value, constant viscosity at the average temperature value, and linear viscosity variation with temperature. The relationship, however, does not approximate the actual fluid viscosities nearly as well as the empirical relationship used by Zebib.[23] The viscosity predictions of the various simplifying assumptions and the actual fluid viscosities for water between 25°C and 130°C are plotted in Figure 4.2. Actual fluid values are plotted, but they can be regarded as the predicted results of the empirical relationship used by Zebib. Critical Rayleigh value predictions based on the constant viscosity assumptions can be in great error. A comparison between a Ra_c prediction based on the new viscosity variation assumption and one based on Zebib's work, presented later in this study, showed good agreement.

The complete derivation of the model for predicting the onset of convection of a single fluid in a porous medium heated from below is presented in Appendix C. The initial assumptions used to derive the model are that Darcy's Law of fluid motion holds, the Boussinesq density approximation[25] is valid, the viscosity varies as described earlier, and all other fluid and solid properties are constant. The Boussinesq approximation assumed the effects of fluid density variation with temperature were only felt in the buoyancy term. The cylindrical porous medium is assumed to occupy the region bounded by: $-L \leq z \leq 0$; $0 \leq r \leq R$; and $0 \leq \phi \leq 2\pi$, as illustrated in Figure 4.3.

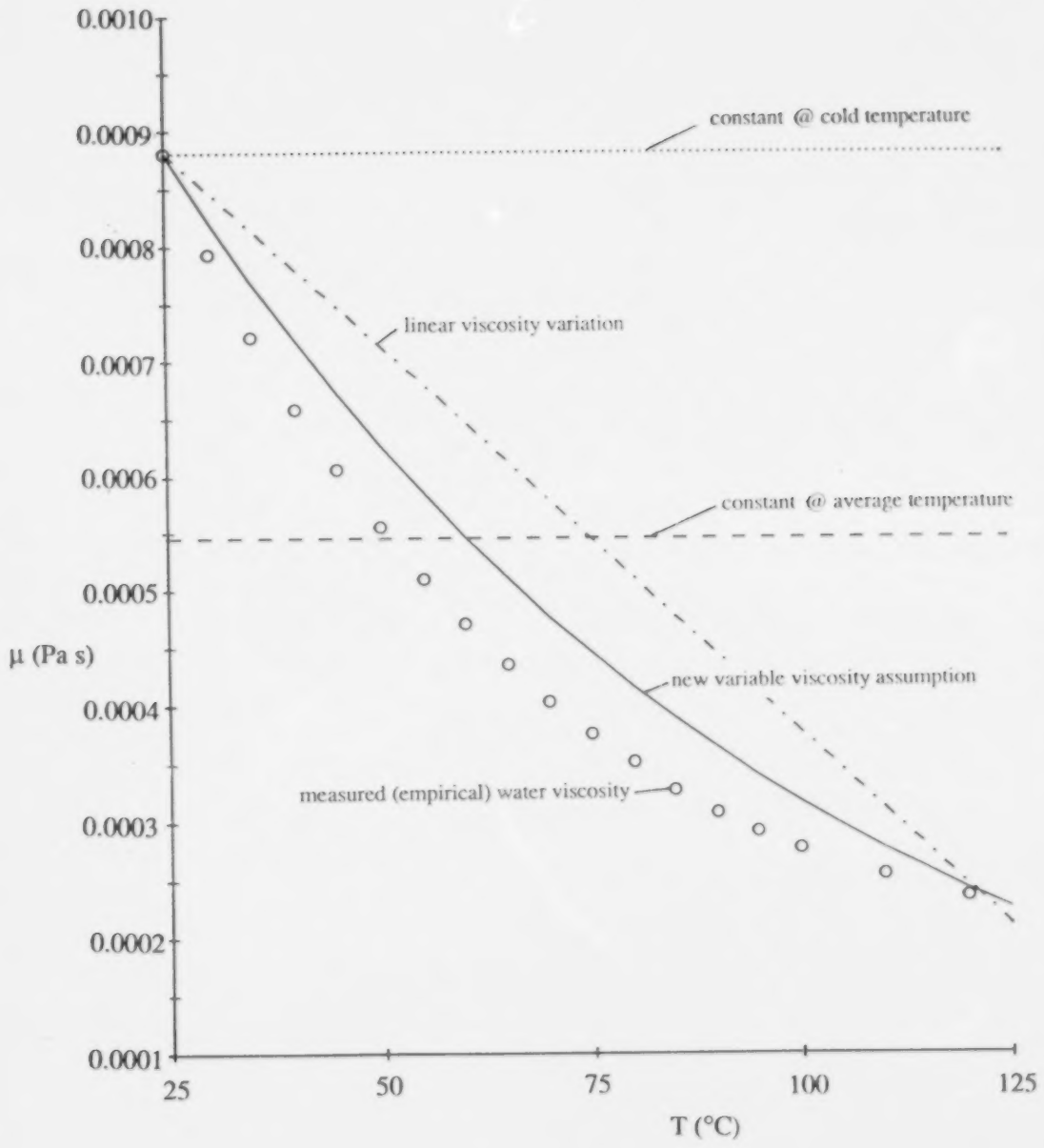

Figure 4.2 Variable Viscosity Predictions

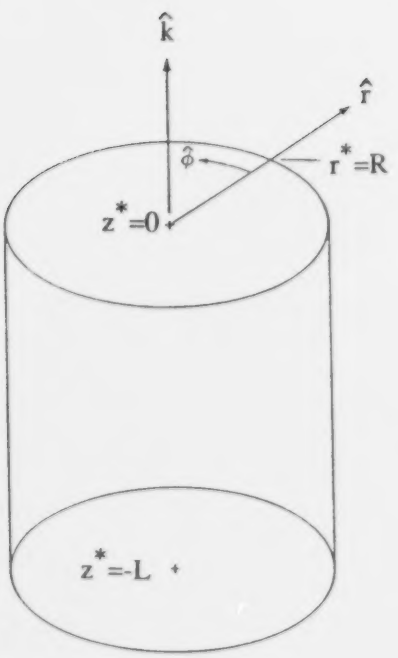

Figure 4.3 Sand Pack Layout

The dimensional conservation equations used to describe the low velocity motion of a single fluid in a porous medium and heat transfer in the medium are:

Conservation of mass:

$$\frac{\partial \rho^*}{\partial t^*} + \nabla^* \cdot (\rho \tilde{u}^*) = 0 \qquad 4.2$$

Conservation of momentum:

$$\frac{\rho^*}{\phi_p} \frac{\partial \tilde{u}_b^*}{\partial t^*} = \tilde{F}^* - \nabla P^* - \frac{\mu}{k} \tilde{u}_b^* \qquad 4.3$$

Conservation of energy:

$$(\rho C_p)_m \frac{\partial T}{\partial t^*} + \phi (\rho C_p)_f \tilde{u}^* \cdot \nabla^* T = \lambda_m \nabla^{*2} T \qquad 4.4$$

Substituting in the viscosity-temperature relationship, normalizing, simplifying, linearizing and examining only the vertical component yield the following dimensionless equation:

$$0 = Ra \nabla_1^2 \theta \mu_R^{\theta - z} + \ln \mu_R^{\theta - z} \nabla^2 \left(\frac{\partial \theta}{\partial z} \right) + \nabla^4 \theta \qquad 4.5$$

where:

Ra = Rayleigh number = $[g_a k \beta (T_{bot} - T_{top}) L \rho^2 C_p] / (\mu \lambda_m)$

$\nabla_1^2 ( ) = \nabla^2 ( ) - \partial^2 ( ) / \partial z^2$

θ = perturbed temperature $(((T - T_0) + (T_1 - T_0)(z^* / L))/(T_1 - T_0))$

μ_R = viscosity ratio (μ_{top} / μ_{bot})

z = dimensionless height (z^* / L)

Modelling of the test pack was done using two sets of boundary conditions. The first boundary condition set used was the one[7] commonly used for the convection of a single fluid in a confined porous medium heated from below; the sidewalls were assumed to be adiabatic and impermeable, and the upper and lower surfaces were assumed to be isothermal and impermeable. Additionally, an attempt to model more accurately the effect of the heat flux meters was made by developing a unique, second set of boundary conditions. The top and bottom boundaries of the sand pack were assumed to be separated from the isothermal, impermeable surfaces by an impermeable layer of finite thermal conductivity. The linearized dimensionless boundary conditions are:

Boundary Conditions: Set 1; Isothermal:

$$\begin{aligned} &@\ z = 0: \quad \theta = 0\ ;\ \nabla^2\theta = 0 \\ &@\ z = -1: \quad \theta = 0\ ;\ \nabla^2\theta = 0 \\ &@\ r = s: \quad \partial\theta/\partial r = 0\ ;\ \partial\nabla^2\theta/\partial r = 0 \end{aligned} \qquad 4.6$$

Boundary Conditions: Set 2; Finite Conductive Layer:

$$\begin{aligned} &@\ z = 0: \quad \partial\theta/\partial z = -\alpha\theta;\ \nabla^2\theta = 0 \\ &@\ z = -1: \quad \partial\theta/\partial z = \alpha\theta;\ \nabla^2\theta = 0 \\ &@\ r = s: \quad \partial\theta/\partial r = 0\ ;\ \partial\nabla^2\theta/\partial r = 0 \end{aligned} \qquad 4.7$$

The next step was to separate variables using:

$$\theta = g(z)\, J_m(\lambda r)\cos(m\phi) \qquad 4.8$$

where:

J_m = Bessel function of first kind
r = dimensionless radius (r^*/L)
λ = eigenvalue
m = mode of Bessel function
ϕ = angle
g = height function
z = dimensionless height (z^*/L)
s = dimensionless outer radius (R/L)
α = $(\lambda_L / L_L) / (\lambda_m / L)$

The simplified equation describing the fluid motion then becomes:

$$g^{iv} - z \ln\mu_R g^{iii} - 2\lambda^2 g^{ii} + z\lambda^2 \ln\mu_R g^{i} + [\lambda^4 - ((\lambda^2 Ra)/\mu_R{}^z)] g = 0 \qquad 4.9$$

and the boundary conditions become:

Set 1; Isothermal:

$$\begin{aligned} &@\ z = 0: \quad g(0) = 0;\ g^{ii}(0) - \lambda^2 g(0) = 0 \\ &@\ z = -1: \quad g(-1) = 0;\ g^{ii}(-1) - \lambda^2 g(-1) = 0 \\ &@\ r = s: \quad J_m{}^{i}(\lambda s) = 0 \end{aligned} \qquad 4.10$$

Set 2; Finite Conductive Layer:

$$\begin{aligned} &@\ z = 0: \quad g^{i}(0) = -\alpha g(0);\ g^{ii}(0) - \lambda^2 g(0) = 0 \\ &@\ z = -1: \quad g^{i}(-1) = \alpha g(-1);\ g^{ii}(-1) - \lambda^2 g(-1) = 0 \\ &@\ r = s: \quad J_m{}^{i}(\lambda s) = 0 \end{aligned} \qquad 4.11$$

where s = aspect ratio of porous medium = R/L .

The planar cylindrical boundary condition equations @ r = s are Bessel function roots and have been tabulated in many handbooks.[51] The fourth order linear ordinary differential equation in g(z) does not have an analytical solution and must be solved numerically as a boundary value problem with conditions as at z = 0 and z = -1. Finite difference methods based on separation of the fourth order problem into two coupled second order equations were attempted but were unstable and did not work. The technique successfully used for this boundary value problem is a modification of the shooting technique developed by Kalaba[52] to solve linear boundary value problems. His method was to solve a series of unique initial value problems and linearly combine (superimpose) them to give the correct boundary values and, hence, the solution. The linear combination of solutions is valid for linear equations only. The four initial value problems for the present work were solved by a 4th order, 100 step Runge-Kutta technique. The four solutions were then combined to give the proper boundary values, if possible. The critical Rayleigh value was the lowest non-zero Rayleigh value that allowed a solution. The critical Rayleigh value was found by treating it as the lowest root of the linear superposition process. This was done numerically with a Newton-Raphson technique. This method is more clearly illustrated below:

Four initial value problems ($0 \geq z \geq -1$):

a) $g(0) = 1;\ g^{i}(0) = g^{ii}(0) = g^{iii}(0) = 0$

b) $g(0) = 0;\ g^{i}(0) = 1;\ g^{ii}(0) = g^{iii}(0) = 0$

c) $g(0) = g^{i}(0) = 0;\ g^{ii}(0) = 1;\ g^{iii}(0) = 0$

d) $g(0) = g^{i}(0) = g^{ii}(0) = 0;\ g^{iii}(0) = 1$

4.12

The four initial value problems are linearly combined to satisfy the z = 0 boundary conditions and the final solution values (Runge-Kutta) at z = -1 are combined with the same relationship. The combined final solution values are compared with the boundary conditions at z = -1 and the input value of Ra modified (Newton-Raphson) until a match occurs. Critical Rayleigh values for viscosity ratios from one to ten and for the first seventeen modes of convective motion were found for the isothermal boundary condition case and are presented in Appendix D. It should be noted that the tabulated values are limited to a cell of 0.343 aspect ratio with impermeable, isothermal upper and lower surfaces. Interpolating between the tabulated values allowed the rapid prediction of the critical Rayleigh value. This was done by estimating the Ra_c, calculating the lower (hot) surface temperature, finding the corresponding hot fluid viscosity, calculating the viscosity ratio, and finding the new predicted Ra_c. This process was iterated until the Ra_c value stabilized at the final predicted value of Ra_c.

The new viscosity variation assumption was verified by comparing the new method's results with Zebib's[23] results for a water saturated cylindrical porous medium of 0.343 aspect ratio with a 125°C bottom temperature and a 25°C top temperature. Zebib's method was used to predict a critical Rayleigh value of 23.2. The evaluation of Zebib's method was done using the graphical information from his papers,[23,32] as he suggested, and the determination accuracy was probably about ± 0.5. The new model predicted a critical value of 24.2. The small difference, 4.3%, clearly showed the new method's validity. Both methods predicted a critical Rayleigh value of 52 for the constant viscosity case. The new viscosity variation relationship reliably predicted Ra_c for a large viscosity variation that reduced Ra_c to 45% of its constant viscosity value. This performance is adequate for the experimental conditions encountered in this study. Details of the calculations for the comparison are shown in Appendix E.

4.1.2 Heat Transfer Rate

When fluid velocity levels are high, models based upon Darcy's law do not accurately predict heat transfer rates and models utilizing extensions to Darcy's law[26,27] are used. The low permeability sand packs used in this study allow the use of models based on Darcy's law. A flow model by Bau[14] was used in the present study to find the amplitude of fluid motion and hence heat transfer rate by using power integral techniques to extend the linearized equations previously used for finding the onset of convection. This method is applicable for Rayleigh numbers of up to approximately five times the critical Rayleigh value,[37,40] which is well above the maximum Rayleigh number measured in the present study. No extensions of the theory nor development of new models was done in this section.

The constant viscosity power integral extension technique of Bau[14] was applied to the fluid velocity profiles resulting from the variable viscosity, onset of convection model. The application of this technique revealed that the isothermal boundary conditions model and the finite thermal conductivity layer boundary conditions model resulted in the same set of equations, presented below:

$$Nu = 1.0 + (1.0 - \{Ra_c / Ra\}) [I_1^2 / (I_2 - I_1^2)]$$

where:

$$I_1 = \int g \ (g^{ii} - \lambda^2 g) \ dz \quad \text{limits of integration: -1 to 0}$$

$$I_2 = \int g^2 \ (g^{ii} - \lambda^2 g)^2 \ dz \quad \text{limits of integration: -1 to 0}$$

I_1 and I_2 are numerically integrated in a trapezoidal scheme from the output of the linear stability analysis for both sets of boundary conditions. The final Nusselt number equation is different for the two boundary conditions as the integrals are different for each set of boundary conditions. Complete details of the derivation of the heat transfer rate equations are shown in Appendix F.

4.2 Single Fluid Experiments

This study utilized a 40-70 Unimin (quartz) sand pack of 26.5 Darcy (26.5×10^{-12} m^2) permeability and 32.4% porosity. The sand pack porosity was calculated based on the mass of the sand pack, from a mass balance during packing, and the known volume of the heat transfer cell. The sand pack permeability was calculated from the results of the permeability and porosity testing of 25.4 mm diameter, 254 mm long sample cores taken from sand packs made with the same sand, the same packing techniques, and the same cell walls. The dry sand was packed into the cell using a particle distributor, as described by Wygal.[53] The sand pack was then saturated to 99.25% with de-ionized water. Saturation was checked by injecting a known volume of water and measuring the pressure rise.

Five experiments, denoted W-S #1-#5, were done. They were done to supply enough data to test adequately the models that were used in the analysis of further experiments. The first two experiments were done with the sand pack heated from the top, in which the temperature gradient stabilizes the fluid and the Rayleigh number is negative. These experiments were certain not to have convection occurring and were conducted to determine the thermal conductivity of the matrix. The next two experiments were done with the sand pack heated from the bottom which yielded positive, but subcritical Rayleigh numbers. A fifth experiment was done with the sand pack heated from the bottom and yielded a positive and supercritical Rayleigh number. For the first four experiments the Nusselt number was 1.0, while for the last it was 1.76. Isotherms that were flat for the first four experiments became steeply inclined at angles up to approximately 45° to the horizontal for the fifth experiment, as shown in Figure 4.4. The inclined isotherms appeared three days after the start of the experiment, long before steady state was reached. The early appearance of the inclined isotherms was used as a qualitative indicator of convection, but steady state Nusselt numbers are more reliable and informative. The detailed analysis of the experimental work is presented in Appendix G. Non-dimensional results for the five experiments are shown in Figure 4.5. These results indicate that the actual critical Rayleigh number for this system must fall between 21.8 and 27.0.

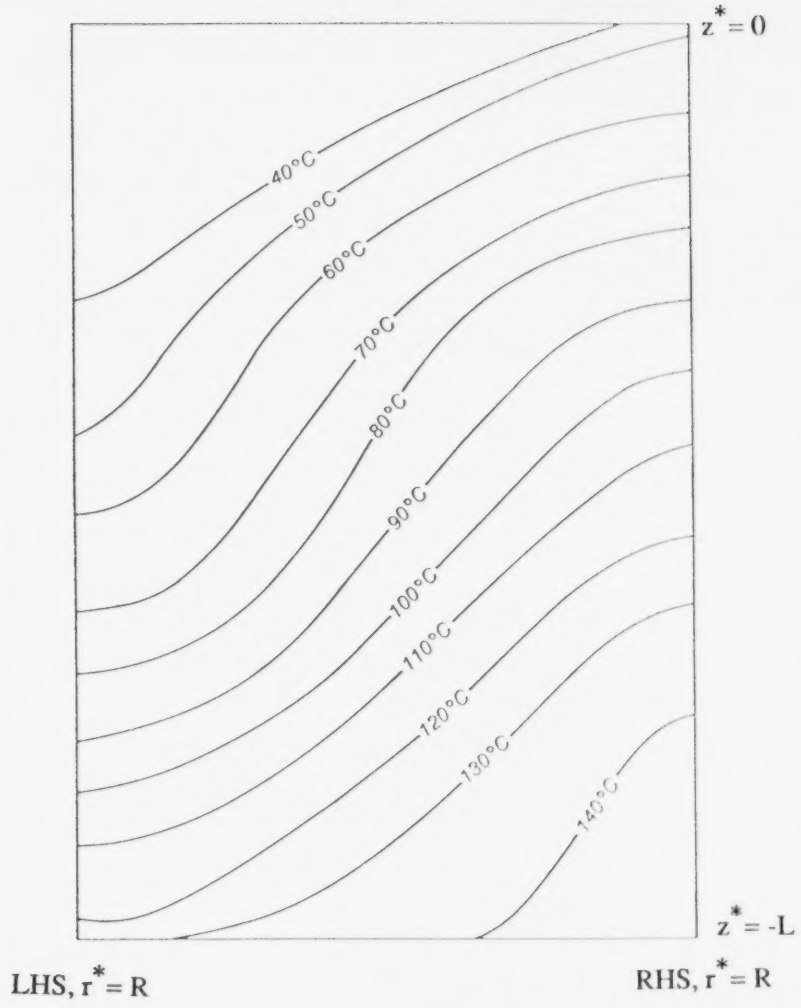

Figure 4.4 Convective Isotherms (Elevation), Water in Sand, Run W-S #5

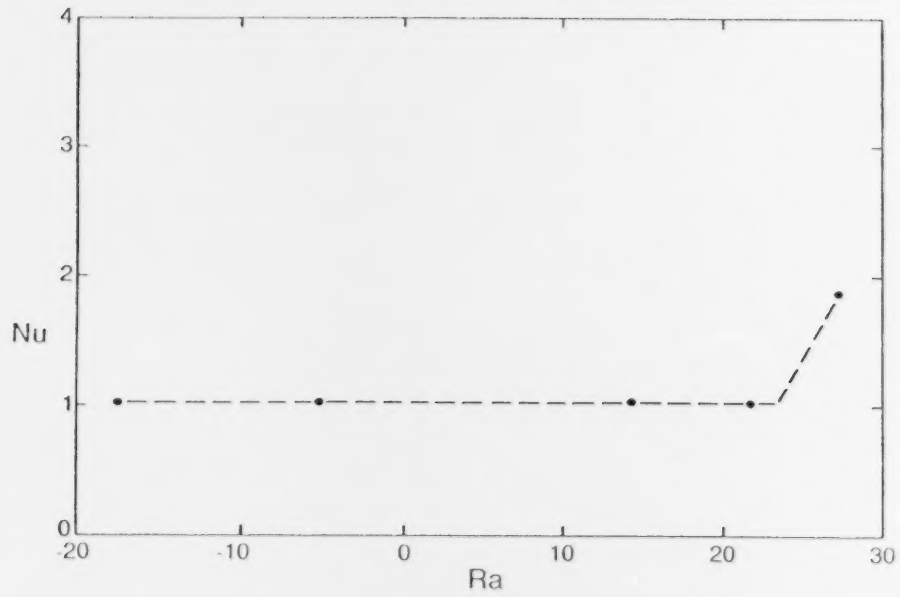

Figure 4.5 Measured Heat Transfer Rates, Water in Sand, Runs W-S #1-#5

4.3 Single Fluid: Comparison of Results

4.3.1 Onset of Convection

The onset of convection of water in the sand pack contained in the heat transfer cell was predicted based on three separate cases. All three cases shared the assumptions that the cell walls were adiabatic and impermeable, the top and bottom confining surfaces were impermeable, all properties, excepting density and viscosity, were constant, and the Boussinesq approximation[25] was invoked. The first case assumed the top and bottom surfaces were isothermal and the water viscosity to be constant; the critical Rayleigh value was predicted to be 52.08. The second case assumed the top and bottom surfaces were isothermal, but the water viscosity to be variable, which resulted in a critical Rayleigh value prediction of 24.78. The third case assumed both the top and bottom boundary had a layer of finite thermal conductivity between it and an isothermal surface and a variable water viscosity. The third case, with its novel boundary conditions used to more accurately model the heat flux meters, resulted in a critical Rayleigh prediction of 22.27. For details on these calculations see Appendix C.

The experiments determined that the actual critical Rayleigh number must fall between 21.8 and 27.0. The prediction based on the first, constant viscosity case is in complete disagreement. Both the second and third cases predicted a critical Rayleigh value within the measured range. Results of the second and third cases are plotted along with the experimental results in Figure 4.6. With only one experimental point it is impossible to differentiate truly between case 2 and case 3.

4.3.2 Heat Transfer Rate

Both the isothermal boundary condition (case 2) and the finite conductivity layer boundary condition (case 3) model results were used to predict heat transfer rates. Results of these two predictions are plotted along with the experimental results in Figure 4.7. Both predictions apparently under-predict the actual results, but with only one experimental data point, clear determination of this was not possible. The finite conductivity layer prediction (heat flux meter effect) appears to be the more accurate, but not sufficiently more to be worth using. Models and calculations are presented, in detail, in Appendix G.

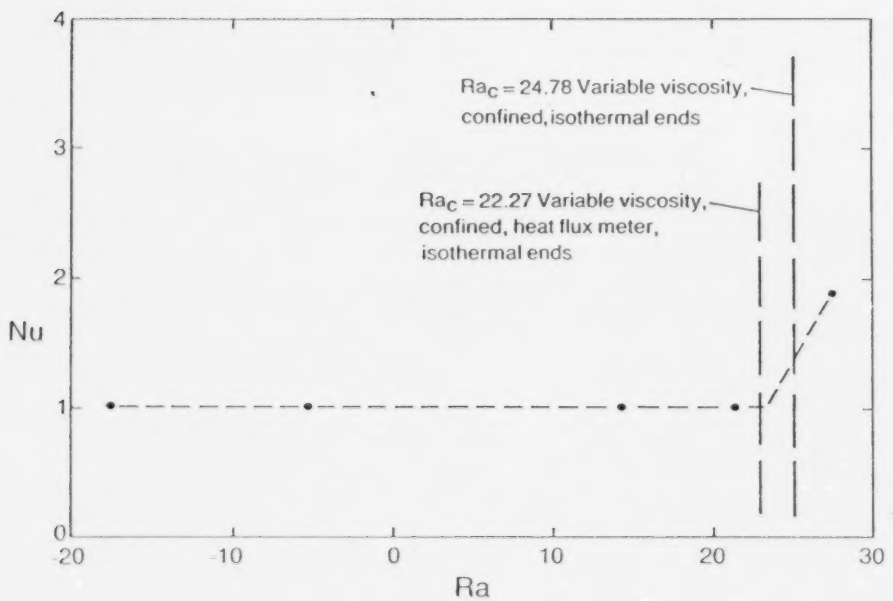

Figure 4.6 Comparison of Predicted and Measured Critical Rayleigh Values, Water in Sand, Runs W-S #1-#5

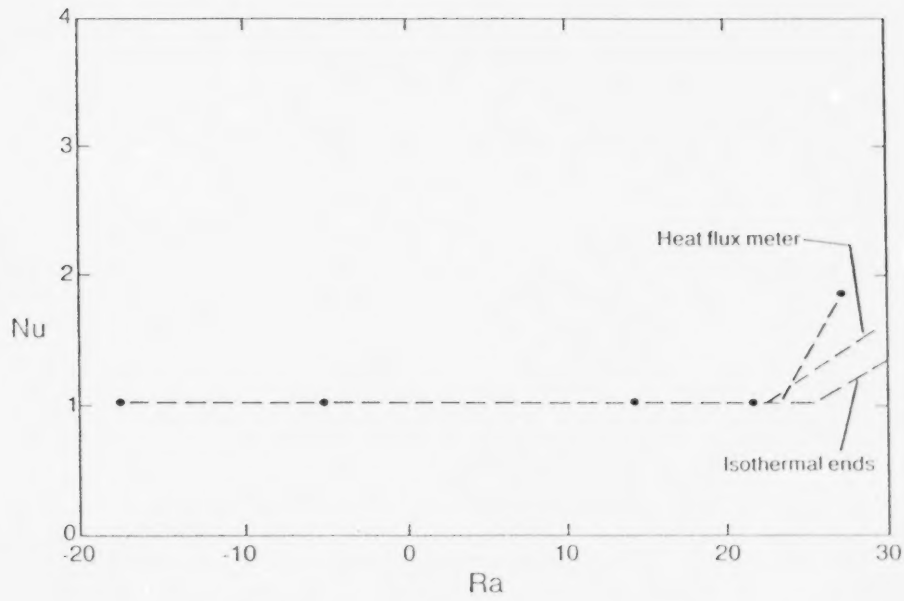

Figure 4.7 Comparison of Predicted and Measured Heat Transfer Rates, Water in Sand, Runs W-S #1-#5

CHAPTER 5. NATURAL CONVECTION OF LIQUID/CONDENSIBLE VAPOUR

A liquid which saturates a porous medium heated from below begins to boil when the temperature of the lower surface exceeds the liquid boiling point. Boiling in the moderately permeable porous media predominantly considered in this study creates an almost isothermal two phase (vapour/liquid) zone in which the vapour rises as bubbles from the bottom surface to the top of the two phase zone, where it condenses and flows downwards as a liquid.[14] A schematic of this system is shown in Figure 5.1. The zone is not perfectly isothermal because of superheating, subcooling and the effects of capillary pressure. Vapour pressure of the fluid is dependent on the capillary pressure, which depends upon the liquid saturation. As the liquid saturation varies throughout the two phase zone the capillary pressure and hence vapour pressure, boiling point, and temperature vary.[15] The capillary pressure of the bubbles can fluidize the porous medium unless an overburden pressure exceeding the capillary pressure is placed on the medium.[14] In the present study an overburden pressure of 100 kPa above pore fluid pressure was applied to the sand pack.

If the heat flux into the lower surface is increased, eventually a point will be reached where the rate of boiling is greater than the rate at which liquid can trickle down to the lower surface. At this point a single phase vapour zone will form at the lower surface. This is referred to as dry out.[16] If the thermal conductivity of the liquid saturated media is such that at the boiling point the heat flux is greater than the dryout heat flux then a two phase zone will not develop, only a lower vapour zone and an upper liquid zone. In high permeability sand packs the two phase and/or dry vapour zones may reach to the upper surface of the sand pack. In low permeability sand packs an overlying liquid zone develops above the two phase zone. The overlying liquid zone position is maintained by the condensation of penetrating vapour fingers as they enter the colder liquid zone.[50] The quantitative permeabilities required for "high" or "low" behaviour depend on the thermal characteristics of the porous medium and saturating fluid.

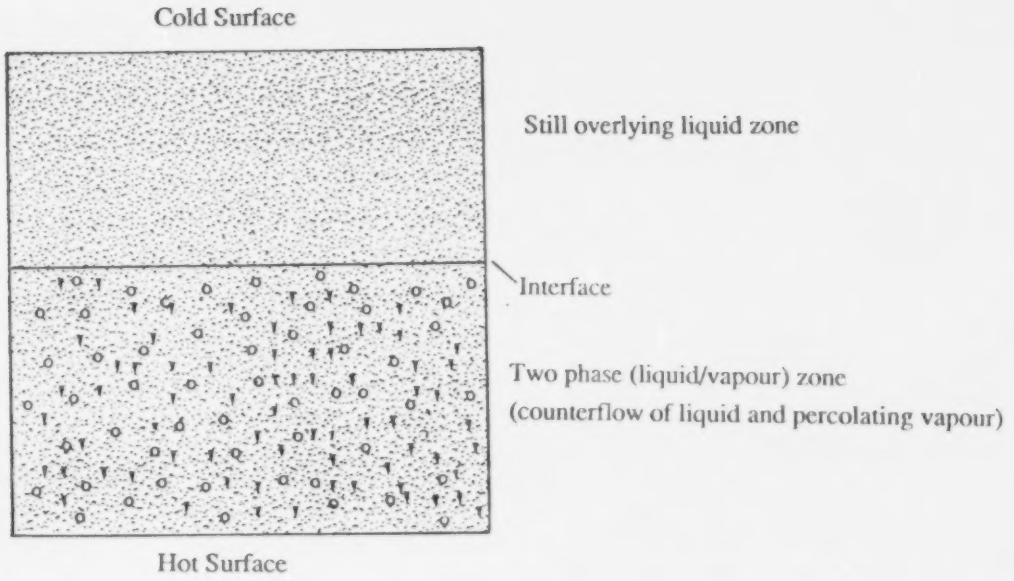

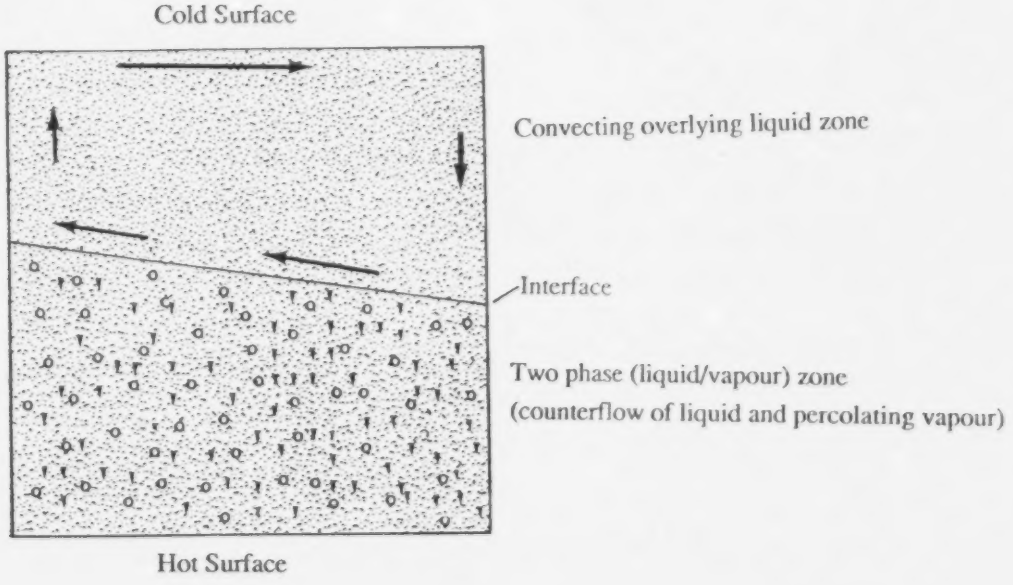

Figure 5.1 Schematic of the Natural Convection of a Liquid/Vapour in a Porous Medium Heated from Below

5.1 Steam/Water Models

Models of water/steam natural convection[14-18] in packs of the correct permeability range for the formation of an overlying water zone have been primarily limited to examining the two phase region, with very cursory treatments of the overlying water zone. Typically, analysis of the two phase zone is accomplished by assuming that the two phase zone is in a state of one-dimensional, counter-current steam-water flow. For a given heat transfer rate, a saturation profile is calculated, which allows relative permeability and, if necessary, capillary pressure to be calculated. These are then used to find the mass flow rate and the pressure gradient.

Both Bau[14,17,18] and Sondergeld and Turcotte[16], in their modelling of the two phase zone, assumed a constant saturation throughout the two phase zone and relative permeabilities that were simply linear functions of saturation. Udell[15] conducted a more thorough analysis in which a non-linear saturation profile and relative permeabilities that were cubic functions of the net saturation were assumed. Udell obtained the net saturation by subtracting the irreducible water saturation from the actual saturation. The saturation profile was determined by maximizing the heat transfer rate through the two phase zone. Both Udell and Bau assumed that the overlying water zone was in strictly conductive heat transfer mode, and on that assumption calculated the water zone thickness and hence the two phase zone thickness and the overall Nusselt number. The primary sources of error of these two methods are an error in counter-current flow liquid/vapour relative permeability, and an error in the assumption of a strictly conductive overlying water zone.

Sondergeld and Turcotte,[16] who detected overlying water zone convection, concentrated their analysis on the two phase zone, with only an extremely limited and flawed stability analysis of the overlying water zone. They based their analysis of the overlying zone on the density difference between steam and water and neglected the critical effects of heat transfer in stabilizing the interface. In the analysis of their experimental results, they used the measured total steam volume and the calculated steam saturation to determine both the two phase zone and water zone thicknesses. The primary source of error in this approach is the assumption of a constant saturation of steam in the two phase zone, as the steam saturation is most definitely not constant.[15]

The most useful model for the theoretical analysis of the boiling natural convection of a liquid and a condensible vapour in a low permeability porous medium would appear to be

one in which the overlying liquid zone and the two phase zone are treated separately. Udell's model of the two phase zone seems to be adequate. However, previous treatments of the overlying liquid zone are not adequate, and the purpose of this section of this work is to develop a method to accurately model the heat transfer mode and Nusselt number of the overlying liquid zone.

The literature on natural convection in porous media does not suggest a method for prediction of the Nusselt number of the overlying water zone. The first step in the process developed in the current study for predicting the Nusselt number of the overlying water zone was to determine the heat transfer mode. Published experimental studies[14-19] have shown the overlying water zone can be either in a conductive or in a convective state. The overlying water zone has been experimentally found to be in the convection mode by three different research efforts, [16,17] including the present study. The part of this study with a steam/water system in a 26.5 Darcy (26.5×10^{-12} m^2) sand pack in the heat transfer cell found three dimensional natural convection occurring in the overlying water zone. Natural convection was indicated by the steeply inclined isotherms in the overlying water zone, as shown in Figure 5.2. The convection was triggered by boiling and was not due to single fluid convection prior to boiling. Sondergeld and Turcotte[16] detected two dimensional natural convection (roll cells) of the overlying water zones in their high aspect ratio (5.0), low permeability (70 Darcy, 70×10^{-12} m^2) glass bead pack. The high aspect ratio of their pack forced two and not three dimensional convection. Later visualization studies by Sondergeld and Turcotte[19] in their thin rectangular pack confirmed the presence of two dimensional natural convection triggered by the onset of boiling. Bau and Torrance[17] detected three dimensional convection of the overlying water zone in their experiments with a low aspect ratio (0.238), high permeability (1400 Darcy, 1400×10^{-12} m^2) cylindrical sand pack. This occurred in a system undergoing three dimensional natural convection prior to boiling, unlike both the system of Sondergeld and Turcotte[16] and the system described in this study.

In Bau and Torrance's[18] study of the steam/water system without convection prior to boiling, three dimensional convection in the overlying water zone was not detected after boiling began. Bau and Torrance used three different, low permeability porous mediums in the same apparatus. The permeabilities of the porous mediums used ranged from 8.5 to 64 Darcies (8.5×10^{-12} m^2 to 64×10^{-12} m^2).

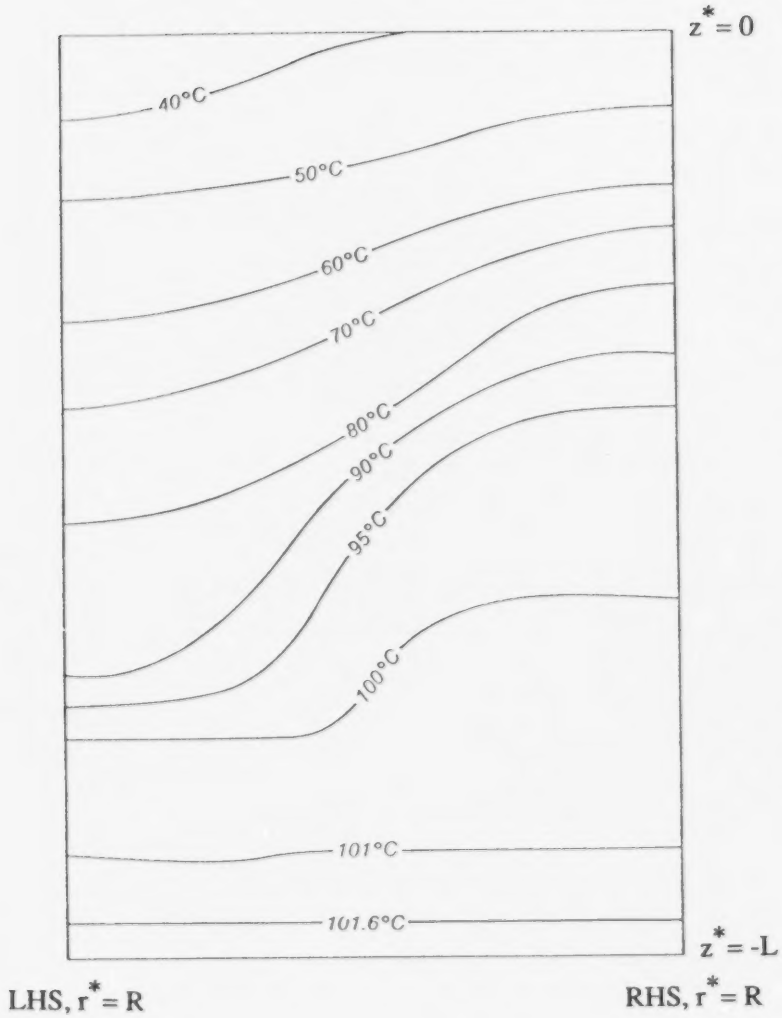

Figure 5.2 Moderate Permeability Isotherm Contours (Elevation), Water/Steam in Sand, Run W/S-S #1

The contradictory results of these experimental investigations have not been adequately explained in the literature. Bau[14] attempted to explain the contradictory results of Sondergeld and Turcotte[16] by claiming that their water was in two dimensional convection before the two phase zone developed and the motion impressed itself onto the two phase system. However, the single fluid system of Sondergeld and Turcotte, when treated by the methods described in Chapter 4, has a predicted critical Rayleigh number of 13 and a maximum experimental Rayleigh value of 8. Additionally, their separate flow visualization study[19] showed no two dimensional convection prior to the onset of boiling. Thus, Bau's attempted explanation of their results was incorrect. Sondergeld and Turcotte[16] tried to explain their two dimensional water zone convection by proposing a two phase Rayleigh number based on the density difference between the water zone and the two phase zone. This explanation ignores the critical stabilizing influence of heat transfer[50] and cannot explain the lack of overlying water zone convection in Bau's experiments.[14]

The model developed in the present study for predicting the heat transfer mode of the overlying water zone is based on the system's behaviour at the onset of boiling. If, at the onset of boiling, either single fluid natural convection is already occurring, or the interface between the steam phase and the water phase is unstable, then natural convection in the overlying water zone will be initiated.

The occurrence of single fluid natural convection prior to boiling will result in convection in the overlying water zone. This can be predicted by determining the critical Rayleigh value (Ra_c) and the Rayleigh number at the onset of boiling (Ra_b) by the techniques presented in Chapter 4. Natural convection will occur if Ra_b is greater than Ra_c.

The interface between the steam and water phases is primarily stabilized because the fingers of steam penetrating the water zone lose heat to the water zone and condense, forcing the interface back down. The interface will become unstable when the overlying water zone cannot remove heat sufficiently rapidly from the steam finger to condense and collapse it. If the overlying water zone is initially in a conductive heat transfer mode, there is a limit as to how much heat it can remove from a finger of steam. If a greater amount of heat removal is required the interface will become unstable and move upwards. This results in a non-horizontal interface (isotherm) under the water zone and the immediate initiation of natural convection in the overlying water zone.[54-56] The natural convection mode of heat transfer can remove heat at a greater rate from the steam fingers and may be able to stabilize the interface. The "angle" of the interface determines the

level of convection, and an "angle" sufficiently steep for natural convection to stabilize the interface may be possible. If a greater amount of heat removal is required than can be provided by natural convection caused by an interface at the maximum spatially allowable angle, then the overlying water zone is unstable and will collapse. Nucleate boiling will commence with the whole pack acting as a two phase zone. Under these conditions pockets of cool water near the bottom of the pack and fluids at saturation temperature encompassing the entire pack have been observed.

The model predicting the stability of the steam-water interface is based on simplifying and extending Straus and Schubert's[50] work on the satability of water over steam in geothermal reservoirs to a specific case. Their model does not exactly correspond to the situation presently dealt with in that they used a non-isothermal steam zone instead of an almost isothermal two phase zone. Additionally, they used a permeable top surface instead of an impermeable top surface. The difference in zone treatment is a significant, but a necessary simplification that can be corrected by empirical correlation. The development of the model is shown in Appendix H. The model determines a dimensionless stability number (W) representing the ratio of the marginally stable perturbation wavelength to the maximum horizontal dimension of the porous medium. If the stability number is too small the interface will not stabilize and convection will occur. The stability number is evaluated at the onset of boiling (W_b) for each experiment. If W_b is less than some critical value, W_{bc}, the interface between the steam and water phases is unstable, and water zone convection will occur. The value of W_{bc} is determined empirically to correct for the necessary simplifications in the model.

For water at ambient pressure and $T_{sat} = 100°C$, W_b is (from Appendix H):

$$W_b = \frac{1.7019 \times 10^{-8} \lambda_m (100 - T_o)}{L (1.349 \times 10^{6} k + 6.9337 \times 10^{-7} \lambda_m)} \qquad 5.1$$

where:

W_b = dimensionless stability number at onset of boiling
λ_m = thermal conductivity of medium [W/m K]
L = height of sand pack [m]
k = permeability of sand pack [m^2]
T_o = upper surface temperature of sand pack [°C]

Once the heat transfer mode of the overlying water zone has been established, the Nusselt number for the overlying water zone can be predicted. If the overlying water zone is in the conductive mode the Nusselt number is, of course, one. If the overlying water zone is convective the Nusselt number can be predicted from the following empirical model, the development of which is shown in Appendix H:

$$Nu_w = 1.0 + \Omega[(Q / Q_b)^{1.5} - 1.0] \{W_{bc} - W_b\} \quad 5.2$$

where:
Nu_w = Nusselt number of overlying liquid zone
Ω = correction factor
Q = imposed heat flux [W/m^2]
Q_b = heat flux at onset of boiling [W/m^2]
W_{bc} = critical boiling stability number
W_b = boiling stability number

5.2 Steam/Water Experiments

The study of the natural convection of a liquid and a condensible vapour in a porous medium was conducted using water. Several previously published experimental studies have also used water,[15] with most using a permeable top surface.[14,16-19] The results from most of these studies seem to agree fairly well, in that a water layer was formed above a two-phase zone. However, Sondergeld and Turcotte[16,19] found the overlying water layer to be convecting in a system that was not convecting prior to the onset of boiling, while Bau and Torrance[14,18] did not.

The initial phase of the study of the natural convection of a liquid and a condensible vapour in a porous medium was intended to examine the behaviour of the overlying water zone. A 40-70 Unimin (quartz) sand pack of 26.5 Darcy (26.5×10^{-12} m^2) permeability and 32.4% porosity initially saturated to 99.25% with de-ionized water was utilized. Pore fluid pressure was maintained at atmospheric pressure and the sand pack was heated from below. Three experiments, denoted W/S-S #1 - #3, were done at progressively higher heat flux rates and all had the lower surface of the sand pack above the boiling point. The results of these experiments are listed in Table 5.1 and shown in Figure 5.3. The top of the two phase zone was located by interpolating the average temperatures measured for each horizontal layer of temperature probes in the sand pack. The top of the two phase zone was thus defined as the average height of the two phase zone.

Table 5.1 Water/Steam in Sand: Experimental Results

Description	W/S-S #1	W/S-S #2	W/S-S #3
$q(W/m^2)$ lower surface	370.4	878.0	1254.9
$T_1(°C)$ bottom of two phase zone	101.76	100.26	102.56
$T_M(°C)$ top of two phase zone	99.31	98.95	101.22
$T_0(°C)$ top of overlying water zone	38.68	39.61	51.92
$\Delta y_w(m)$ thickness of overlying water zone	0.382	0.255	0.233
$\Delta y_{sw}(m)$ thickness of two phase zone	0.341	0.469	0.491
Nu_o overall	1.636	4.152	7.201
Nu_w water zone	0.984	1.596	2.520
Nu_{sw} two phase zone	18.17	117.12	174.24

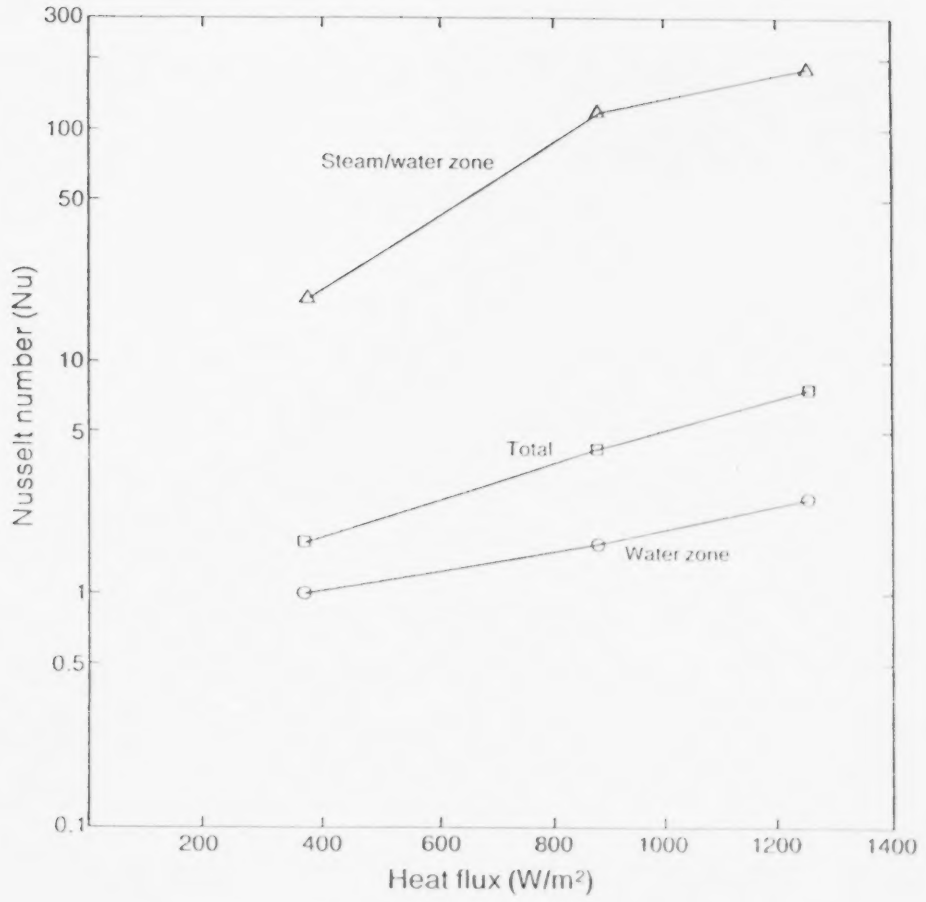

Figure 5.3 Experimental Results; Water/Steam in Sand, Runs W/S-S #1-#3

The average thickness of the overlying water zone was determined by subtracting the two phase zone height from the overall pack height. The resulting Nusselt numbers were based on the average zone thickness, the temperature drop across the zone, the measured heat flux, and the thermal conductivity calculated as if the zone was water saturated and at the average zone temperature. The thermal conductivity was predicted using actual thermal conductivity measurements conducted with the same pack during the single fluid experiments.

A two phase zone with an overlying water layer existed for all three experiments. The overlying water zone had non-horizontal isotherms, increasing in declination as the heat flux increased, indicating natural convection. The non-horizontal isotherms in the overlying water zone above the two phase zone are shown for the first experiment in Figure 5.2. However, the Nusselt number of the overlying water zone for the first experiment was approximately one, indicating no convection. Consequently, the level of convection in the first experiment was considered too low to be detectable on the basis of heat flux. In the other two experiments Nusselt numbers were greater than one, clearly indicating convection.

The two phase zone underlying the water zone apparently imposed a non-horizontal isotherm on the lower surface of the water zone. The overlying water zone behaved similarly to a porous medium saturated with a single fluid confined between sloping isothermal surfaces and heated from below. Such an inclined system has a critical Rayleigh value of zero[54-56] (i.e. convective heat transfer is always occurring). The heat transfer rate through such a system increases with increasing slope (which agrees with experimental data discussed later). A detailed analysis of these experiments is presented in Appendix I.

The second phase of the study of the natural convection of a liquid and a condensible vapour in a porous medium was conducted using water in a high permeability sand pack. The intent of these experiments was to determine where the upper limit to the permeability that can support an overlying water zone may be. The experiments were conducted using a 6-9 Colorado (quartz) sand pack of 2100 Darcy (2100×10^{-12} m^2) permeability and 34.0% porosity saturated with de-ionized water. The sand pack was heated from below.

The first two water/steam-sand experiments, denoted W/S-S II #1 and #2, were done with the pore fluid pressure maintained at atmospheric pressure. The first experiment, W/S-S II #1, had an applied heat flux of 822.3 W/m^2. The second experiment, W/S-S II #2, had

an applied heat flux of 1110.8 W/m^2. Both experiments were in the convective regime and the heat transfer through the sand pack was so efficient the temperature at the bottom of the sand pack never approached the boiling point. The next three water/steam-sand experiments, denoted W/S-S II #3- #5, were conducted with the pore fluid pressure maintained, by a vacuum pump, at 28.5 kPa absolute. The first of this second set of water/steam experiments, W/S-S II #3, had an applied heat flux of 964.2 W/m^2, but the bottom sand pack temperature still did not reach the boiling point. The second of this set, W/S-S II #4, had an applied heat flux of 1079.1 W/m^2 and boiling did occur. A water and a dry steam zone developed, both extending from the bottom to the top of the sand pack. The temperature profiles for this experiment are shown in Figure 5.4, clearly illustrating the lack of an overlying water zone. The last water/steam experiment, W/S-S II #5, with an applied heat flux of 1185.1 W/m^2, also had boiling occur, and the entire sand pack was filled with dry steam.

The results of these high permeability experiments clearly show that there is an upper limit to the permeability that will allow the formation of an overlying water zone. Overlying water zones have been found in previously published works to exist for permeabilities ranging from 8.5 Darcy to 1400 Darcy (8.5 to 1400 x 10^{-12} m^2) .[14-19] The permeability upper limit for the existence of an overlying water zone near the onset of boiling could then be expected to fall between 1400 and 2100 Darcy (1400 and 2100 x 10^{-12} m^2) .

5.3 Steam/Water: Comparison of Results

The initial comparison of the steam/water system results was done to determine the relative significance of the overlying water zone and the two phase zone. The experimental results of this study (denoted Exp.) are compared with the results of two different models (A and B) in Table 5.2. The first model (model A) was based on Bau's[14] model, in which the overlying water zone is assumed conductive and the two phase zone is modelled as one-dimensional. The second model (model B) assumed the two phase zone to be isothermal and, as no predictive model of the two phase zone had been published, utilized the measured Nusselt number of the overlying water zone. Further details of these two models are in Appendix J. The comparison in Table 5.2 clearly shows that, in terms of zone thickness, it is much more accurate (up to 28%) to assume an infinite two-phase zone Nusselt number (isothermal two-phase zone) and calculate the overlying water zone Nusselt number, than to calculate the two phase zone Nusselt number and assume a conductive overlying water zone.

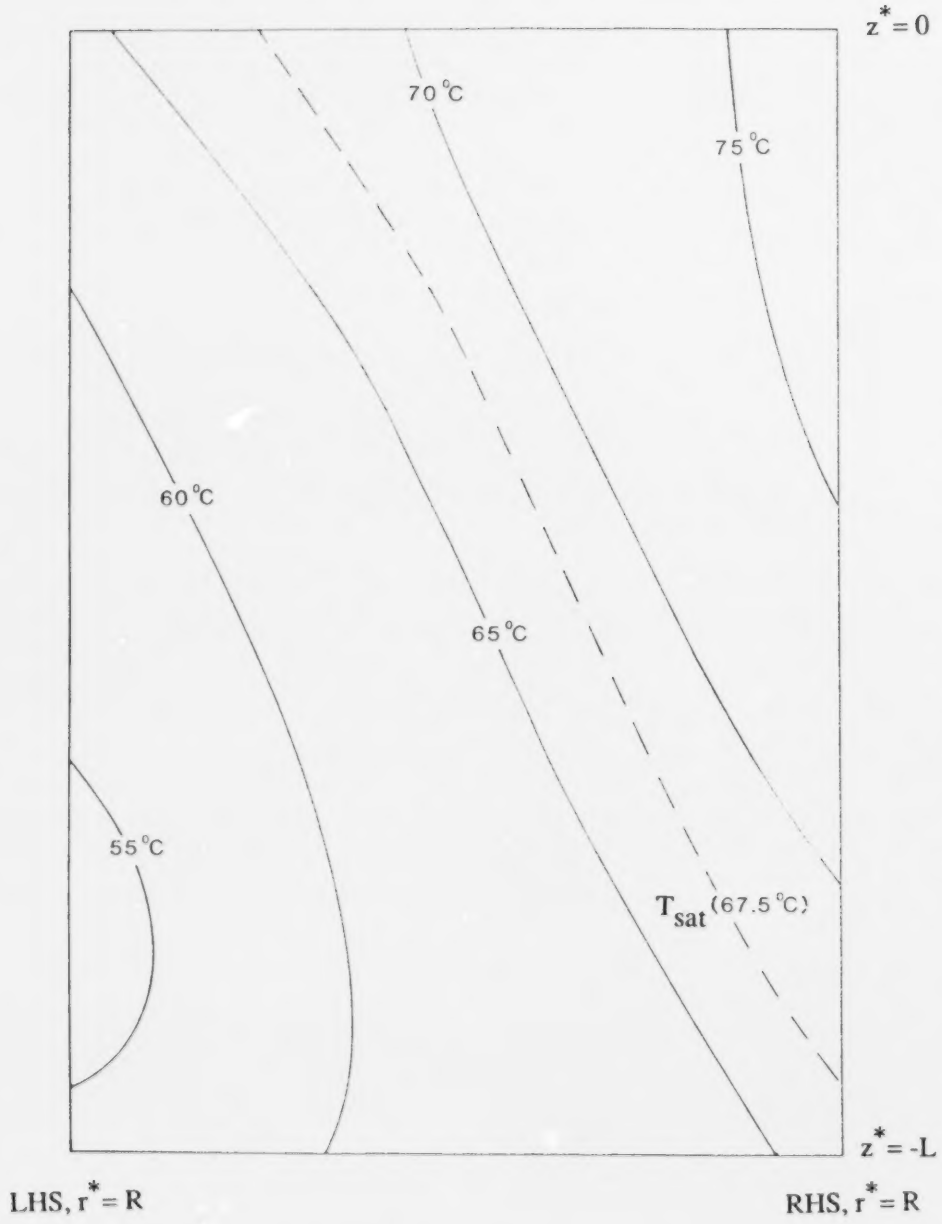

Figure 5.4 High Permeability Isotherm Contours (Elevation), Water/Steam in Sand, Run W/S-S II #4

Table 5.2 Water/Steam in Sand: Comparison of Models

Desc	W/S-S #1			W/S-S #2			W/S-S #3		
Source	Exp.	A	B	Exp.	A	B	Exp.	A	B
q lower surface[W/m^2]	370.4	370.4	370.4	878.0	878.0	878.0	878.0	878.0	878.0
Nu_{sw} 2 phase zone	18.17	∞	∞	117.12	∞	∞	174.24	∞	∞
Nu_w water zone	0.984	1.0	0.984	1.596	1.0	1.596	2.520	1.0	2.520
Nu_o overall	1.636	1.833	1.833	4.152	4.4	4.44	7.201	7.836	7.836
Δy_w water zone [m]	0.3822	0.3946	0.3883	0.2548	0.1629	0.2601	0.2325	0.0923	0.2326
Δy_{sw} 2 phase zone [m]	0.3411	0.3287	0.3350	0.4685	0.5604	0.4632	0.4908	0.6310	0.4907
ERROR in Δy_{sw}	0	-3.6%	-1.8%	0	19.6%	-1.1%	0	28.6%	-0.02%

In an attempt to confirm the interface stability model developed in this study the experimental results of this study and of those previously published by others were compared with the results of the interface stability model. The stability number (W) was evaluated at the onset of boiling (W_b) for this study's experiments, and for experiments reported by Bau[14,17,18] and Sondergeld and Turcotte.[16] These are presented in Table 5.3. An examination of Table 5.3 indicates that if W_{bc} falls between 0.11 and 0.19 then the interface stability model predicts the conductive state found by Bau and the convective state found by Sondergeld and Turcotte.

Table 5.3 Water/Steam in Sand: Overlying Water Zone Modes

Source	$k(10^{-12}\ m^2)$	L(m)	λ_m(W/m K)	T_o(°C)	W_b	Mode
Bau [14]	8.5	0.187	0.92	19	0.560	conduction
Bau [14]	11.0	0.159	0.96	18	0.544	conduction
Bau [14]	64.0	0.217	2.60	16.5	0.193	conduction
S & T[16]*	70.4	0.198	0.83	16	0.063	convection
S & T[16]	70.4	0.105	0.83	28	0.102	convection
EHT**	26.5	0.668	2.40	39	0.108	convection

* S & T = Sondergeld and Turcotte; ** EHT = Present work

The empirical model developed in this study for the prediction of the overlying water zone Nusselt number was fitted both to the Sondergeld and Turcotte[16] experimental results for a 0.198 m high pack and to the present study results. The results of this fitting are shown in Figure 5.5. The fitting yielded:

$\Omega = 1.29$

$W_{bc} = 0.17$

and hence: $Nu_w = 1.0 + 1.29\ [\ (Q / Q_b)^{1.5} - 1.0\ ]\ \{0.17 - W_b\}$ 5.3

It should be noted that the W_{bc} resulting from the fitting of this model falls within the limits found earlier. This lends support to both the model for determining heat transfer mode and the model for determining overlying liquid zone Nusselt number.

The new model for predicting the overlying water zone heat transfer mode explains the apparently contradictory findings of the present study, Bau's studies,[14] and Sondergeld and Turcotte's work.[16] Bau's lower permeability experiments did not convect because, at the onset of boiling, the imposed heat flux through his thin pack was large enough to stabilize the interface and maintain a conductive regime. The present study's earlier experiments found convection occurring because the thicker pack used allowed a lower imposed heat flux at the onset of boiling, even though the sand pack permeability fell within the range of those examined by Bau. Sondergeld and Turcotte's experiments used sand packs of approximately the same thickness and of similar permeability as Bau's, but the substantially lower thermal conductivity of their pack (0.83 vs. 2.60 W/m K) forced a lower heat flux at the onset of boiling. The lower heat flux was not able to stabilize the interface and convection occurred.

The predictive performance of the model of the overlying water zone Nusselt number is compared with experimental results from Sondergeld and Turcotte[16] and from the present work in Figure 5.5. Nusselt numbers are plotted as a function of the ratio of applied heat flux to the onset of boiling heat flux. This study's experimental results (triangles) agree very closely with the model results (dotted line). Sondergeld and Turcotte's experimental results for a 0.198 m thick pack (squares) agree fairly well with the model results (dashed line), with only a small amount of scatter about the model's prediction. Sondergeld and Turcotte's results for a 0.108 m thick pack (circles) show overlying water zone Nusselt numbers of less than one at lower heat fluxes. This anomaly is due to their prediction of two phase height, and hence overlying water zone Nusselt number, by using a calculated constant steam saturation. Their model for the saturation fails for the lower heat flux, thinner model case and causes the anomalous results. However, as the heat flux is increased their experimental results approach the model predictions (dot-dash line).

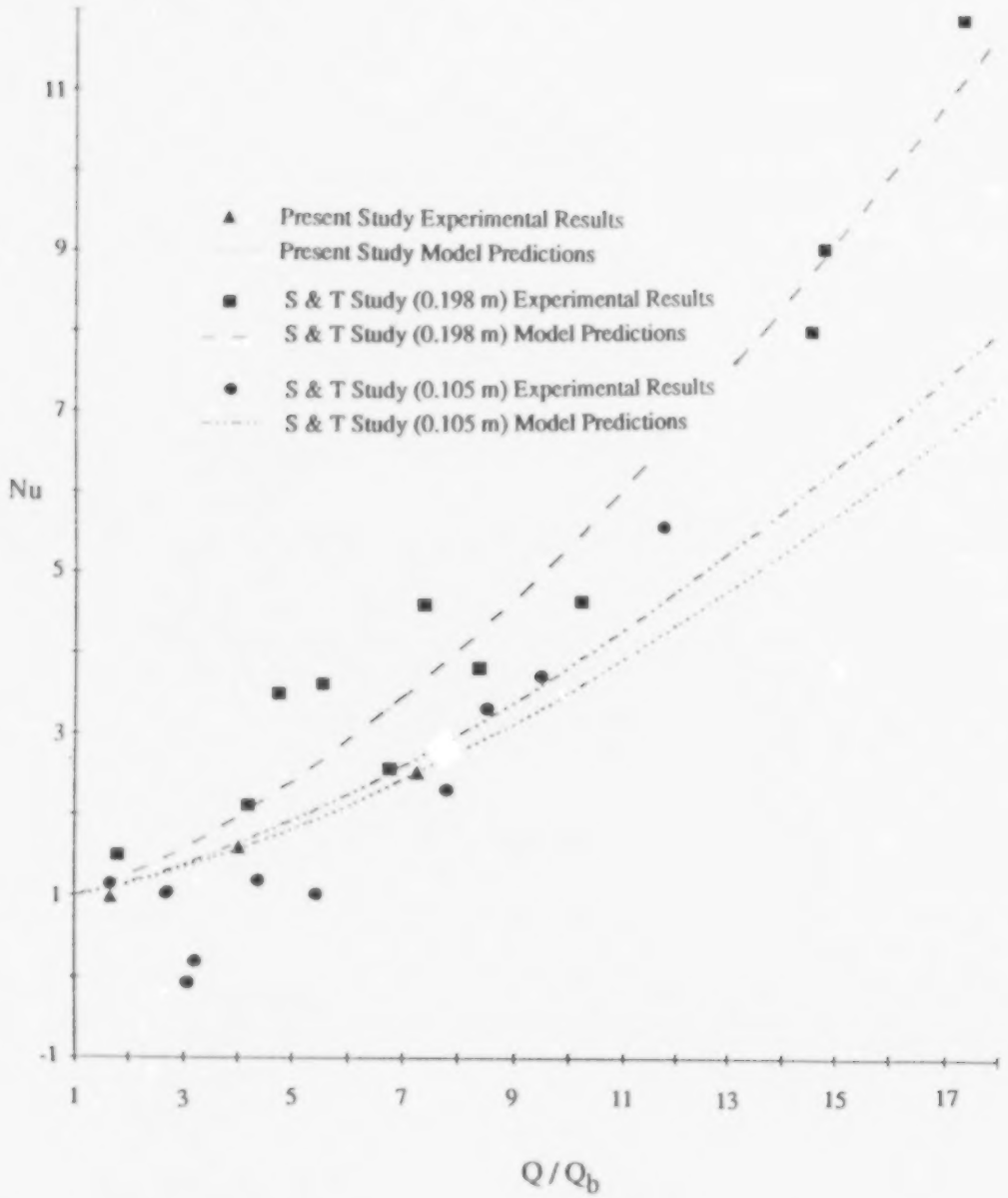

Figure 5.5 Overlying Water Zone Nusselt Number Model Predictions

CHAPTER 6. NATURAL CONVECTION OF TWO IMMISCIBLE LIQUIDS

A porous medium saturated with two immiscible liquids may have the liquids separated into two distinct layers or the liquids may be evenly distributed throughout the medium. The evenly distributed fluids may have one or both of the liquids wetting the solid phase. The Alberta oil sands deposits are water wet and have the water and oil distributed throughout the deposit. To represent the actual system adequately, this phase of the study was primarily concerned with a mixture of two immiscible fluids, with water being the wetting phase. When the saturated porous medium is heated from below, each constituent fluid has a destabilizing influence on the system, similar to that for a single fluid. This destabilizing influence is modified by many factors,[57] including: wetting,[58] capillary pressure, saturation, surface tension, continuous or discontinuous phases, drag, etc. Many of these factors are represented to some extent by the relative permeability.[59] Relative permeability is measured with each of the different fluids being driven by the same applied pressure gradient. The actual pressure gradient applied to each phase is slightly modified by the capillary pressure of that fluid. The fluids in a natural convection system, however, are driven by buoyancy forces which can be very different for each fluid.

6.1 Two Immiscible Fluids: Models

There have been no reports in the open literature describing theoretical or experimental studies of the natural (thermal) convection of two immiscible liquids in a porous medium although several studies of miscible fluids have been published.[11-13] The aim of this part of the present study was to examine the natural convection of two immiscible liquids in a porous medium, particularly in ways that may potentially be applied to reservoir modelling. This part of the study will be restricted to the prediction of the onset of convection. Prediction of the rates of heat transfer of two immiscible fluids undergoing natural convection in a porous medium would require numerical modelling with a mesh size too small to be integrated into a reservoir model. Therefore, the prediction of the rates of heat transfer for two immiscible fluids were considered outside the scope of this study.

6.1.1 Psuedo-Fluid Model

As no previously published work was available for guidance, an extremely simple model was initially used. This simple model was based on the assumption that the two fluids

could be treated as a single, "pseudo-fluid". The model uses the actual thermal conductivity of the media, the absolute permeability, and mass averaged fluid properties. These values are used in the single fluid model. This method ignored all those factors caused by the presence of two immiscible fluids. These factors were expected to modify the destabilizing influence of the thermal gradient significantly. Because of its oversimplification the "pseudo-fluid" model was not expected to predict accurately the behaviour of the experiments.

6.1.2 Relative Permeability Models

A much more detailed set of five theoretical models for predicting the onset of convection was developed in which the effects of relative permeability are predominant. The set of models gives each of the two fluids its own Rayleigh number, based on the individual fluid properties and the effective permeability at the given fluid saturation. The effective permeability is the product of the absolute and relative permeabilities. Critical Rayleigh values are then predicted for each phase as if each individual fluid is the only fluid present in the porous medium. Also, the values of relative permeability measured in the pressure drive experiments may need to be altered to be used in the buoyancy drive situation. Five of the possible methods of altering the measured relative permeability values are denoted as Models 1 through 5.

The Rayleigh number for a fluid is defined by this set of models as:

$$Ra_{rf} = k_{rf} [g_a k \beta (T_{bot} - T_{top}) L \rho^2 C_p] / \{ \mu \lambda_m \}$$

where the physical properties are as for that one fluid except for:

λ_m = saturated overall medium thermal conductivity [W/m K]
(includes effect of other fluid)

k_{rf} = relative permeability of the fluid in the porous medium
at the given fluid saturations

The various models in the set would alter the values of k_{rf} so as to match the behaviour of the system. The alterations in k_{rf} would represent the difference between the relative

permeability found in a pressure driven system and that found in a buoyancy driven system.

Examination of the equation describing Ra_{rf} shows that two different fluids in the same porous medium and under the same imposed temperature difference are almost certain to have different values of Ra_{rf}, due to their different physical properties and relative permeabilities. In order to graphically represent the experimental results two horizontal Ra_{rf} axes, one for each fluid, must be used. The two axes are dimensioned such that a value of Ra_{rf} for one fluid at a certain temperature difference will directly correspond to the different, correct value of Ra_{rf} for the other fluid at the same temperature difference. For example, a temperature difference of 100°C may correspond to a Ra_{rf} of 23 for fluid 1 and a Ra_{rf} of 35 for fluid 2. The graph would thus be constructed such that the Ra_{rf} value of 23 for fluid 1 will directly correspond to the Ra_{rf} value of 35 for fluid 2. This graphical representation is used throughout the rest of this section, including Figure 6.1, which portrays the proposed five models of the set.

The first model treated the system as if pressure driven relative permeability completely describes the interactions between the fluids. Effects of the difference in driving force between pressure driven relative permeability and buoyancy driven natural convection were ignored. This model is illustrated in Figure 6.1a. The second model assumed the convective movement of the more mobile phase may have more drag on the less mobile phase than predicted by pressure driven relative permeability ($k_{rf2} > k_{rf2}$ measured). For this model, convection would occur in the less mobile phase before it was predicted. This model is illustrated in Figure 6.1b. The third model assumed the convective motion of the more mobile phase was retarded by the presence of the less mobile phase to a greater extent than predicted by pressure driven relative permeability ($k_{rf1} < k_{rf1}$ measured). This would cause convective flow in the more mobile phase to be retarded until after the predicted critical Rayleigh value was exceeded. The third model is illustrated in Figure 6.1c. The fourth model is a combination of the second and third. Onset of convection of the more mobile phase was assumed to be additionally retarded by the second phase, and the additional drag on the less mobile phase was assumed to cause it to convect earlier than predicted ($k_{rf1} < k_{rf1}$ measured ; $k_{rf2} > k_{rf2}$ measured). The fourth model is illustrated in Figure 6.1d. The fifth model was an extreme case of the fourth. The additional flow retardation on the most mobile phase and the additional drag effects on the least mobile phase were assumed to be enough to cause both fluids to begin convecting at the same imposed temperature difference. The fluids would behave as if one fluid with intermediate properties and low effective permeability. The fifth model is illustrated in Figure 6.1e.

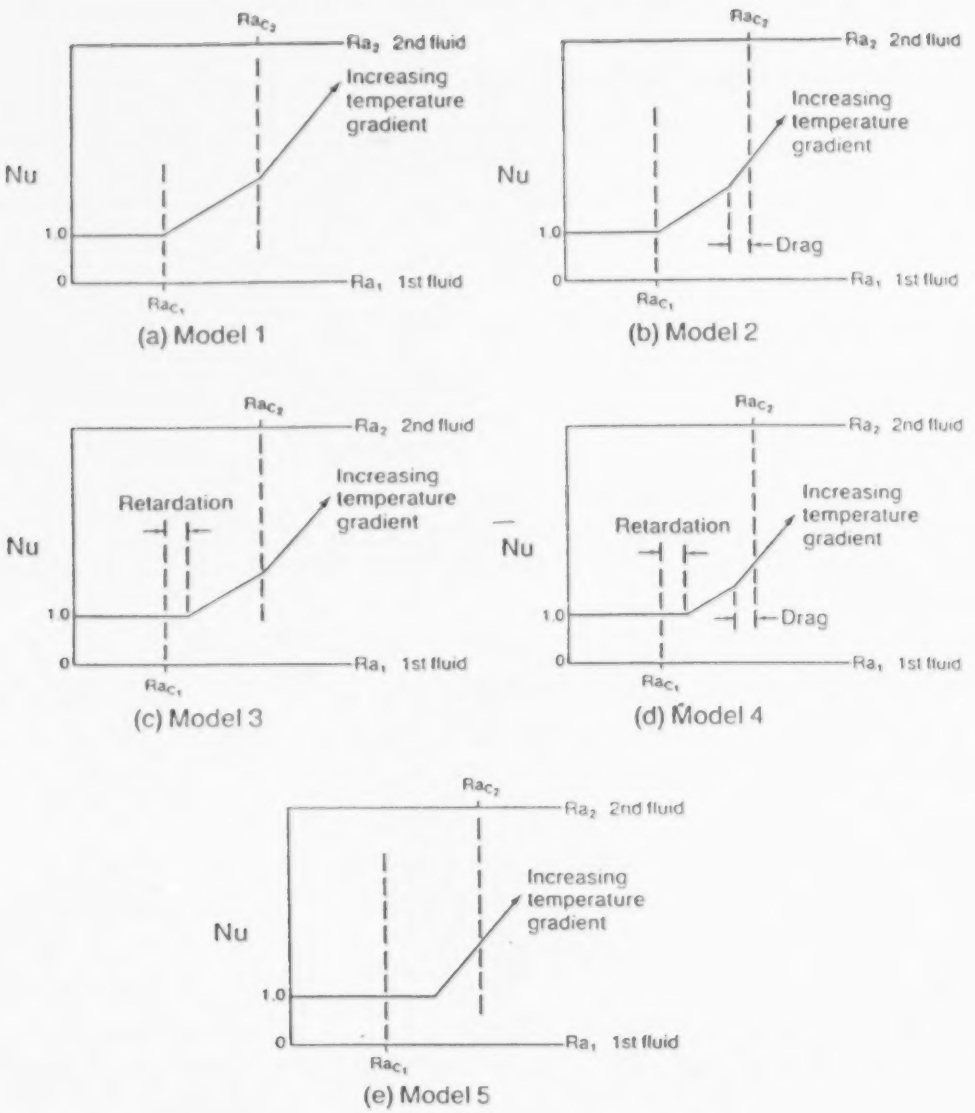

Figure 6.1 Proposed Relative Permeability Models

6.2 Tetrachloroethylene/Water Experiments

The initial experiments in this part of the study utilized a 40-70 Unimin sand pack of 26.5 Darcy (26.5×10^{-12} m^2) permeability and 32.4% porosity. The sand pack was initially saturated to 99.12% with de-ionized water. Tetrachloroethylene was then flooded through the pack (2.8 pore volumes injected) until a water saturation of 14.27%, and a tetrachloroethylene saturation of 85.73%, was achieved. Saturations were determined by a mass balance. Tetrachloroethylene was selected because it is totally immiscible in water, inflammable, only moderately reactive with the heat transfer cell liner and, as a single fluid, convects at a lower imposed temperature gradient than water. This provided the maximum mechanistic difference between the experiments using tetrachloroethylene and the later experiments using oil, as the oil requires a greater imposed temperature gradient to convect than water. The other fluids considered that could achieve this convective capability were either extremely flammable or highly reactive with the heat transfer cell liner.

Five tetrachloroethylene water/sand experiments, denoted T/W-S #1-#5, in which the sand pack was heated from below, were attempted. The first three progressed to steady state and resulted in Nusselt numbers of about one. Each experiment took approximately 14 days to reach steady state. The fourth experiment had to be curtailed before steady state was reached due to an extended series of electrical power failures. The resulting Nusselt value of 1.53 indicated convection, but an examination of the experimental isotherms showed them to be flat and that no convection occurred. It was concluded that steady state conditions had not been reached, and the high Nusselt number was due to transient effects alone. The fourth experiment, however, had progressed far enough to clearly show no convection was possible for this system under the imposed temperature gradient value. The experiments in the single fluid portion of the present study had shown that when convection is going to occur in a system the isotherms show convective effects long before steady state is achieved, and the isotherms from the fourth experiment showed no evidence of convection. The fifth experiment was terminated shortly after commencement due to the development of a large leak. This was due to liner damage by the tetrachloroethylene. Results of the four experiments are shown in Figure 6.2. The experimental analysis can be found in Appendix K.

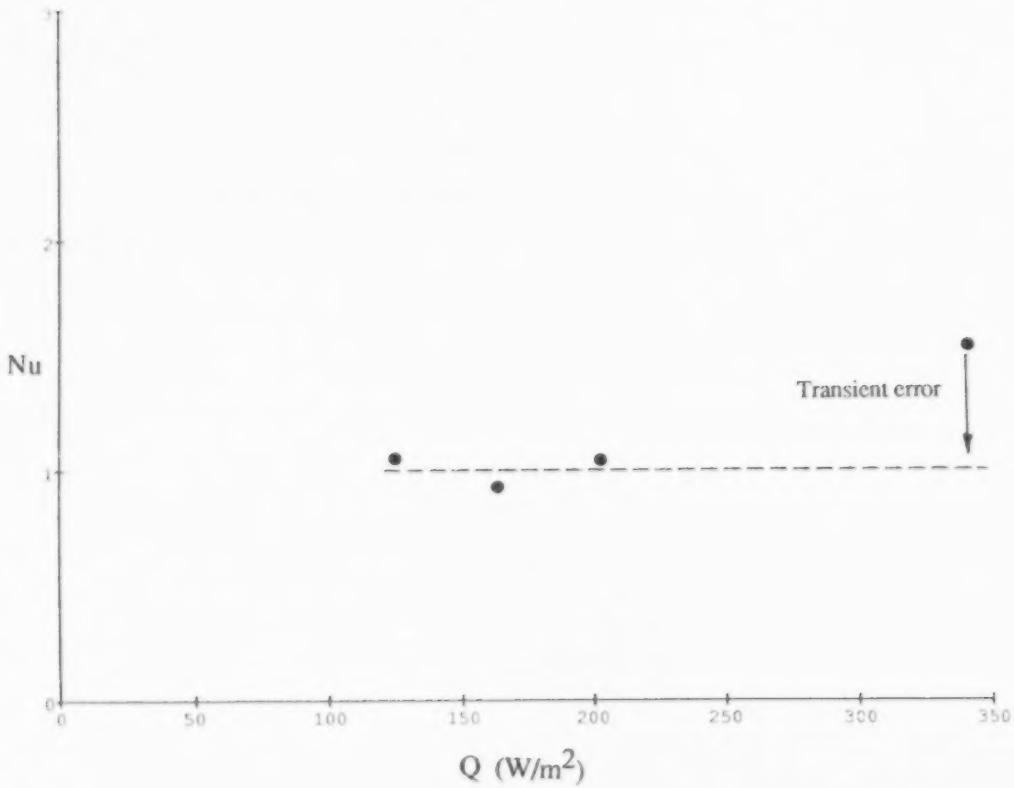

Figure 6.2 Experimental Results, Tetrachloroethylene/Water in Sand, Runs T/W-S #1-#4

The latter phase of this part of the study utilized a 6-9 Colorado sand pack of 2100 Darcy (2100×10^{-12} m^2) permeability and 34.0% porosity. The sand pack was initially saturated with de-ionized water. Tetrachloroethylene was then flooded through the pack (10.3 pore volumes injected) until a water saturation of 7.9%, and a tetrachloroethylene saturation of 92.1%, was achieved. Four experiments, denoted T/W-S II #1-#4, in which the sand pack was heated from below were done. Natural convection occurred in all four experiments and the results are shown in Figure 6.3.

6.3 Mentor 29/Water Experiments

The initial phase of this portion of the study utilized a 6-9 Colorado sand pack of 1950 Darcy (1950×10^{-12} m^2) permeability and 33.4% porosity. The sand pack was initially saturated with de-ionized water. Mentor 29, a light oil produced by Esso Petroleum Canada, was then flooded through the pack (2.2 pore volumes injected) until a water saturation of 16.5%, and a Mentor 29 saturation of 83.5%, was achieved. Mentor 29 was selected because it was totally immiscible in water, safe, and had a viscosity only six times that of water. Seven oil/water-sand experiments, denoted O/W-S #1 - #7, were done. Two experiments, O/W-S #1 and #4, were heated from above, and were duplicates of each other. Hence, the results from O/W-S #4 were not reported. The other five experiments were heated from below and four of the five showed natural convection. Experimental results are shown in Figure 6.4. After this experimental series was complete, de-ionized water was flooded through the pack (1.5 pore volumes injected) until a water saturation of 75.4%, and a Mentor 29 saturation of 24.6%, was achieved. Five experiments, denoted O/W-S II #1 - #5, were then done. Two experiments, O/W-S II #1 and #4, were heated from above, resulting in negative heat flux values and Rayleigh numbers. The other three experiments were heated from below and natural convection occurred in all three. Experimental results are shown in Figure 6.5.

Figure 6.3 Experimental Results, Tetrachloroethylene/Water in High Permeability Sand, Runs T/W-S II #1-#4

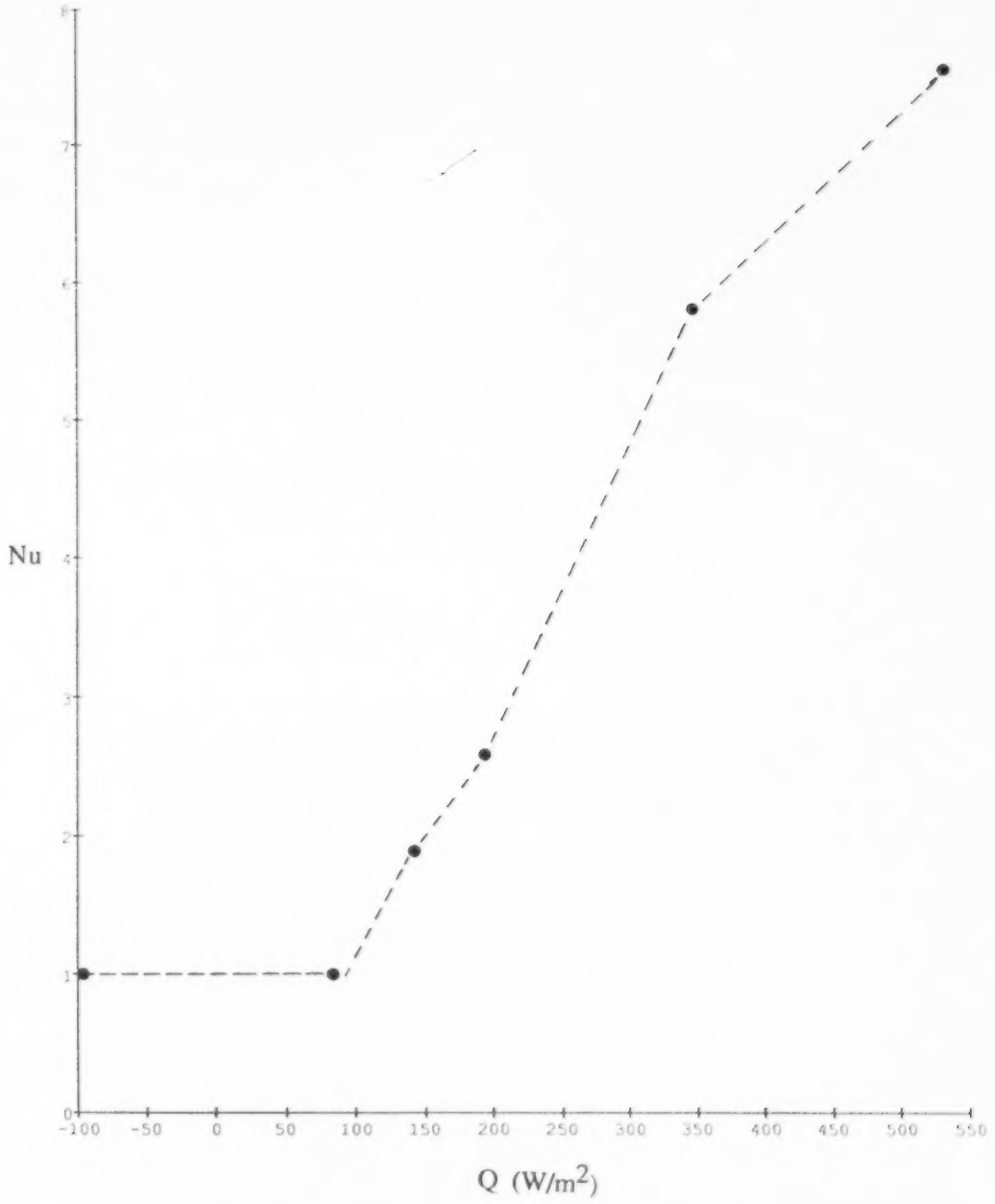

Figure 6.4 Experimental Results, Mentor 29/Water in High Permeability Sand, Runs O/W-S #1-#3, #5-#7

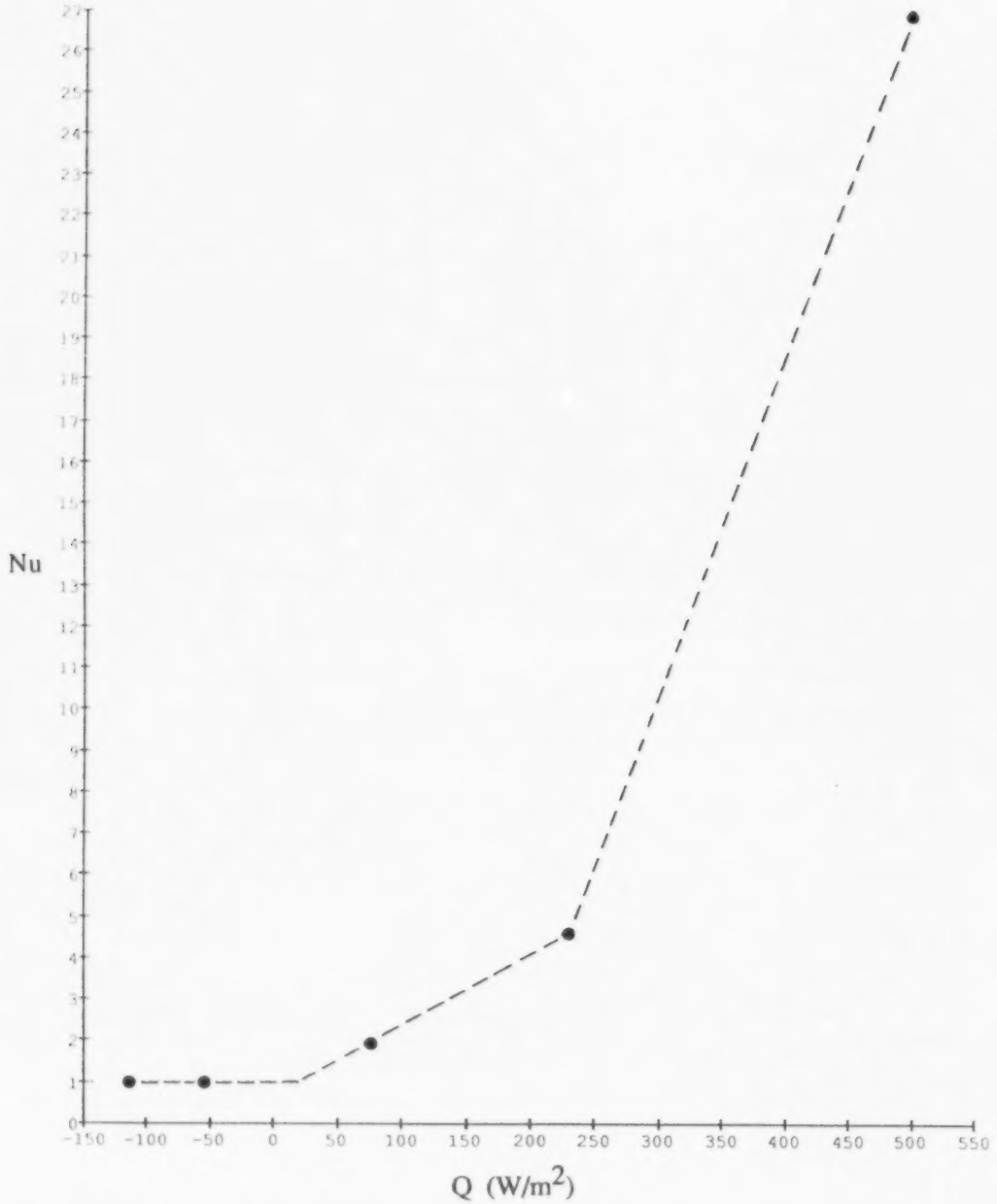

Figure 6.5 Experimental Results, Mentor 29/Water in High Permeability Sand, Runs O/W-S II #1-#5

6.4 Two Immiscible Liquids: Comparison of Results

6.4.1 Psuedo-Fluid Model Results

The predicted onset of convection, as calculated by the "psuedo-fluid" model, is shown, along with the experimental results, in Figures 6.6 to 6.9. The experimental results are plotted as values of Ra Psuedo. The Ra Psuedo values result from inserting experimental values into the "psuedo-fluid" model definition of the Rayleigh number. The experimentally indicated critical Rayleigh values are compared with the predictions of the "pseudo-fluid" model in Table 6.1. The pseudo-fluid treatment appears to consistently underpredict the critical Rayleigh value, although the actual critical Rayleigh number was not exactly determined by the experiments. Further details of the calculations can be found in Appendix L.

Table 6.1 Psuedo-fluid Model Predictions

Exp. Series	Ra_c Exp.	Ra_c Psuedo	Error
T/W-S	>38.3	32.8	>14.4 %
T/W-S II	~66.7	51.6	~23 %
O/W-S	~65.8	42.1	~36 %
O/W-S II	~54.9	47.7	~13 %

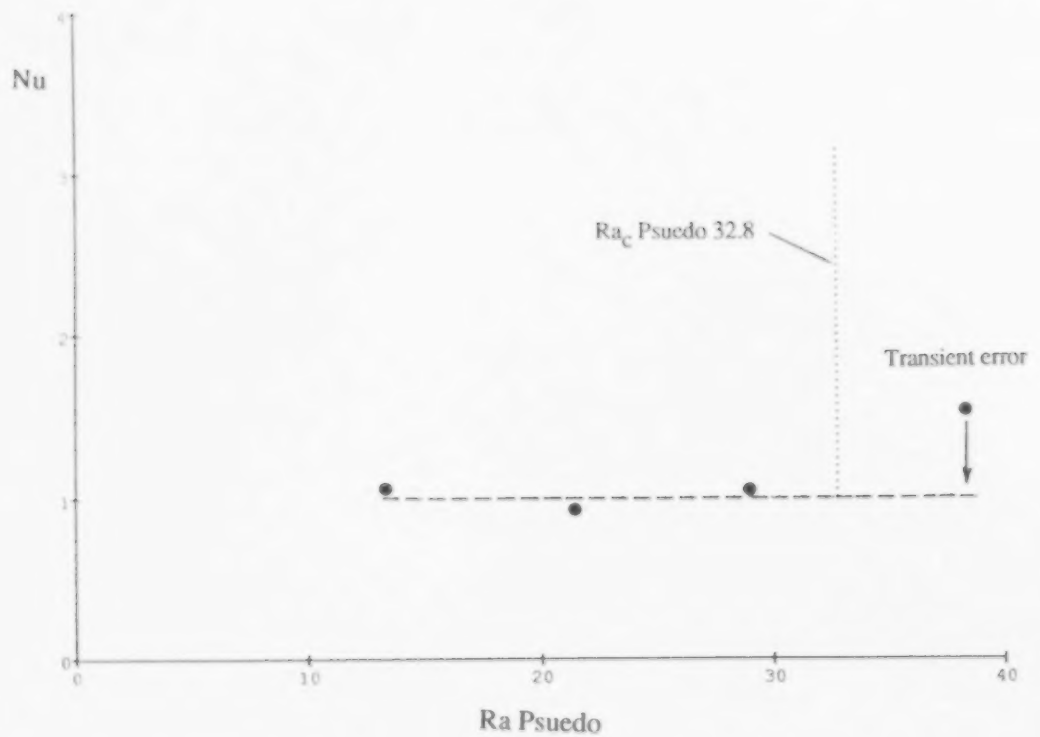

Figure 6.6 Comparison of Predicted and Measured Critical Rayleigh Values, Pseudo-Fluid, Tetrachloroethylene/Water in Sand, Runs T/W-S #1-#4

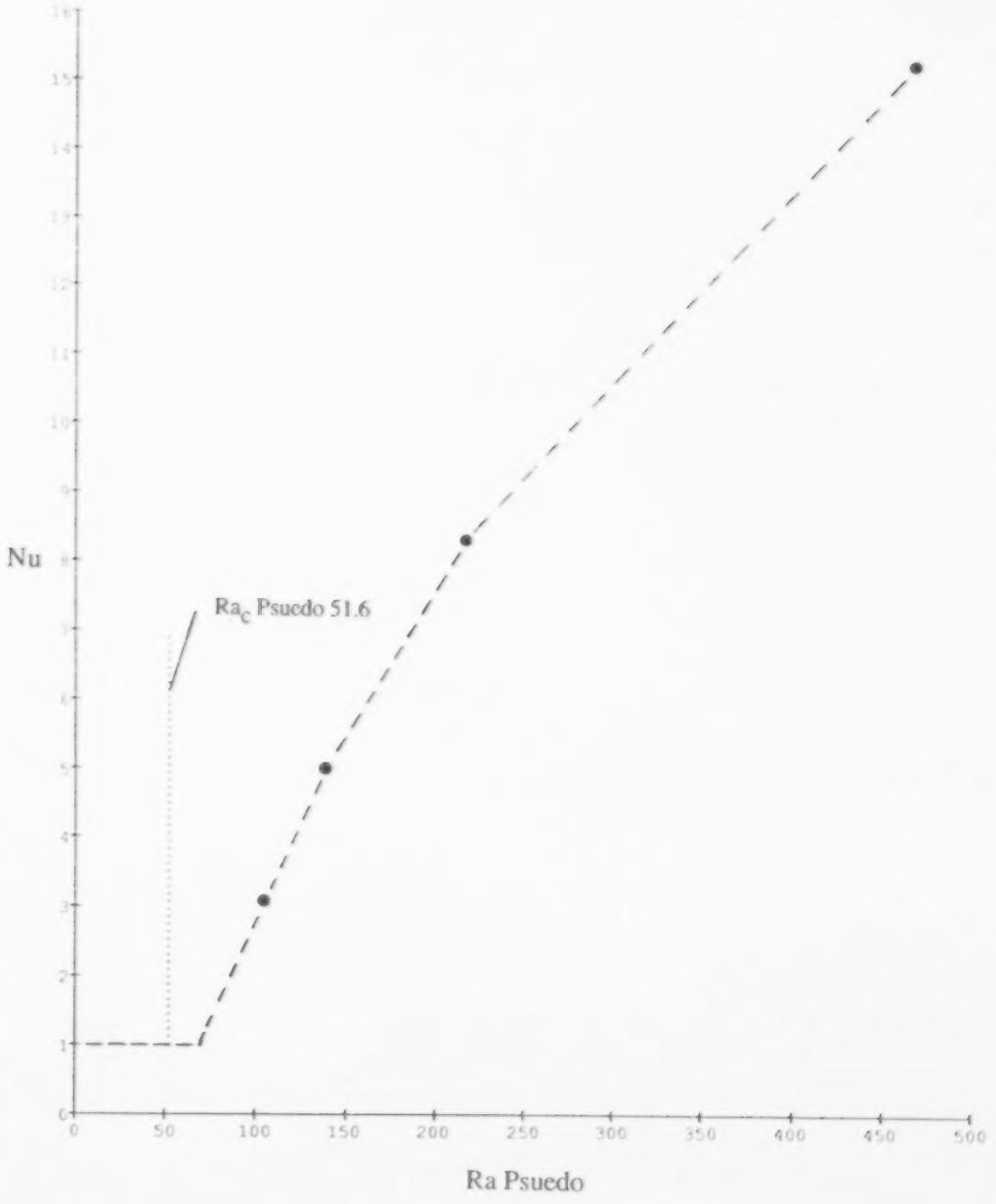

Figure 6.7 Comparison of Predicted and Measured Critical Rayleigh Values, Pseudo-Fluid, Tetrachloroethylene/Water in High Permeability Sand, Runs T/W-S II #1-#4

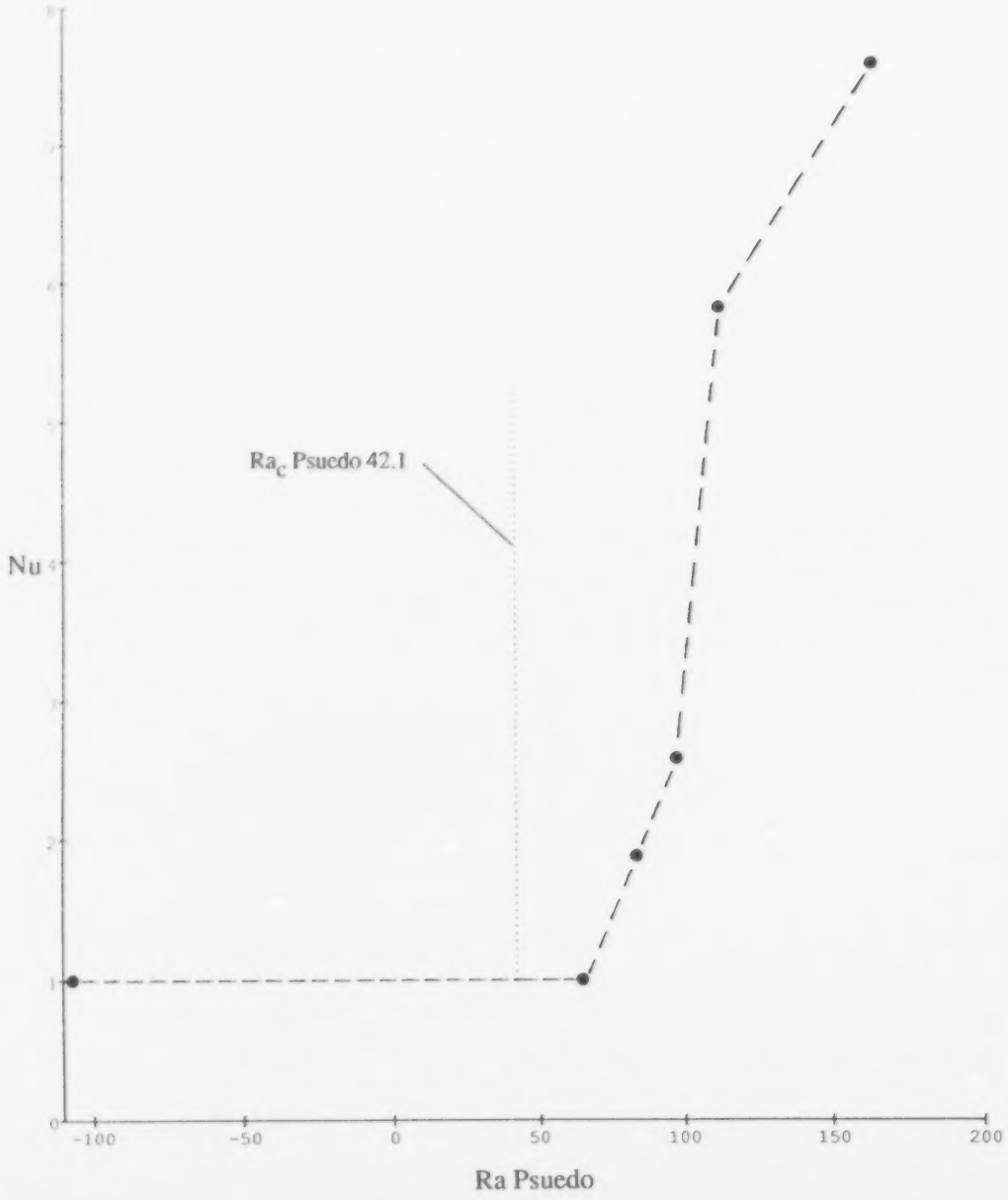

Figure 6.8 Comparison of Predicted and Measured Critical Rayleigh Values, Pseudo-Fluid, Mentor 29/Water in High Permeability Sand, Runs O/W-S #1-#3, #5-#7

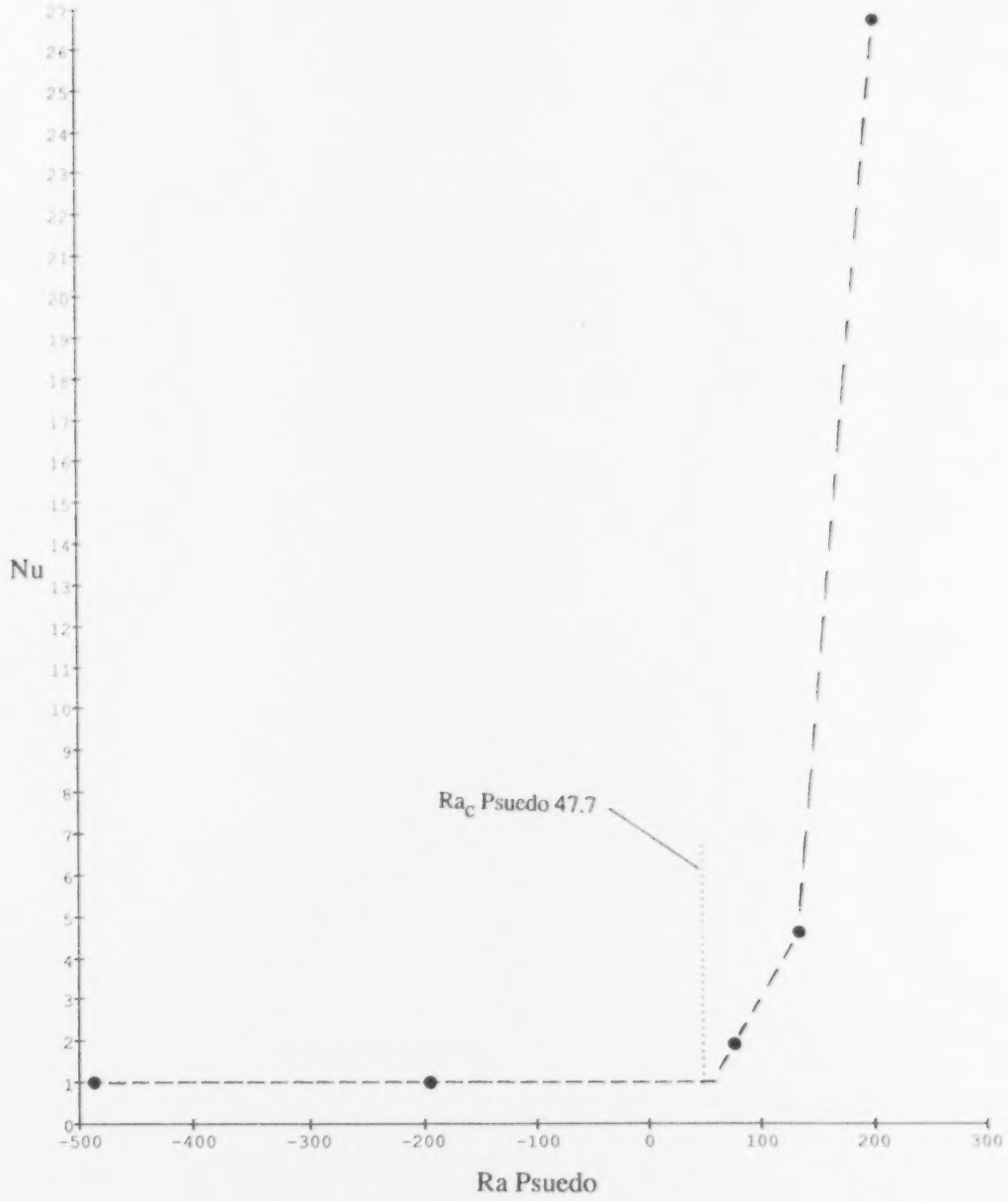

Figure 6.9 Comparison of Predicted and Measured Critical Rayleigh Values, Pseudo-Fluid, Mentor 29/Water in High Permeability Sand, Runs O/W-S II #1-#5

6.4.2 Relative Permeability Models Results

The first of the five relative permeability models was used to predict the critical Rayleigh values for the four experimental series. The calculations used relative permeabilities from Appendix M. The effects of viscosity variation were obtained for the first mode of natural convection from Appendix C. The predicted critical Rayleigh values are plotted versus experimental values for the four experimental series in Figures 6.10, 6.11, 6.12 and 6.13. The experimental results are plotted as values of Ra Rel Perm #1 for both phases. The Ra Rel Perm #1 values result from inserting experimental values into the relative permeability #1 model definition of the Rayleigh number for both phases. Further details of the calculations can be found in Appendix N. The experimentally indicated critical Rayleigh values for the two phases are compared with the predictions of relative permeability Model 1 in Table 6.2.

Table 6.2 Relative Permeability Model 1 Predictions

Exp. Series	Ra_c Oil Exp.	Ra_c Oil Rel Perm 1	Error Oil	Ra_c Water Exp.	Ra_c Water Rel Perm 1	Error Water
T/W-S	>20	35.5 *	?	impossible	impossible	
T/W-S II	~41.6	51.3	~23 %	impossible	impossible	
O/W-S	~37.2	37.6	~1 %	~41.8	38.8	~7 %
O/W-S II	>5.84	18.7	?	~47.3	47.7	~1 %

The results of the second tetrachloroethylene/water-sand experiments (Figure 6.11) indicated the relative permeability of the oil phase would have to be changed from 0.70 to 0.87 for the predicted and experimental values to match. The required change is beyond any uncertainty in relative permeability. The first series of Mentor 29 oil/water-sand experiments (Figure 6.12) indicated the relative permeability of the oil phase would have to be changed form 0.83 to 0.84 and that of the water phase from 0.059 to 0.054 for the predicted and experimental critical values to match. The second series of Mentor 29 oil/water-sand experiments (Figure 6.13) indicated the relative permeability of the water phase would have to be changed from 0.69 to 0.694 for the predicted and experimental critical values to match.

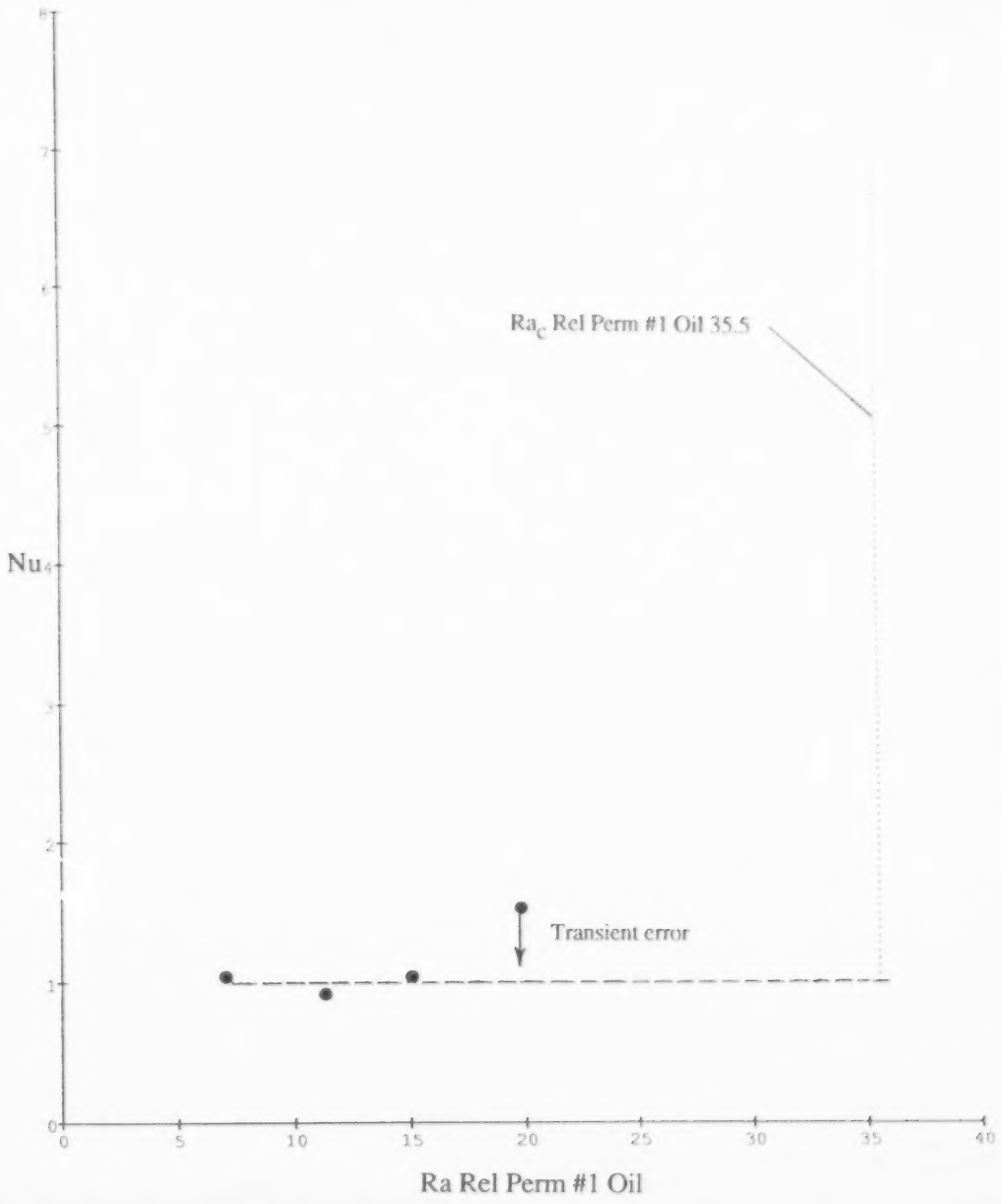

Figure 6.10 Comparison of Predicted and Measured Critical Rayleigh Values, Relative Permeability Model 1, Tetrachloroethylene/Water in Sand, Runs T/W-S #1-#4

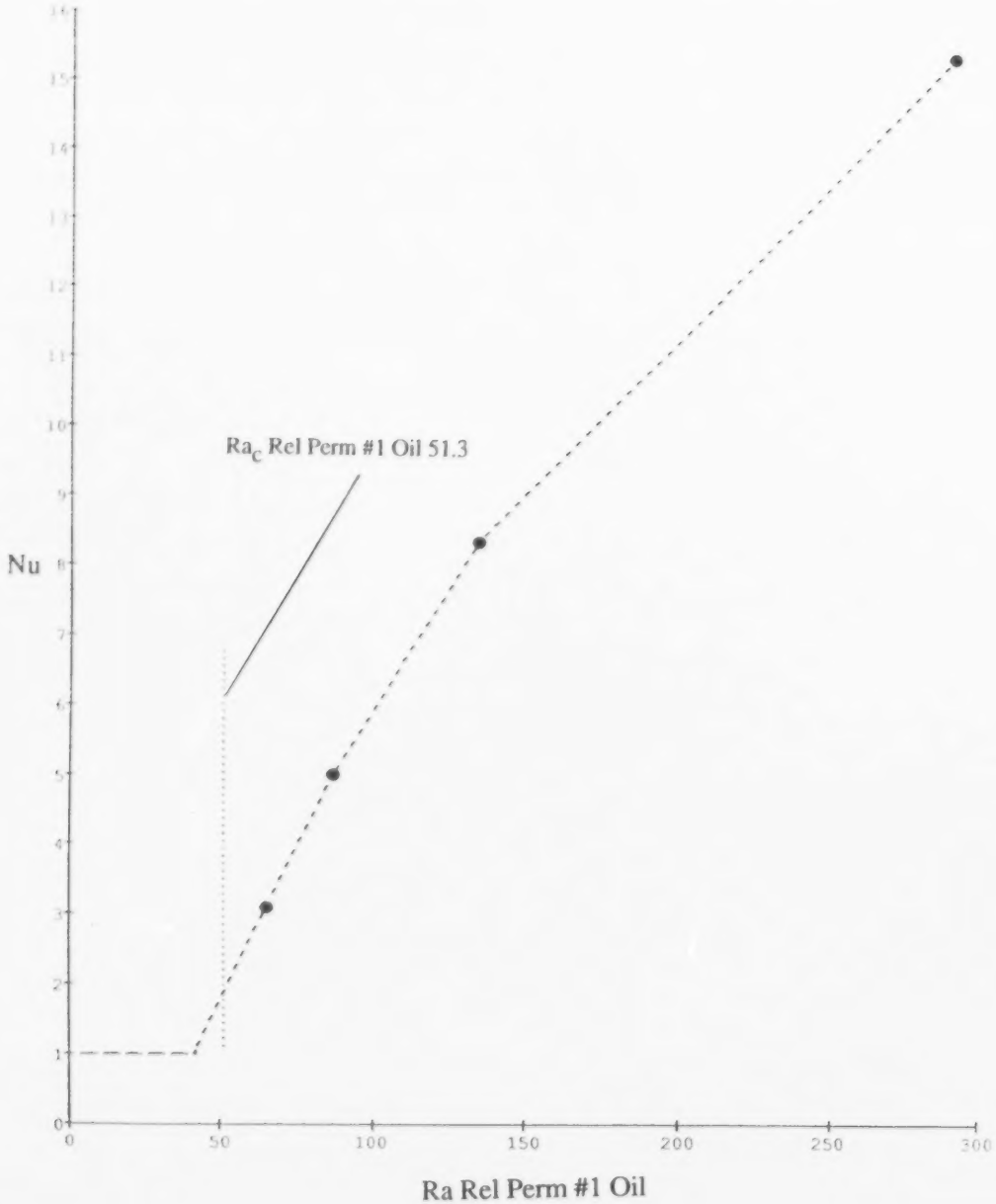

Figure 6.11 Comparison of Predicted and Measured Critical Rayleigh Values, Relative Permeability Model 1, Tetrachloroethylene/Water in High Permeability Sand, Runs T/W-S II #1-#4

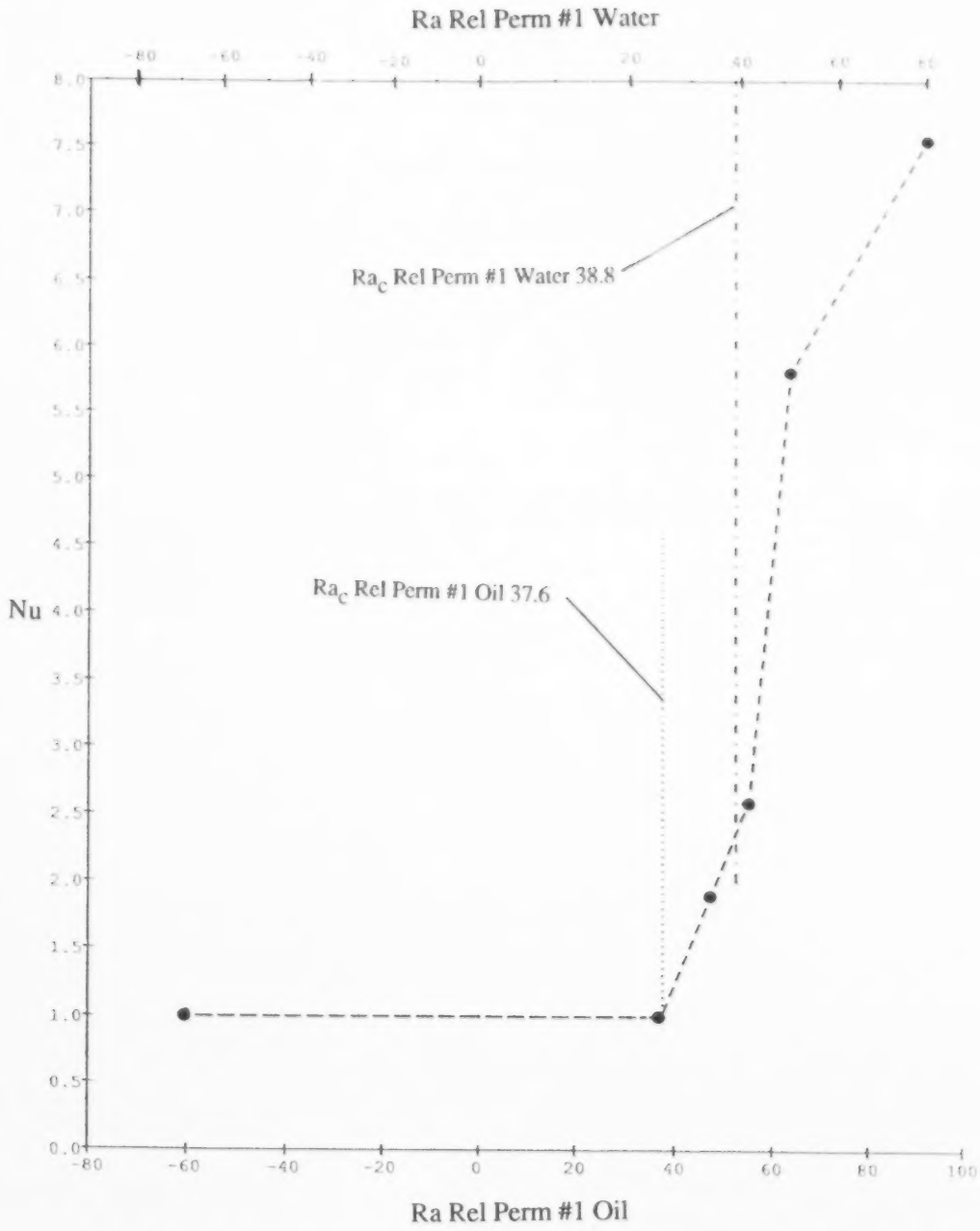

Figure 6.12 Comparison of Predicted and Measured Critical Rayleigh Values, Relative Permeability Model 1, Mentor 29/Water in High Permeability Sand, Runs O/W-S #1-#3, #5-#7

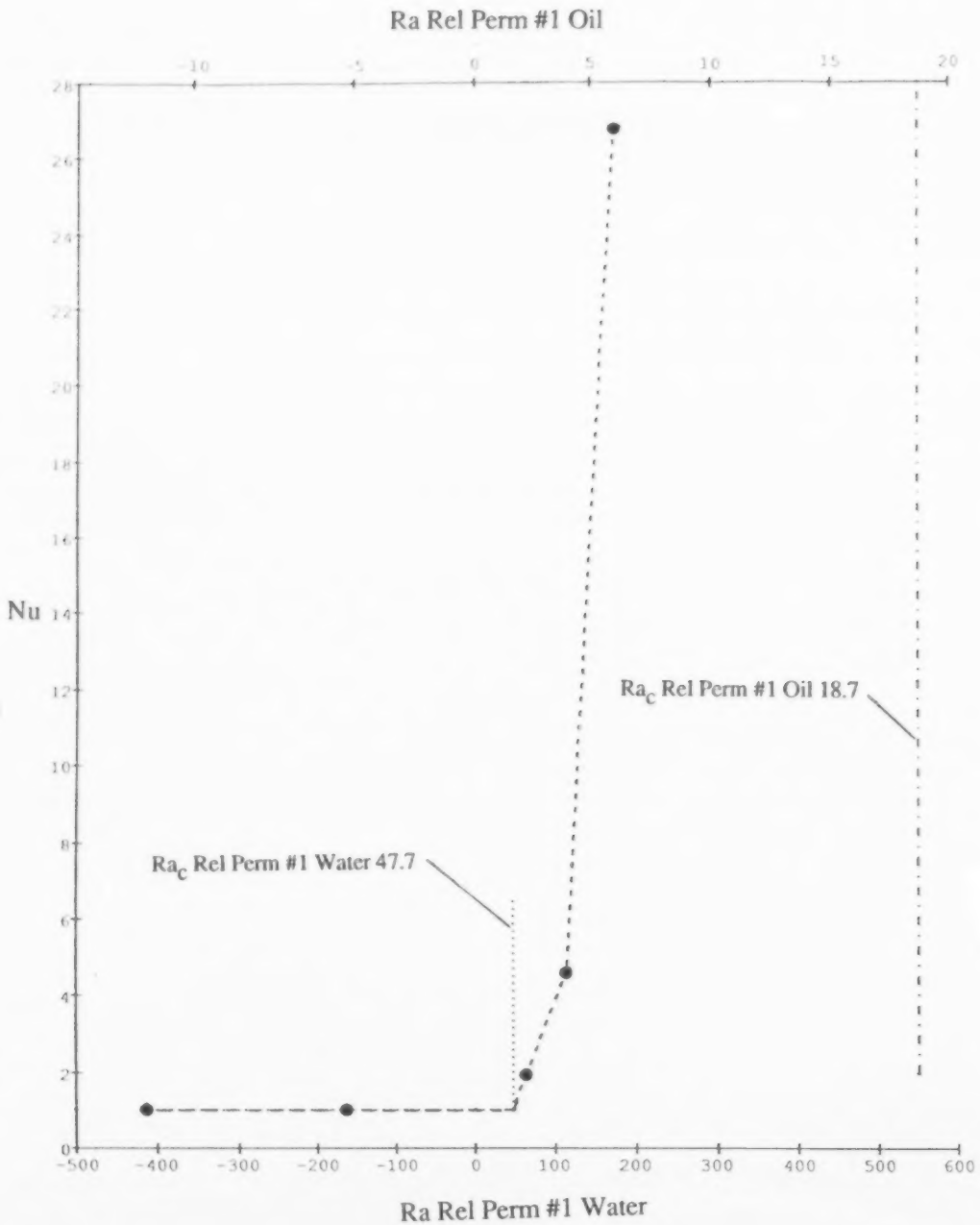

Figure 6.13 Comparison of Predicted and Measured Critical Rayleigh Values, Relative Permeability Model 1, Mentor 29/Water in High Permeability Sand, Runs O/W-S II #1-#5

The agreement between prediction and experiment for both series of Mentor 29 oil/water-sand experiments seems remarkably good, especially considering the non-wetting phase was the most mobile in the first series, while the wetting phase was the most mobile in the second series. The second tetrachloroethylene/water-sand series showed poorer agreement between prediction and experiment, and the discrepancy is too large to be explained by the experimental uncertainty in the relative permeability data. The most reasonable explanation for the discrepancy is that in cases where the non-wetting phase is much more mobile than the wetting phase the pressure driven relative permeability underestimates the buoyancy driven relative permeabilty. Fortunately, this circumstance is very unlikely in the water wet oil sands reservoirs.

6.4.2.1 Relative Permeability Sensitivity

One concern is the limited accuracy of the predictions of relative permeability at intermediate fluid saturations. The predictions were made based upon linear interpolations from measured relative permeabilities at irreducible water and oil saturations (end points). The sensitivity of the results to variations in relative permeability was tested by varying the water relative permeability used in the predictions and analysis of the first Mentor 29 oil/water-sand (O/W-S) series by plus and minus 10%. This was equivalent to using water relative permeabilities of 0.065 and 0.053 instead of 0.059. The experimental water phase Rayleigh numbers changed by $\pm$ 10%, but the predicted critical water phase Rayleigh numbers changed, by +2.3% and -2.1%, respectively. The small changes in the predicted critical Rayleigh values indicate the predictions are insensitive to small errors in the measurement of relative permeability. These results are shown in Figures 6.14 and 6.15. The reduction of water relative permeability by only 10% (Figure 6.15) was adequate to allow Model 1 behavior to perfectly describe the O/W-S system. Given the accuracy of available relative permeability information Model 1 seems to give an adequate description of the onset of natural convection of two immiscible liquids.

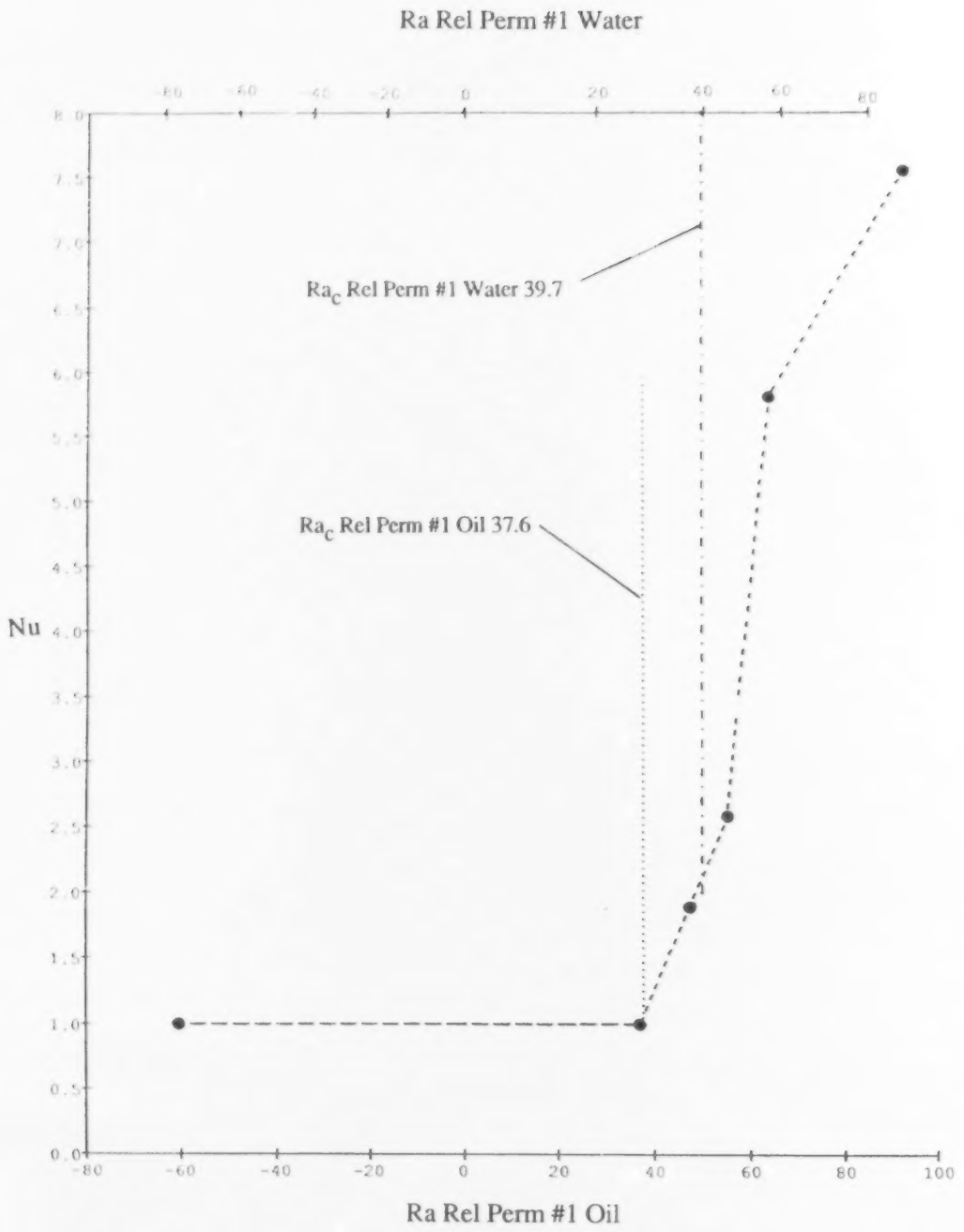

Figure 6.14 Comparison of Predicted and Measured Critical Rayleigh Values, Relative Permeability Model 1, Mentor 29/Water in High Permeability Sand, Runs O/W-S #1-#3, #5-#7, Water Rel. Perm. + 10%

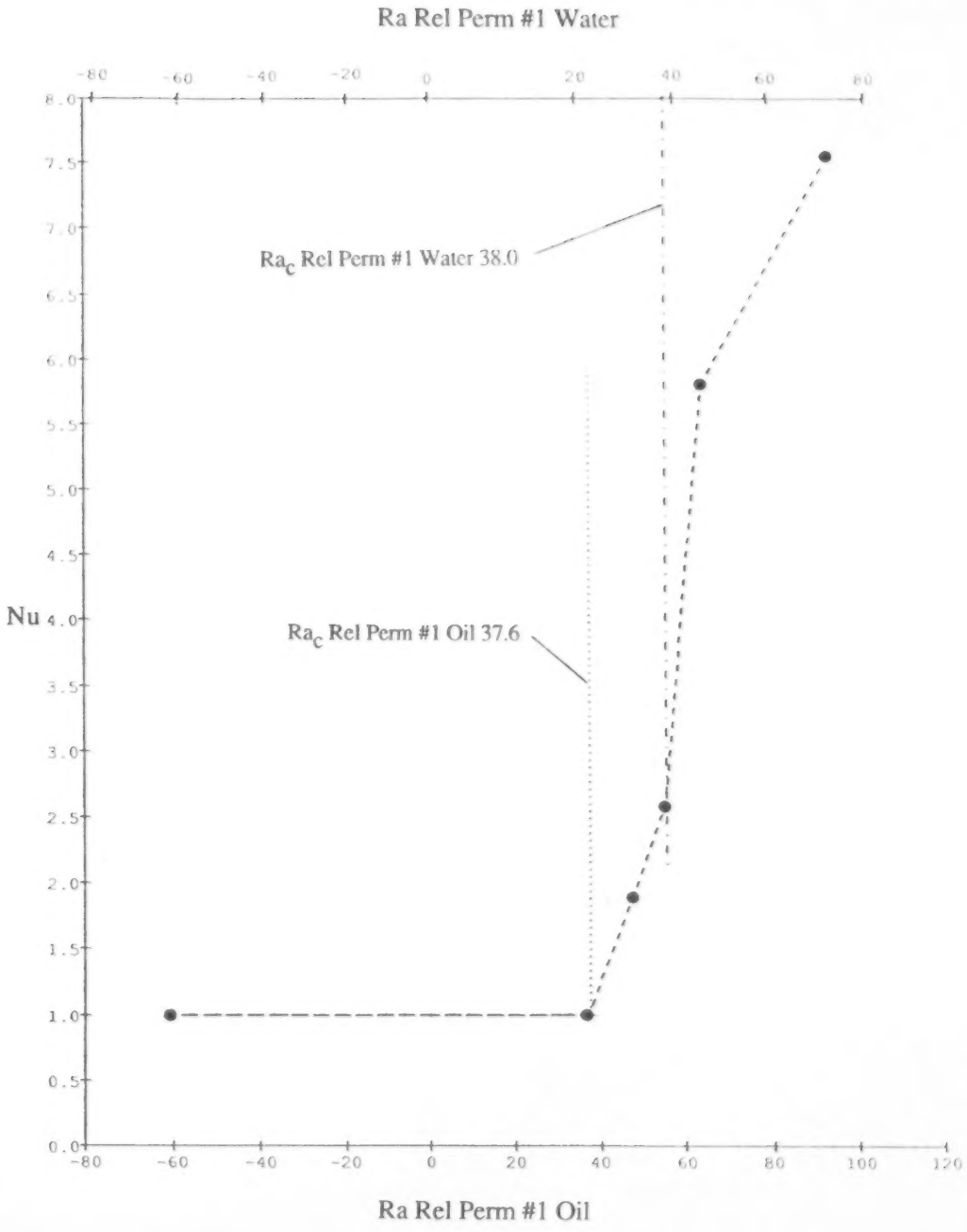

Figure 6.15 Comparison of Predicted and Measured Critical Rayleigh Values, Relative Permeability Model 1, Mentor 29/Water in High Permeability Sand, Runs O/W-S #1-#3, #5-#7, Water Rel. Perm. - 10%

CHAPTER 7. CONCLUSIONS

The study of the steady state natural convection of a single fluid saturating a cylindrical porous medium heated from below has shown that the convection of water can be adequately predicted by previously developed techniques. However, a novel viscosity-temperature relationship based on the ratio between the fluid viscosity at the maximum and minimum temperature has been proposed and models based on the relationship were developed. The models allow the more rapid prediction of the natural convection of fluids (including fluids other than water), especially when cold end temperatures are not fixed at 25°C. The models based on this new relationship would be useful tools for the examination of any viscosity sensitive thermal natural convection in a porous medium.

The examination of the boiling of water in a cylindrical porous medium heated from below focussed on the liquid (water) zone overlying the two phase (steam/water) zone. The overall thermal characteristics of the system are controlled by the behaviour of the overlying liquid zone. A new model, based on the stability of the interface between a condensible vapour zone and a overlying liquid zone, has been developed. The model predicts the heat transfer mode of the overlying liquid zone. Additionally, an empirical model has been developed that predicts the Nusselt number of the convecting overlying liquid zone. Using these models, the differing behaviour of the overlying liquid zone, reported by others, can now be explained. Additionally, the experimental results provide a data set for the verification of numerical simulators incorporating steam/water stability interactions.

The study of the steady state natural convection of a mixture of two immiscible fluids in a cylindrical porous medium is new. A simple "pseudo"-fluid model based on mass averaged fluid properties was found to underpredict the critical Rayleigh value for the onset of convection. A different model was developed that more adequately predicted the onset of convection. The model treated each phase independently and used experimentally determined relative permeability values to quantify the impact of one phase on the other. The experimental results can be used to test the validity of numerical simulators intended to describe the natural convection of two immiscible fluids.

The interface stability model developed in the boiling section of this work could be adapted to oil sands reservoirs, particularly to the liquid saturated zones between steam chambers and colder oil sands, such as occurs around horizontal wells and in gravity drainage. The heat transfer mode of these zones is critical, as the heat transfer through these zones control the total rate of heat transfer from the steam chamber to the cold oil sands. The total rate of heat transfer controls the rate of oil production from the reservoir. However, based on the results of the experiments with two immiscible liquids and the high oil viscosities and low permeabilities of oil sands reservoirs, it is unlikely that large scale natural convection would occur in the undisturbed regions of a typical reservoir.

CHAPTER 8. REFERENCES

1. Outtrim, C.P., Evans, R.G.: "Alberta's Oil Sands Reserves and Their Evaluation"; The Oil Sands of Canada-Venezuela 1977, CIM Spl. V 17, Can. Inst. Min. Metall., pp 36-66.
2. Takamura, K.:"Microscopic Structure of Athabasca Oil Sand"; Can. J. Chem. Eng., V 60, 1982, pp 538-545.
3. Kunii, D., Smith, J.M.: "Heat Transfer Characteristics of Porous Rocks"; A.I.Ch.E.J., V 6, 1960, pp 71-78.
4. Lillico, D.A.:"Development of an Oil Sands Heat Transfer Cell"; MSc Thesis, U of Alberta, Fall 1986.
5. Cervenan, M.R., Vermeulen, F.E., Chute, F.S.:"Thermal Conductivity and Specific Heat of Oil Sand Samples"; Can. J. Earth Sci., V 18, 1981, pp 926-931.
6. Ward, C.E., Ward, G.D.:"Heat Transfer and Oil Displacement Mouels for Tar Sand Reservoirs"; 59th Tech. Conf., Am. Inst. Min. Met. Pet. Eng., S.P.E., Houston, Sept. 1984, SPE 13222(10).
7. Lapwood, E.R.: "Convection of a Fluid in a Porous Medium"; Proc. Cambridge Phil. Soc., V 44, 1948, pp 508-521.
8. Muskat, M.:"The Flow of Homogeneous Fluids Through Porous Media"; McGraw-Hill, 1937.
9. Prasad, V., Kulacki, F.A.:"Natural Convection in a Rectangular Porous Cavity with Constant Heat Flux on One Vertical Wall"; Heat Transfer in Porous Media, Winter Ann. Mtg. ASME, Phoenix, USA, Nov 14-19, 1982, pp 35-41.
10. Kassoy, D.R. and Zebib, A.:"Variable Viscosity Effects on the Onset of Convection in Porous Media"; Phys. Fluids, V 18, 1975,pp 1649-1651.
11. Lawson, M.L., Yang, W.J.: "Thermal Stability of Binary Gas Mixtures in a Porous Medium"; J. Heat Transfer, V 97, 1975, pp 378-381.
12. Brand, H., Steinberg, V.: "Convective Instabilities in Binary Mixtures in a Porous Medium"; Physica, V 119A, 1983, pp 327-338.
13. Davidson, M.R.: "Natural Convection of Gas/Vapour Mixtures in a Porous Medium"; Int. J. Heat Mass Transfer, V 29, 1986, pp 1371-1381.
14. Bau, H.H.: "Experimental and Theoretical Studies of Natural Convection in Laboratory-Scale Models of Geothermal Systems", Ph.D. Thesis, Cornell University, Ithaca, N.Y., 1980.
15. Udell, K.S.: "Heat Transfer in Porous Media Considering Phase Change and Capillarity - the Heat Pipe Effect"; Int. J. Heat Mass Transfer, V 28, 1985, pp 485-495.

16. Sondergeld, C.H., Turcotte, D.L.: "An Experimental Study of Two-Phase Convection in a Porous Medium with Applications to Geological Problems"; J. Geophys. Res., V 82, 1977, pp 2045-2053.
17. Bau, H.H., Torrance, K.E.: "Thermal Convection and Boiling in a Porous Medium"; Winter Annual Meeting, ASME, (Heat Transfer), 1981.
18. Bau, H.H., Torrance, K.E.: "Boiling in Low Permeability Porous Materials"; Int. J. Heat Mass Transfer, V 25, 1982, pp 45-55.
19. Sondergeld, C.H., Turcotte, D.L.: "Flow Visualization Studies of Two-Phase Thermal Convection in a Porous Layer"; Pure Appl. Geophys., 1978, pp 321-330.
20. Schubert, G. and Straus, J.M.:"Two-phase Convection in a Porous Medium"; J. Geophys. Res., V 82, 1977, pp 3411-3421.
21. Wankat, P.C.: "Convective Stability of Newtonian Fluids in Multicomponent and Multiphase Systems"; PhD Thesis, Princeton Univ., 1970.
22. Beck, J.L.: "Convection in a Box of Porous Material Saturated with Fluid"; Phys. of Fluids, V 15, 1972, pp 1377-1383.
23. Zebib, A.: "Onset of Natural Convection in a Cylinder of Water Saturated Porous Media"; Phys. Fluids, V 21, 1978, pp 699-700.
24. Rayleigh, L.: "On Convection Currents in a Horizontal Layer of Fluid, when the Higher Temperature is on the Underside"; Phil. Mag., V 32, 1916, pp 529-546.
25. Holst, P.H., Aziz, K.: "A Theoretical and Experimental Study of Natural Convection in a Confined Porous Medium"; Can. J. Chem. Eng., V 50, 1972, pp 232-241.
26. Somerton, C.W., McDonough, J.M., Catton, I.: "Natural Convection in Porous Media: A Mixed Finite Difference - Galerkin Solution with Wavenumber Predictions"; Proc. of 79th Intl Heat Transfer Conf., 1982, pp 347-350.
27. Geordiadis, J.G., Catton, I.: "Prandtl Number Effect on Benard Convection in Porous Media"; J. Heat Transfer, V 108, 1986, pp 284-290.
28. Horton, C.W. and Rogers, F.T.:"Convection Currents in a Porous Medium"; J. Appl. Phy., V 16, 1945, pp 367-370.
29. Katto, Y., Masuoka, T.: "Criterion for the Onset of Convective Flow in a Fluid in a Porous Medium"; J. Heat Transfer, V 10, 1967, pp 297-309.
30. Joseph, D.D.: "Stability of Fluid Motions II"; Springer Tracts in Natural Philosophy, 1976, pp 52-90.
31. Ribando, R.J., Torrance, K.E.: "Natural Convection in a Porous Medium: Effects of Confinement, Variable Permeability, and Thermal Boundary Conditions"; J. Heat Transfer, Trans. ASME, 1976, pp 42-48.
32. Zebib, A.; "Onset of Natural convection in a Box of Water-Saturated Porous

Media with Large Temperature Variation"; Phys. Fluids, V 20, 1977, pp 4-9.

33. Gary, J., Kassoy, D.R., Tadjeran, H., Zebib, A.: "The Effects of Significant Viscosity Variation on Convective Heat Transport in Water-Saturated Porous Media"; J. Fluid Mech., V 117, 1982, pp 233-249.
34. Masuoka, T.: "Heat Transfer by Free Convection in a Porous Layer Heated from Below"; Heat Trans. Jap. Res., V 1, 1972, pp 39-45.
35. Schneider, K.J.: "Investigation of the Influence of Free Thermal Convection on Heat Transfer Through Granular Material"; Intl. Inst. of Refrig., Proc. 1963, pp 247-253.
36. Busse, F.H., Joseph, D.D.: "Bounds for Heat Transport in a Porous Layer"; J. Fluid Mech., 1972, pp 521-543.
37. Palm, E., Weber, J.E., Kvernvold, O.: "On Steady Convection in a Porous Medium"; J. Fluid Mech., V 54, 1972, pp 153-161.
38. Sorey, J.L.: "Numerical Modeling of Liquid Geothermal Systems"; Geological Surv. Prof. Paper 1044-D, 1978.
39. Cheng, P.:"Heat Transfer in Geothermal Systems"; Adv. Heat Trans., V 14, 1979, pp 1-105.
40. Bau, H.H., Torrance, K.E.: "An Experimental and Analytical Study of Low Rayleigh Number Thermal Convection in a Vertical Cylinder Filled with Porous Material"; 20th ASME/AIChE Natl. Heat Transfer Conf., 1981, Milwaukee, Wis., pp 17-24.
41. Horne, R.N.: "Three-Dimensional Natural Convection in a Confined Porous Medium Heated from Below"; J. Fluid Mech., V 92, 1979, pp 751-766.
42. Straus, J.M., Schubert, G.: "On the Existence of Three-Dimensional Convection in a Rectangular Box Containing Fluid-Saturated Porous Material"; J. Fluid Mech., V 87, 1978, pp 385-394.
43. Straus, J.M. and Schubert, G.:"Three-Dimensional Convection in a Cubic Box of Fluid-Saturated Porous Material"; J. Fluid Mech., V 91, 1979, pp 155-165.
44. Bories, S. and Deltour, A.:"Influence des Conditions aux Limites sur la Convection Naturelle dans un Volume Poreux Cylindrique"; Intl. J. Heat Mass Transfer, V 23, 1980,pp 765-771.
45. Bau, H.H., Torrance, K.E.: "Low Rayleigh Number Thermal Convection in a Vertical Cylinder Filled with Porous Materials and Heated from Below"; J. Heat Transfer, Trans. ASME, V 104, 1982, pp 166-172.
46. Rogers, F.T. and Morrison, H.L.:"Convection Currents in Porous Media. III. Extended Theory of the Critical Gradient"; J. Appl. Phys., V 21, 1950, pp 1177-1180.

47. Straus, J.M. and Schubert, G.:"Thermal Convection of Water in a Porous Medium: Effects of Temperature- and Pressure-Dependent Thermodynamic and Transport Properties"; J. Geophys. Res., V 82, 1977, pp 325-333.

48. Wooding, R.A.:"Steady State Free Thermal Convection of Liquid in a Saturated Permeable Medium"; J. Fluid Mech., V 2, 1957, pp 273-285.

49. Riahi, N.: "Nonlinear Convection in a Porous Layer with Finite Conducting Boundaries"; J. Fluid Mech., V 129, 1983, pp 153-171.

50. Schubert, G., Straus, J.M.: "Gravitational Stability of Water Over Steam in Vapor-Dominated Geothermal Systems"; J. Geophys. Res., V 85, 1980, pp 6505-6512.

51. Abramowitz, M., Stegun, I.A., ed.: "Handbook of Mathematical Functions"; Dover Pub., N.Y.

52. Kalaba, R.: "Some Aspects of Quasi Linearization"; Intl. Symp. Nonlinear Diff. Eq. and Nonlinear Mech., 1961, Col. Springs, Academic Press, pp 135-146.

53. Wygal, R.J.: " On the Construction of Models that Simulate Oil Reservoirs"; 23rd Tech. Conf. Pet. Prod., Penn. State Univ., 1962.

54. Combarnous, M.A., Bories, S.A.: "Hydrothermal Convection in Saturated Porous Media"; Adv. Hydrosci., 1975, pp 231-307.

55. Bories, S.A., Combarnous, M.A.; "Natural Convection in a Sloping Porous Layer"; J. Fluid Mech., 1973, pp 63-79.

56. Kaneko, T., Mohtadi, M.F., Aziz, K.: "An Experimental Study of Natural Convection in Inclined Porous Media"; Int. J. Heat Mass Transfer,1974, pp 485-496.

57. Raghavan, R., Marsden, S.S.: "The Stability of Immiscible Liquid Layers in a Porous Medium"; J. Fluid Mech., 1971, pp 143-159.

58. Fatt, I., Waldemar, A.K.: "Effect of Fractional Wettability on Multiphase Flow Through Porous Media"; AIME Tech. Note 2043, AIME Trans., V 216, 1959, pp 426-431.

59. Wyllie, M.R.J.: "Relative Permeability"; Petroleum Production Handbook, V 2, Ch. 25, McGraw-Hill, New York, 1962.

60. Ruth, D.W.: "A Model for Convection in Horizontal Porous Media Layers"; AIAA 18th Aerospace Sci., 1980, Pasadena, Ca.

61. "Encyclopedia of Chemical Technology"; 2nd Ed., J. Wylie & Sons, V 5, pp 195-203.

62. Somerton, W.H., Keese, J.A., Chu, S.L.: "Thermal Behavior of Unconsolidated Oil Sands"; Soc. Pet. Eng. J., V 14, 1974, pp 513-521.

APPENDICES

A. HEAT TRANSFER CELL

A.1 Cell Design

A diagram of the heat transfer cell is shown in Figure A.1. An asbestos-cement (A/C) water transmission pipe rated at 4.8 MPa and with a 460 mm inner diameter was selected for the wall of the cell due to its low thermal conductivity (~ 1 W/m K), high temperature durability, and pressure capability. The ends of the pipe were capped by 12.7 mm thick 316SS rings welded to 26 gauge 316SS sheet cladding the inside of the pipe. Discs 31.8 mm thick and 454 mm in diameter made of Colorceran, a material commonly used for laboratory counter tops, were used for heat flux meters, as the thermal conductivity (~ 1 W/m K) was suitable and the material was robust. Heating/cooling heads, as detailed in Figures A.2, and A.3 were installed at each end of the pipe. The lower head contained a sandwich of a liquid cooling plate, an electrical heating plate and a sealing plate, and a copper temperature moderating plate. The upper head additionally contained an overburden applying piston assembly. The sealing plates contained temperature control thermocouples, ports for sensor leads and fluid injection, and the sealing surface for the flexible asbestos-metal (Flexitallic) gasket used against the asbestos-cement pipe ends. Each heat flux meter was separated from the copper moderating plate by a silicone rubber pad. A 762 mm diameter steel pipe surrounded the cell and acted as both a temperature guard against radial heat losses and as protection against pore fluids if the asbestos-cement pipe fails. Heaters were located on the top, centre and bottom of the guard and the cold end also contained a water-fed cooling coil. The cell assembly was compressed by two 24" 600-pound flanges which used 12 studs to axially load the system. The flanges had welded-on rings to contain the steel pipe guard. Asbestos-cement pads were used between the flanges and the heating/cooling heads as high strength thermal insulation. Rock wool insulation was installed between the cell walls and the guard, and an insulating cap of fiberglass surrounded the entire assembly.

There were two groups of heaters: the main heating plates and the guard heaters. The main heater plates, as shown in Figure A.4, were two identical 635 mm diameter, 12 mm thick discs that contained coiled tubular electric heaters embedded in Thermon heat transfer cement and enclosed in stainless steel. Stainless steel spacers filled the areas between heaters and provided the required compressive strength. There were two separate heaters inside each heating plate, one heating the inner 381 mm diameter and the other heating the outer annulus. The heaters were run by computer-controlled power

controllers and operated at either 103 VAC or 260 VAC. On 260 VAC the maximum total power consumption of both main heating plates was 15 kW.

The guard heaters were metal clad electric bar heaters clamped around the hot end, the centre, and the cold end of the guard. These ran on 120 VAC and consumed up to 2000 watts. Control was accomplished with three solid state temperature controllers, one for each heater.

The cell heat transfer fluid circuits are shown in Figure A5. Two cooling fluids were used, Dow Corning 210H, a high temperature silicone heat transfer oil, and water. The oil was pumped and kept at a constant high temperature by a Haake N-3B circulator, and was run through the 25 mm thick stainless steel cooling plate, shown in Figure A.6, contained in the lower heating/cooling head. Cooling water was normally used on the cold upper end of the cell and also ran through a cooling plate. The cooling plates had three parallel counter-current paths inside them. Water was also used to cool the low temperature end of the guard pipe. The guard cooler was made of flattened 12.7 mm diameter copper tubing wound onto the guard and then embedded in Thermon heat transfer cement.

A schematic diagram of the pore fluid control system is shown in Figure A.7. Pore fluids were contained in an expansion tank which was connected via a manifold to six injection ports in each of the sealing plates contained in the heating/cooling heads. Pore pressure was maintained by high pressure nitrogen gas acting on the expansion tank pore fluids. The head of pore fluid inside the expansion tank was measured by a Rosemount differential pressure transmitter and the pore fluid pressure was measured by a Rosemount absolute pressure transmitter. A low pressure nitrogen blanket was maintained over the circulator in order to reduce oil oxidation at high temperatures. A high pressure nitrogen blanket was maintained on a sample cylinder filled with oil connected to the overburden assembly. The oil pressure forced a piston down, applying the overburden to the cell contents.

A.2 Cell Monitoring and Control

Monitoring and control of the heat transfer cell was handled by a Hewlett-Packard 3054A data acquisition and control system with an uninterruptable power supply. The 3054A system included a 3456A digit voltmeter with 6 1/2 digit capability and a 3497A multiplexer with a 3498A multiplexer extender. The total capacity of the multiplexers was 15 data acquisition and control cards. The system used three software thermocouple-

compensated 20-channel multiplexer cards, two uncompensated 20-channel multiplexer cards, one 8-channel actuator output card and two 2-channel programmable 0-20 mA current supply cards. The 3054A was controlled by a HP85B computer through an HPIB bus.

Temperature measurements throughout the cell were made by E-type thermocouples monitored using the three software thermocouple-compensated multiplexer cards. A typical layout for the major temperature measurement points is shown in Figure A.8. Thermocouples were initially calibrated both by using a Hewlett-Packard quartz thermometer in a stable ice or oil bath for temperatures up to 150°C, and by using a high purity (ACS certified) tin solidification bath for a 231°C calibration. The special limits of error wire was found to be adequately accurate and calibration was discontinued.

Pressure measurements were taken with two Rosemount Alphaline 4000 pressure transmitters powered by a Hammond 24 VDC supply. The output currents of 4-20 mA from the transmitters was converted to 0.2 - 1.0 VDC by two precision 50 ohm resistors and the voltages were read by channels two and three of the first software thermocouple-compensated multiplexer card. Channel one of the first software thermocouple-compensated multiplexer card recorded the on or off state of the Haake circulator.

The heat flux meters, shown in Figure A.9, were grooved Colorceran discs with thermocouples glued into the grooves with silicone adhesive. The leads for the heat flux meters ran through the copper moderating plate, through the sealing plate, and exited through teflon and silicone rubber pressure seals.

The probes for monitoring sample temperatures are shown in Figure A.10. The probes were 3.2 mm stainless steel tubing with E-type thermocouples at the measurement points. The temperature sensor leads were brought through ports in the cell wall.

The monitoring and control program for this system was written in HP Basic and utilized HP-supplied subroutines wherever possible. The computer system first warned the operator and then aborted the experiment if the pore fluid pressure or differential pressure in the pore fluid expansion tank varied beyond user-selected limits. An experiment was also aborted if the Haake circulator shut down, if temperature variations across the sealing plate exceeded user-selected limits, or if the user requested a shut-down.

During normal operation the computer system continuously read only that data necessary for main heater control and abort testing. At user selectable time steps the system read and stored, on tape, all sensor output. Upon a status request the system read and printed only the most significant data. Upon a data request the system read and stored, on tape, all sensor output.

A printout of the stored data occurred when an experiment was aborted. The program did not permit sealing plate set point temperatures to be modified while the experiment was underway.

The Haake cooling oil circulator was individually controlled and only reported its on or off condition to the computer. This was accomplished by the closing or opening of an integral relay. When closed the relay caused a 24 VDC reading to be placed on channel 1 of the first software thermocouple-compensated card.

The power system for the cell is shown in Figure A.11 and used both the actuator output card to control the system relays, and the current supply cards to control the main heater power controllers. Main heater control was accomplished by PID control and by voltage selection. The PID control had two rates of gain: a high rate for far from the set point, and a very low rate for close to the set point. The rates of gain, as well as the integral and derivative control constants, were user-selectable. The main heaters were run on either 260 VAC or 103 VAC, depending on user preference, with computer-controlled relays selecting the voltage and setting the controller for that voltage. Usually 260 VAC was used for fast warmup, and 103 VAC was used for minimum error at steady state conditions.

The guard heaters were controlled by independent temperature controllers. The temperature controllers monitored the radial temperature difference across the insulation between the guard and the cell wall. The difference was measured by a two-point thermopile with the voltage produced being amplified so that a 1°C temperature difference produced a 1 mV signal to the temperature controllers.

A.3 Operating Procedures

The first step in the experimental procedure was to install the lower Flexitallic gasket, already coated with Loctite 515, onto the lower sealing plate. Then a porous Nomex collar was slipped onto the copper moderating plate. The porous collar prevented sand from entering the gasket area and blocking up the cell walls, hence not allowing sufficient

gasket compression for a seal. Next, an O-ring made of thin walled 8 mm Teflon tubing was placed on the sealing plate inside the gasket. The O-ring was of sufficient strength to hold the cell walls off the gasket until the upper flange was put in place. The tubing then collapsed and the cell wall contacted the gasket. The Loctite 515 sealant was anaerobic and the O-ring delayed the onset of sealant set up until the lower gasket was compressed. This rather complicated lower gasket assembly is shown in Figure A.12.

The next step in the experimental procedure was to pack the heat transfer cell with clean, dry sand. This consisted of first positioning and connecting the sample temperature sensing probes and then packing sand into the cell by pouring it through a distributor constructed similarly to that described by Wygal.[53] The distributor used 5 layers of 10 mesh 304 stainless steel screen spaced 50 mm apart to distribute the sand which then fell 350 mm into the cell. The distributor was contained in a 460 mm diameter stainless steel tube. The tube was grounded to reduce static electricity effects. The resulting porosity with 40-70 mesh Unimin sand was 32.4% and the permeability was 26.5 Darcies ($26.5 \times 10^{-12}\ m^2$).

The sand pack was packed to a height such that the overburden pressure applying piston could apply pressure to the top of the pack without exceeding travel limitations. Once the sand pack was in place, the guard was put on, had its cooler connected, and had the space between the cell wall and guard tightly packed with rock wool insulation. It should be noted that at every step of the assembly process, the sensors in every new component attached were connected and tested. The upper heating/cooling head with Loctite 515 coated gasket was then placed on top of the cell. Then the asbestos-cement pad was lowered onto the upper heating/cooling head, followed by the upper flange at which point the teflon O-ring collapsed. The flange was tightened using six Holmatro hydraulic stud tensioning jacks. The jacks were placed on one set of six studs (every other stud) and the correct hydraulic pressure for the required stud stress was applied. The stud nuts were then brought into contact with the flange and the jacks removed and placed onto the other set of six studs. The process was repeated three to four times in order to very accurately and evenly tighten the studs so as not to damage the cell walls. The normal necessary hydraulic pressure was 20 MPa for a stud stress of 94 MPa and a gasket sealing stress of 40 MPa. Once the flanges were tightened, the cell was pressure tested for leaks. If no leaks were found, rock wool insulation was packed around the studs and then a large

fiberglass insulation cap of 150 mm thickness was placed over the cell.

Saturation of the pack was done by flowing three to five pore volumes of fluid through the cell by connecting into the six injection tubes. The fluid was then injected and extracted from different ports in order to thoroughly sweep the cell. The mass of the extracted fluid and the the injected fluid were measured in order to do a mass balance to find the residual saturation in the sand pack. Additionally, residual gas volume was found by injecting 100 ml of fluid and measuring the pore fluid pressure rise.

Following sample saturation, the extraction and injection manifolding, if necessary, were filled with water while the expansion tank was only partially filled with water. The pressure monitoring portion of the system was filled with water and the differential pressure transmitter was set to about 2 kPa by adjusting the height of water in the column above it. Nitrogen gas pressure was then applied to the expansion tank through a gas regulator; pressure control was achieved by very slowly bleeding the gas off.

Once the cell was pressurized, the experiment was begun and the computer-controlled data acquisition and control system was started. The general program flowchart is presented in Figure A.13 and the subroutine flowchart is shown in Figure A.14. The temperatures for the upper and lower sealing plates as well as the operating pressure and temperature limits were keyed into the computer. With the experiment in operation the hot oil circulator bath temperature and the water cooling flow rates were adjusted so that the heaters on the guard and in the heating/cooling heads would act only as trimmers. The guard heater temperature controllers were set so that the guard temperature was the same as or slightly above the temperature of the cell wall.

Once the experimental parameters were set correctly, the experiment was checked occasionally with status requests, data runs were taken at automatic intervals, and when steady state conditions exist one to four data runs were made. Steady state conditions usually required about a week to appear. The cell was brought up to operating temperatures with 260 VAC on the main heaters, and 103 VAC was then used to reduce fluctuations at steady state.

Upon completion of an experiment the computer program was aborted and a new pair of upper and lower sealing plate temperatures were selected. The pore fluid pressure was

then adjusted if necessary, to maintain pore fluids in the correct phase and a new experiment was begun. An experiment usually took 10 to 14 days to complete. Upon completion of the entire experimental series the program was aborted and the cell was cooled by completely opening the water cooler valves. The cell was then disassembled. Sampling for analysis of the cell contents was then done if necessary.

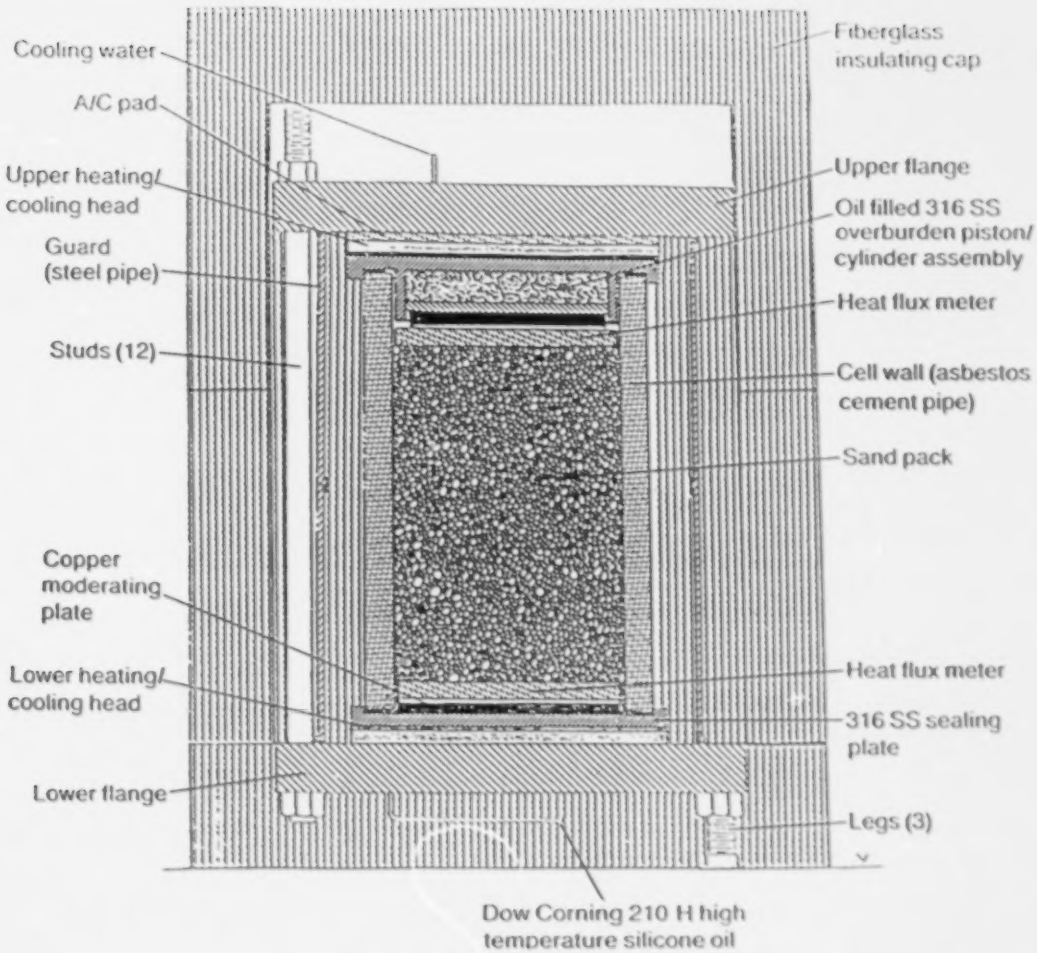

Figure A.1 Heat Transfer Cell

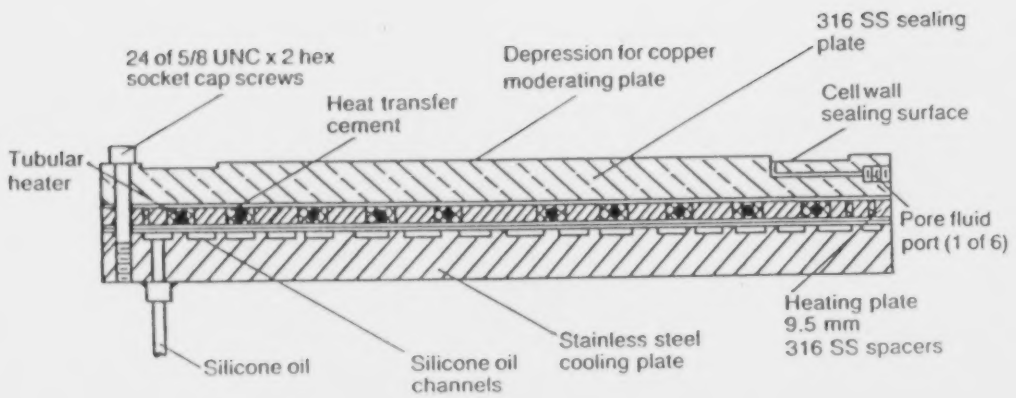
316 SS sealing plate
24 of 5/8 UNC x 2 hex socket cap screws
Depression for copper moderating plate
Heat transfer cement
Cell wall sealing surface
Tubular heater
Pore fluid port (1 of 6)
Heating plate 9.5 mm 316 SS spacers
Stainless steel cooling plate
Silicone oil
Silicone oil channels

Figure A.2 Lower Heating/Cooling Head Section

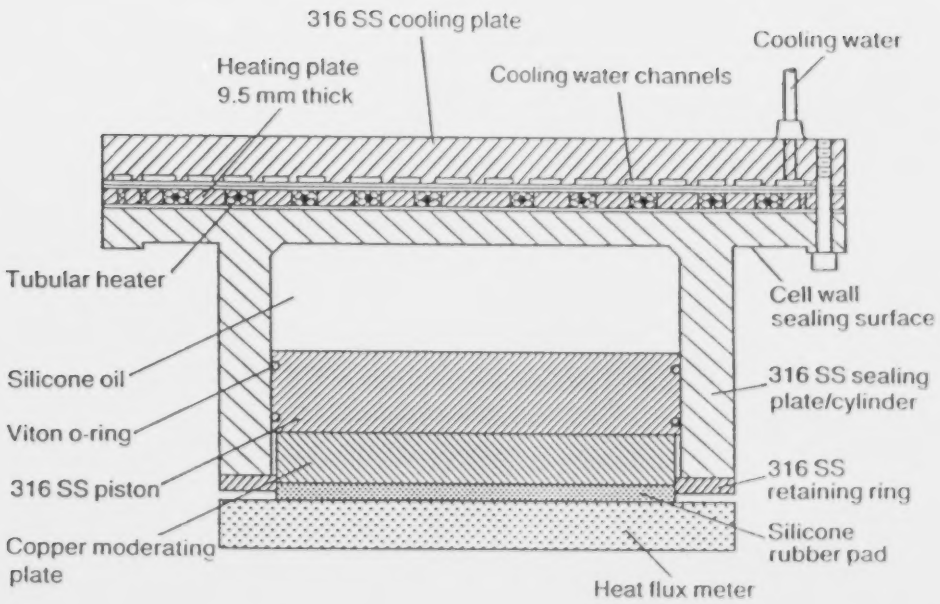

Figure A.3 Upper Heating/Cooling Head and Overburden Assembly Section

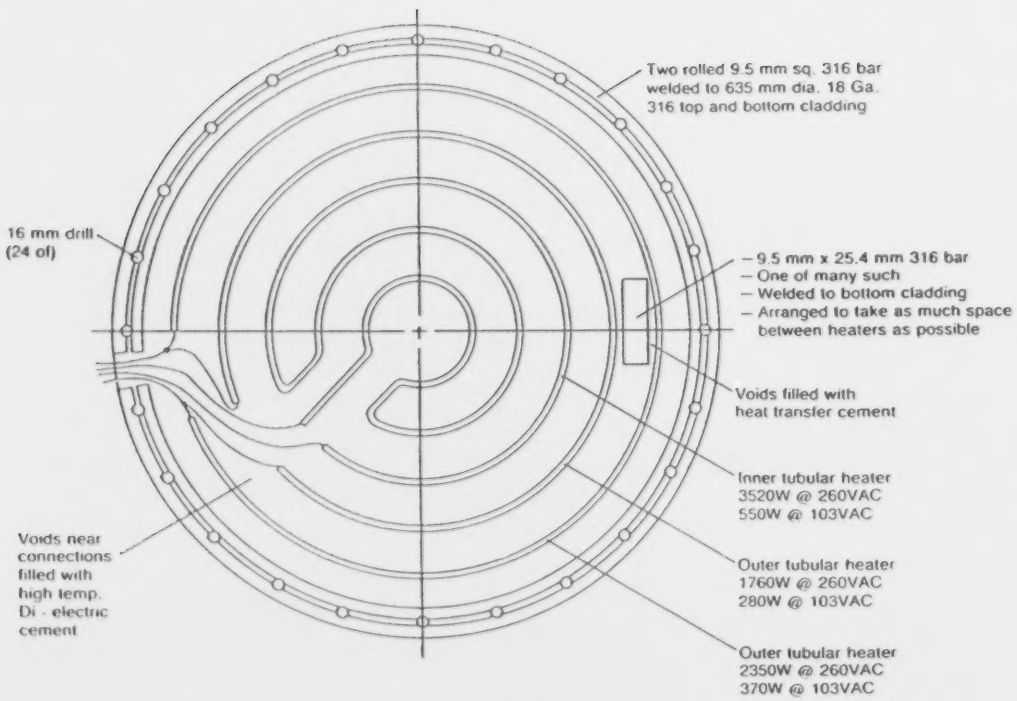

Figure A.4 Main Heater Plate

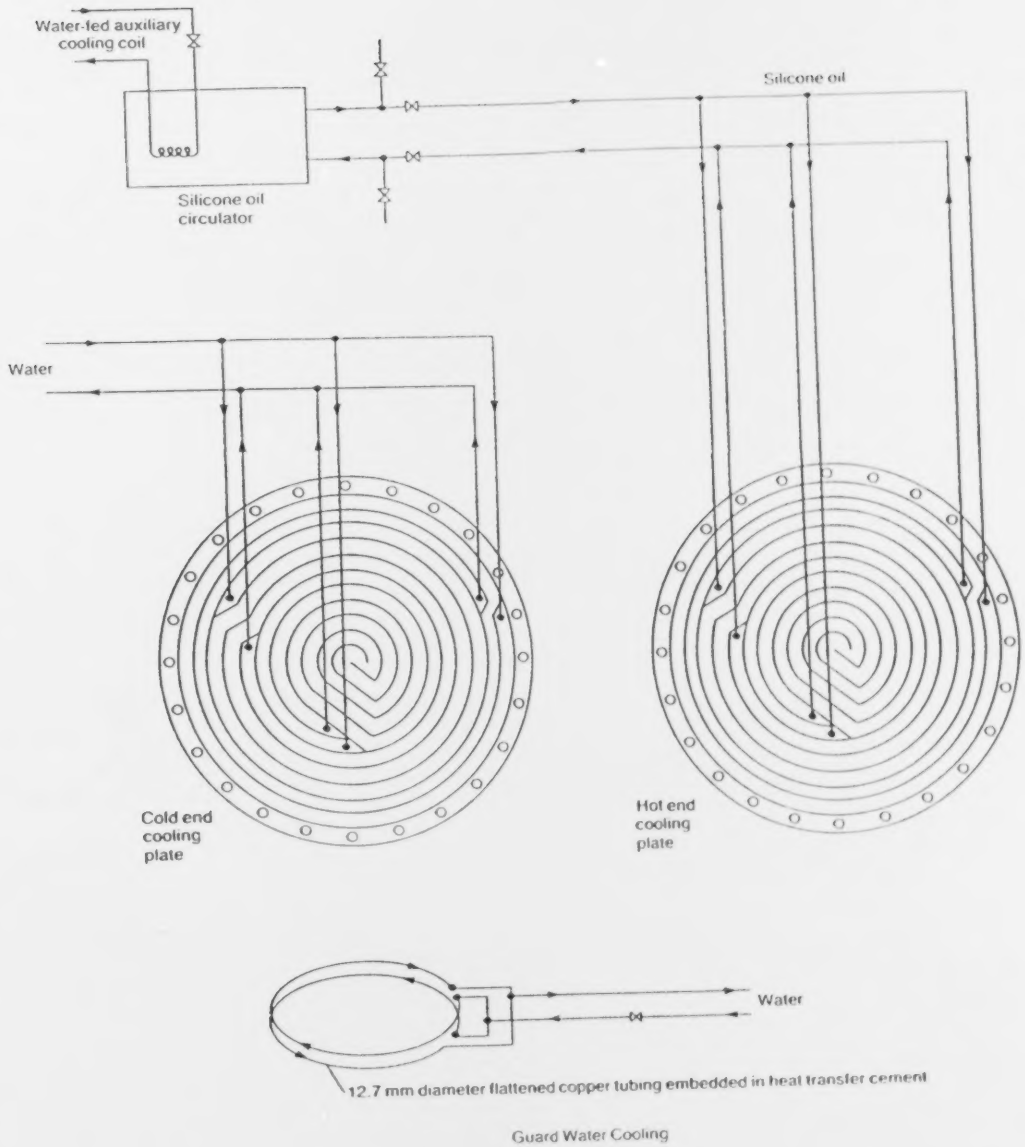

Figure A.5 Heat Transfer Fluid Circuits

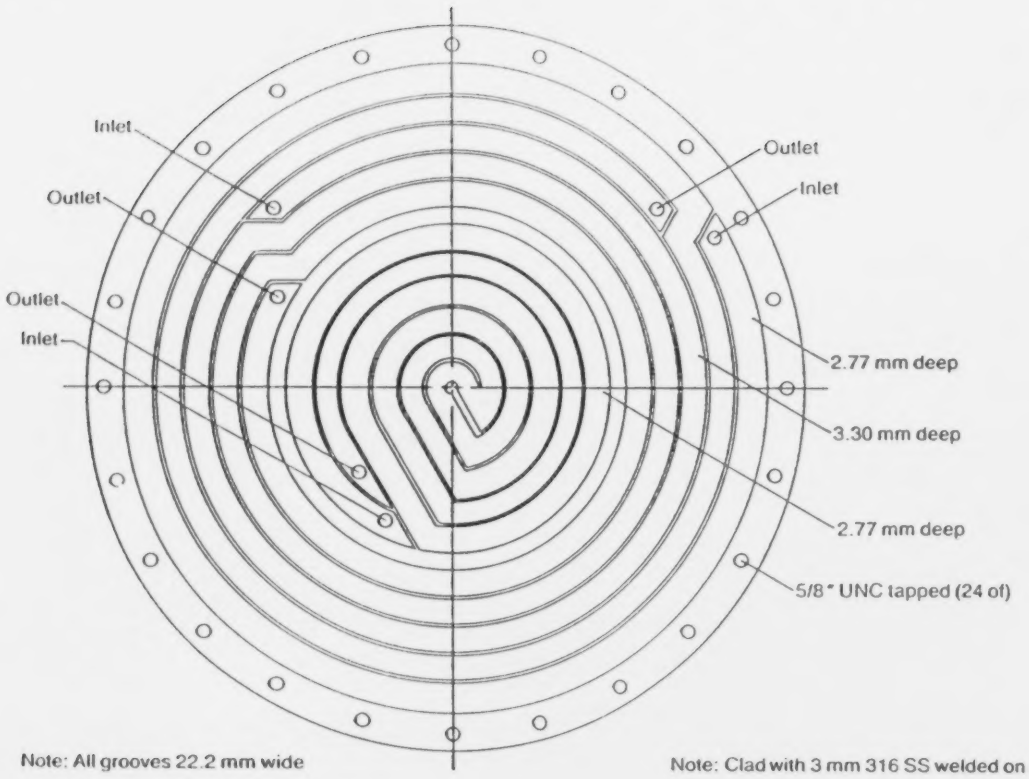

Figure A.6 Cooling Plate

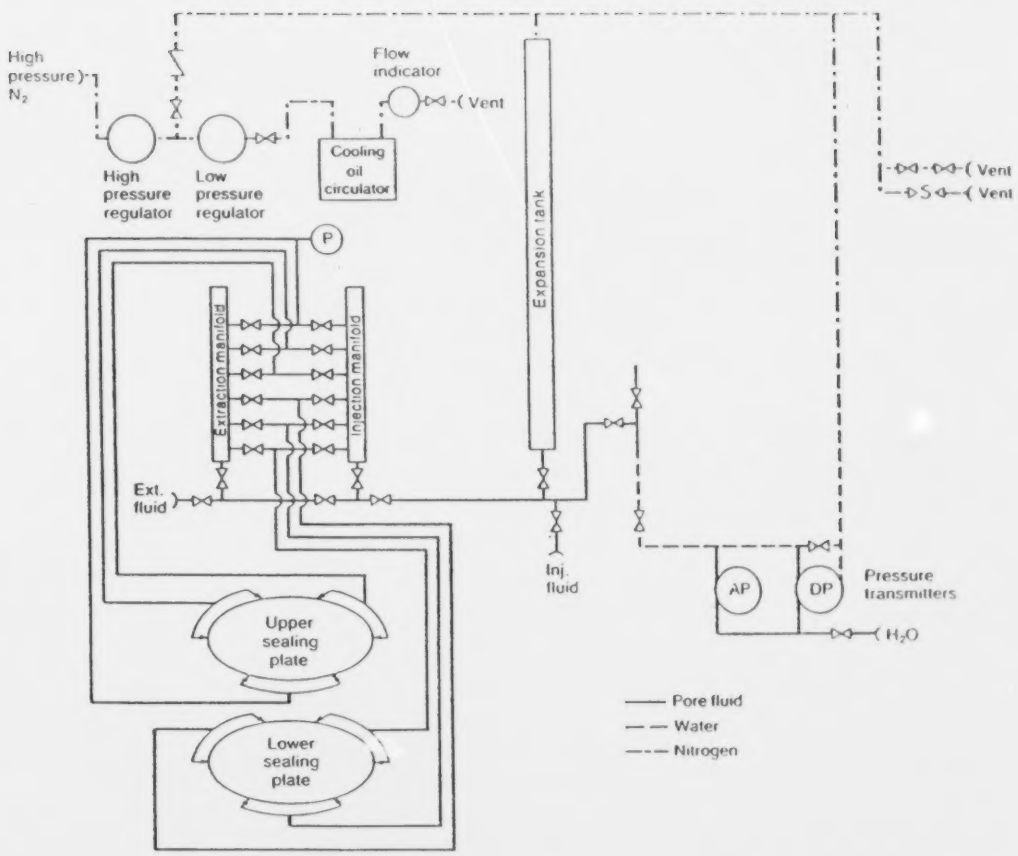

Figure A.7 Pore Fluid Control System

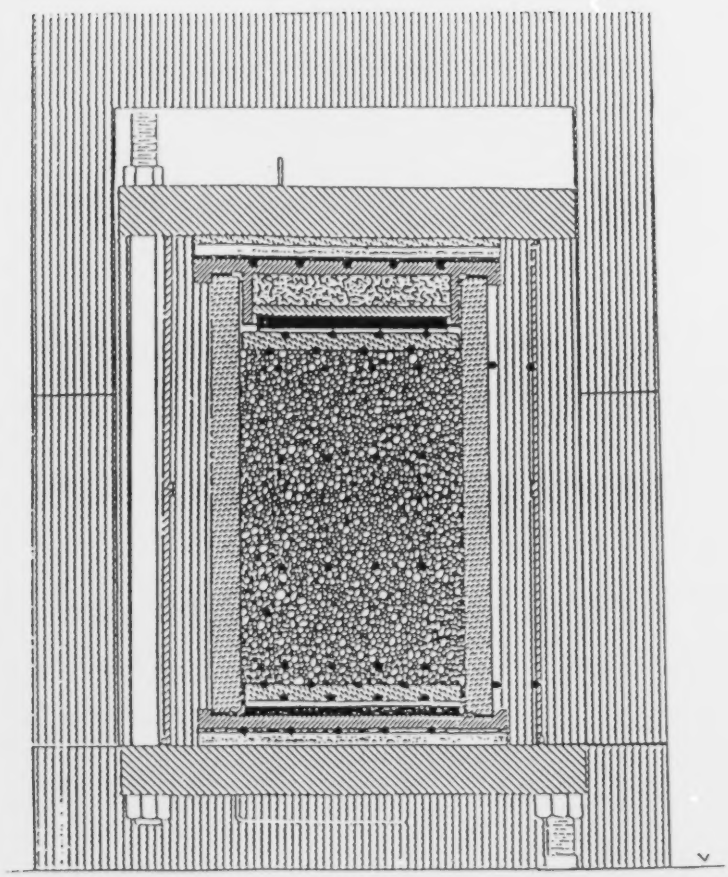

• Thermocouple - E type

Figure A.8 Primary Thermocouple Locations

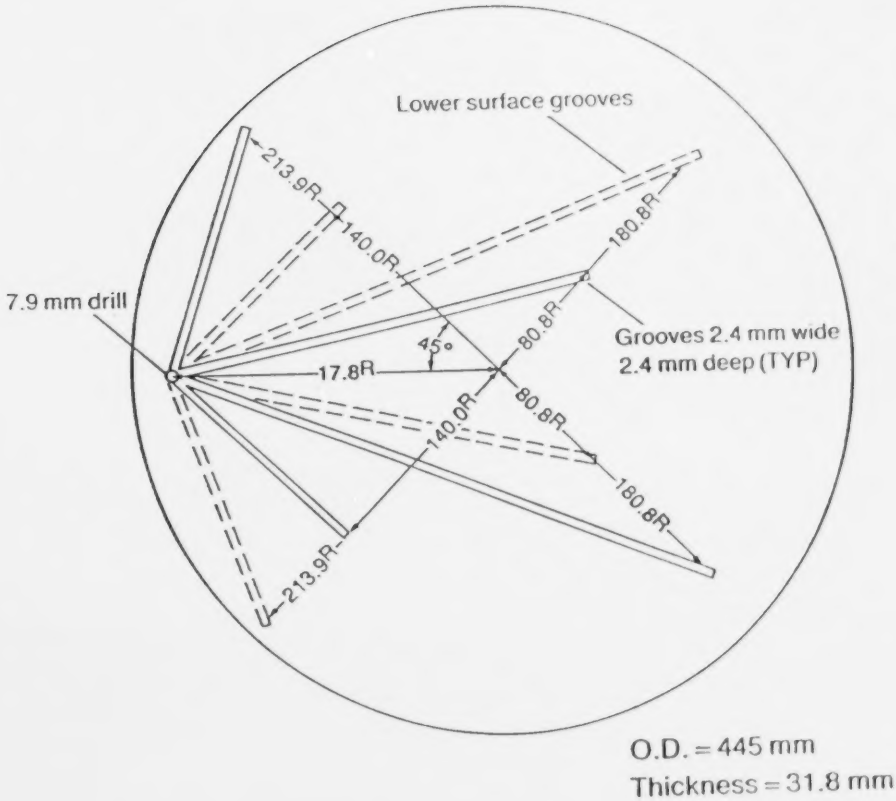

Figure A.9 Heat Flux Meter

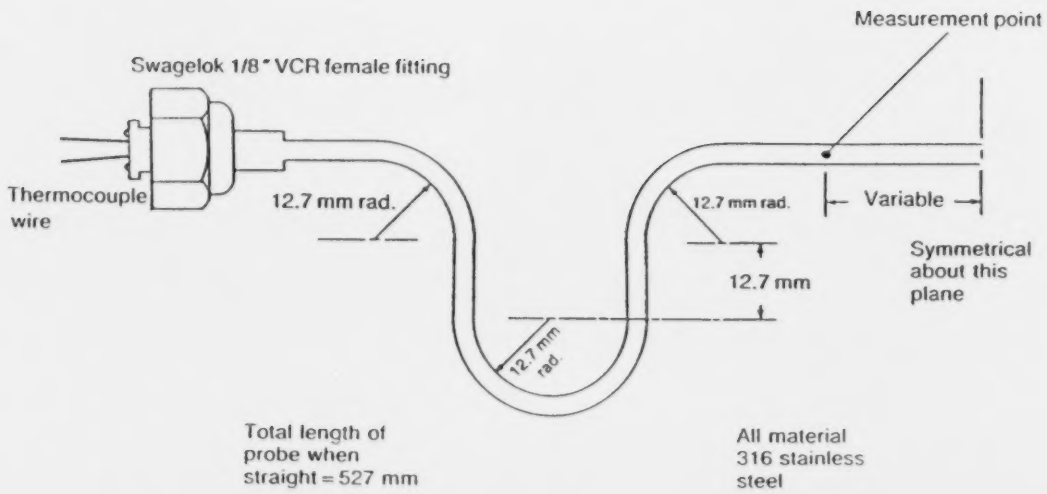

Figure A.10 Temperature Probes

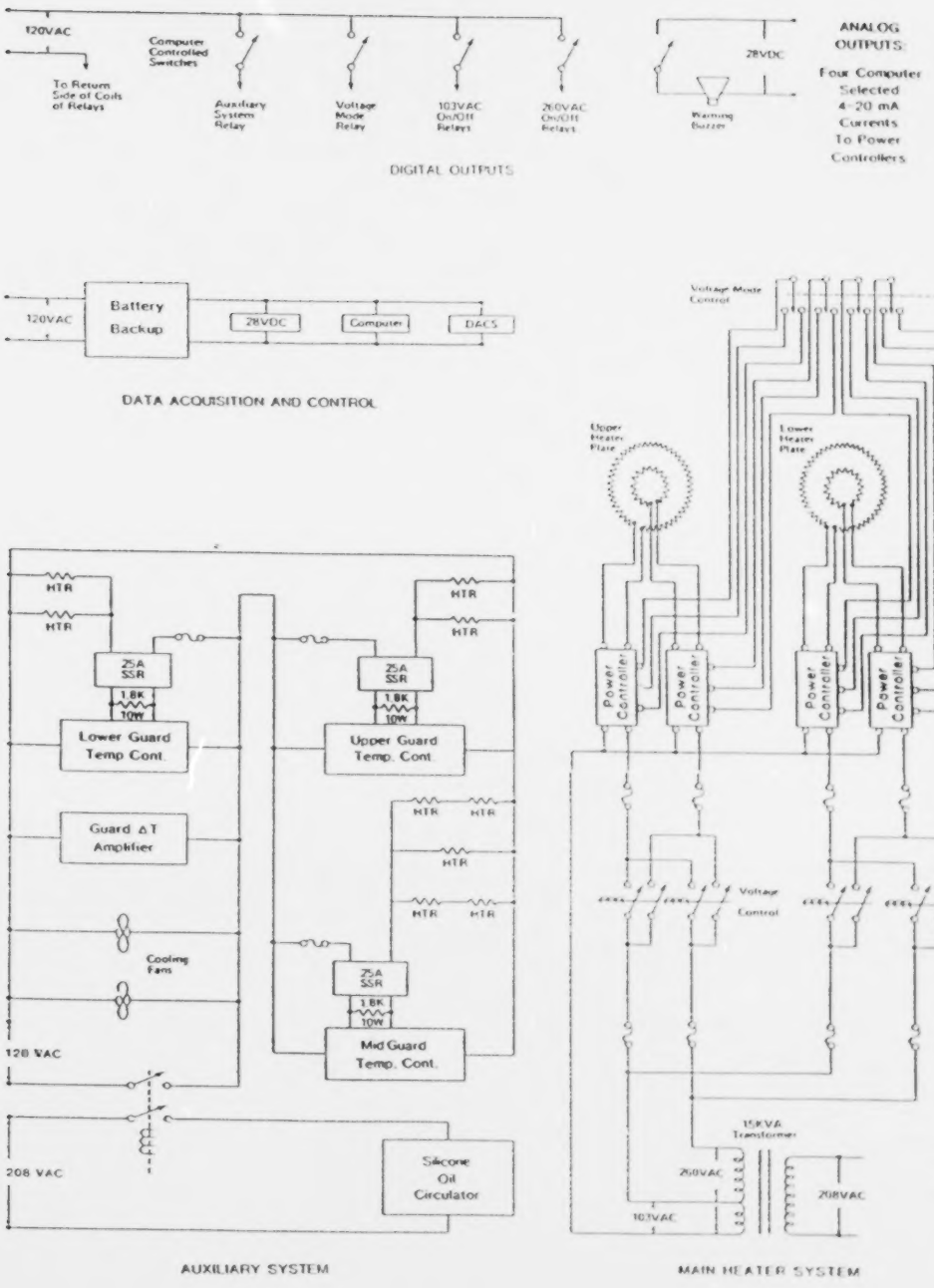

Figure A.11 Cell Power System

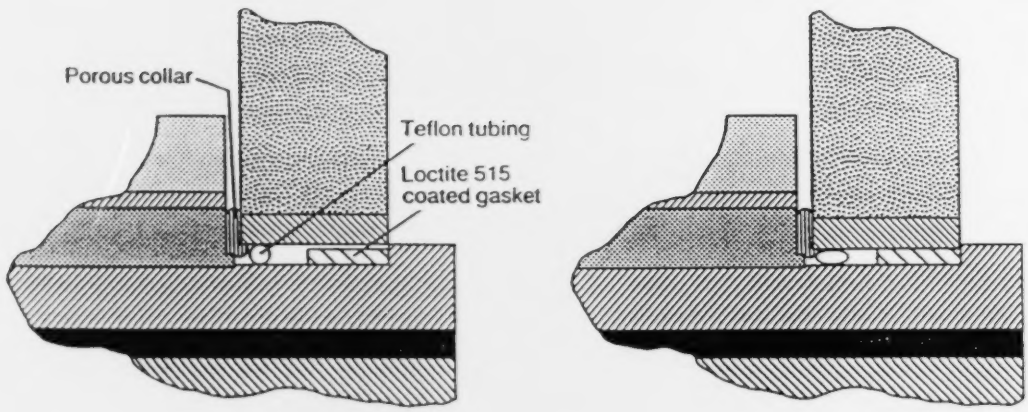

Lower gasket detail no. 1
Before compression

Lower gasket detail no. 2
After compression

Figure A.12 Lower Gasket Assembly

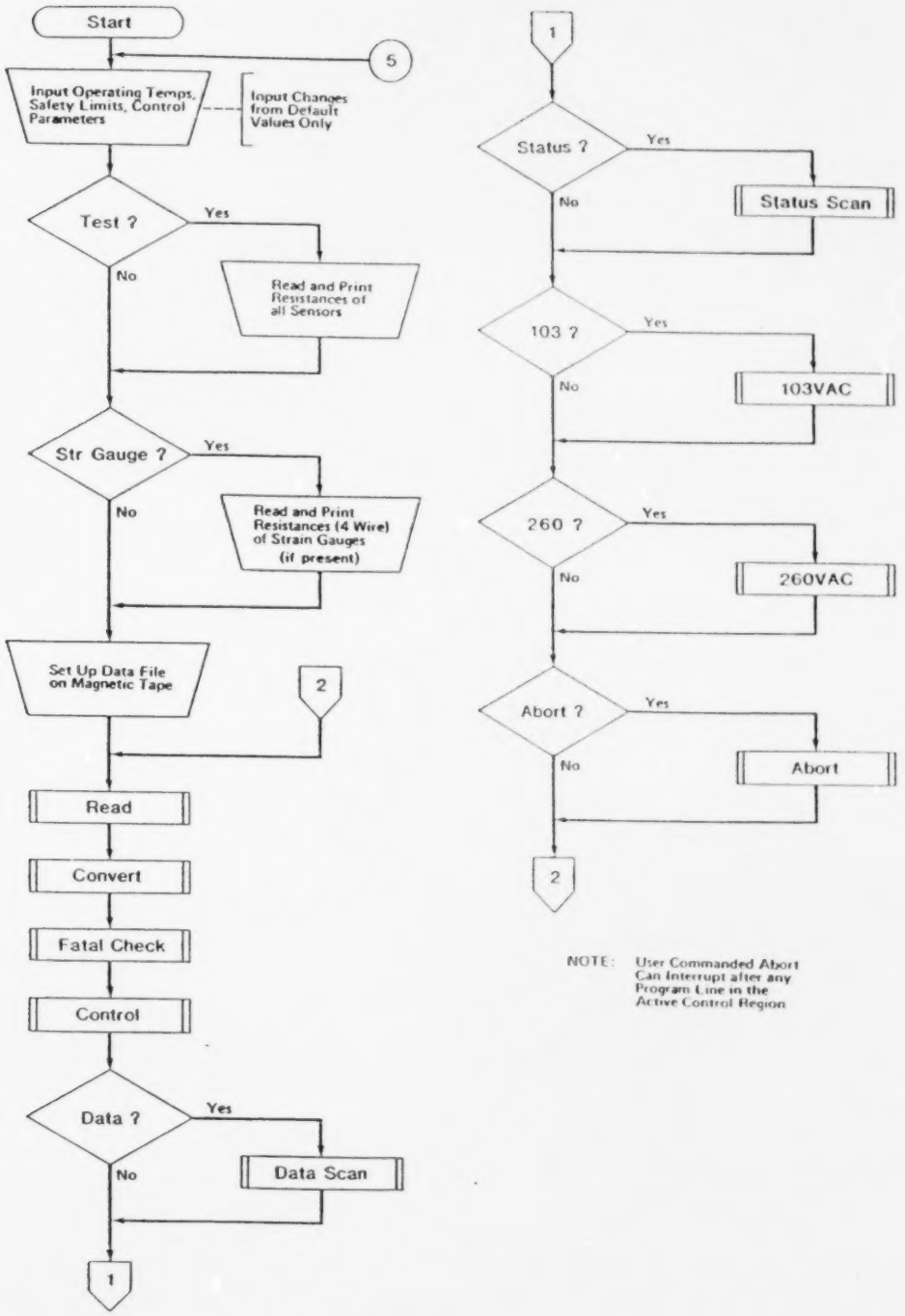

Figure A.13 Basic Flow Chart of Data Acquisition and Control Program

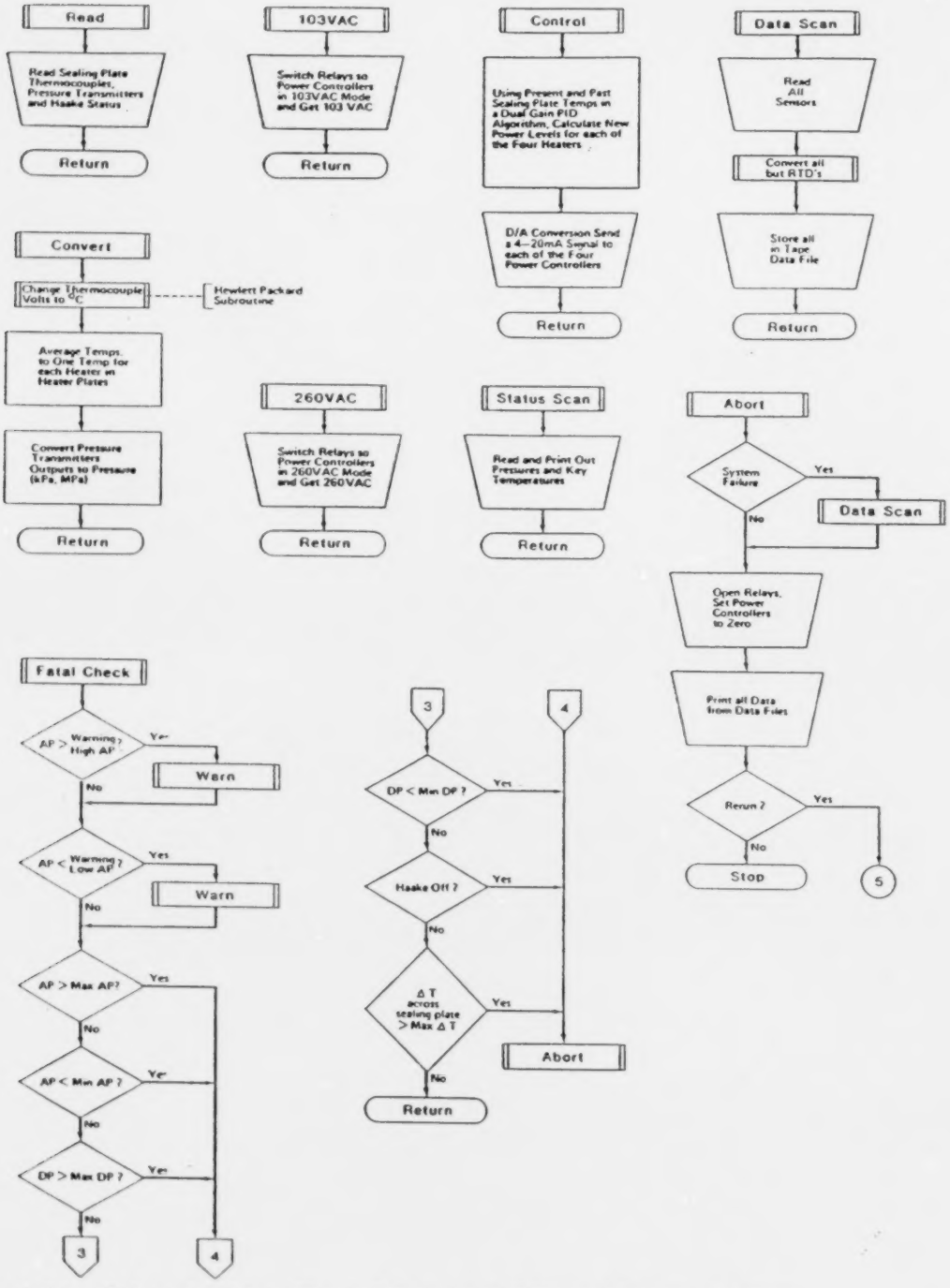

Figure A.14 Subroutine Flow Chart of Data Acquisition and Control Program

B. HEAT TRANSFER CELL CALIBRATION

Calibration of the heat transfer cell was done by analyzing the results of conduction mode experiments to allow prediction of the heat transfer rate from the temperature differences across the heat flux meters. The analysis was based on the known thermal conductivity of the water saturated sand pack used. The thermal conductivity of the water-saturated sand was measured by an independent laboratory (Tempest Geophysical Consultants) and is shown in Appendix O. The calibration analysis was done in three phases: first, a steady-state series solution ignoring wall effects; second, a steady-state numerical solution including wall effects; and third, a final steady-state series solution with a correction factor for the wall effects. The final solution will allow prediction of the heat flux without using a numerical model for each prediction.

Systematic errors in the heat transfer cell measurement of heat fluxes must be considered for an accurate calibration analysis to be done. As heat fluxes are lowered the temperature differences across the heat flux meters are reduced. However, the offset between the various thermocouples measuring this temperature difference remain the same. Hence, as the heat flux drop, the relative error in the heat flux measurement increases. Conversely, as the heat fluxes increase the complicated structure (overburden piston/cylinder assembly) above the upper heat flux meter reduces its accuracy markedly. This was due to the highly nonuniform overburden assembly forcing non-level isotherms and rendering the thermocouple measurements invalid for determining heat flux.

Four experiments were utilized for calibrating the heat transfer cell. The first two experiments were conducted with low heat fluxes and with the top of the cell hot and the bottom cold. The low heat fluxes meant a generally reduced accuracy due to thermocouple offset but allowed both top and bottom heat flux meters to be utilized. The other two experiments were typical of actual experiments and had relatively high heat fluxes and with the bottom of the cell hot and the top cold. The high heat fluxes meant a generally increased accuracy due to less relative thermocouple offset but did not allow the upper heat flux meter to be utilized. Experimental conditions and results for all four experiments are shown in Table B.1.

The sand pack thermal conductivity must be corrected from the outside measured value to compensate both for a small difference in porosity between the measured sample and the actual sand pack and for the differences in average sand pack temperature in the four experiments.

from Tempest Geophysical Consultants (Appendix O)

$$\lambda_s = \lambda_w^{\phi} \lambda_{solid}^{1-\phi}$$

λ_s = thermal conductivity of saturated sample
λ_{solid} = measured thermal conductivity of solid = 4.945 [W/m K]
λ_w = thermal conductivity of water = 0.602 [W/m K]
ϕ = porosity = 0.324
λ_s = 2.50 [W/m K] @ 26.1°C

temperature effects (from Somerton, et al[62])

$\lambda_{sT} = \lambda_{s51.7} - 0.002304\ (T-51.7°C)\ (\lambda_{s51.7} - 1.419)$
λ_{sT} = λ_s @ temperature T [°C]
$\lambda_{s51.7}$ = λ_{sT} @ 51.7°C [W/m K]

$\therefore \lambda_{sT} = 2.56 - 0.002352\ T$

$\therefore$ for water saturated samples:

$$\lambda_m = 2.56 - 0.002352\ T$$

The thermal conductivities of the sand pack for the four experiments are also shown in Table B.1.

The first phase of the calibration process is the steady-state, series analysis ignoring wall effects:

$$q = (\lambda_m \Delta T_s) / \Delta y_s = (\lambda_{hfm1} \Delta T_{hfm}) / \Delta y_{hfm}$$

where:

q	=	heat flux [W/m^2]
λ_m	=	sand pack thermal conductivity @ T_{avs} [W/m K]
T_{avs}	=	average sand pack temperature [°C]
ΔT_s	=	sand pack temperature difference [°C]
Δy_s	=	distance between thermocouples measuring ΔT_s [m]
λ_{hfm1}	=	heat flux meter thermal conductivity of phase 1 @ T_{avhfm} [W/m K]
T_{avhfm}	=	average heat flux meter temperature [°C]
ΔT_{hfm}	=	heat flux meter temperature difference [°C]
Δy_{hfm}	=	distance between thermocouples measuring ΔT_{hfm} [m]

The values of λ_{hfm1} are listed in table B.1. The dependence of λ_{hfm1} on T_{avhfm} was best represented by:

$$\lambda_{hfm1} = 1.50 - 2.05 \times 10^{-3} T_{avhfm}$$

which is also listed in Table B.1. The accuracy and range of applicability of the calibration was improved by breaking the calibration relationship up into its various parts, i.e. parallel effect of walls, variation of thermal conductivity of heat flux meter material with temperature and undetermined systematic errors. However, the thermal conductivity of the heat flux meter material was not known at elevated temperatures, at the time the cell was being calibrated, and it was lumped in with the other undetermined errors. The parallel effect of the walls was determined by a combined numerical-analytic technique. A steady-state, finite difference numerical model which included the cell walls was operated with the given sand pack and wall thermal conductivity and λ_{hfm1} heat flux meter thermal conductivity. The results of the numerical model were then analyzed using a simple series method in order to determine the parallel wall correction factor (PW). The effect of the walls on the cell calibration should, physically, be only a function of heat flux (ΔT_{hfm}), as the wall thermal conductivity was considered constant. Therefore, the parallel wall correction factor was:

$$PW = \{C_1 + C_2 \Delta T_{hfm}\}$$

and using the numerical results:

$$q = (\lambda_m \Delta T_s) / \Delta y_s = (\lambda_{hfm1} \Delta T_{hfm} \bullet PW) / \Delta y_{hfm}$$

A least squares fit for the four numerical runs yielded:

$$PW = 1.0137 + 1.623 \text{ X } 10^{-3} \Delta T_{hfm}$$

When PW was applied to the experimental results one obtained:

$$\lambda_{hfm2} = \lambda_{hfm1} / PW$$

The values of λ_{hfm2} are listed in Table B.1. The third and final phase of the calibration was to find a relationship that predicted λ_{hfm2}. This relationship was a combination of the heat flux meter material thermal conductivity (λ_{hfmm}), which was temperature dependent (and unknown at the time of calibration) :

$$\lambda_{hfmm} = \lambda_{hfmm} @ T_0 + C_3 \bullet T_{avhfm}$$

and the true calibration relationship (CR), which was primarily a function of heat flux (ΔT_{hfm}):

$$CR = C_4 + C_5 \bullet \Delta T_{hfm}$$

Combining the two relationships yielded:

$$\lambda_{hfm2} = \lambda_{hfmm} \bullet CR$$

$$= C_4 \bullet \lambda_{hfmm} + C_3 \bullet C_4 \bullet T_{avhfm} + C_5 \bullet \lambda_{hfmm} \bullet \Delta T_{hfm} + \text{higher order terms}$$

$$\therefore \quad \lambda_{hfm2} = C_6 + C_7 \bullet T_{avhfm} + C_8 \bullet \Delta T_{hfm}$$

a least squares fit with the experiment results yields:

$$\lambda_{hfm2} = 1.446 - 5.7 \times 10^{-3} \Delta T_{hfm} - 1.55 \times 10^{-3} T_{hfm}$$

combining with PW gives:

$$\lambda_{hfm3} = PW \bullet \lambda_{hfm2}$$

The final calibration equation is thus:

$$\lambda_{hfm3} = (1.0137 + 1.623 \times 10^{-3} \Delta T_{hfm}) \bullet (1.446 - 5.7 \times 10^{-3} \Delta T_{hfm} - 1.55 \times 10^{-3} T_{hfm})$$

The values of λ_{hfm3} are listed in Table B.1.

Table B.1 Heat Transfer Cell Calibration

Description	W/S #1	W/S #2	W/S #3	W/S #4
T_s (top) [°C]	74.85	115.94	26.34	29.12
T_s (bottom) [°C]	62.51	93.18	108.04	128.63
ΔT_s [°C]	12.34	22.76	81.70	99.51
T_{avs} [°C]	68.68	104.56	67.19	78.88
λ_m [W/m K]	1.353	1.294	1.256	1.205
λ_{hfm1} [W/m K]	1.359	1.283	1.259	1.209
λ_{hfm2} [W/m K]	1.332	1.272	1.224	1.171
λ_{hfm3} [W/m K]	1.354	1.293	1.253	1.206

C. SINGLE FLUID: ONSET OF CONVECTION

The derivation presented here is based on the work of Joseph,[30] Bau[14], and Zebib.[23]

Conservation of Momentum:

$$\frac{\rho^*}{\phi_p}\frac{\partial \tilde{u}_b^*}{\partial t^*} = \tilde{F}^* - \nabla P^* - \frac{\mu}{k}\tilde{u}_b^* \qquad \text{C.1}$$

Conservation of Mass:

$$\frac{\partial \rho^*}{\partial t^*} + \nabla^* \cdot (\rho \tilde{u}^*) = 0 \qquad \text{C.2}$$

Conservation of Energy:

$$(\rho C_p)_m \frac{\partial T}{\partial t^*} + \phi(\rho C_p)_f \tilde{u}^* \cdot \nabla^* T = \lambda_m \nabla^{*2} T \qquad \text{C.3}$$

where

$( )_m$ = saturated media values

$( )_f$ = fluid values.

Darcy's Law:

$$\tilde{u}_b^* = -\frac{k}{\mu}\left(\nabla^* P^* + \rho g_a \hat{k}\right) \qquad \text{C.4}$$

Note: $\tilde{u}_b^*$ is the bulk velocity

The Boussinesq Approximation:[25]

- density variations modify only effects of gravity.

$$\therefore \; dilation = 0 \quad \therefore \quad div\, \tilde{u}^* = 0$$

$$\rho = \rho_0[1 - \beta(T - T_0)]$$

where $(\ )_0$ = condition at upper surface

$(\ )_1$ = condition at lower surface

also

$$\tilde{F}^* = -\rho g_a \hat{k}$$

$$\frac{\partial \rho}{\partial t^*} = 0$$

$$\nabla^* \cdot (\rho \tilde{u}^*) = \rho \nabla^* \cdot \tilde{u}^*$$

applying the Bousinesq Approximation to C.1 yields:

$$\frac{\rho_o^*}{\phi_p} \frac{\partial \tilde{u}_b^*}{\partial t^*} = -\nabla^* P^* + \rho_o g_a \hat{k} \beta (T - T_o) - \frac{\mu}{k} \tilde{u}_b^* - \rho_o g_a \hat{k} \qquad \text{C.5}$$

and applying Boussinesq Approximation to C.2 yields:

$$\nabla^* \cdot \tilde{u}^* = 0 \qquad \text{C.6}$$

Re-arrange temperature profile:

$$T = T_o - (T_1 - T_0)\frac{z^*}{L} + (T_1 - T_0)\theta$$

therefore:

$$\frac{\partial T}{\partial t^*} = (T_1 - T_0)\frac{\partial \theta}{\partial t^*}$$

$$\nabla^* T = -\frac{(T_1 - T_0)}{L}\hat{k} + (T_1 - T_0)\nabla^*\theta$$

$$T - T_0 = (T_1 - T_0)\left\{\theta - \frac{z^*}{L}\right\}$$

$$\nabla^{*2} T = (T_1 - T_0)\nabla^{*2}\theta$$

Rewrite the pressure profile as:

$$p^* = P^* + \rho_0 g_a\left[z^* + \frac{\beta(T_1 - T_0)(z^*)^2}{2L}\right] + P_o^*$$

where: P_o^* = constant, applied pressure

$$\nabla^* p^* = \nabla^* P^* + \rho_0 g_a\left[\hat{k} + \frac{\beta(T_1 - T_o)}{L} z^* \hat{k}\right] + 0$$

Substitute temperature profile and pressure profile into C.5

$$\frac{\rho_0^*}{\phi_p}\frac{\partial \tilde{u}_b^*}{\partial t^*} = -\nabla^* P^* + \rho_0 g_a \beta (T_1 - T_0)\left\{\theta - \frac{z^*}{L}\right\}\hat{k}$$

$$\frac{\rho_o^*}{\phi_p}\frac{\partial \tilde{u}_b^*}{\partial t^*} = -\left[\nabla^* P^* + \hat{k}\rho_0 g_a\left[\beta (T_1 - T_0)\frac{z^*}{L} + 1\right]\right] + \rho_0 g_a \beta (T_1 - T_0)\theta\hat{k} - \frac{\mu}{k}\tilde{u}_b^*$$

$$\frac{\rho_0^*}{\phi_p}\frac{\partial \tilde{u}_b^*}{\partial t^*} = -\nabla^* p^* + \rho_0 g_a \beta (T_1 - T_0)\theta\hat{k} - \frac{\mu}{k}\tilde{u}_b^* \qquad \text{C.7}$$

Substitute temperature profile into C.3

$$(\rho C_p)_m \frac{\partial \theta}{\partial t^*} + \phi(\rho C_p)_f \tilde{u}^* \cdot \left(\nabla^* \theta - \frac{1}{L}\hat{k}\right) = \lambda_m \nabla^{*2}\theta \qquad \text{C.8}$$

note: $\phi\tilde{u}^* = \tilde{u}_b^*$ *on volume average*

represent viscosity variation as:

$$\mu = \mu_0\left(\frac{\mu_0}{\mu_1}\right)^{-\left[\frac{T-T_0}{T_1-T_0}\right]}$$

$$\frac{T-T_0}{T_1-T_0} = \theta - \frac{z^*}{L}$$

$$\mu = \mu_0\left(\frac{\mu_0}{\mu_1}\right)^{\left(\frac{z^*}{L}-\theta\right)}$$

$$\mu = \mu_0\left(\frac{\mu_0}{\mu_1}\right)^{z^*/L}\left(\frac{\mu_1}{\mu_0}\right)^{\theta}$$

substitute into C.7

$$\frac{\rho_0^*}{\phi_p}\frac{\partial \tilde{u}_b^*}{\partial t^*} = -\nabla^* p^* + \rho_0 g_a \beta (T_1 - T_0)\theta \hat{k} - \frac{\mu_0}{k}\left(\frac{\mu_0}{\mu_1}\right)^{\left(\frac{z^*}{L}-\theta\right)} \tilde{u}_b^* \qquad \text{C.9}$$

Normalize:

$$\tilde{x} = \frac{\tilde{x}^*}{L}; \tilde{u} = \frac{\tilde{u}^* \rho_f C_{pf} L}{\lambda_m \sqrt{Ra}}$$

$$t = \frac{t^* \lambda_m}{L^2 \rho_{0f} C_{pf}}$$

$$p = \frac{k \rho_{0f} C_{pf}}{\mu_0 \lambda_m} p^*$$

substitute into C.9

$$\frac{1}{\phi_p}\frac{\lambda_m^2 \sqrt{Ra}}{C_{pf} L^3 \rho_{0f} C_{pf}}\frac{\partial \tilde{u}_b}{\partial t} = -\frac{\mu_0 \lambda_m}{k \rho_{0f} C_{pf} L}\nabla p$$

$$+ \rho_0 g_a \beta (T_1 - T_0)\theta \hat{k}$$

$$-\frac{\mu_0}{k}\left(\frac{\mu_0}{\mu_1}\right)^{z-\theta}\frac{\lambda_m \sqrt{Ra}}{\rho_{of} C_{pf} L}$$

multiply by:

$$\frac{kL\rho_{of}C_{pf}}{\mu_0\lambda_m\sqrt{Ra}}$$

$$\frac{1}{\phi_p}\frac{k\lambda_m}{L^2C_{pf}\mu_0}\frac{\partial\tilde{u}_b}{\partial t}=-\frac{1}{\sqrt{Ra}}\nabla p+\frac{\rho_{0f}^2 g_a\beta(T_1-T_0)kLC_{pf}}{\mu_0\lambda_m\sqrt{Ra}}\theta\hat{k}-\left(\frac{\mu_0}{\mu_1}\right)^{z-\theta}\tilde{u}_b$$

for porous media under consideration

$$B=\frac{k\lambda_m}{L^2C_{pf}\mu_0}\to 0$$

therefore:

$$0=-\frac{1}{\sqrt{Ra}}\nabla p+Ra^{1/2}\theta\hat{k}-\left(\frac{\mu_0}{\mu_1}\right)^{(z-\theta)}\tilde{u}_b$$

note:

$$\frac{\mu_0}{\mu_1}=\mu_R$$

$$0=-(Ra)^{-1/2}\nabla p+Ra^{-1/2}\theta\hat{k}-\mu_R^{z-\theta}\tilde{u}_b \qquad \text{C.10}$$

normalize C.8

$$\frac{(\rho C_p)_m \lambda_m}{L^2 \rho_{0f} C_{pf}} \frac{\partial \theta}{\partial t} + \frac{\rho_{0f} C_{pf} \lambda_m \sqrt{Ra}\tilde{u}_b}{\rho_{0f} C_{pf} L} \cdot \left(\frac{1}{L} \nabla\theta - \frac{1}{L} \hat{k} \right) = \frac{\lambda_m}{L^2} \nabla^2 \theta$$

$$\frac{(\rho C_p)_m}{(\rho_0 C_p)_f} \frac{\partial \theta}{\partial t} + Ra^{1/2} \tilde{u}_b \cdot (\nabla\theta - \hat{k}) = \nabla^2 \theta$$

$$\frac{(\rho C_p)_m}{(\rho_0 C_p)_f} = \gamma$$

$$\gamma \frac{\partial \theta}{\partial t} + Ra^{1/2} \tilde{u}_b \cdot (\nabla\theta - \hat{k}) = \nabla^2 \theta \qquad \text{C.11}$$

$$\nabla \cdot \tilde{u}_b = 0 \qquad \text{C.12}$$

substitute into C.5

$$Ra^{1/2} \tilde{u}_b \cdot (\nabla\theta - \hat{k}) = \nabla^2 \theta \qquad \text{C.13}$$

linearizing C.13 given:

$$\frac{\partial \theta}{\partial x} \ll 1; \frac{\partial \theta}{\partial y} \ll 1; \frac{\partial \theta}{\partial t} \ll 1$$

then

$$-Ra^{1/2}\tilde{u}_b \cdot \hat{k} = \nabla^2\theta$$

note:

$$\omega = \tilde{u}_b \cdot \hat{k}$$

$$-Ra^{1/2}\omega = \nabla^2\theta \qquad \text{C.14}$$

$\nabla \times C.10$ *yields*:

$$0 = -(Ra)^{-1/2}\nabla\times\nabla p + Ra^{1/2}\nabla\times\theta\hat{k} - \nabla\times\left(\mu_R^{z-\theta}\tilde{u}_b\right)$$

$$\nabla\times\nabla p = 0$$

$\nabla\times(\nabla\times C.10)$ *yields*

$$0 = Ra^{1/2}\nabla\times(\nabla\times\theta\hat{k}) - \nabla\times\left(\nabla\times\left(\mu_R^{z-\theta}\tilde{u}_b\right)\right)$$

in Cartesian coordiantes

$$\nabla\times(\nabla\times\theta\hat{k}) = -\frac{\partial^2\theta}{\partial x\partial z}\hat{i} + \frac{\partial^2\theta}{\partial x\partial z}\hat{j} - \left(\frac{\partial^2\theta}{\partial x^2} + \frac{\partial^2\theta}{\partial y^2}\right)\hat{k}$$

$$\nabla\times\left(\nabla\times\left(\mu_R^{z-\theta}\tilde{u}_b\right)\right) = \nabla\left(\nabla\cdot\left(\mu_R^{z-\theta}\tilde{u}_b\right)\right) - \nabla^2\left(\mu_R^{z-\theta}\tilde{u}_b\right)$$

$$\nabla\cdot\left(\mu_R^{z-\theta}\tilde{u}_b\right) = \left(\nabla\mu_R^{z-\theta}\right)\cdot\tilde{u}_b + \mu_R^{z-\theta}\left(\nabla\cdot\tilde{u}_b\right)$$

Note C.12:

$$\nabla \cdot \tilde{u}_b = 0$$

$$\left(\nabla \mu_R^{z-\theta}\right) \cdot \tilde{u}_b = \mu_R^{z-\theta}\left(\ln \mu_R^{z-\theta}\right)\hat{k} \cdot \tilde{u}_b = \mu_R^{z-\theta}\left(\ln \mu_R^{z-\theta}\right)\omega$$

$$\nabla\left(\nabla \cdot \left(\mu_R^{z-\theta}\tilde{u}_b\right)\right) = \nabla\left(\mu_R^{z-\theta}\left(\ln \mu_R^{z-\theta}\right)\omega\right)$$

$$\nabla \times \left(\nabla \times \left(\mu_R^{z-\theta}\tilde{u}_b\right)\right) = \nabla\left(\mu_R^{z-\theta}\left(\ln \mu_R^{z-\theta}\right)\omega\right) - \nabla^2\left(\mu_R^{z-\theta}\tilde{u}_b\right)$$

consider only the $\hat{k}$ component

note

$$\nabla_1^2() = \nabla^2() - \frac{\partial^2()}{\partial z^2}$$

$$\hat{k} \cdot \left(\nabla \times \left(\nabla \times \theta \hat{k}\right)\right) = -\nabla_1^2 \theta$$

$$\hat{k} \cdot \left(\nabla \times \left(\nabla \times \left(\mu_R^{z-\theta}\tilde{u}_b\right)\right)\right) = \frac{\partial}{\partial z}\left(\mu_R^{z-\theta}\left(\ln \mu_R^{z-\theta}\right)\omega\right) - \nabla^2\left(\mu_R^{z-\theta}\omega\right)$$

$$= \mu_R^{z-\theta}\ln \mu_R^{z-\theta}\left[\frac{\partial \omega}{\partial z} + \omega\left(1 + \ln \mu_R^{z-\theta}\right)\right]$$

$$-\mu_R^{z-\theta}\nabla^2\omega - \mu_R^{z-\theta}\ln \mu_R^{z-\theta}\omega\left(1 + \ln \mu_R^{z-\theta}\right)$$

$$= \mu_R^{z-\theta}\left[\left(\ln \mu_R^{z-\theta}\right)\frac{\partial \omega}{\partial z} - \nabla^2\omega\right]$$

thus $\hat{k} \cdot \nabla \times (\nabla \times C.10)$ yields:

$$0 = Ra^{1/2}\nabla_1^2\theta + \mu_R^{z-\theta}\left[\left(\ln\mu_R^{z-\theta}\right)\frac{\partial\omega}{\partial z} - \nabla^2\omega\right] \qquad \text{C.15}$$

$$\nabla^2(C.14) \rightarrow \nabla^4\theta = -Ra^{1/2}\nabla^2\omega$$

$$\rightarrow \nabla^2\omega = -Ra^{-1/2}\nabla^4\theta$$

$$\frac{\partial}{\partial z}\ (C.14) \rightarrow \frac{\partial}{\partial z}\nabla^2\theta = -Ra^{1/2}\frac{\partial\omega}{\partial z}$$

$$\rightarrow \frac{\partial\omega}{\partial z} = -Ra^{-1/2}\nabla^2\left(\frac{\partial\theta}{\partial z}\right)$$

substitute into C.15

$$0 = Ra^{1/2}\nabla_1^2\theta + \mu_R^{z-\theta}\left\{\left(\ln\mu_R^{z-\theta}\right)\left\{-Ra^{-1/2}\nabla^2\left(\frac{\partial\theta}{\partial z}\right)\right\} + Ra^{-1/2}\nabla^4\theta\right\}$$

multiply by:

$$\frac{Ra^{1/2}}{\mu_R^{z-\theta}}$$

$$0 = Ra\nabla_1^2\theta\mu_R^{\theta-z} + \ln\mu_R^{\theta-z}\nabla^2\left(\frac{\partial\theta}{\partial z}\right) + \nabla^4\theta \qquad \text{C.16}$$

The boundary conditions must now be found. Two sets of boundary conditions will

be considered. The first set is the classic set for a confined porous media and assumes adiabatic impermeable side walls and isothermal, impermeable top and bottom surfaces.[23,30] The second set is one never before considered in the literature. The side walls are assumed adiabatic and impermeable. The top and bottom surfaces are assumed impermeable, but with a finitely conductive layer between the porous media surface and an isothermal surface. The closest approach in the literature is by Riahi,[49] who assumed a finitely conductive semi-infinite mass at each surface. The physical layout and coordinate system of the sand pack is shown in Figure C.1.

Thermal Boundary Conditions

side walls:

$$\hat{r} \cdot q = 0 @ r^* = R$$

$$\frac{\partial T}{\partial r^*} = 0 @ r^* = R$$

normalize

$$\frac{\partial \theta}{\partial r} = 0 @ r = \frac{R}{L}$$

set R/L = s

$$\frac{\partial \theta}{\partial r} = 0 @ r = s$$

isothermal top surface: $T = T_0 @ z^* = 0$

normalize $\theta = 0 @ z = 0$

isothermal bottom surface: $T = T_1 @ z^* = -L$

normalize $\theta = 0 @ z = -1$

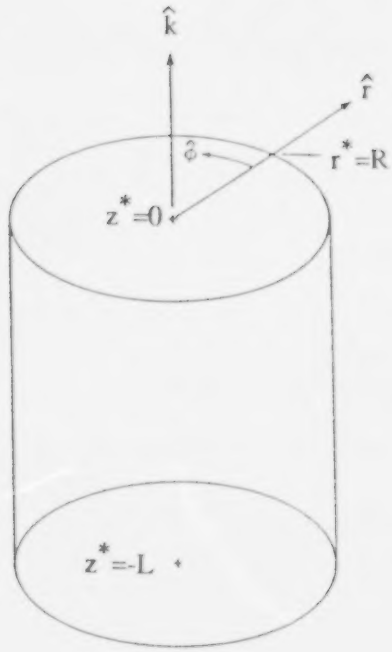

Figure C.1 Sand Pack Layout

The finite conductivity layer boundary conditions are complex but can be simplified considerably by linearizing them. Before convection occurs, conduction is the only mode of heat transfer, and the temperatures of the isothermal surfaces can hence by determined given the sand pack surface temperatures and the thermal conductivities of the sand pack and conductive layer.

top surface:

$$T_a = T_0 - \left(\frac{L_L}{L}\right)\left(\frac{\lambda_{ST}}{\lambda_L}\right)(T_1 - T_0)$$

where:

T_a = temperature of isothermal surface above conductive layer

L_L = thickness of conductive layer

λ_L = thermal conductivity of conductive layer

similarly bottom surface:

$$T_b = T_1 + \left(\frac{L_L}{L}\right)\left(\frac{\lambda_{ST}}{\lambda_L}\right)(T_1 - T_0)$$

where:

T_b = temperature of isothermal surface below conductive layer.

The heat flux through the sand pack surface is assumed to be steady-state conductive only, with no transient effects, i.e.

top surface:

$$\left.\frac{\partial T}{\partial z^*}\right|_{z^*=0} = \left(\frac{\lambda_L}{\lambda_{ST}}\right)\left.\frac{\partial T_{LT}}{\partial z^*_{LT}}\right|_{z^*_{LT}=0} = \left(\frac{\lambda_L}{\lambda_{ST}}\right)\left(\frac{T_a - T|_{z^*=0}}{L_L}\right)$$

where:

T_{LT} = temperature in conductive layer

$z_{LT}^{\cdot}$ = height above sand pack surface.

Similarly, bottom surface:

$$\left.\frac{\partial T}{\partial z^*}\right|_{z^*=-L} = -\left(\frac{\lambda_L}{\lambda_{ST}}\right)\left.\frac{\partial T_{LB}}{\partial z_{LB}^*}\right|_{z_{LB}^*=0} = \left(\frac{\lambda_L}{\lambda_{ST}}\right)\left(\frac{T|_{z^*=-L} - T_b}{L_L}\right)$$

T_{LB} = temperature conductive layer

$z_{LB}^{\cdot}$ = height below sand pack surface.

substitute isothermal temperatures and normalize:

top surface:

$$\frac{\partial \theta}{\partial z} = -\left(\frac{\lambda_L}{\lambda_{ST}}\frac{L}{L_L}\right)\theta$$

set

$$\alpha = \frac{\lambda_L}{\lambda_{ST}}\frac{L}{L_L}$$

$$\frac{\partial \theta}{\partial z} = -\alpha\theta \;@\; z=0$$

bottom surface:

$$\frac{\partial \theta}{\partial z} = \alpha\theta \;@\; z=-1$$

Flow boundary conditions:

bottoms and top surface

$$\tilde{u}_b^* \cdot \hat{k} = \omega^* = 0 \,@\, z^* = 0, -L$$

normalize

$$\omega = 0 \,@\, z = 0, -1$$

substitute C.14

$$\nabla^2 \theta = 0 \,@\, z = 0, -1$$

sidewalls:

$$\tilde{u}_b^* \cdot \hat{r} = 0 \,@\, r^* = R$$

set s = R/L

normalize

$$\tilde{u}_b \cdot \hat{r} = 0 \,@\, r = s$$

take $\hat{\phi} \cdot (\nabla \times c.10)$:

$$\hat{\phi} \cdot \left[0 = -Ra^{1/2} \nabla \times \nabla p + Ra^{1/2} \nabla \times \theta \hat{k} - \nabla \times \mu_R^{z-\theta} \tilde{u}_b \right]$$

ignore viscosity variation, $\mu_R = 1.0$

$$0 = -Ra^{1/2}\frac{\partial\theta}{\partial r} - \frac{1}{r}\frac{\partial(\hat{r}\cdot\tilde{u}_b)}{\partial z} + \frac{1}{r}\frac{\partial\omega}{\partial r}$$

from thermal boundary conditions

$$\frac{\partial\theta}{\partial r} = 0 \;@\; r = s$$

from flow boundary conditions

$$\hat{r}\cdot\tilde{u}_b = 0 \;@\; r = s$$
$$\frac{\partial}{\partial z}(\hat{r}\cdot\tilde{u}_b) = 0 \;@\; r = s$$
$$0 = \left(\frac{1}{r}\frac{\partial\omega}{\partial r}\right) @\; r = s$$
$$\frac{\partial\omega}{\partial r} = 0 \;@\; r = s$$

substitute C.14

$$\frac{\partial(\nabla^2\theta)}{\partial r} = 0 \;@\; r = s$$

summarize boundary conditions

Set 1: Isothermal:

@ $z = 0$: $\theta = 0$; $\nabla^2\theta = 0$

@ $z = -1$: $\theta = 0$; $\nabla^2\theta = 0$ C.17

@ $r = s$: $\partial\theta/\partial r = 0$; $\partial\nabla^2\theta/\partial r = 0$

Set 2: finite Conductive Layer:

@ $z = 0$: $\partial\theta/\partial z = -\alpha\theta$; $\nabla^2\theta = 0$

@ $z = -1$: $\partial\theta/\partial z = -\alpha\theta$; $\nabla^2\theta = 0$ C.18

@ $r = s$: $\partial\theta/\partial r = 0$; $\partial\nabla^2\theta/\partial r = 0$

separation of variables: propose $\theta = g(z, \lambda)\, h(r, \phi, \lambda)$ is a solution of C.16 then:

$$\nabla^2\theta = \frac{1}{r}\left[\frac{\partial}{\partial r}\left(r\frac{\partial\theta}{\partial r}\right) + \frac{\partial}{\partial\phi}\left(\frac{1}{r}\frac{\partial\theta}{\partial\phi}\right) + \frac{\partial}{\partial z}\left(r\frac{\partial\theta}{\partial z}\right)\right]$$

$$\nabla^2\theta = \frac{1}{r}\left[r\frac{\partial^2\theta}{\partial r^2} + \frac{\partial\theta}{\partial r} + \frac{1}{r}\frac{\partial^2\theta}{\partial\phi^2} + r\frac{\partial^2\theta}{\partial z^2}\right]$$

$$\nabla^2\theta = \frac{\partial^2\theta}{\partial r^2} + \frac{1}{r}\frac{\partial\theta}{\partial r} + \frac{1}{r^2}\frac{\partial^2\theta}{\partial\phi^2} + \frac{\partial^2\theta}{\partial z^2}$$

$$\frac{\partial\theta}{\partial z} = h\frac{dg}{dz} = hg'$$

$$\frac{\partial\theta}{\partial r} = g\frac{\partial h}{\partial r} = gh_r$$

$$\nabla^2\theta = g\left[h_{rr} + \frac{1}{r}h_r + \frac{1}{r^2}h_{\phi\phi}\right] + g''h$$

$$\nabla^2\left(\frac{\partial\theta}{\partial r}\right) = g\left[h_{rrr} + \frac{1}{r}h_{rr} + \frac{1}{r^2}h_{r\phi\phi}\right] + g''h_r$$

substitute into C.18

$$g(0,\lambda)\left[h_{rr} + \frac{1}{r}h_r + \frac{1}{r^2}h_{\phi\phi}\right] + g''(0,\lambda)h = 0 \qquad \text{(A)}$$

$$g(-1,\lambda)\left[h_{rr}+\frac{1}{r}h_r+\frac{1}{r^2}h_{\phi\phi}\right]+g''(-1,\lambda)h=0 \tag{B}$$

$$g\left[h_{rr}(s,\phi,\lambda)+\frac{1}{s}h_r(s,\phi,\lambda)+\frac{1}{s^2}h_{\phi\phi}(s,\phi,\lambda)\right]+g''h_\lambda(s,\phi,\lambda)=0 \tag{C}$$

$$g'(0,\lambda)h=-\alpha g(0,\lambda)h \tag{D}$$

$$g'(-1,\lambda)h=\alpha g(-1,\lambda)h \tag{E}$$

$$gh_\lambda(s,\phi,\lambda)=0 \tag{F}$$

simplify (F)

$$h_\lambda(s,\phi,\lambda)=0 \tag{G}$$

substituting into (C) gives

$$h_{rr}(s,\phi,\lambda)+\frac{1}{s}h_r(s,\phi,\lambda)+\frac{1}{s^2}h_{\phi\phi}(s,\phi,\lambda)=0 \tag{H}$$

simplify (D)

$$g'(0,\lambda) = -\alpha g(0,\lambda) \tag{I}$$

simplify (E)

$$g'(-1,\lambda) = \alpha g(-1,\lambda) \tag{J}$$

simplify (A)

$$g(0,\lambda)\left[h_{rr} + \frac{1}{r}h_r + \frac{1}{r^2}h_{\phi\phi}\right] = -g''(0,\lambda)h$$

$$\frac{1}{h}\left[h_{rr} + \frac{1}{r}h_r + \frac{1}{r^2}h_{\phi\phi}\right] = -\frac{g''(0,\lambda)}{g(0,\lambda)} = \textit{some constant depending on } \lambda$$

$$= G_1(\lambda) \tag{K}$$

similarly (B) yields

$$\frac{1}{h}\left[h_{rr} + \frac{1}{r}h_r + \frac{1}{r^2}h_{\phi\phi}\right] = -\frac{g''(-1,\lambda)}{g(0,\lambda)} = G_2(\lambda) \tag{L}$$

propose

$$h(r,\phi,\lambda) = a(r,\lambda)b(\phi,\lambda)$$

$$\frac{1}{h}\left[h_{rr} + \frac{1}{r}h_r + \frac{1}{r^2}h_{\phi\phi}\right] = \frac{1}{ab}\left[a''b + \frac{1}{r}a'b + \frac{1}{r^2}ab''\right] = G_1(\lambda)$$

$$a''b + \frac{1}{r}a'b + \frac{1}{r^2}ab'' = G_1(\lambda)ab$$

$$\left[a'' + \frac{1}{r}a' - G_1(\lambda)a\right]b = -\frac{1}{r^2}ab''$$

$$\left[a'' + \frac{1}{r}a' - G_1(\lambda)a\right]\frac{r^2}{a} = -\frac{b''}{b} = m^2 \ \ (constant)$$

$$b = \cos m\phi \qquad \text{(M)}$$

(must be periodic in 2π therefore m is integer)

$$a'' + \frac{1}{r}a' - G_1(\lambda)a = \frac{m^2 a}{r^2}$$

$$a'' + \frac{1}{r}a' + \left(-G_1(\lambda) - \frac{m^2}{r^2}\right)a = 0 \qquad \text{(N)}$$

from page 362 of Handbook of Mathematic Functions[51] equation 91.53 yields

$$r^2a'' + (1-2p)ra' + (\lambda^2q^2r^{2q} + p^2 - m^2q^2)a = 0 \qquad (O)$$

$$a = r^p(BF)_m(\lambda r^q)$$

where p, q are constants in above equation and do not extend beyond equation (O). $(BF)_m$ is various Bessel functions or combinations thereof.

the solution must be bounded at r = 0

$(BF)_m = J_m$ (Bessel function of first kind)

to match (O) and (N) set p = 0; q = 1

$a = J_m(\lambda r)$

(O) becomes:

$$r^2a'' + ra' + (\lambda^2r^2 - m^2)a = 0 \qquad (P)$$

r^2 (N) *is* $\qquad r^2a'' + ra' + \left(-G_l(\lambda)r^2 - m^2\right)a = 0$

therefore

$$-G_l(\lambda) = \lambda^2 \qquad (Q)$$

(P) becomes

$$r^2J_m'' + rJ_m' + (\lambda^2r^2 - m^2)J_m = 0 \qquad (R)$$

therefore

$$\theta = g(z) J_m(\lambda r) \cos(m\phi)$$

$$\nabla^2\theta = \left\{ g\left[J_m'' + \frac{1}{r} J_m' - \frac{m^2}{r^2} J_m \right] + g'' J_m \right\} \cos m\phi \qquad \text{C.19}$$

manipulate (R)

$$J_m'' + \frac{1}{r} J_m' - \frac{m^2}{r^2} J_m = -\lambda^2 J_m \qquad \text{C.20}$$

$$\nabla^2\theta = J_m \cos m\phi \{ g'' - \lambda^2 g \}$$

$$\frac{\partial\theta}{\partial z} = J_m \cos m\phi\, g' \qquad \nabla^2\left(\frac{\partial\theta}{\partial z}\right) = J_m \cos m\phi \{ g''' - \lambda^2 g' \}$$

$$\frac{\partial\theta}{\partial r} = J_m' \cos m\phi\; g$$

$$\nabla^2\left(\frac{\partial\theta}{\partial r}\right) = J_m' \cos m\phi \{ g'' - \lambda^2 g \}$$

$$\nabla^4\theta = \nabla^2(\nabla^2\theta) = \nabla^2 \{ J_m \cos m\phi \{ g'' - \lambda^2 g \} \}$$

$$\nabla^4\theta = \cos m\phi\left[(g'' - \lambda^2 g)\left\{J_m'' + \frac{1}{r}J_m' - \frac{m^2}{r^2}J_m\right\} + J_m\{g^{IV} - \lambda^2 g''\}\right]$$

$$\textit{note:}\quad \left\{J_m'' + \frac{1}{r}J_m' - \frac{m^2}{r^2}J_m\right\} = -\lambda^2 J_m$$

$$\nabla^4\theta = J_m \cos m\phi[g^{IV} - 2\lambda^2 g'' + \lambda^4 g]$$

$$\nabla_1^2\theta = \nabla^2\theta - \frac{\partial^2\theta}{\partial z^2} = -J_m\lambda^2 \cos m\phi$$

sub into C.16

$$0 = J_m \cos m\phi\left\{g^{IV} - 2\lambda^2 g'' + \lambda^4 g - \lambda^2 Ra\mu_R^{\theta - z} g + \ln\mu_R^{\theta - z}(g''' - \lambda^2 g')\right\} \quad \text{C.21}$$

$$g^{IV} + g'''\ln\mu_R^{\theta - z} - 2\lambda^2 g'' - g'\lambda^2 \ln\mu_R^{\theta - z} + \left(\lambda^4 - \lambda^2 Ra\mu_R^{\theta - z}\right)g = 0$$

to simplify, note the small perturbations of temperature from the linear gradient do not effect viscosity significantly.

$$g^{IV} - \ln\mu_R^z g''' - 2\lambda^2 g'' + \lambda^2 \ln\mu_R^z g' + \left(\lambda^4 - \frac{\lambda^2 Ra}{\mu_R^z}\right)g = 0$$

$$g^{IV} - z\ln\mu_R g''' - 2\lambda^2 g'' + z\lambda^2 \ln\mu_R g' + \left(\lambda^4 - \frac{\lambda^2 Ra}{\mu_R^z}\right)g = 0 \quad \text{C.22}$$

now rewrite boundary conditions:

Set 1; Isothermal:

@ z = 0 $g(0) = 0; g''(0) - \lambda^2 g(0) = 0$

@ z = -1: $g(-1) = 0; g''(-1) - \lambda^2 g(-1) = 0$

@ r = s: $J_m'(\lambda s) = 0$

Set 2; Finite Conductive Layer:

@ z = 0: $g'(0) = \alpha g(0); g''(0) - \lambda^2 g(0) = 0$

@ z = -1: $g'(-1) = \alpha g(-1); g''(-1) - \lambda^2 g(-1) = 0$

@ r = s: $J_m'(\lambda s) = 0$

where s = aspect ratio of porous medium = R/L.

can find eigenvalues from the Handbook of Mathematical Function,[51] but must calculate s from experiment

$$s = \frac{R}{L} = \frac{0.2289m}{0.67m} = 0.343$$

now find zeroes of $J_m'(\lambda s)$

the results for the first seven eigenvalues are listed in Table C.1

Table C.1
Model Eigenvalues

MODE M	EIGENVALUE FOR 1st ZERO	EIGENVALUE FOR 2nd ZERO
0	0	11.179
1	5.373	15.560
2	8.914	
3	12.262	
4	15.522	
5	18.727	

The different modes and zeroes result in different planforms of motion. The planforms of motion corresponding to m = 1, first zero; m = 2, first zero; m = 0, second zero, for a constant viscosity liquid are illustrated in Figure C.2. These are the three first modes of natural convection.

The fourth order linear ordinary differential equation C.22 does not have an analytical solution and must be solved numerically. Finite difference methods were attempted but could not handle the high order of the problem. The technique successfully used for this boundary value problem was a modification of the shooting technique published by Kalaba.[52] A series of unique initial value problems were solved and linearly superimposed to give the correct boundary values.

For example: given boundary conditions:
$g(0) = 0;\ g^{II} = 0$
$g(-1) = 0;\ g^{II}(-1) = 0$
solve the following initial value problems by a 4th order, 100 step Runge-Kutta technique.
$g(0) = g^{I}(0) = g^{II}(0) = g^{III}(0) = 0$
$g^{I}(0) = 1.0;\ g(0) = g^{II}(0) = g^{III}(0) = 0$
$g^{III}(0) = 1.0\ ;\ g(0) = g^{I}(0) = g^{II}(0) = 0$

The first initial value problem gave a trivial, zero, result but the second was multiplied by -0.46 and added to the third to give the correct result. The critical Rayleigh value was 24.78. This same method was applied to the conductive layer boundary conditions and the critical Rayleigh value was found to be 22.27.

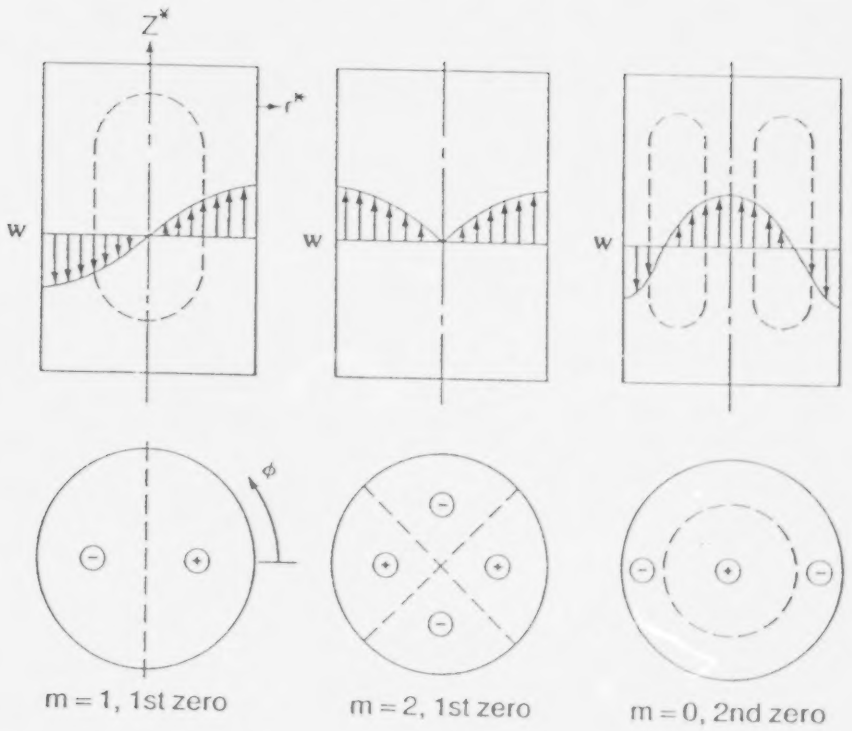

Figure C.2: Convective Motion Planforms

D. CRITICAL RAYLEIGH VALUES

The following is a series of tables and graphs delineating the critical Rayleigh numbers for viscosity ratios from one to ten. The critical Rayleigh numbers are found for the first seventeen modes of convective motion. The solutions are found for isothermal top and bottom surfaces, and the corresponding eigenvalues are noted on each graph. The solution technique used was presented in Chapter 4 and Appendix C.

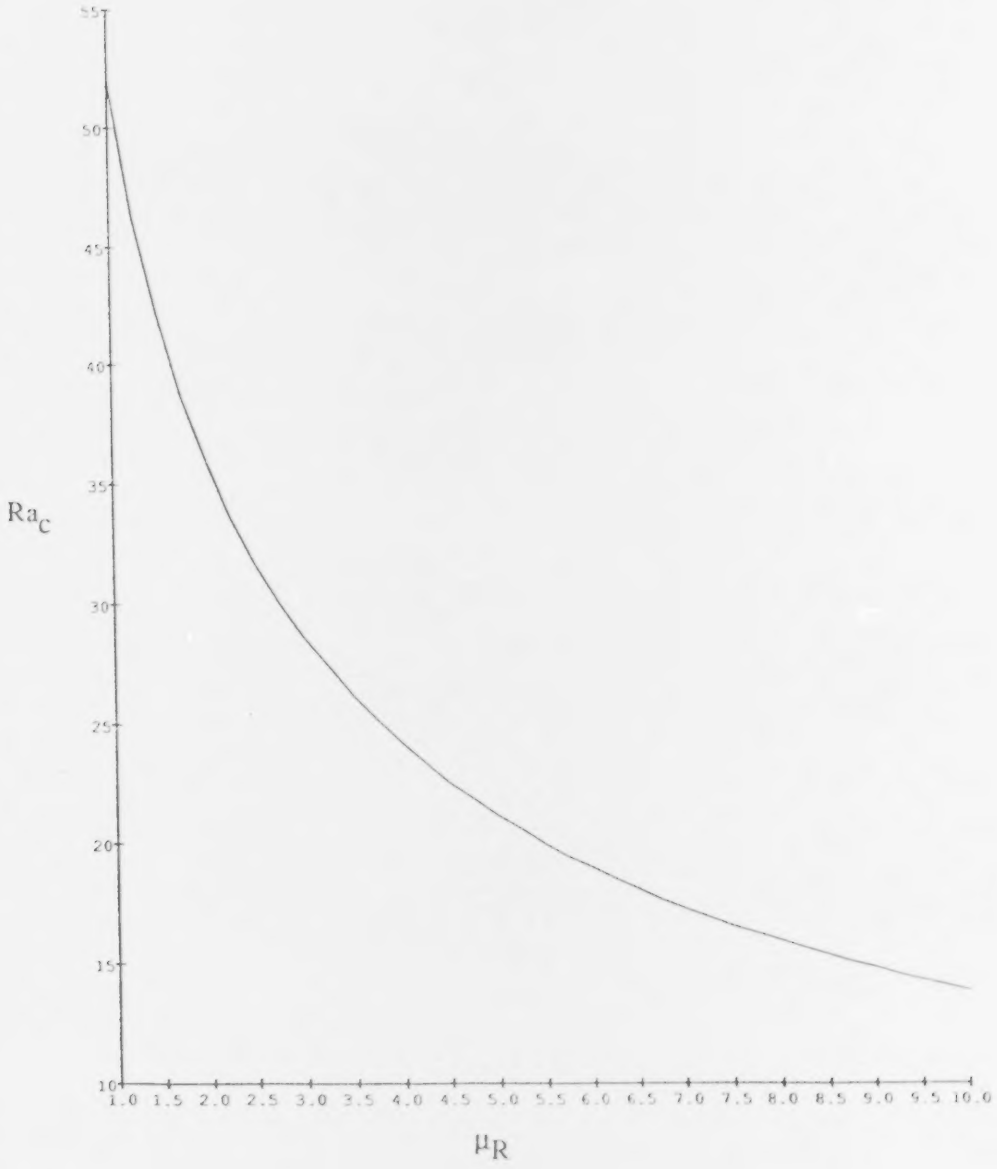

Figure D.1 Predicted Critical Rayleigh Values, Mode 1

Table D.1 Predicted Critical Rayleigh Values, Mode 1, $\lambda = 5.3742$

μ_R	Ra_c
1.00	51.99393
1.25	46.30601
1.50	42.03699
1.75	38.68106
2.00	35.95409
2.25	33.68231
2.50	31.75256
2.75	30.08752
3.00	28.63233
3.25	27.34678
3.50	26.20071
3.75	25.17093
4.00	24.23929
4.25	23.39138
4.50	22.61558
4.75	21.90237
5.00	21.24394
5.25	20.63373
5.50	20.06625
5.75	19.53683
6.00	19.04149
6.25	18.57680
6.50	18.13980
6.75	17.72789
7.00	17.33883
7.25	16.97062
7.50	16.62151
7.75	16.28995
8.00	15.97454
8.25	15.67405
8.50	15.38737
8.75	15.11350
9.00	14.85154
9.25	14.60067
9.50	14.36015
9.75	14.12931
10.00	13.90754

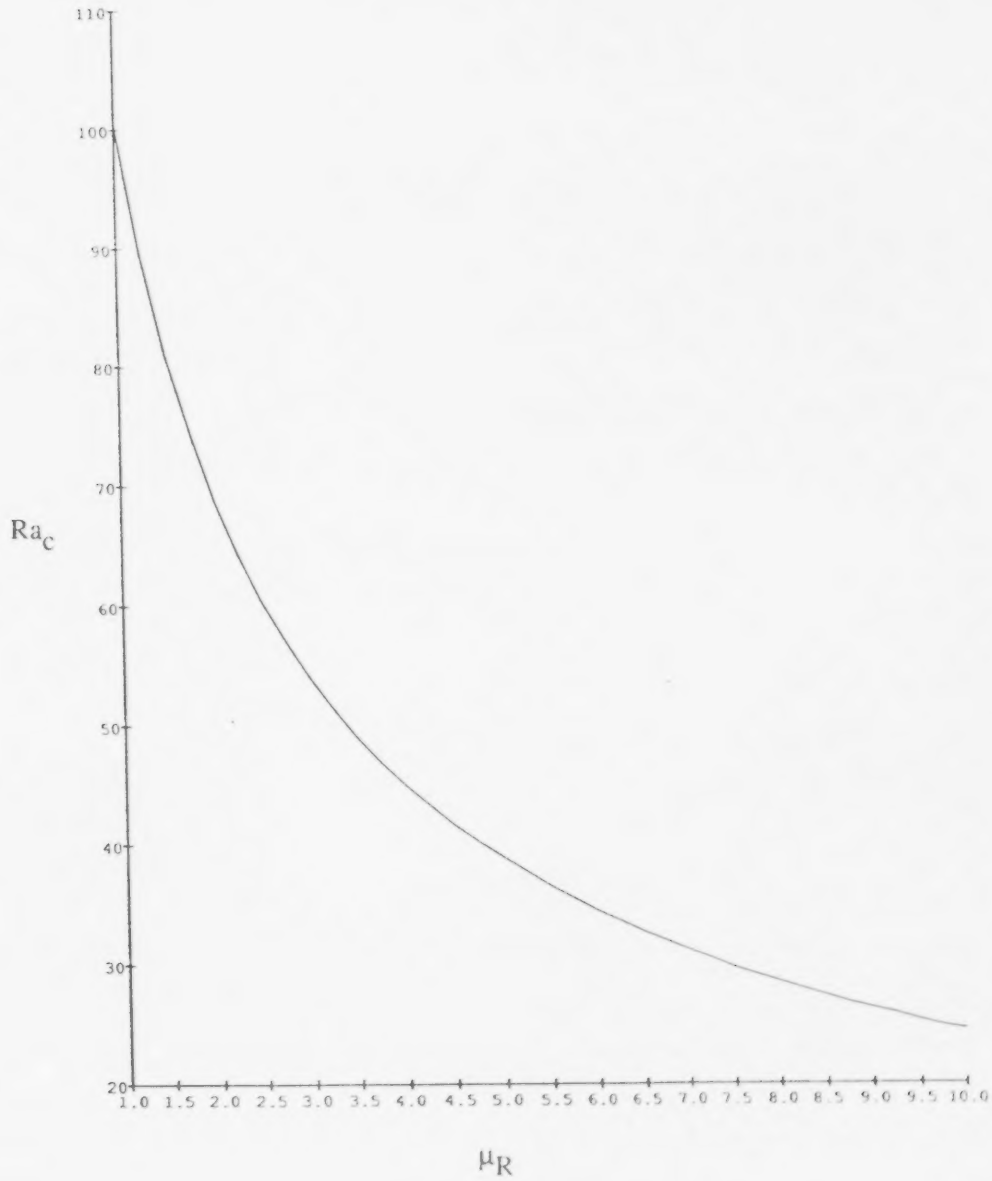

Figure D.2 Predicted Critical Rayleigh Values, Mode 2

Table D.2 Predicted Critical Rayleigh Values, Mode 2, $\lambda = 8.9148$

μ_R	Ra_c
1.00	100.43855
1.25	89.47081
1.50	81.07042
1.75	74.37843
2.00	68.89286
2.25	64.29680
2.50	60.37860
2.75	56.99072
3.00	54.02669
3.25	51.40752
3.50	49.07319
3.75	46.97725
4.00	45.08304
4.25	43.36128
4.50	41.78822
4.75	40.34440
5.00	39.01370
5.25	37.78263
5.50	36.63983
5.75	35.57564
6.00	34.58181
6.25	33.65121
6.50	32.77769
6.75	31.95588
7.00	31.18108
7.25	30.44917
7.50	29.75649
7.75	29.09981
8.00	28.47625
8.25	27.88323
8.50	27.31846
8.75	26.77985
9.00	26.26554
9.25	25.77384
9.50	25.30320
9.75	24.85223
10.00	24.41967

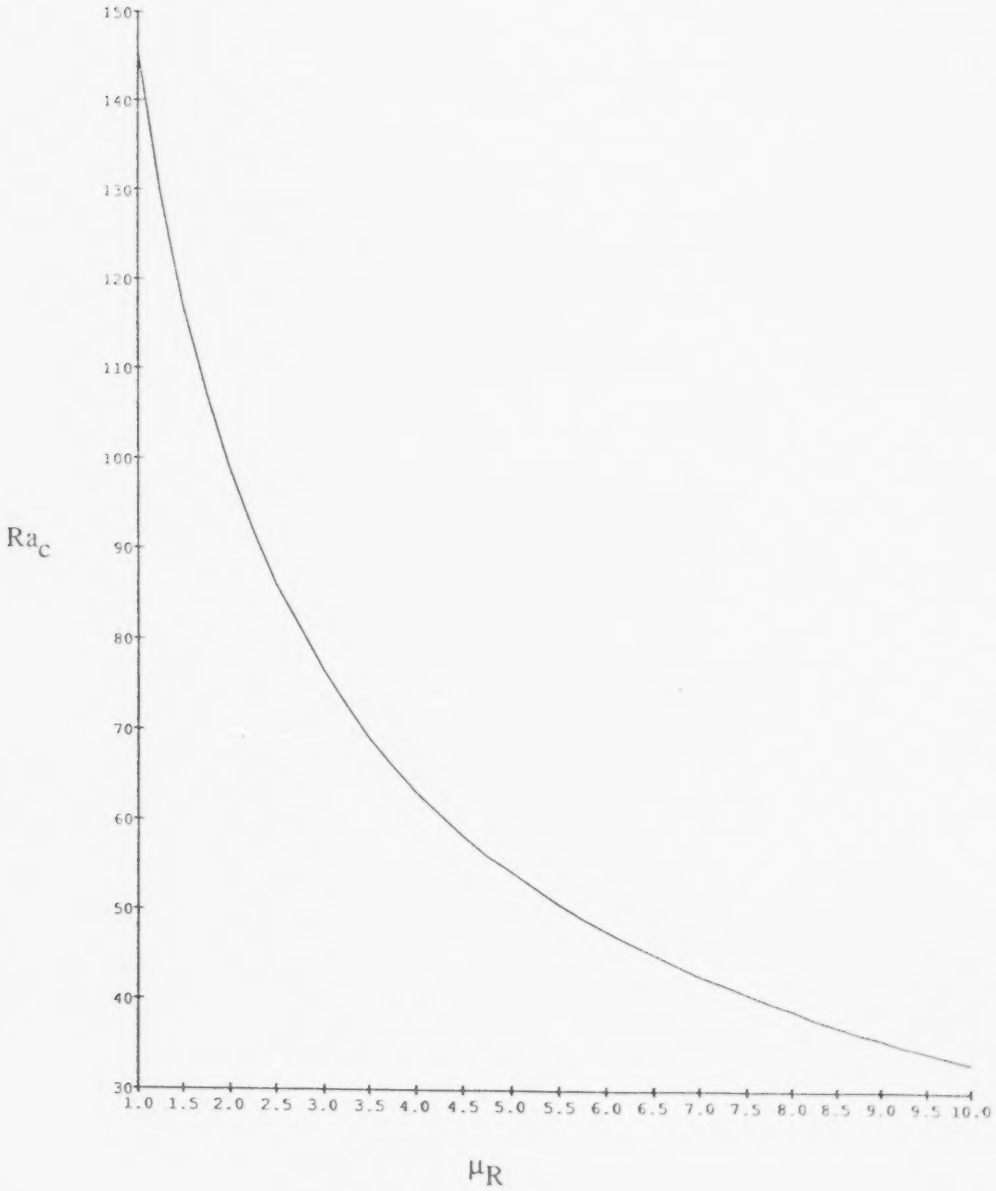

Figure D.3 Predicted Critical Rayleigh Values, Mode 3

Table D.3 Predicted Critical Rayleigh Values, Mode 3, $\lambda = 11.1842$

μ_R	Ra_c
1.00	145.60429
1.25	129.59838
1.50	117.14730
1.75	107.14403
2.00	98.91020
2.25	92.00123
2.50	86.11194
2.75	81.02525
3.00	76.58235
3.25	72.66422
3.50	69.17986
3.75	66.05843
4.00	63.24396
4.25	60.69159
4.50	58.36494
4.75	56.23415
5.00	54.27453
5.25	52.46541
5.50	50.78941
5.75	49.23174
6.00	47.77980
6.25	46.42273
6.50	45.15113
6.75	43.95685
7.00	42.83273
7.25	41.77253
7.50	40.77070
7.75	39.82235
8.00	38.92313
8.25	38.06916
8.50	37.25696
8.75	36.48340
9.00	35.74568
9.25	35.04125
9.50	34.36782
9.75	33.72330
10.00	33.10578

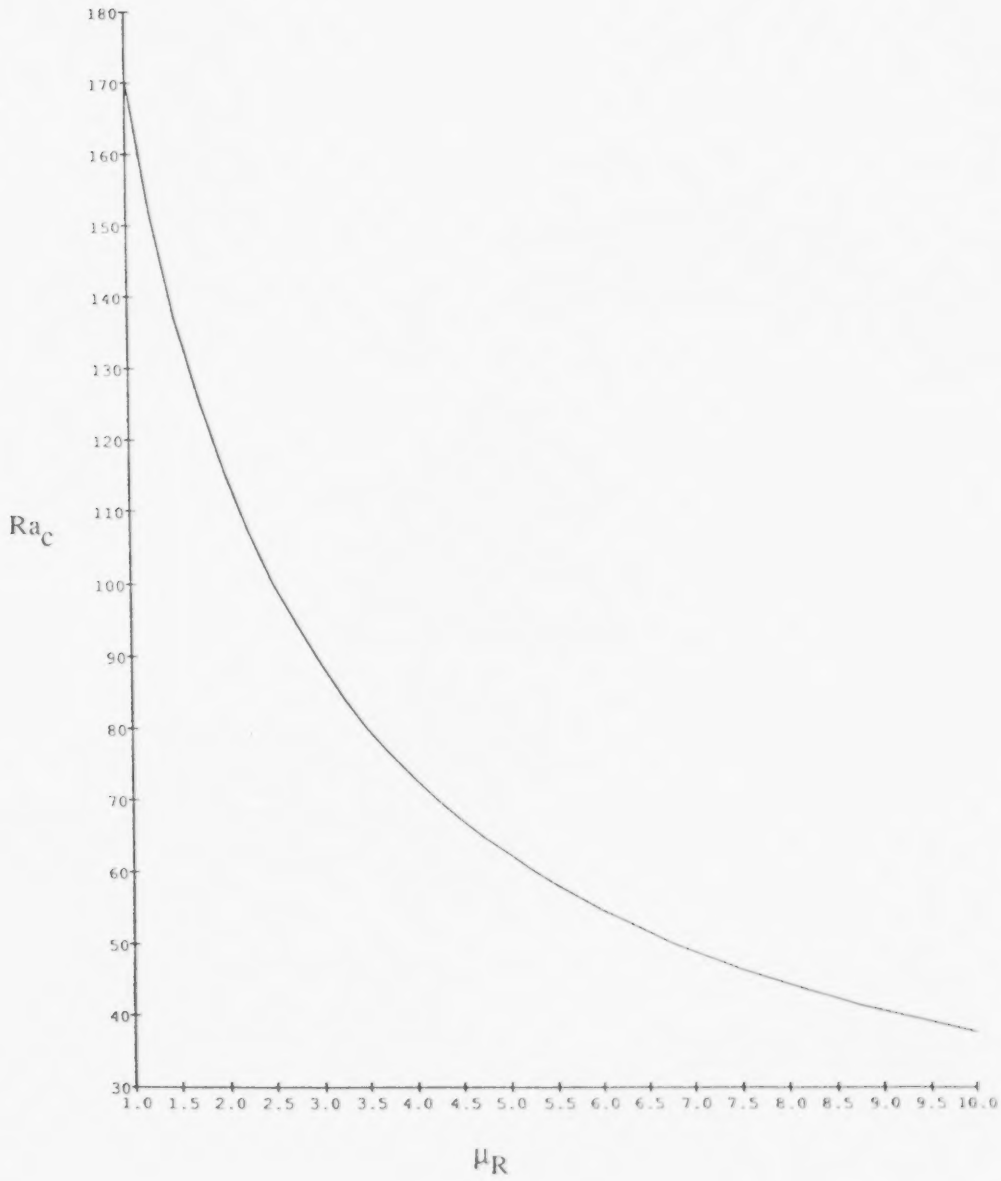

Figure D.4 Predicted Critical Rayleigh Values, Mode 4

Table D.4 Predicted Critical Rayleigh Values, Mode 4, $\lambda = 12.2627$

μ_R	Ra_c
1.00	170.76088
1.25	151.90587
1.50	137.12300
1.75	125.20377
2.00	115.38178
2.25	107.14165
2.50	100.12380
2.75	94.06960
3.00	88.78881
3.25	84.13827
3.50	80.00835
3.75	76.31362
4.00	72.98657
4.25	69.97311
4.50	67.22939
4.75	64.71948
5.00	62.41365
5.25	60.28709
5.50	58.31889
5.75	56.49135
6.00	54.78933
6.25	53.19985
6.50	51.71167
6.75	50.31504
7.00	49.00143
7.25	47.76336
7.50	46.59425
7.75	45.48826
8.00	44.44022
8.25	43.44550
8.50	42.49998
8.75	41.59995
9.00	40.74208
9.25	39.92335
9.50	39.14103
9.75	38.39266
10.00	37.67598

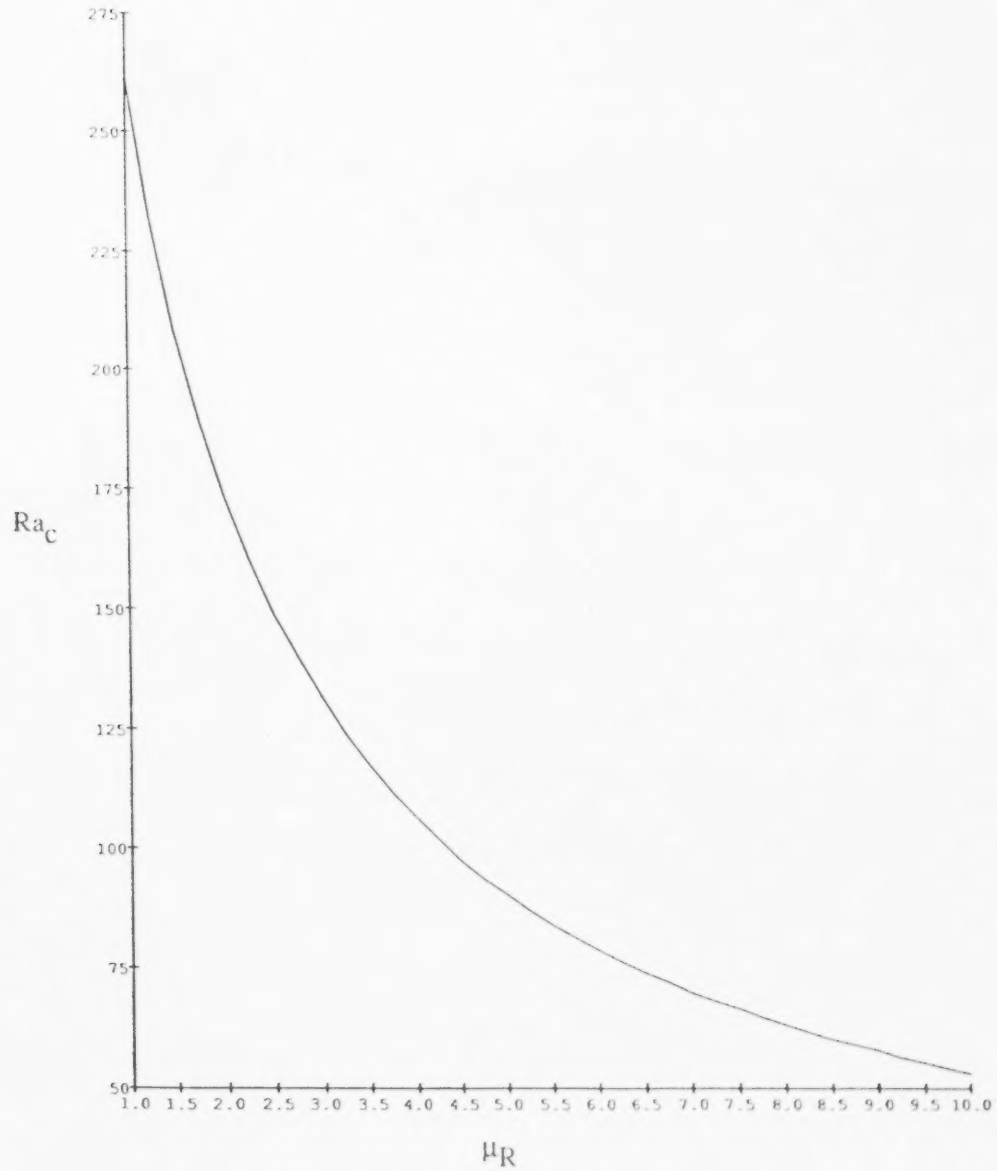

Figure D.5 Predicted Critical Rayleigh Values, Mode 5

Table D.5 Predicted Critical Rayleigh Values, Mode 5, $\lambda = 15.5213$

μ_R	Ra_c
1.00	261.05434
1.25	231.73196
1.50	208.18477
1.75	189.06055
2.00	173.31026
2.25	160.14676
2.50	148.99089
2.75	139.41666
3.00	131.10736
3.25	123.82446
3.50	117.38542
3.75	111.64849
4.00	106.50207
4.25	101.85712
4.50	97.64177
4.75	93.79740
5.00	90.27565
5.25	87.03636
5.50	84.04581
5.75	81.27553
6.00	78.70127
6.25	76.30229
6.50	74.06069
6.75	71.96097
7.00	69.98965
7.25	68.13490
7.50	66.38635
7.75	64.73481
8.00	63.17217
8.25	61.69120
8.50	60.28544
8.75	58.94912
9.00	57.67703
9.25	56.46451
9.50	55.30731
9.75	54.20162
10.00	53.14395

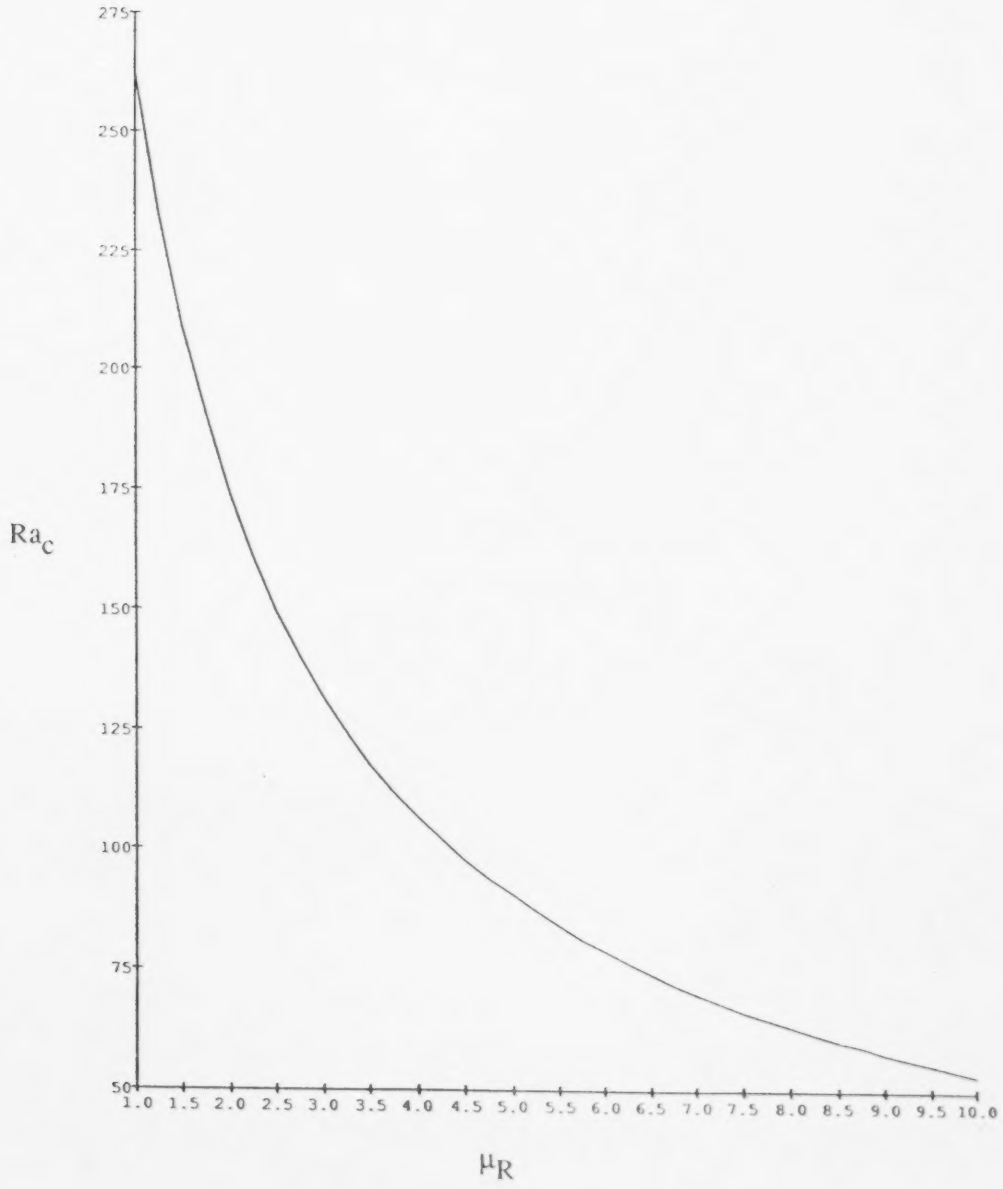

Figure D.6 Predicted Critical Rayleigh Values, Mode 6

Table D.6 Predicted Critical Rayleigh Values, Mode 6, $\lambda = 15.5616$

μ_R	Ra_c
1.00	262.30482
1.25	232.83496
1.50	209.16246
1.75	189.93553
2.00	174.10134
2.25	160.86864
2.50	149.65496
2.75	140.03180
3.00	131.60055
3.25	124.36131
3.50	117.89047
3.75	112.12549
4.00	106.95412
4.25	102.28683
4.50	98.05136
4.75	94.18876
5.00	90.65043
5.25	87.39598
5.50	84.39151
5.75	81.60840
6.00	79.02229
6.25	76.61231
6.50	74.36049
6.75	72.25124
7.00	70.27100
7.25	68.40790
7.50	66.65149
7.75	64.99257
8.00	63.42297
8.25	61.93543
8.50	60.52345
8.75	59.18123
9.00	57.90355
9.25	56.68570
9.50	55.52345
9.75	54.41293
10.00	53.35066

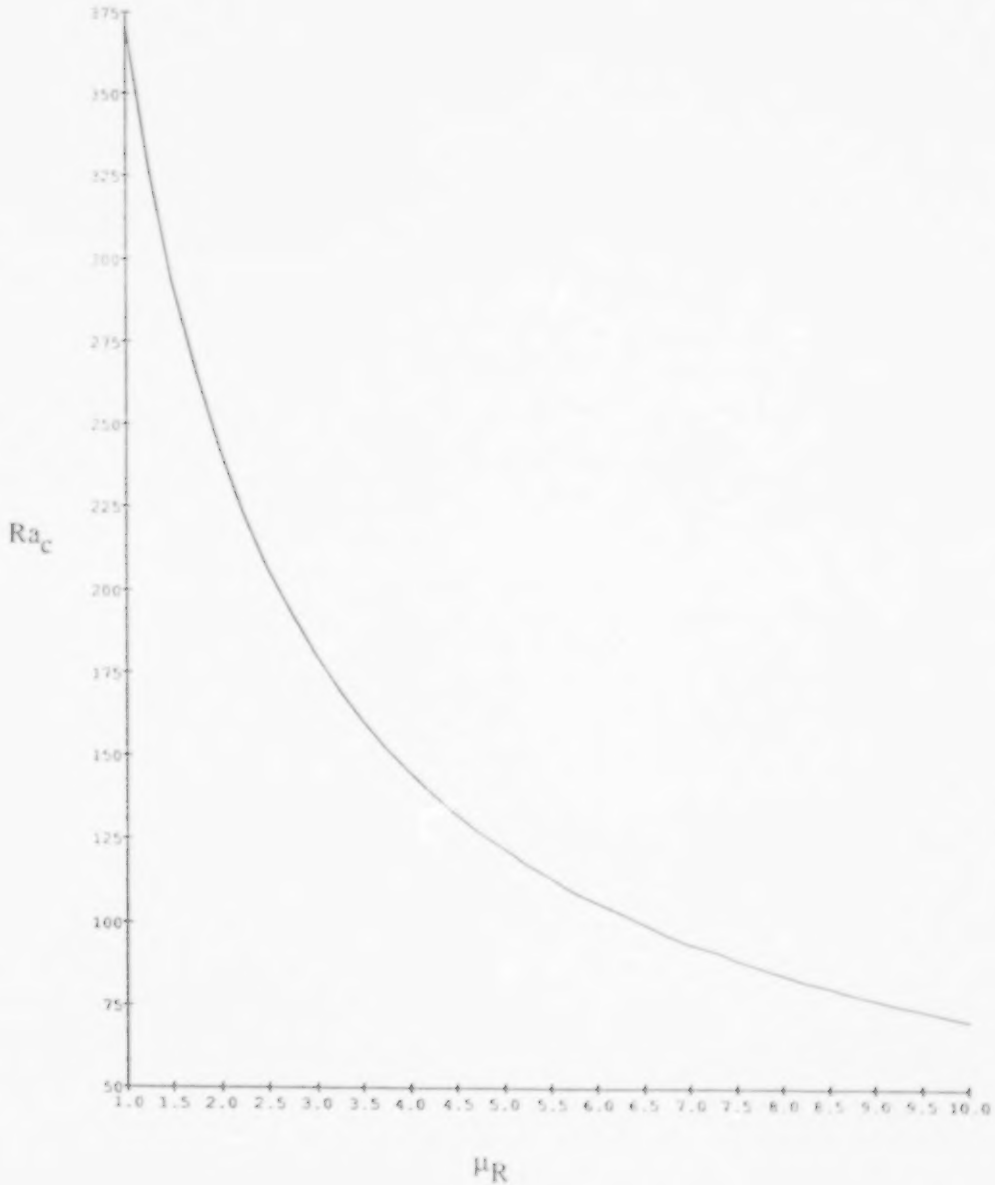

Figure D.7 Predicted Critical Rayleigh Values, Mode 7

Table D.7 Predicted Critical Rayleigh Values, Mode 7, $\lambda = 18.7262$

μ_R	Ra_c
1.00	370.68754
1.25	328.17610
1.50	293.30951
1.75	264.97456
2.00	241.76413
2.25	222.48895
2.50	206.25112
2.75	192.38953
3.00	180.41579
3.25	169.96454
3.50	160.75826
3.75	152.58287
4.00	145.27078
4.25	138.68904
4.50	132.73081
4.75	127.30929
5.00	122.35323
5.25	117.80357
5.50	113.61095
5.75	109.73378
6.00	106.13675
6.25	102.78971
6.50	99.66674
6.75	96.74542
7.00	94.00626
7.25	91.43226
7.50	89.00847
7.75	86.72174
8.00	84.56042
8.25	82.51416
8.50	80.57374
8.75	78.73091
9.00	76.97828
9.25	75.30919
9.50	73.71761
9.75	72.19812
10.00	70.74578

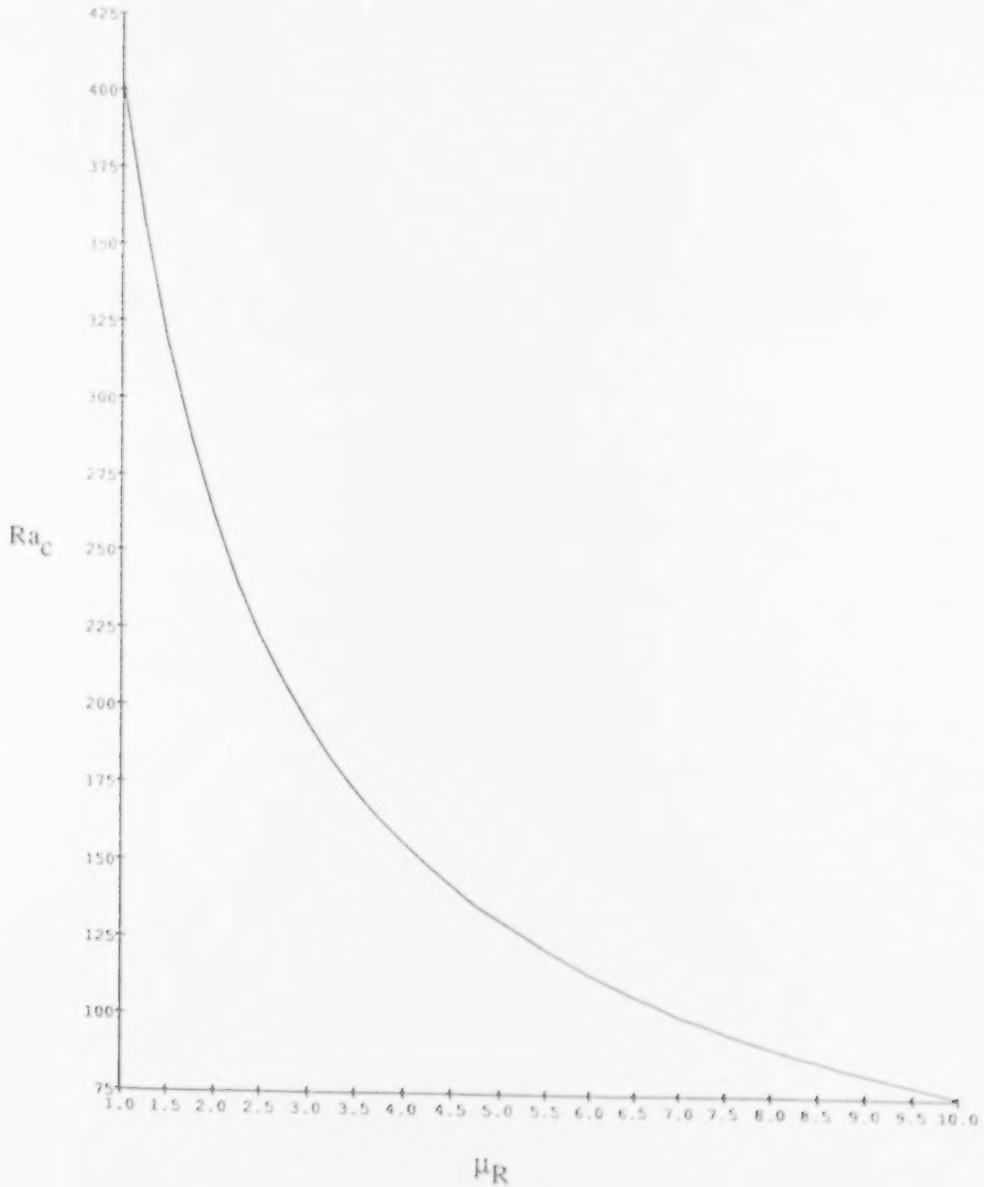

Figure D.8 Predicted Critical Rayleigh Values, Mode 8

Table D.8 Predicted Critical Rayleigh Values, Mode 8, $\lambda = 19.5741$

μ_R	Ra_c
1.00	403.13886
1.25	356.62899
1.50	318.30020
1.75	287.17827
2.00	261.73251
2.25	240.63832
2.50	222.89492
2.75	207.76739
3.00	194.71434
3.25	183.33178
3.50	173.31342
3.75	164.42342
4.00	156.47743
4.25	149.32937
4.50	142.86200
4.75	136.98016
5.00	131.60578
5.25	126.67422
5.50	122.13149
5.75	117.93212
6.00	114.03755
6.25	110.41485
6.50	107.03573
6.75	103.87574
7.00	100.91363
7.25	98.13087
7.50	95.51118
7.75	93.04023
8.00	90.70534
8.25	88.49526
8.50	86.39993
8.75	84.41041
9.00	82.51865
9.25	80.71739
9.50	79.00012
9.75	77.36092
10.00	75.79443

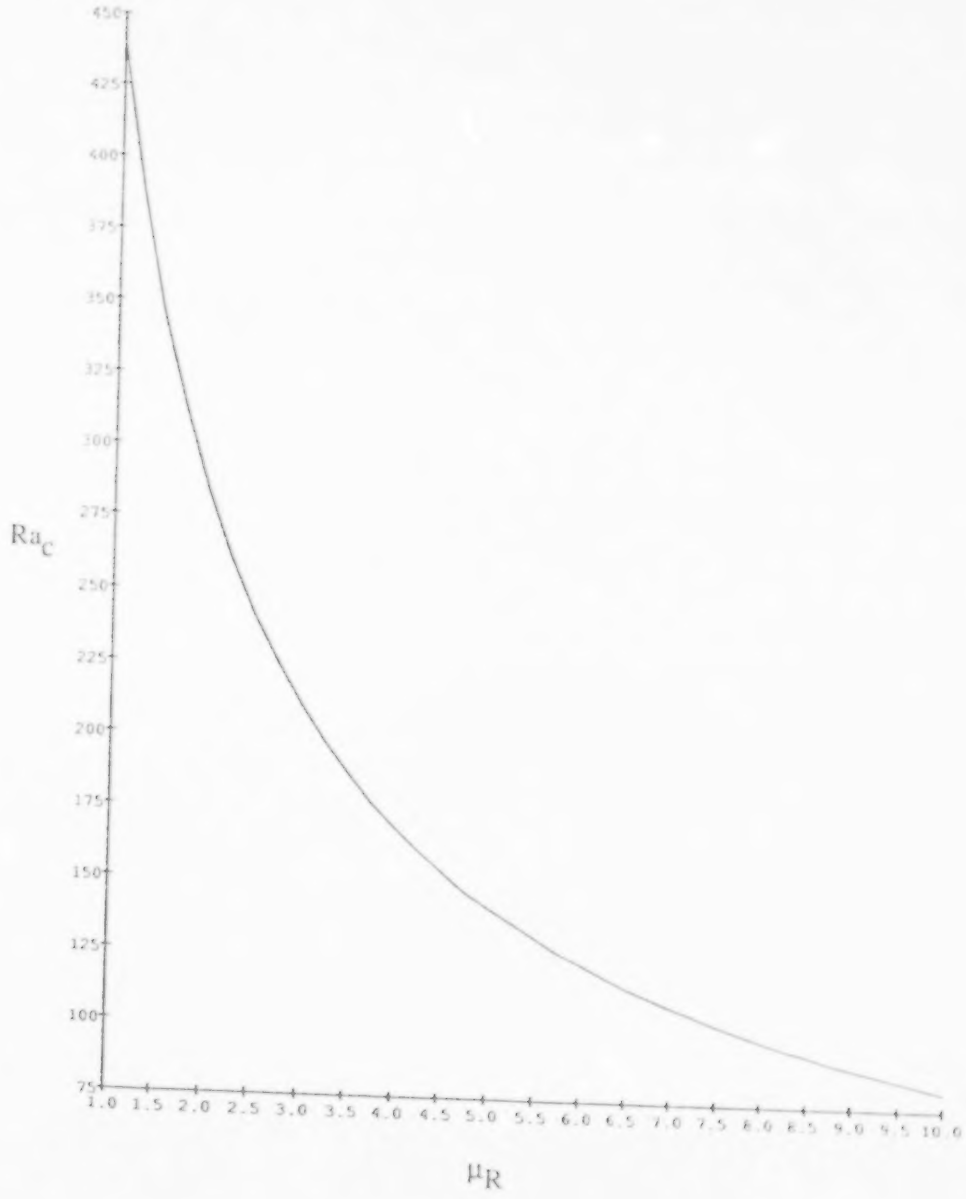

Figure D.9 Predicted Critical Rayleigh Values, Mode 9

Table D.9 Predicted Critical Rayleigh Values, Mode 9, $\lambda = 20.4775$

μ_R	Ra_c
1.00	439.29952
1.25	388.28627
1.50	346.05049
1.75	311.80046
2.00	283.85528
2.25	260.73185
2.50	241.31141
2.75	224.77528
3.00	210.52230
3.25	198.10500
3.50	187.18490
3.75	177.50176
4.00	168.85252
4.25	161.07641
4.50	154.04460
4.75	147.65257
5.00	141.81469
5.25	136.46010
5.50	131.52964
5.75	126.97354
6.00	122.74960
6.25	118.82181
6.50	115.15926
6.75	111.73522
7.00	108.52650
7.25	105.51285
7.50	102.67653
7.75	100.00190
8.00	97.47513
8.25	95.08395
8.50	92.81743
8.75	90.66580
9.00	88.62029
9.25	86.67302
9.50	84.81688
9.75	83.04544
10.00	81.35288

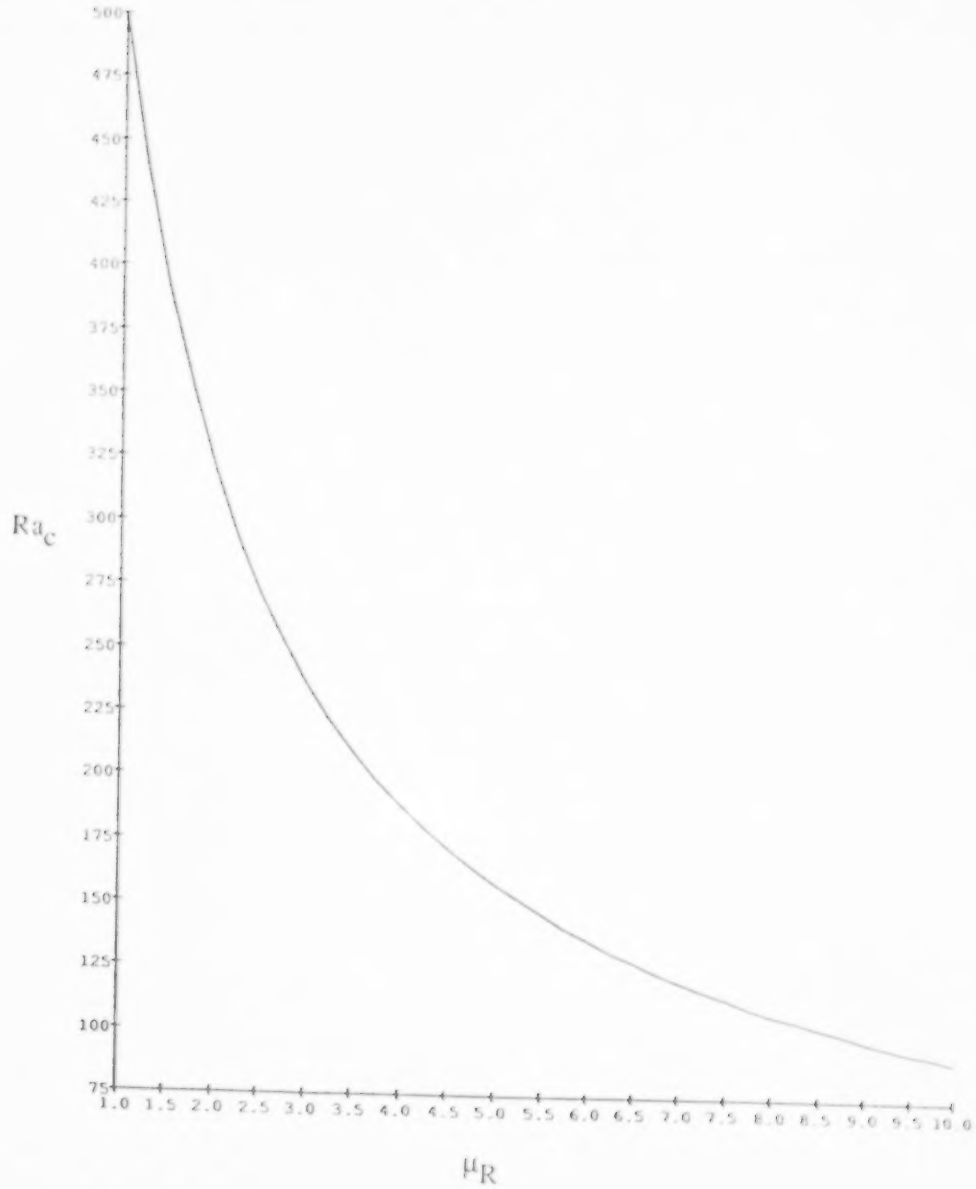

Figure D.10 Predicted Critical Rayleigh Values, Mode 10

Table D.10 Predicted Critical Rayleigh Values, Mode 10, $\lambda = 21.8952$

μ_R	Ra_c
1.00	499.34217
1.25	440.74443
1.50	391.92268
1.75	352.43753
2.00	320.32777
2.25	293.83187
2.50	271.62897
2.75	252.75857
3.00	236.51895
3.25	222.38987
3.50	209.97895
3.75	198.98530
4.00	189.17460
4.25	180.36174
4.50	172.39853
4.75	165.16496
5.00	158.56281
5.25	152.51088
5.50	146.94147
5.75	141.79765
6.00	137.03121
6.25	132.60104
6.50	128.47185
6.75	124.61320
7.00	120.99863
7.25	117.60511
7.50	114.41242
7.75	111.40278
8.00	108.56047
8.25	105.87154
8.50	103.32357
8.75	100.90546
9.00	98.60728
9.25	96.42007
9.50	94.33577
9.75	92.34709
10.00	90.44742

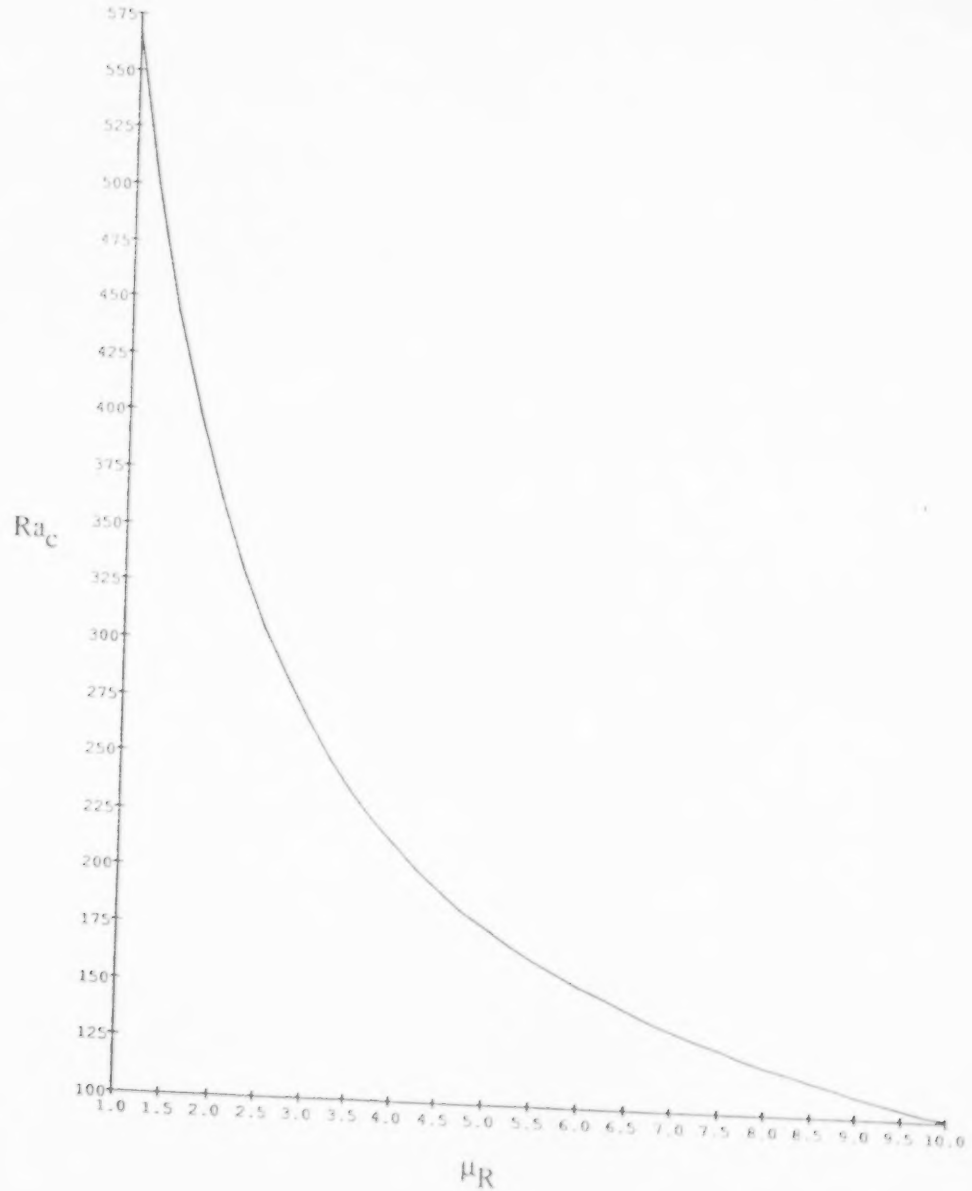

Figure D.11 Predicted Critical Rayleigh Values, Mode 11

Table D.11 Predicted Critical Rayleigh Values, Mode 11, $\lambda = 23.3952$

μ_R	Ra_c
1.00	567.25259
1.25	499.92499
1.50	443.53145
1.75	398.07885
2.00	361.24393
2.25	330.93142
2.50	305.58502
2.75	284.08082
3.00	265.60196
3.25	249.54500
3.50	235.45623
3.75	222.98862
4.00	211.87235
4.25	201.89464
4.50	192.88544
4.75	184.70718
5.00	177.24741
5.25	170.41325
5.50	164.12733
5.75	158.32466
6.00	152.95024
6.25	147.95719
6.50	143.30533
6.75	138.95996
7.00	134.89102
7.25	131.07228
7.50	127.48077
7.75	124.09629
8.00	120.90099
8.25	117.87902
8.50	115.01631
8.75	112.30027
9.00	109.71961
9.25	107.26420
9.50	104.92491
9.75	102.69348
10.00	100.56242

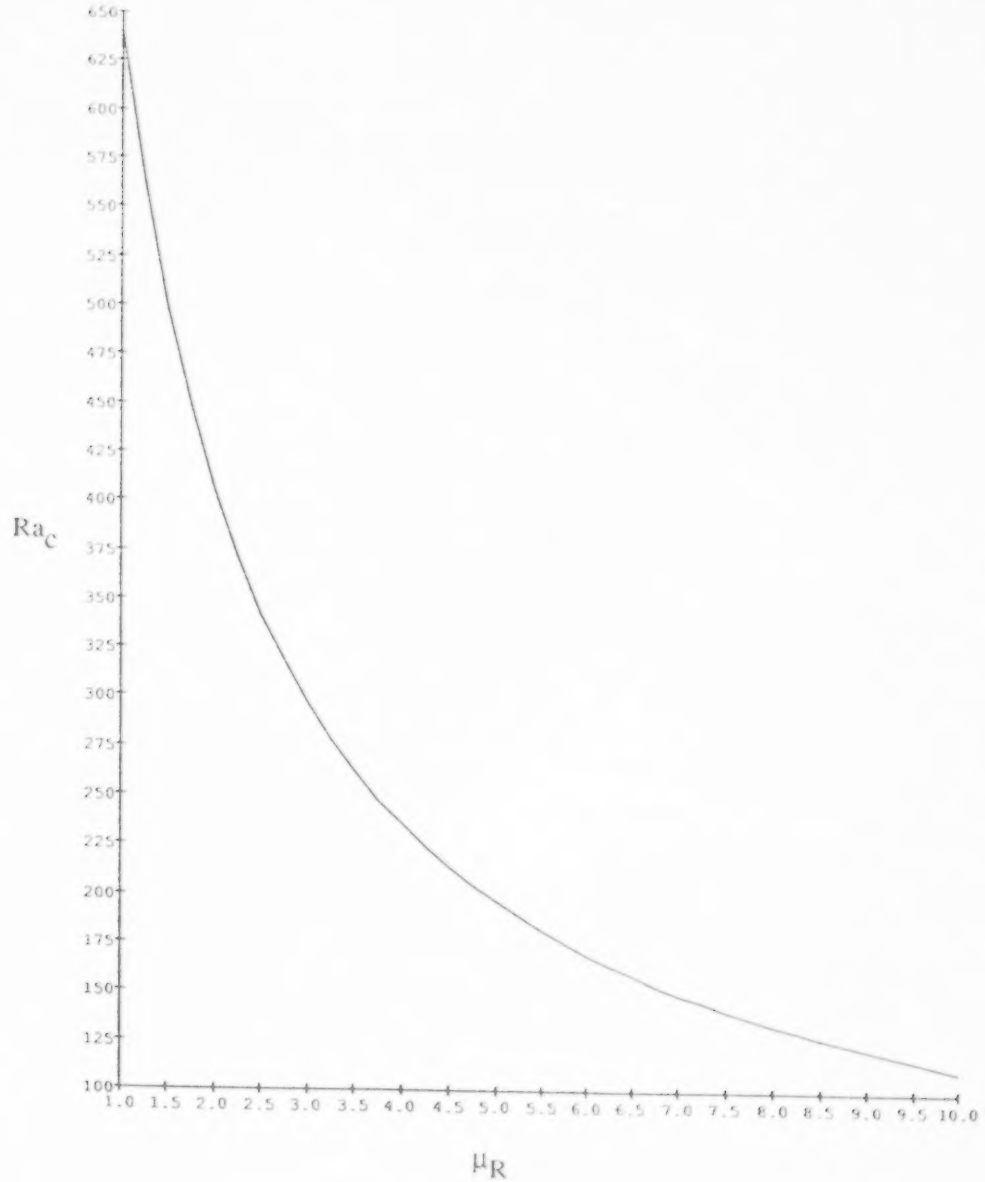

Figure D.12 Predicted Critical Rayleigh Values, Mode 12

Table D.12 Predicted Critical Rayleigh Values, Mode 12, $\lambda = 24.9162$

μ_R	Ra_c
1.00	640.71350
1.25	563.77454
1.50	499.07297
1.75	447.12539
2.00	405.16705
2.25	370.72543
2.50	341.98285
2.75	317.63621
3.00	296.74302
3.25	278.60886
3.50	262.71361
3.75	248.65987
4.00	236.13934
4.25	224.90939
4.50	214.77617
4.75	205.58314
5.00	197.20243
5.25	189.52858
5.50	182.47375
5.75	175.96425
6.00	169.93774
6.25	164.34114
6.50	159.12895
6.75	154.26195
7.00	149.70611
7.25	145.43183
7.50	141.41314
7.75	137.62723
8.00	134.05396
8.25	130.67547
8.50	127.47587
8.75	124.44096
9.00	121.55804
9.25	118.81569
9.50	116.20362
9.75	113.71254
10.00	111.33402

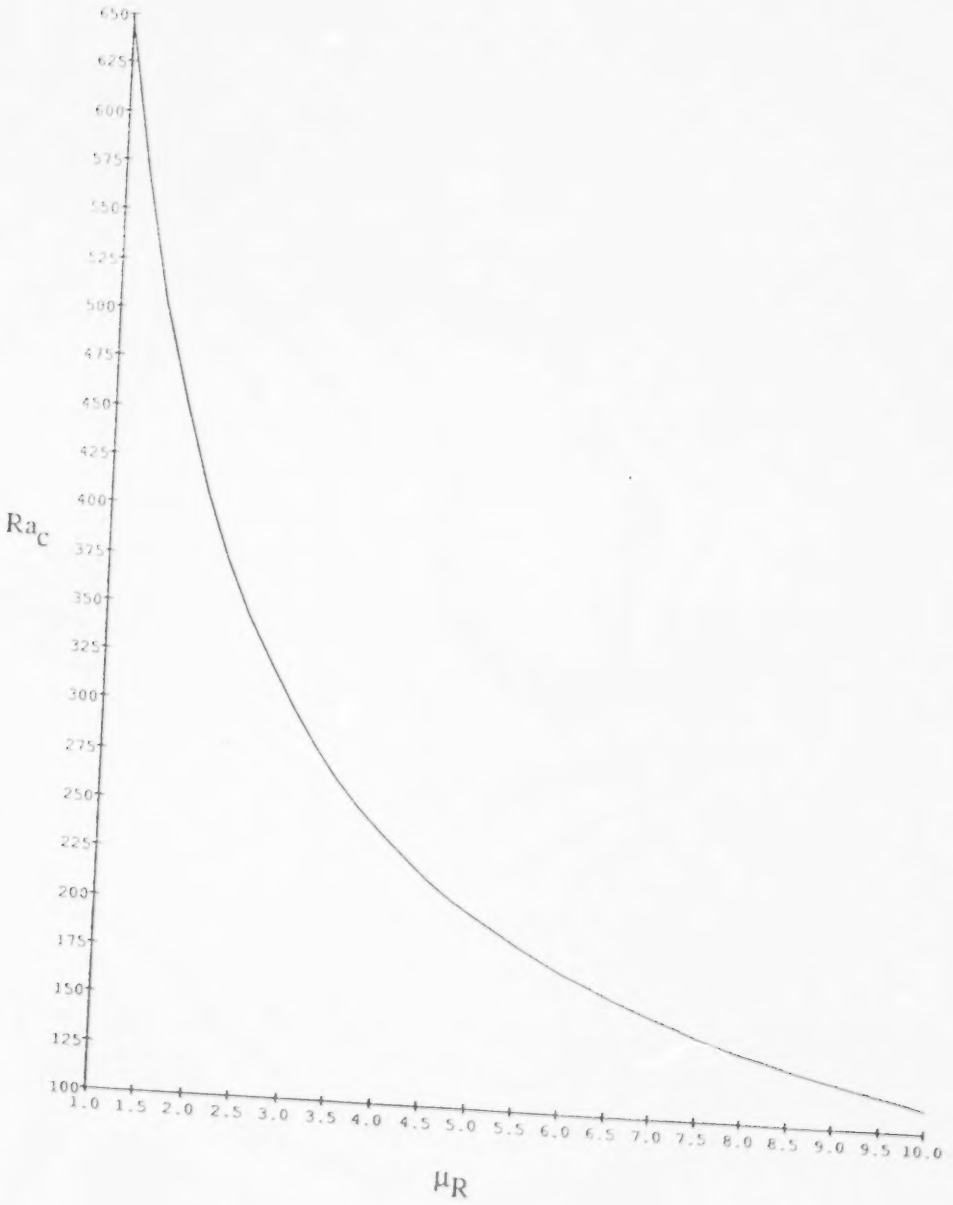

Figure D.13 Predicted Critical Rayleigh Values, Mode 13

Table D.13 Predicted Critical Rayleigh Values, Mode 13, $\lambda = 25.0374$

μ_R	Ra_c
1.00	646.76575
1.25	569.02882
1.50	503.63825
1.75	451.15387
2.00	408.77246
2.25	373.99026
2.50	344.96808
2.75	320.38783
3.00	299.29586
3.25	280.99092
3.50	264.94718
3.75	250.76302
4.00	238.12716
4.25	226.79435
4.50	216.56879
4.75	207.29244
5.00	198.83615
5.25	191.09336
5.50	183.97542
5.75	177.40792
6.00	171.32792
6.25	165.68181
6.50	160.42366
6.75	155.51387
7.00	150.91811
7.25	146.60647
7.50	142.55276
7.75	138.73394
8.00	135.12969
8.25	131.72197
8.50	128.49476
8.75	125.43372
9.00	122.52603
9.25	119.76016
9.50	117.12575
9.75	114.61339
10.00	112.21459

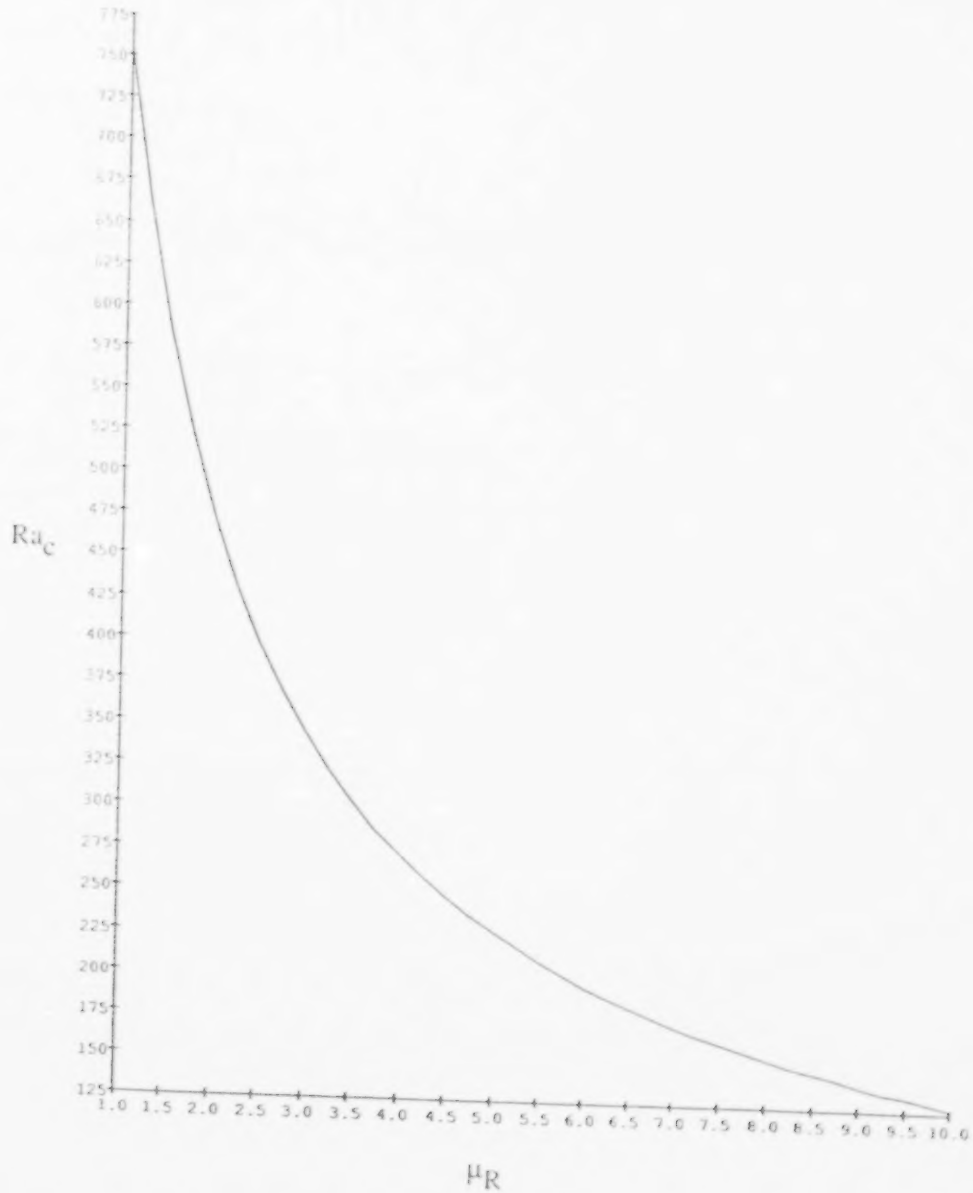

Figure D.14 Predicted Critical Rayleigh Values, Mode 14

Table D.14 Predicted Critical Rayleigh Values, Mode 14, $\lambda = 27.0940$

μ_R	Ra_c
1.00	753.95492
1.25	661.88551
1.50	584.20160
1.75	522.18225
2.00	472.31150
2.25	431.50586
2.50	397.53459
2.75	368.81817
3.00	344.21663
3.25	322.89449
3.50	304.22839
3.75	287.74383
4.00	273.07162
4.25	259.92444
4.50	248.07111
4.75	237.32552
5.00	227.53652
5.25	218.57915
5.50	210.34929
5.75	202.75995
6.00	195.73753
6.25	189.21942
6.50	183.15194
6.75	177.48890
7.00	172.19022
7.25	167.22107
7.50	162.55091
7.75	158.15295
8.00	154.00350
8.25	150.08162
8.50	146.36862
8.75	142.84789
9.00	139.50453
9.25	136.32512
9.50	133.29764
9.75	130.41120
10.00	127.65594

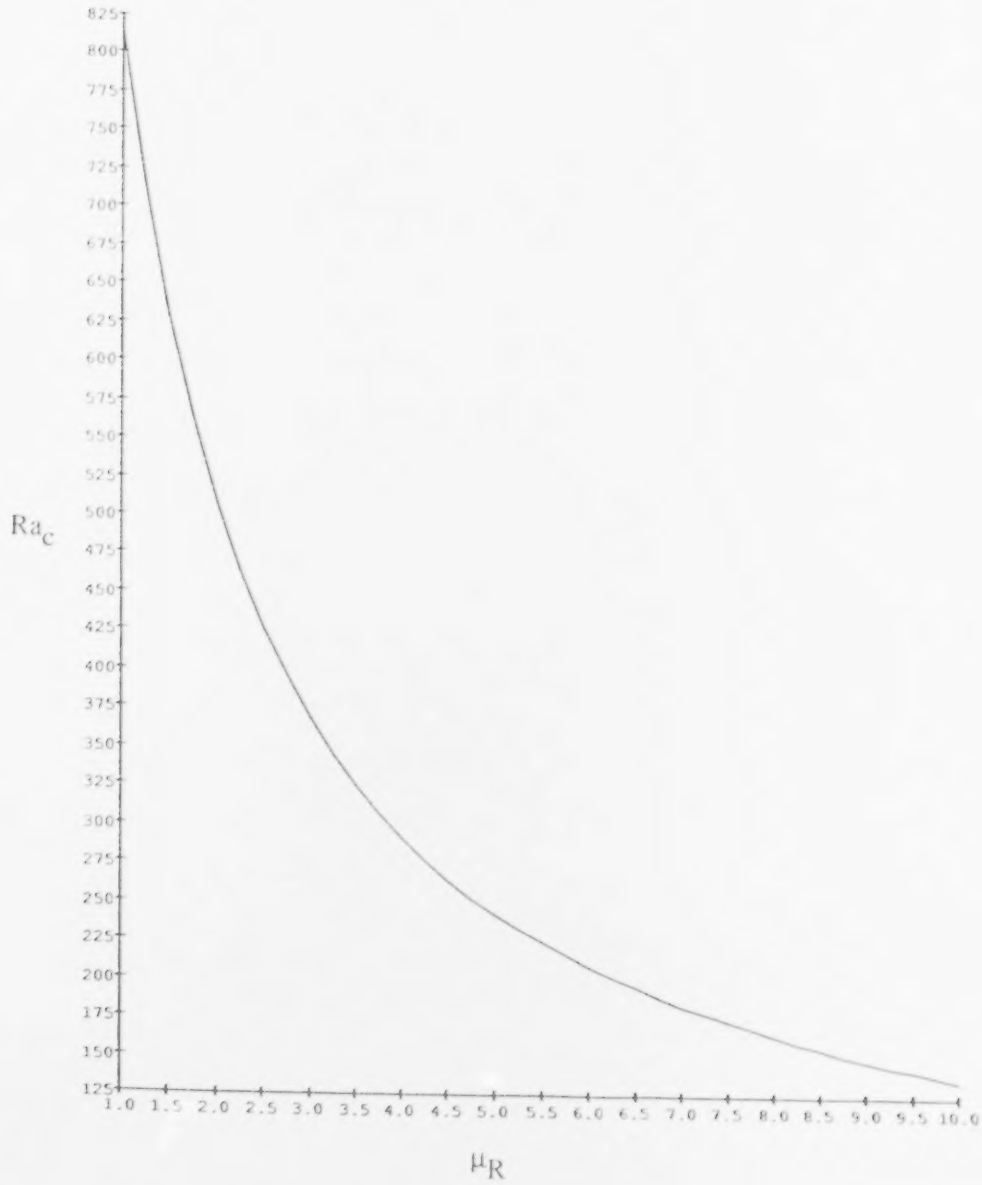

Figure D.15 Predicted Critical Rayleigh Values, Mode 15

Table D.15 Predicted Critical Rayleigh Values, Mode 15, $\lambda = 28.1594$

μ_R	Ra_c
1.00	812.81345
1.25	712.76931
1.50	628.24315
1.75	560.97086
2.00	506.98225
2.25	462.86532
2.50	426.18398
2.75	395.20077
3.00	368.67447
3.25	345.70257
3.50	325.60159
3.75	307.85902
4.00	292.07488
4.25	277.93593
4.50	265.19322
4.75	253.64585
5.00	243.12961
5.25	233.50968
5.50	224.67306
5.75	216.52647
6.00	208.99043
6.25	201.99705
6.50	195.48846
6.75	189.41487
7.00	183.73318
7.25	178.40594
7.50	173.39996
7.75	168.68666
8.00	164.24042
8.25	160.03856
8.50	156.06117
8.75	152.29023
9.00	148.70983
9.25	145.30536
9.50	142.06405
9.75	138.97412
10.00	136.02493

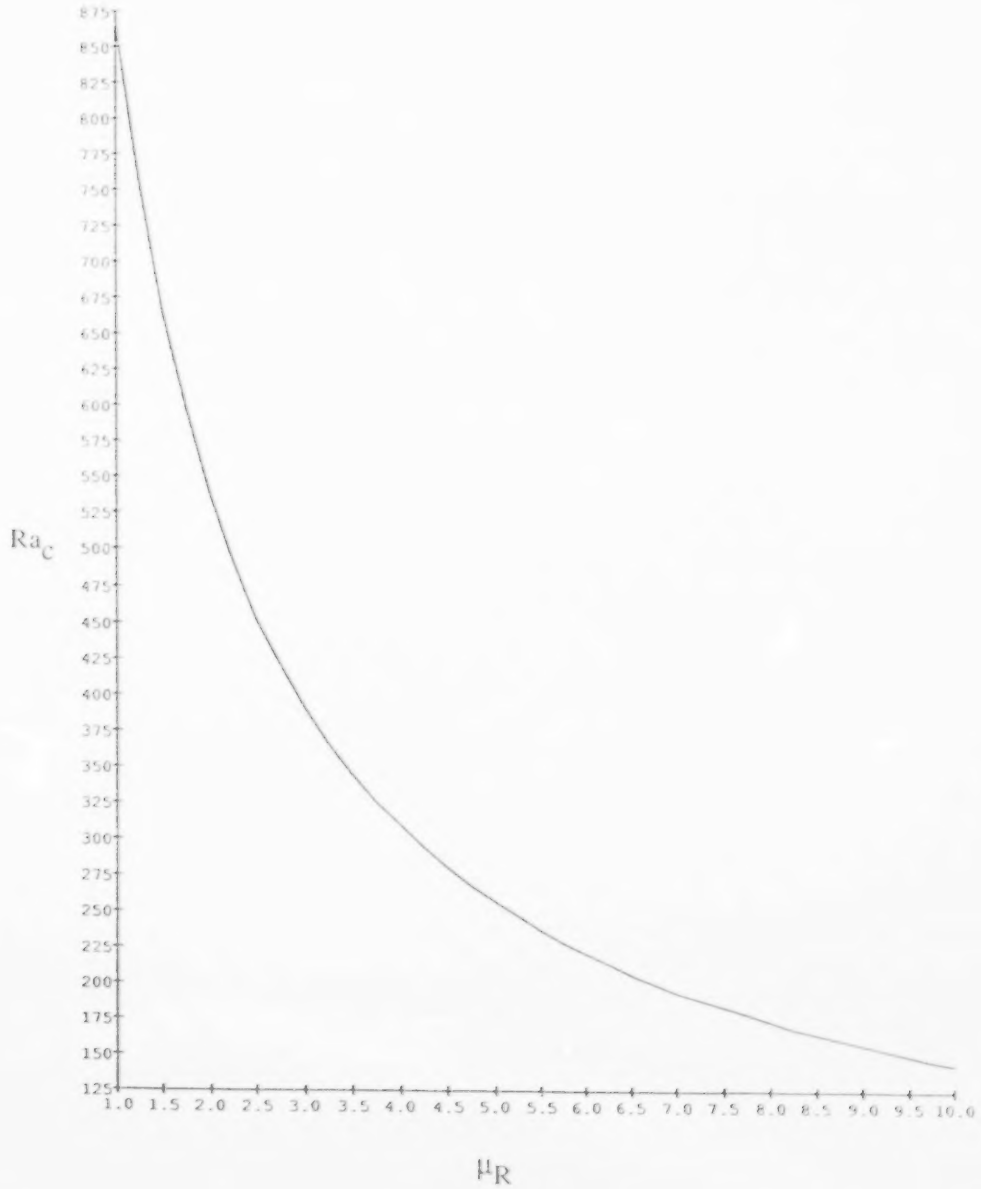

Figure D.16 Predicted Critical Rayleigh Values, Mode 16

Table D.16 Predicted Critical Rayleigh Values, Mode 16, $\lambda = 29.0995$

μ_R	Ra_c
1.00	866.67420
1.25	759.15253
1.50	668.43749
1.75	596.32696
2.00	538.57389
2.25	491.41717
2.50	452.26886
2.75	419.20882
3.00	390.93019
3.25	366.45125
3.50	345.04075
3.75	326.15004
4.00	309.35229
4.25	294.30986
4.50	280.75676
4.75	268.47874
5.00	257.29870
5.25	247.07473
5.50	237.68652
5.75	229.03202
6.00	221.02866
6.25	213.60194
6.50	206.69165
6.75	200.24482
7.00	194.21434
7.25	188.56112
7.50	183.24973
7.75	178.24941
8.00	173.53323
8.25	169.07670
8.50	164.85866
8.75	160.86017
9.00	157.06412
9.25	153.45510
9.50	150.01926
9.75	146.74417
10.00	143.61870

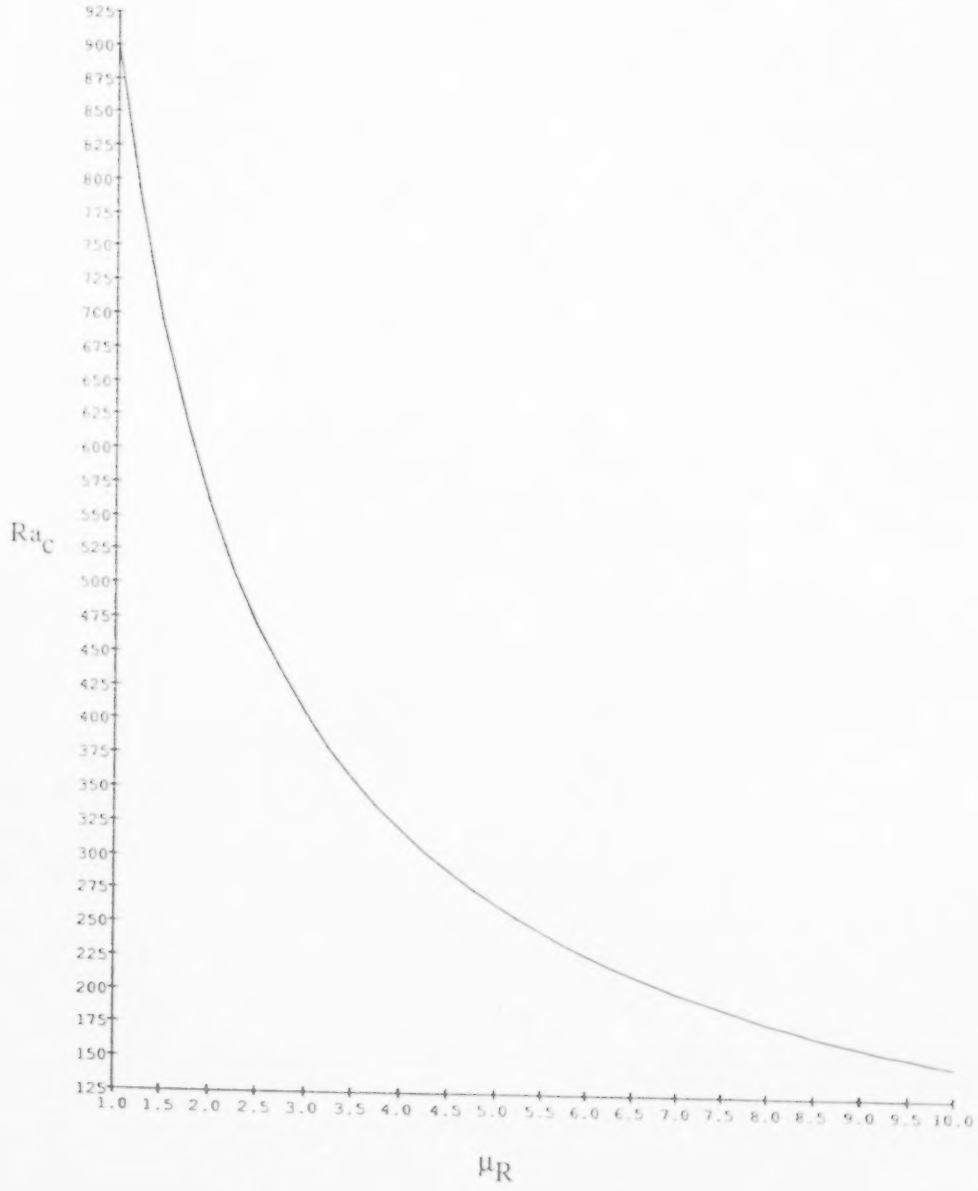

Figure D.17 Predicted Critical Rayleigh Values, Mode 17

Table D.17 Predicted Critical Rayleigh Values, Mode 17, $\lambda = 29.6950$

μ_R	Ra_c
1.00	901.49885
1.25	789.33356
1.50	694.36425
1.75	619.38656
2.00	559.05781
2.25	509.89530
2.50	469.15325
2.75	434.76567
3.00	405.35257
3.25	379.89751
3.50	357.63625
3.75	337.99930
4.00	320.54280
4.25	304.91300
4.50	290.83647
4.75	278.08169
5.00	266.47336
5.25	255.85698
5.50	246.11013
5.75	237.12687
6.00	228.81956
6.25	221.11265
6.50	213.94240
6.75	207.25295
7.00	200.99684
7.25	195.13227
7.50	189.62280
7.75	184.43655
8.00	179.54516
8.25	174.92368
8.50	170.54993
8.75	166.40399
9.00	162.46815
9.25	158.72643
9.50	155.16468
9.75	151.76978
10.00	148.53006

E. SINGLE FLUID: ONSET MODELS COMPARISON

Following is a comparison of the onset of convection model used in the present study and the one presented by Zebib.[23,32] The models' predicted critical Rayleigh numbers (onset of convection) for a water saturated cylindrical porous medium heated from below were compared.

ZEBIB'S MODEL:

Note: Zebib used different symbols than were used in the present work. They are used in this context only in this appendix.

$z_{m,k}$ = Bessel function root parameter, mode = m,k
τ = Dimensionless temperature difference, $(T_1 - T_0) / T_0$
R_c = Critical Rayleigh value

1. Aspect Ratio:

   $s = R / L = 0.3426$ .....(1)[23]

2. Eigenvalue:

   $\lambda = z_{m,k} / s$ .....(5)[23]

   for (m,k) = (1,1)
   $z_{m,k} = 1.841$ .....Table 1[23]

   $\lambda = 5.374$
   $\lambda / \pi = 1.711$

3. Temperature Difference:

   $\tau = (T_1 - T_0) / T_0$ .....(2)[32]
   $T_0 = 25°C = 298$ K
   $T_1 = 126.32°C$
   $\tau = 0.34$

4. Ra_c:

From R_c vs. λ curve @ $\tau = 0.34$ .....Figure 2[32]

for $\lambda / \pi = 1.711$

$R_c / \pi^2 = 2.35 \pm 0.05$ (graphical uncertainty)

$Ra_c = 23.2 \pm 0.5$

PRESENT MODEL:

water @ $T_0 = 25°C \rightarrow \mu_0 = 8.80637E\text{-}04$ [Pa s]

water @ $T_1 = 126.32°C \rightarrow \mu_1 = 2.20485E\text{-}04$ [Pa s]

$\therefore \mu_R = \mu_0 / \mu_1 = 3.994$

from Appendix D, Table D.1, (Ra_c for eigenvalue = 5.3742; mode 1)

$Ra_c = 24.2$

F. SINGLE FLUID: HEAT TRANSFER RATE

This work is based on the power integral technique used by Bau,[14] and Ruth.[60]

The temperature is represented as an average value over the horizontal cross-section superposed with a fluctuating quantity.

$$T = T_z(z^*) + \tau^*(\tilde{x}^*) \qquad \text{F.1}$$

where

$$T_z = \frac{1}{A^*}\iint_{A^*} T\,dA^*$$

$$\iint_{A^*} \tau^*\,dA^* = 0$$

Steady state conditions are assumed. Taking the horizontal cross-sectional average of C.3 and substituting F.1 gives:

$$\frac{1}{A^*}\iint_{A^*} \nabla^{*2} T\,dA^* = \frac{1}{A^*}\iint_{A^*} \frac{(\rho C_p)_f}{\lambda_{ST}}\,\tilde{u}_b^* \cdot \nabla^* T\,dA^*$$

$$\frac{d^2 T_z}{dz^{*2}} + \frac{1}{A^*}\iint_{A^*} \nabla^{*2}\tau^*\,dA^* = \frac{(\rho C_p)_f}{A^*\lambda_{ST}}\left\{\iint_{A^*} \tilde{u}_b^* \cdot \nabla^*\tau^*\,dA^* + \frac{dT_z}{dz^*}\iint_{A^*} \omega^*\,dA^*\right.$$

No net vertical fluid flow leads to:

$$\iint_{A^*} \omega^*\,dA^* = 0$$

$$\iint_{A^*} \nabla^{*2} \tau^* \, dA^* = \nabla^{*2} \iint_{A^*} \tau^* \, dA^*$$

$$\tilde{u}_b^* \cdot \nabla^* \tau^* = \nabla^* \cdot (\tilde{u}_b^* \tau^*) - \tau^* (\nabla^* \cdot \tilde{u}_b^*)$$

$$\nabla^* \cdot \tilde{u}_b^* = 0$$

$$\frac{1}{A^*} \iint_{A^*} \nabla^* \cdot (\tilde{u}_b \tau^*) \, dA^* = \frac{1}{A^*} \nabla^* \cdot \iint_{A^*} \tilde{u}_b \tau^* \, dA^*$$

$$= \frac{1}{A^*} \frac{d}{dz^*} \iint_{A^*} \omega^* \tau^* \, dA^*$$

$$\frac{d^2 T_z}{dz^{*2}} = \frac{(\rho C_p)_f}{A^* \lambda_{ST}} \frac{d}{dz^*} \iint_{A^*} \omega^* \tau^* \, dA^* \qquad \text{F.2}$$

$$\frac{dT_z}{dz^*} = \frac{(\rho C_p)_f}{A^* \lambda_{ST}} \iint_{A^*} (\omega^* \tau^*) \, dA^* + C_1$$

integrating:

$$T_z = \frac{(\rho C_p)_f}{A^* \lambda_{ST}} \int_0^{z^*} \left(\iint_{A^*} \omega^* \tau^* \, dA^* \right) dz^* + C_1 z^* + C_2 \qquad \text{F.3}$$

$$T_1 - T_0 = -\left\{ C_1 L + \frac{(\rho C_p)_f}{A^* \lambda_{ST}} \int_{-1}^{0} \left(\iint_{A^*} \omega^* \tau^* \, dA^* \right) dz^* \right\} \qquad \text{F.4}$$

Apply Boundary Conditions

set 1: Isothermal

i) $T = T_0$; @ $z^* = 0$

$\tau^* = 0; T_z = 0$; @ $z^* = 0$

substituting into F.4 yields $C_2 = T_0$

ii) $T = T_1$; @ $z^* = -L$

$\tau^* = 0$; $T_z = T_1$; @ $z^* = -L$

$$T_1 - T_0 = -\left\{C_1 L + \frac{(\rho C_p)_f}{A^* \lambda_{ST}} \int_{-1}^{0} \left(\iint_{A^*} \omega^* \tau^* dA^* \right) dz^* \right\}$$

<> = integral over volume of porous media

$$T_1 - T_0 = -\left\{C_1 L + \frac{(\rho C_p)_f}{\lambda_{ST}} <\omega^* \tau^*> \right\}$$

$$C_1 = -\left\{(T_1 - T_0) + \frac{(\rho C_p)_f}{\lambda_{ST}} <\omega^* \tau^*> \right\} \frac{1}{L}$$

sub. into F.3, F.4

$$\frac{dT_z}{dz^*} = \frac{(\rho C_p)_f}{\lambda_{ST}} \left\{ \frac{1}{A^*} \iint_{A^*} (\omega^* \tau^*) \, dA^* \cdot \frac{1}{L} <\omega^* \tau^*> \right\} - \frac{(T_1 - T_0)}{L} \qquad \text{F.5}$$

$$T_z = \frac{(\rho C_p)_f}{\lambda_{ST}}\left\{\frac{1}{A^*}\int_0^{z^*}\left(\iint_{A^*}\omega^*\tau^* dA^*\right)dz^* - \frac{z^*}{L}<\omega^*\tau^*>\right\} - \frac{(T_1 - T_0)}{L}z^* + T_0$$

F.6

set 2; conductive layer

$$T \text{ is variable, but } \iint_{A^*} T dA^* = T_z$$
$$\therefore T_z = T_o \ @ \ z^* = 0$$
$$T_z = T_1 \ @ \ z^* = -L$$

and hence 2 boundary conditions give the same results as set 1.

Must normalize:

$$\tilde{x} = \frac{\tilde{x}^*}{L}; \tilde{u}_b = \tilde{u}_b^* L \frac{(\rho C_p)_f}{\lambda_{ST}}; \Theta = \frac{(T - T_0)}{(T_1 - T_0)}Ra$$

$$P = \frac{P^*(\rho C_p)_f k}{\mu \lambda_{ST}}; \tau = \frac{\tau^*}{(T_1 - T_0)}Ra$$

Normalize F.2, F.5, F.6, F.1

$$\frac{d^2\Theta_z}{dz^2} = \frac{d}{dz}\left(\frac{1}{A}\iint_A \omega\tau dA\right) \qquad \text{F.7}$$

$$\frac{d\Theta_z}{dz} = \frac{1}{A}\int\int_A \omega\tau\, dA - (Ra + <\omega\tau>) \qquad \text{F.8}$$

$$\Theta_z = \int_0^z \left\{\frac{1}{A}\int\int_A \omega\tau\, dA\right\} dz - (Ra + <\omega\tau>)z \qquad \text{F.9}$$

$$\Theta = \Theta_z + \tau \qquad \text{F.10}$$

Normalize C.5, invoke B $\rightarrow$ 0, constant viscosity, as variable viscosity effects can be neglected.[14]

$$0 = -\nabla P + \tau\hat{k} - \tilde{u}_b \qquad \text{F.11}$$

Normalize C.3, steady state

$$0 = \nabla^2\Theta - \tilde{u}_b \cdot \nabla\Theta \qquad \text{F.12}$$

$<\tilde{u}_b \cdot F.11>$ *yields:*

$$0 = -<\nabla P \cdot \tilde{u}_b> + <\tau\hat{k} \cdot \tilde{u}_b> - <\tilde{u}_b \cdot \tilde{u}_b>$$

(divergence theorem)

$$<\nabla P \cdot \tilde{u}_b> = \int_s P\tilde{u}_b \cdot \hat{n}\, dS$$

(impermeable boundaries)

$$\tilde{u}_b \cdot \hat{n} = 0 \quad on\ S$$
$$<\tau \hat{k} \cdot \tilde{u}_b> = <\tau \omega>$$

$$0 = <\tau \omega> - <\tilde{u}_b \cdot \tilde{u}_b> \qquad \text{F.13}$$

substitute F.7, F.8, F.10 into F.12

$$\tilde{u}_b \cdot \nabla(\tau + \Theta_z) = \nabla^2(\Theta_z + \tau)$$

$$\tilde{u}_b \cdot \nabla \Theta_z = \tilde{u}_b \cdot \frac{d\Theta_z}{dz}\hat{k}$$
$$= \omega \left\{ \frac{1}{A} \int\int_A \omega \tau \, dA - (Ra + <\omega \tau>) \right\}$$

$$note: \quad \int\int_A \tau \, dA = 0$$

therefore

$$<\tau \frac{d}{dz}\left(\frac{1}{A} \int\int_A \omega \tau \, dA \right)> = 0$$

$$<\tau\omega<\omega\tau>>=<\omega\tau>^2$$

$$<\omega\tau\left(\frac{1}{A}\iint_A \omega\tau\, dA\right)>=<\left(\frac{1}{A}\iint_A \omega\tau\, dA\right)^2>$$

$$<\left(\frac{1}{A}\iint_A \omega\tau\, dA\right)^2> - Ra<\tau\omega> - <\omega\tau>^2 = <\tau\nabla^2\tau> \qquad \text{F.15}$$

Assume the values of velocity and temperature are merely the product of the results of the linear stability analysis and of finite amplitudes B_1 and B_2, i.e.

$$\omega = -B_1\left(g''(z) - \lambda^2 g(z)\right) J_m(\lambda r)\cos m\phi \qquad \text{F.16}$$

$$\tau = B_2 g(z)\, J_m(\lambda r)\cos m\phi \qquad \text{F.17}$$

substitute F.16, F.17 into F.15

$$<\left(\frac{1}{A}\iint_A \omega\tau\, dA\right)^2> = B_1^2 B_2^2\left(\iint_A J_m^2\cos^2 m\phi\, dA\right)^2 \int_{-1}^{0} g^2(g'' - \lambda^2 g)^2\, dz$$

$$<\tau\omega> = -B_1 B_2\left(\iint_A J_m^2\cos^2 m\phi\, dA\right)\int_{-1}^{0} g(g'' - \lambda^2 g)\, dz$$

$$<\tau\omega>^2 = B_1^2 B_2^2\left(\iint_A J_m^2\cos^2 m\phi\, dA\right)^2\left(\int_{-1}^{0} g(g'' - \lambda^2 g)\, dz\right)^2$$

$$<\tau\nabla^2\tau> = B_2^2\left(\iint_A J_m^2\cos^2 m\phi\, dA\right)\int_{-1}^{0} g(g'' - \lambda^2 g)\, dz$$

$$\text{Set:} \quad C = B_1 B_2 \int\int_A J_m^2 \cos^2 m\phi \, dA$$

$$I_1 = \int_{-1}^{0} g(g'' - \lambda^2 g) dz$$

$$I_2 = \int_{0}^{-1} g^2 (g'' - \lambda^2 g)^2 dz$$

$$C^2 I_2 + CRaI_1 - C^2 I_1^2 = C\frac{B_2}{B_1} I_1 \qquad \text{F.18}$$

divide F.18 by C and collect:

$$C = \left(\frac{B_2}{B_1} - Ra\right)\left(\frac{I_1}{I_2 - I_1^2}\right)$$

as Ra $\rightarrow$ Ra_c (from above) $|C| \rightarrow 0$ (infinitesimal motion)

$$\frac{B_2}{B_1} = Ra_c$$

$$C = \left(\frac{I_1}{I_2 - I_1^2}\right)(Ra_c - Ra) \qquad \text{F.19}$$

$$Nu = \frac{L}{\lambda_{ST}(T_1 - T_0)} \frac{1}{A^*} \int\int_{A^*} q \, dA^*$$

$$\frac{1}{A^*}\iint_{A^*} q\,dA^* = \frac{1}{A^*}\left(\iint_{A^*} -\lambda_{ST}\frac{\partial T}{\partial z^*} + (\rho C_p)_f \omega^* \tau^*\right) dA^*$$

$$= -\lambda_{ST}\frac{dT_z}{dz^*} + \frac{(\rho C_p)_f}{A^*}\iint_{A^*} \omega^* \tau^*\, dA^*$$

$$Nu = \frac{-L}{T_1 - T_o}\frac{dT_z}{dz^*} + \frac{(\rho C_p)_f L}{\lambda_{ST}(T_1 - T_o)}\frac{1}{A^*}\iint_{A^*} \omega^* \tau^*\, dA^* \qquad \text{F.20}$$

normalize

$$Nu = \frac{1}{Ra}\left(-\frac{d\Theta}{dz} + \frac{1}{A}\iint_A \omega\tau\, dA\right)$$

substitute F.8:

$$Nu = \frac{1}{Ra}(Ra + <\omega\tau>) \qquad \text{F.21}$$

$$Nu = 1 + \frac{<\omega\tau>}{Ra}$$

substitute F.16, F.17;

$$Nu = 1 - \frac{Cl_1}{Ra} \qquad \text{F.22}$$

substitute F.19

$$Nu = 1 - \frac{I_1^2}{I_2 - I_1^2}\left(\frac{Ra_c - Ra}{Ra}\right)$$

$$Nu = 1 + \left(1 - \frac{Ra_c}{Ra}\right)\left[\frac{I_1^2}{I_2 - I_1^2}\right] \qquad \text{F.23}$$

The integrals are calculated numerically using the output from the linear stability analysis for both sets of boundary conditions in a trapezoidal scheme.

Set 1. Isothermal Boundary Conditions

$$Nu = 1 + 1.835\left(1 - \frac{Ra_c}{Ra}\right)$$
$$Ra_c = 24.782$$

Set 2. Finite Conductive Layer Boundary Conditions

$$Nu = 1 + 2.233\left(1 - \frac{Ra_c}{Ra}\right)$$
$$Ra_C = 22.27$$

G. SINGLE FLUID EXPERIMENTAL ANALYSIS

(i) The Rayleigh number is defined[29] as:

$$Ra = [g_a \, k \, \beta \, (T_{Bot} - T_{Top}) \, L \, \rho^2 \, C_p] / (\mu \, \lambda_m)$$

where:

g_a	=	gravity = 9.81 [m/s^2]
k	=	permeability
β	=	fluid coeff. of vol thermal expansion
	=	1/2 (β @ T_{Bot} + β @ T_{Top}) [1/K]
T_{Bot}	=	T at bottom surface of sand pack [°C, K]
T_{Top}	=	T at top surface of sand pack [°C, K]
L	=	height of sand pack = 0.67 [m]
C_p	=	fluid heat capacity @ T_c [J/kg K]
ρ	=	fluid density @ T_c [kg/m^3]
μ	=	fluid viscosity @ T_c [Pa s]
T_c	=	T at coldest surface of sand pack [°C, K]
λ_m	=	saturated medium thermal conductivity
	=	2.56 - 0.002352 T_{av} [W/m K] (Appendix B)
T_{av}	=	1/2 (T_{Bot} + T_{Top}) [°C, K]

(ii) The Nusselt number is defined as:

$$Nu = q \bullet \{L / [\lambda_m (T_{Bot} - T_{Top})]\}$$

where:

$$q = [1.446 - 5.7 \times 10^{-3} \Delta T_{hfm} - 1.55 \times 10^{-3} T_{hfm}] \bullet [1.10137 + 1.623 \times 10^{-3} \Delta T_{hfm}] \bullet [\Delta T_{hfm} / \Delta y_{hfm}]$$

iii) Finding sand pack surface temperatures is difficult as the probes are of necessity a small distance away from the surfaces. The temperature profile in the region of the lower surface is shown in Figure G.1. The most accurate way to find the surface temperatures is to extrapolate the two probe layer temperature measurements to the

surface. The distances Δy_B and Δy_T are from the nearest probe layer to the lower and upper surfaces, respectively.

$$T_{Bot} = T@76.2\text{ mm} + (T@76.2\text{ mm} - T@285.77\text{ mm}) \bullet [\Delta y_B / 209.55]$$

$$T_{Top} = T@704.85\text{ mm} + (T@704.85\text{ mm} - T@495.3\text{ mm}) \bullet [\Delta y_T / 209.55]$$

It should be noted that the height measurements for the probes are with respect to the bottom of the cell wall, not the sand pack.

The values of Δy_B and Δy_T are evaluated from the first four, conductive, experiments where the Nusselt number is known to be one. The total height of the sand pack is known and by using the height and the Nusselt number the necessary values of Δy_B and Δy_T were calculated for each of the four experiments. The values, when averaged are:

$$\Delta y_B = 19.01\text{ mm}$$

$$\Delta y_T = 21.54\text{ mm}$$

When Δy_B and Δy_T are added to the distance between the top and bottom probe layers the calculated sand pack height is 669.2 mm. The actual sand pack height is 670 mm giving an error of 0.8 mm or 0.1%. The sum of Δy_B and Δy_T are known from the total pack height minus the distance between the probe layers, but the above calculations gives their individual values.

iv) With T_{TOP} and T_{BOT} found, the Rayleigh number and Nusselt number for the five single fluid experiments were calculated, and are presented in Table G.1.

Table G.1 Single Fluid: Experimental Results

DESCRIPTION	W-S #1	W-S #2	W-S #3	W-S #4	W-S #5
T_{BOT} (°C)	62.16	92.71	110.46	131.23	136.25
T_{TOP} (°C)	75.27	116.94	23.60	25.58	33.53
C_P (J/kg K)	4182	4204	4179	4178	4175
ρ (kg/m^3)	982.1	963.3	997.6	997.0	994.6
$\mu \times 10^4$ (Pa s)	4.560	2.993	9.122	8.704	7.411
$\beta \times 10^4$ (1/K)	5.73	7.76	5.22	5.89	6.40
Ra	-4.83	-18.45	14.99	21.77	27.03
Nu	1.003	1.001	1.000	1.005	1.756

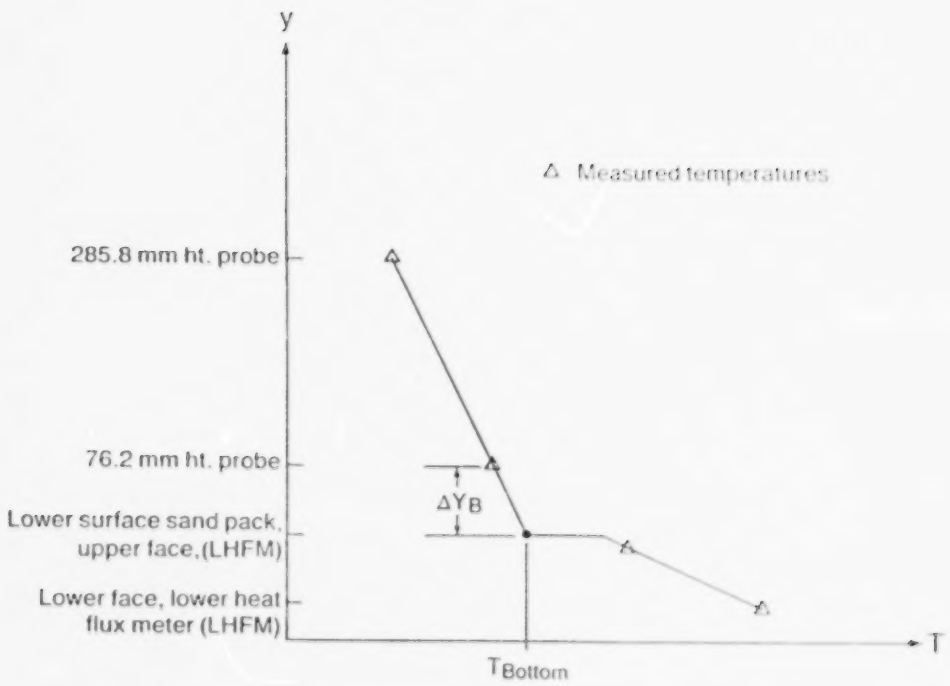

Figure G.1: Lower Surface Temperature Profile.

H. LIQUID/CONDENSIBLE VAPOUR: STEAM/WATER INTERFACE STABILITY

The interface between the steam and water phases is primarily stabilized because the fingers of steam that penetrate the water zone, and bring the interface up, lose heat to the water zone and condense, causing the interface do drop back to the stable position. The interface will become unstable when the overlying water zone cannot remove heat rapidly enough from the steam finger to condense and collapse it. The steam fingers will then penetrate and the interface will be unstable and move up. Further details of the physical logic behind the proposed theory for the interface stability can be found in Chapter 5.

The model developed in this appendix for predicting the stability of the steam-water interface is based on simplifying Straus and Schubert's[50] work to a specific case. Their model does not exactly correspond to the situation dealt with here, in that they used a non-isothermal steam zone instead of an almost isothermal two phase zone. Additionally, they used a permeable top surface instead of an impermeable top surface. The difference in zone treatment is a significant, but necessary simplification that can be corrected by empirical correlation. Straus and Schubert's notation is used throughout and reference to their paper must be made to interpret the following. Straus and Schubert developed an equation for the growth rate of interface perturbations and then presented some numerical solutions and some simplified analytical cases. The purpose of this appendix is to simplify their equation for the growth rate of interface perturbations into an analytical case useful for the boiling of liquids in a confined porous medium heated from below.

Strauss and Shubert's result for the growth rate of interface perturbation ($\bar{\sigma}$) is:

$$0 = \left(f_{18} + f_{15}\bar{\sigma} + f_{19}\sqrt{\bar{\sigma}}\right)\bar{\lambda}_v \coth \bar{\lambda}_v(1-\delta)$$

$$+\left(f_{17} + f_{15}\bar{\sigma} - f_{16}\sqrt{\bar{\sigma}}\right)\bar{\lambda}_l \coth \bar{\lambda}_l\delta \qquad \text{H.1}$$

$$+\left(f_{12} + f_{11}\sqrt{\bar{\sigma}}\right)\bar{\lambda}_l \operatorname{csch} \bar{\lambda}_l\delta - f_7 + f_8\bar{\sigma} + f_9\sqrt{\bar{\sigma}}$$

Strauss and Shubert's parameters are listed below. The se symbols are limited to this appendix alone.

$\bar{\sigma}$	=	dimensionless growth rate of perturbations
$\bar{l}$	=	dimensionless wave number , 2 π d/w,
δ	=	overlying zone thickness/total thickness,
$\bar{\lambda}_l$	=	dimensionless wave number parameter for liquid phase
$\bar{\lambda}_v$	=	dimensionless wave number parameter for vapour phase
f_i	=	various complicated functions
Δ	=	density ratio $(\rho_l - \rho_v) / \rho_l$
$\mathfrak{L}$	=	latent heat parameter
		$h_{lv}/((-dT/dz) \cdot$ total thickness $\cdot$liquid specific heat)
$\bar{\Gamma}$	=	$((-dT/dz) \cdot (dP/dT)_c)/ (\rho_l g_a)$
ψ_3	=	viscosity ratio μ_v/μ_l
Q^*	=	$d \cdot \rho_l^2$
Γ	=	$-dT/dz = q/\lambda m$
d	=	total thickness
d^*	=	overlying zone thickness
$(\,)_l$	=	liquid phase value
$(\,)_v$	=	vapour phase value

as $\bar{\sigma} \rightarrow 0$

$\bar{\lambda}_v, \bar{\lambda}_1 \rightarrow \bar{l}$

$\coth \bar{\lambda}_v (1 - \delta) \rightarrow 1$

$\coth \bar{\lambda}_1 (1 - \delta) \rightarrow 1$

$\operatorname{csch} \bar{\lambda}_1 (1 - \delta) \rightarrow 0$

and H.1 becomes

$$0 = \left\{(f_{18} + f_{17})\bar{l} - f_7\right\} + \left\{\bar{l}(f_{19} - f_{16}) + f_9\right\}\bar{l}\bar{\sigma} \qquad \text{H.2}$$

for the experimental conditions feasible in porous media:

$$\left\{(f_{19} - f_{16})\bar{l} + f_9\right\} > 0$$

therefore for the growth rate to be negative and hence a stable interface to exist:

$$\left\{(f_{18} + f_{17})\bar{l} - f_7\right\} \geq 0 \qquad \text{H.3}$$

substituting expressions for functions:

$$\bar{l}\left[\frac{\Delta(1-\Delta)}{f_1}\mathcal{L}Q^* \cosh \bar{l}\delta \sinh \bar{l}(1-\delta) + \frac{2}{\Gamma}(1-\Delta)\right.$$

$$\left.\frac{+2\Delta\psi_3}{\Gamma f_1}\cosh \bar{l}\delta \cosh \bar{l}(1-\delta) - 2\bar{l}\right] \geq 0$$

for the experimental conditions feasible in porous media:

$$set \quad \sinh \bar{l}(1-\delta) = \cosh \bar{l}(1-\delta)$$

$$\bar{l}\left[\frac{\Delta}{f_1}\cosh \bar{l}\delta \cosh \bar{l}(1-\delta)\left((1-\Delta)\mathfrak{L}Q^* + \frac{2\psi_3}{\bar{\Gamma}}\right) + \frac{2}{\bar{\Gamma}}(1-\Delta) - 2\bar{l}\right] \geq 0$$

set equal to zero

$$\frac{\Delta}{f_1}\cosh \bar{l}\delta \cosh \bar{l}(1-\delta)\left((1-\Delta)\mathfrak{L}Q^* + \frac{2\psi_3}{\bar{\Gamma}}\right) + \frac{2}{\bar{\Gamma}}(1-\Delta) - 2\bar{l} = 0 \qquad \text{H.4}$$

solve H.4 for $\bar{l}$

$$\bar{l} = \frac{(1-\Delta)}{\bar{\Gamma}} + \frac{\Delta}{2f_1}\cosh \bar{l}\delta \cosh \bar{l}(1-\delta)\left[(1-\Delta)\mathfrak{L}Q^* + \frac{2\psi_3}{\bar{\Gamma}}\right] \qquad \text{H.5}$$

for the experimental conditions feasible $(1 - \Delta) / \bar{\Gamma}$ is negligible

note:

$$f_1 = (1-\Delta)\sinh \bar{l}\delta \sinh \bar{l}(1-\delta) + \psi_3 \cosh \bar{l}(1-\delta)\cosh \bar{l}\delta$$

for the experimental conditions feasible in porous media:

$$set \quad \sinh \bar{l}\delta = \cosh \bar{l}\delta$$

$$\therefore \quad f_1 = (1-\Delta+\psi_3)\cosh \bar{l}\delta \cosh \bar{l}(1-\delta) \qquad \text{H.6}$$

sub H.6 into H.5

$$\bar{l} = \frac{\Delta\left[(1-\Delta)\mathfrak{L}Q^{*} + \frac{2\psi_3}{\bar{\Gamma}}\right]}{2(1-\Delta+\psi_3)} \qquad \text{H.7}$$

substitute in experimental properties:

$$\bar{l} = \frac{(\rho_l - \rho_v)\rho_l g_a\left[\frac{\rho_v h_{fg} k}{\lambda_m} + \frac{2\mu_v}{\left(\frac{dP}{dT}\right)_c}\right]}{2\Gamma(\mu_l\rho_v + \rho_l\mu_v)} \qquad \text{H.8}$$

solve H.8 for w/d = W (Stability Number)

$$W = \frac{w}{d} = \frac{4\pi q(\mu_l\rho_v + \rho_l\mu_v)}{(\rho_l - \rho_v)\rho_l g_a\left[\rho_v h_{fg} k + \frac{2\mu_v\lambda_m}{\left(\frac{dP}{dT}\right)_c}\right]} \qquad \text{H.9}$$

at the onset of boiling

$$q = \frac{\lambda_m(T_{sat} - T_o)}{L} \qquad \text{H.10}$$

$$\therefore W_b = \frac{w}{d} = \frac{4\pi\lambda_m(T_{sat}-T_o)(\mu_l\rho_v+\rho_l\mu_v)}{L(\rho_l-\rho_v)\rho_l g_a\left[\rho_v h_{lg}k+\dfrac{2\mu_v\lambda_m}{\left(\dfrac{dP}{dT}\right)_c}\right]} \qquad \text{H.11}$$

for a 100°C interface of water and steam @ 1 atm

$$W_b = \left(\frac{w}{d}\right)\ boiling\ = 1.7019\times10^{-8}\frac{\lambda_m(100-T_o)}{L(1.349\times10^{6}k+6.9337\times10^{-7}\lambda_m)} \qquad \text{H.12}$$

I. LIQUID/CONDENSIBLE VAPOUR: EXPERIMENTAL ANALYSIS

The analysis of the experimental study of the natural convection of steam and water in a cylindrical porous medium was straight forward. The temperature drop across the heat flux meter gave the heat flux. The temperature measurements at each probe level were averaged. The average temperatures at each probe level height were used to determine temperature profiles. The average temperature profile gave the average two-phase zone height, and, when combined with the heat flux, the Nusselt number. The Nusselt number was based on the water saturated thermal conductivity of the sand pack. The Rayleigh number of the overlying water zone was then found, using zone depth and the temperature profile. As an example, the experimental results and conditions for the first water/steam-sand series are shown in Table I.1.

Table I.1: Liquid/Condensible Vapour: Experimental Results

DESCRIPTION	W/S-S #1	W/S-S #2	W/S-S #3
T (°C) @ top sand pack height = 0.7233m	38.678	39.61	51.916
T (°C) @ top 2 phase zone	99.309	98.946	101.224
Height (m) @ top 2 phase zone	0.3411	0.4685	0.4908
T (°C) @ bottom sand pack height = 0.05527 m	101.764	100.258	102.560
q [heat flux] (W/m^2)	370.4	878.0	1254.9
Nu_O overall	1.636	4.152	7.201
Nu_W overlying water zone	0.984	1.5916	2.52
Nu_{SW} two phase zone	18.72	117.12	174.24
Ra overlying water zone	8.858	5.841	5.910

J. LIQUID/CONDENSIBLE VAPOUR: TWO PHASE ZONE THEORETICAL ANALYSIS

The theoretical analysis of the natural convection of liquid and condensible vapour in a porous medium will be focussed on the prediction of Nusselt numbers and thickness of the various zones. Two theoretical analyses will be used, the first, presented in this appendix, dealing with the two phase zone and the second, presented in Appendix H, describing the overlying water zone.

The analytical technique used follows Bau et al.[14,17,18] The assumed mass and heat transfer state is that of a one dimensional, countercurrent flow of liquid down and vapour up in the two phase zone. Liquid is boiled at the bottom surface and vapour condensed in an infinitesimally thin layer at the interface between the two-phase and water zones. Heat transfer occurs only by the latent heat transfer of the vapour.

Mass fluxes must balance:

$$\dot{m}_v = -\dot{m}_l = \dot{m} \qquad \text{J.1}$$

Heat transfer is by latent heat transport alone:

$$q = h_{lv}\dot{m} \qquad \text{J.2}$$

Applying Darcy's Law

$$\dot{m}_l = -[k\, k_{rl} / \nu_l]\{dP/dz + \rho_l g\} \qquad \text{J.3}$$

$$\dot{m}_v = -[k\, k_{rv} / \nu_v]\{dP/dz + \rho_v g\} \qquad \text{J.4}$$

Approximating the relative permeabilities:

$$k_{rl} = S_l \; ; \; k_{rv} = 1 - S_l \qquad \text{J.5}$$

where S_l is the liquid saturation i.e. $S_l = 0$ means 100% vapour and $S_l = 1.0$ means 100% liquid.

Combining J.1, J.3, J.4, J.5 yields

$$\dot{m} = [S_l (1 - S_l) k g_a (\rho_l - \rho_v)] / [(1 - S_l) \nu_l + S_l \nu_v] \qquad J.6$$

which can be solved for saturation.

The thickness of the overlying water zone is determined by

$$q = \lambda_m (T_{sat} - T_{top}) / \Delta y_w \qquad J.7$$

and hence, two phase zone height is

$$\Delta y_{sw} = L - \Delta y_w \qquad J.8$$

The Nusselt number of the overlying water zone is assumed to be one. The Nusselt number of the two phase zone is assumed infinite, but with a maximum (dryout) heat flux[14] of:

$$q_{max} = k h_{lv} g_a (\rho_l - \rho_v) / [(\nu_l)^{0.5} + (\nu_v)^{0.5}]^2 \qquad J.9$$

It should be noted that the work of Udell[15] would result in an improved prediction of saturation but not in Nusselt number or zone thickness.

The second analytical technique predicts the overlying water zone Nusselt number. However, the measured Nusselt numbers for the overlying water zone were used in Table 5.2, in order to show the true significance of the overlying water zone.

The following equation, based on inverting the definition of the overlying water zone Nusselt number gives the overlying water zone thickness.

$$\Delta y_w = [Nu_w \lambda_m (T_{sat} - T_{top})] / q \qquad J.10$$

K. TWO IMMISCIBLE LIQUIDS: EXPERIMENTAL ANALYSIS

As an example, the experimental analysis of the first tetrachloroethylene/water-sand series is presented. The analysis was limited as natural convection was not achieved. The temperature drop across the heat flux meter gave the heat flux. The temperature measurements at each probe level were averaged and the temperature profile (linear) found. The temperature at the top and bottom surface were then extrapolated from the profile. The total temperature difference and the heat flux gave an effective thermal conductivity for each experiment. The thermal conductivity for the first three experiments were then fitted to a model similar to that for water saturated media (Appendix B). The calculated thermal conductivities were then used to find the Nusselt numbers for all four experiments. The results of the analysis are shown in Table K.1. Similar analysis gave the results presented in Table K.2.

Thermal Conductivity Model:

$$\lambda_{sT} = \lambda_{s51.7} - C_1 (T - 51.7)(\lambda_{s51.7} - 1.419)$$

a least squares fit yields:

$$\lambda_{s51.7} = 1.936$$
$$C_1 = 0.01699$$
$$\lambda_{sT} = 2.389 - 8.778 \times 10^{-3} T$$

$$\therefore \lambda_m = 2.389 - 8.778 \times 10^{-3} T$$

The experimental results for all the "oil"/water-sand series are presented in Table K.2.

Table K.1
Tetrachloroethylene/Water in Sand: Experimental Results

DESCRIPTION	T/W-S #1	T/W-S #2	T/W-S #3	T/W-S #4*
q (W/m^2)	124.811	163.355	202.666	341.223
Run Duration (hrs)	161.8	144.0	186.7	96.0
T (°C) @ top sand pack height = 0.7233 m	23.727	25.208	37.848	44.441
λ_m apparent (W/m K)	2.101	1.742	1.792	2.437
T (°C) average	43.357	56.167	75.145	90.548
λ_m calculated (W/m K)	2.009	1.896	1.730	1.595
Nu	1.05	0.92	1.04	1.53

* - not steady state.

Table K.2
Two Immiscible Liquids: Experimental Results

T/W-S Series	#1	#2	#3	#4
q (W/m^2)	124.81	163.36	202.67	341.22
Nu	1.05	0.92	1.04	1.53*

T/W-S II Series	#1	#2	#3	#4
q (W/m^2)	30.72	64.32	160.96	559.07
Nu	3.10	5.00	8.30	15.20

O/W-S Series	#1	#2	#3	#5	#6	#7
q (W/m^2)	-96.46	83.92	348.96	193.70	142.11	535.94
Nu	1.00	1.00	5.80	2.58	1.89	7.55

O/W-S II Series	#1	#2	#3	#4	#5
q (W/m^2)	-113.89	230.11	76.22	-54.71	502.78
Nu	1.00	4.60	1.93	1.00	26.73

* transient, non-convective

L. TWO IMMISCIBLE LIQUIDS: PSEUDO-FLUID

Analysis of the natural convection of two immiscible liquids in a cylindrical porous medium by treating the fluids as a single pseudo-fluid was very simple. The Rayleigh numbers for the experiments were found using actual thermal conductivity, assuming no permeability reduction (no relative permeability) and fluid properties based on a mass average. The critical Rayleigh value was predicted using the single fluid theory, and mass-averaged fluid properties, including viscosity.

As an example, the psuedo-fluid analysis for the first tetrachloroethylene/water sand experimental series is presented. The tetrachloroethylene properties were found in the "Encyclopedia of Chemical Technology".[61] The liquid mixture saturating the sand pack was 9.32% by mass water and 90.68% by mass tetrachloroethylene. The pseudo-fluid properties and resulting Rayleigh numbers are shown in Table L.1.

The critical Rayleigh value was found by using the experimental conditions to estimate the Rayleigh number, finding the resulting viscosity ratio between hot and cold surfaces, and then finding the critical Rayleigh value from Appendix C. This process was iterated until the viscosity ratio matched the critical Rayleigh value accurately. The critical Rayleigh number was found to be 32.76 for the isothermal boundary conditions.

The psuedo-fluid Rayleigh numbers and predicted critical values are presented for all the "oil"/water experiments in Table L.2.

Table L.1
Tetrachloroethylene/Water in Sand: Pseudo-fluid Rayleigh Values

DESCRIPTION	T/W-S #1	T/W-S #2	T/W-S #3	T/W-S #4*
T_{TOP} (°C)	23.727	25.208	37.848	44.441
T_{BOT} (°C)	63.313	87.670	113.213	137.784
ρ_{pseudo} (kg/m^3)	1558.9	1556.7	1536.7	1526.0
Cp_{pseudo} (J/kg K)	1169	1169	1169	1169
$\mu_{pseudo} \times 10^4$ (Pa s)	8.55	8.41	7.38	6.88
$\beta_{pseudo} \times 10^4$ (1/K)	10.17	10.27	10.35	10.44
Ra	13.37	21.50	29.04	38.32

* transient, non-convective

Table L.2
Two Immiscible Liquids: Pseudo-fluid Rayleigh Values

T/W-S Series	#1	#2	#3	#4
Nu	1.05	0.92	1.04	1.53*
Ra_{pseudo}	13.37	21.50	29.04	38.37

$Ra_c = 32.8$

T/W-S II Series	#1	#2	#3	#4
Nu	3.10	5.00	8.30	15.20
Ra_{pseudo}	104.86	139.36	217.88	470.78

$Ra_c = 51.6$

O/W-S Series	#1	#2	#3	#5	#6	#7
Nu	1.00	1.00	5.80	2.58	1.89	7.55
Ra_{pseudo}	-106.81	64.95	112.92	97.92	83.89	164.12

$Ra_c = 42.1$

O/W-S II Series	#1	#2	#3	#4	#5
Nu	1.00	4.60	1.93	1.00	26.73
Ra_{pseudo}	-486.90	134.42	75.44	-195.08	207.35

$Ra_c = 47.7$

* transient, non-convective

M. RELATIVE PERMEABILITY EXPERIMENTS

The relative permeabilities of the oil/water mixtures used in the natural convection experiments were measured at end points in a permeability apparatus. The same sand, 6/9 Colorado, was used in the apparatus. The permeability flow cell was 5.08cm in diameter and 0.594m long. Pressure differentials were measured with a 0-7 kPa differential transmitter. Back pressure was maintained with a regulating valve. No overburden pressure was applied. Water was taken directly from the building's cold water supply as the flow rates were high. Oil was recirculated and pumped by a high volume pump.

The mixture of tetrachloroethylene/water was found to have the following end points;

$k_{ro} = 0.655$ @ $S_o = 0.88$
$k_{rw} = 0.0$ @ $S_o = 0.88$

$k_{ro} = 0.0$ @ $S_o = 0.21$
$k_{rw} = 0.907$ @ $S_o = 0.21$

a linear relationship between end points yields:

$k_{ro} = -0.205 + 0.978\ S_o$
$k_{rw} = 1.191 - 1.354\ S_o$

The mixture of Mentor 29/water was found to have the following end points:

$k_{ro} = 0.891$ @ $S_o = 0.89$
$k_{rw} = 0.0$ @ $S_o = 0.89$

$k_{ro} = 0.0$ @ $S_o = 0.05$
$k_{rw} = 0.90$ @ $S_o = 0.05$

a linear relationship between end points yields:

$k_{ro} = -0.053 + 1.061\ S_o$
$k_{rw} = 0.954 - 1.071\ S_o$

N. TWO IMMISCIBLE LIQUIDS: RELATIVE PERMEABILITY

As an example, the relative permeability model 1 analysis of the first tetrachloroethylene/water-sand series is presented. This sample analysis is limited to calculating the Rayleigh values of the tetrachloroethylene phase, as the water phase has almost no mobility. The relative permeability of tetrachloroethylene in the 90.68% tetrachloroethylene, 9.32% water saturated 40-70 Unimin sand was found, from Appendix M, to be 0.63. The Rayleigh number for a fluid considering relative permeability, is defined as:

$$Ra_{rf} = k_{rf} [g_a k \beta (T_{bot} - T_{top}) L \rho^2 C_p] / \{ \mu \lambda_m \}$$

where properties are for the one fluid as in Appendix G except for:

λ_m = saturated medium thermal conductivity
includes effects of other fluid [W/m K]

k_{rf} = relative permeability of fluid in the porous medium
at the given saturation.

The properties and Rayleigh values are presented in Table N.1

The relative permeability Rayleigh valves and predicted critical Rayleigh values for all the "oil"/water experimental series are presented in Table N.2.

Table N.1
Tetrachloroethylene/Water in Sand:
Tetrachloroethylene Phase Relative Permeability Rayleigh Values

DESCRIPTION	T/W-S #1	T/W-S #2	T/W-S #3	T/W-S #4*
T_{TOP} (°C)	23.727	25.208	37.848	44.441
T_{BOT} (°C)	63.313	87.670	113.213	137.784
ρ_{tetra} (kg/m^3)	1616.6	1614.2	1592.6	1581.1
Cp_{tetra} (J/kg K)	860	860	860	860
μ_{tetra} x 10^4 (Pa s)	8.49	8.39	7.43	6.96
β_{tetra} x 10^4 (1/K)	10.79	10.79	10.79	10.79
k_{rf}	0.63	0.63	0.63	0.63
Ra	7.05	11.29	15.10	19.81

Table N.2
Two Immiscible Liquids: Relative Permeability Rayleigh Values

T/W-S Series	#1	#2	#3	#4
Nu	1.05	0.92	1.04	1.53*
Ra_{oil}	7.05	11.29	15.10	19.81

Ra_c (oil) = 35.5

T/W-S II Series	#1	#2	#3	#4
Nu	3.10	5.00	8.30	15.20
Ra_{oil}	65.40	86.90	135.90	293.60

Ra_c (oil) = 51.3

O/W-S Series	#1	#2	#3	#5	#6	#7
Nu	1.00	1.00	5.80	2.58	1.89	7.55
Ra_{oil}	-60.50	36.80	64.00	55.50	47.60	93.00
Ra_{water}	-69.00	23.60	51.70	41.60	33.60	80.20

Ra_c (oil) = 37.6
Ra_c (water) = 38.8

O/W-S II Series	#1	#2	#3	#4	#5
Nu	1.00	4.60	1.93	1.00	26.73
Ra_{oil}	-11.40	4.03	2.66	-5.28	5.84
Ra_{water}	-412.20	113.80	63.90	-165.10	175.60

Ra_c (oil) = 18.7
Ra_c (water) = 47.7

* transient, non-convective

O. WATER/SAND THERMAL CONDUCTIVITY

The following is a report describing the thermal conductivity of the water-saturated 40-70 Unimin sand used in the initial heat transfer experiments.

THERMAL CONDUCTIVITY MEASUREMENTS

For: Alberta Research Council
Edmonton, Alberta

By: Tempest Geophysical Consultants Limited
24 Quesnell Road
Edmonton, Alberta
T5R 5N2

August 8, 1989

PERMIT TO PRACTICE
TEMPEST GEOPHYSICAL CONSULTANTS LIMITED
Signature
Date Aug 8/89
PERMIT NUMBER: P 3862
The Association of Professional Engineers, Geologists and Geophysicists of Alberta

SUMMARY OF RESULTS

	Km	Ks
Run 1 (Cell 39)	4.95 $Wm^{-1}K^{-1}$	2.40 $Wm^{-1}K^{-1}$
Run 2 (Cell 42)	4.94 $Wm^{-1}K^{-1}$	2.34 $Wm^{-1}K^{-1}$

Km = material conductivity

Ks = conductivity of saturated sample

$Ks = Kw^{\phi} Km^{1-\phi}$

Kw = water conductivity = 0.602 $Wm^{-1}K^{-1}$

ϕ = porosity

----------CELL MEASUREMENTS----------

DATE 7.08 '989

HOLE NO. 1 DEPTH ' CELL NUMBER 39

PUMP 3 CELL HEIGHT 12.99 CELL DIAMETER 36.7

IN.DIA 34.79 THICKNESS 1.23 CELL WEIGHT 5.433

DRY WEIGHT 23.100 WET WEIGHT 26.291 POROSITY 34.394

THERMISTOR NUMBERS ARE:279.280.281.282

ROOM TEMP 27.622 G-NUMB .510

TEMPS. 29.597 29.088 24.179 22.612

-FS: .97 S: 1.27 CONDUCT. 5.44

TEMPS. 29.592 29.086 24.164 22.614

-FS: .98 S: 1.28 CONDUCT. 5.45

TEMPS. 29.600 29.083 24.153 22.516

S: .99 S: .29 CONDUCT. 4.95

DATE 7.08 1989

CORE NO. 2 DEPTH 2 CELL NUMBER 42

PUMP # CELL HEIGHT 13 CELL DIAMETER 36.87

IN.DIA 34.36 THICKNESS 3.24 CELL WEIGHT 5.462

DRY WEIGHT 23.030 WET WEIGHT 26.341 POROSITY 35.54%

THERMISTOR NUMBERS ARE:283.284.287.288

ROOM EMP 27.635 G-NUMB .486

EMPS. 29.637 28.032 24.187 22.506

DIFF .99 S: .22 CONDUCT. 4.94

EMPS. 29.630 28.032 24.135 22.508

DIFF .00 S: .22 CONDUCT. 4.93

EMPS. 29.607 28.033 24.188 22.606

DIFF 1.00 S: .22 CONDUCT. 4.94